THÈSE

En vue de l'obtention du

DOCTORAT DE L'UNIVERSITÉ DE TOULOUSE

Délivré par :

Institut National Polytechnique de Toulouse (INP Toulouse)

Discipline ou spécialité :

Génie des Procédés et de l'Environnement

Présentée et soutenue par :

Mohamed RAII

le : mercredi 12 décembre 2012

Titre :

Formulation, caractérisation et mise en oeuvre des barrières perméables réactives à base de phosphate de calcium, utilisation pour la fixation de polluants

Ecole doctorale :
Mécanique, Energétique, Génie civil et Procédés (MEGeP)

Unité de recherche :

RAPSODEE

Directeur(s) de Thèse :

M. Ange NZIHOU, Professeur, Ecole des Mines d'Albi-Carmaux
M. Javier ESCUDERO SANZ, Chargé de recherche, Ecole des Mines d'Albi-Carmaux

Rapporteurs :

M. Lev FILIPPOV, Professeur des universités, INPL, Nancy
M. Zoubeir LAFHAJ, Professeur, ECL, Lille

Membre(s) du jury :

M. Emmanuel MARTINS, Ingénieur, PRAYON, Belgique

M. Eric CHAMPION, Professeur des universités, SPCTS, Limoges

M. Patrick SHARROCK, Professeur des universités, UPS, Toulouse
M. F. Javier ESCUDERO SANZ, Chargé de recherche, EMAC, ALBI (co-directeur de thèse)
M. Ange NZIHOU, Professeur, EMAC, ALBI (directeur de thèse)

Résumé: L'objectif principal de cette thèse est la formulation des mélanges stables contenant l'hydroxyapatite gel synthétisée (Ca-HA$_{Gel}$). Le comportement rhéologique des mélanges Eau/(sulfate de calcium) et hydroxyapatite/(sulfate de calcium) a été étudié. Les résultats ont montrés que tout les mélanges sont caractérisés par un comportement rhéologique rhéofluidifiant et thixotrope. Le potentiel zêta a été utilisé dans cette étude pour mieux appréhender les interactions entre les particules et leur effet sur le comportement des mélanges. La fixation de sulfate sur la surface de Ca-HA favorise la stabilité de la structure du Ca-HA$_{Gel}$. Les analyses de caractérisation effectuées sur les formulations ont montrées la formation de nouveaux composés tels que le sulfate-phosphate de calcium hydraté et l'Ardealite. Les tests de lixiviation et de percolation ont révélés que le taux de relargage de soufre et strontium à partir des sous-produit de gypse était négligeable pour les mélanges contenant Ca-HA$_{Gel}$. Ca-HA$_{Gel}$ stabilise les métaux lourds relargués à partir du gypse et plâtre. Les particules du gypse améliore les performances hydrauliques de Ca-HA$_{Gel}$ et le plâtre hydraté stabilise la structure de Ca-HA$_{Gel}$ par la formation des particules agglomérées. Le test colonne effectués sur la formulation AWPG2 a montré une grande performance à retenir le plomb et le cadmium avec des capacités de rétention de plus de 99% et 88% respectivement. The traitement des métaux lourds était lié aux particules de Ca-HA et aux phosphate et calcium libres. La formulation AWPG2 peut être utilisée dans les barrières perméables réactives pour traiter les eaux souterraines contaminées.

Mots clés : stabilité de la structure, stabilité chimique, performances hydrauliques, réactivité

Abstract: The main purpose of this thesis was the formulation of stable blends based on synthesized hydroxyapatite-gel (Ca-HA$_{Gel}$). The rheological behavior of water−calcium sulfates and hydroxyapatite−calcium sulfates blends was considered in this study. The results show that all blends and formulations exhibit a shear-thinning effect and thixotropic behavior. The ζ potential was used in this study to understand the interaction between particles and its effect on the global behavior of the blends. Fixation of sulfate on Ca-HA surface promotes the stability of Ca-HA$_{Gel}$ suspension. Characterization analysis of formulation shown the presence of new compounds such as calcium sulfate-phosphate hydrate and Ardealite. Leaching and percolation tests revealed that the release rate of sulfur and strontium from gypsum by-product was negligible in blends based on Ca-HA$_{Gel}$. Ca-HA$_{Gel}$ was stabilized the heavy metals released from plaster and gypsum. Gypsum particles enhanced hydraulic performances of Ca-HA$_{Gel}$ and hydrated plaster stabilized Ca-HA$_{Gel}$ structure by the formation of agglomerated particles. Column test carried out on AWPG2 blend revealed high removal performances for lead and cadmium with retention capacity of 99% and 88% respectively. The reactivity was related to Ca-HA and free calcium and phosphate contained in the selected formulation. AWPG2 blend is to be used as permeable reactive barrier for in-situ contaminated groundwater remediation.

Keywords: structure stability, chemical stability, metal behavior, hydraulic performances, reactivity.

Table of content

Chapter 1
Literature review

<div style="border:1px solid">

Chapter II
Materials & Characterization procedures

</div>

Chapter III
Physicochemical and mineralogical properties of initial materials

---

Chapter IV
Ca-HA$_{Gel}$ – Gypsum and Ca-HA$_{Gel}$ – Plaster formulations

Chapter V
Rheological behavior of gypsum, plaster and hydroxyapatite gel blends

Chapter VI
Rheological behavior of Water—Calcium sulfates—Hydroxyapatite-Gel ternary blends

List of Figures

List of Tables

General introduction

I. Introduction and Motivation

The contamination of natural resources such as groundwater has become a major problem associated to the abusive use of toxic industrial substances. In addition, the preservation and management of water resources has become a major concern in a world that suffers from water scarcity.

Groundwater is the most exploited resource to meet the water needs of populations worldwide. In this case, up to two billion people lack in water table resources, they depend directly on aquifers and 40% of the world's food produced by irrigated agriculture relies heavily on groundwater. The water reserve depends on the global aquifer; up to 35% is intended for human consumption and industrial purposes. The UNESCO report published in 2008 on the hydrogeological map of underground water reserves worldwide shows identification of aquifers and 90 273 in Europe. However, the contamination of aquatic ecosystems including deep groundwater affected by various pollutants, is one of the main problems related to the infiltration of heavy metals and radionuclides, chlorinated compounds and volatile organic compounds through the soil layers. This scenario is often encountered in areas of feeding (fertilization), septic tanks, mines, nuclear operations, uncontrolled landfills and areas of agricultural activity in the non-oriented use of fertilizers. In Europe, the groundwater is polluted with many contaminants such as nitrates, pesticides, hydrocarbons, sulfates and bacteria.

The politics of environmental protection insist on the decontamination and treatment of contaminated soil and groundwater. By the 1980s, the first attempts at treatment were started by using the method "pump and treat", this technique requires significant energy input to high operating costs. In 1999, the guidelines of the Soil Conservation in Germany issued the first laws requiring the highlighting techniques that can be used to clean up contaminated soil source of pollution of groundwater such as excavation and cleaning of soil, heat treatment, solidification and stabilization.

However, research has been focused on the development of a technical book for the effective treatment of soil and groundwater pollution. This book should be of benefit and potential technical and economic criteria that should be in favor of this application; A new technique, called the passive permeable reactive barriers (PRB), is based on the introduction of a reagent or a mixture of reactive porous materials with certain permeability in a cut at the water table to promote the in situ immobilization of pollutants by the passage of the plume along a polluted natural slope and a homogeneous flow through the reactive layer. This natural mechanism completely eliminates the cost of energy by reducing operating costs and offsetting the costs of monitoring and surveillance of the treatment technique of groundwater.

During the last twenty years, the development of PRB by experiments at laboratory scale was conducted at the University of Waterloo and the application of a test driver has been installed in Borden (Ontario, Canada) in 1991. In France, the implementation of the first PRB was in 1994 in Neuville. Currently, the growing interest in this new system has allowed its use in several European countries. Particularly in Europe, 35 permeable reactive barriers were implanted with 20 industrial projects by using reagents with decontamination mechanisms such as chemical degradation, the change in the chemical form of the pollutant, adsorption and biological processes.

II.   Context of the thesis

The general context of this study was the use of synthesized hydroxyapatite in PRB technique as reactive material. Synthesized hydroxyapatite-gel ($Ca_{10}(PO_4)_6(OH)_2$, Ca-HA$_{Gel}$) has shown a high capacity to retain heavy metals in its gel form. Gel form looks like a concentrated suspension already characterized by a unstable structure. The stabilization of concentrated suspensions requires the breakage of powder agglomerates by adding chemical material. Calcium sulfate industrial by-product was used to stabilize gel structure as support material. Hence, the valorization of industrial waste in PRB is a good issue.

III. Objectives

The main goals of this thesis were as follows:

The investigation of rheological behavior of gypsum, plaster, synthesized Ca-HA$_{Gel}$ and blends between materials with different proportions (i.e. binary blends: water/plaster, water/gypsum, Ca-HA$_{Gel}$/plaster and Ca-HA$_{Gel}$/gypsum, and ternary blends: Ca-HA$_{Gel}$/(water/plaster) and Ca-HA$_{Gel}$/(water/gypsum). Furthermore, the rheological behavior of concentrated suspension Ca-HAGel was studied using the steady and dynamic rheological tests to characterize rheological behavior, viscosity and internal structure. Rheological behavior characterizes the matrix stability and hence the consistency. Study of the interaction between particles was considered as a major step to interpret the effects such as attraction and dispersion describing the stability of formulations.

The determination of physicochemical characteristics and the identification of mineral phases present in formulations was examined. The study of the environmental behavior of waste materials (gypsum with different fraction sizes and plaster) and formulations based on gypsum, plaster and Ca-HA$_{Gel}$ using a standardized leaching test. The evaluation of the stabilization of gypsum and plaster chemical elements release using Ca-HA$_{Gel}$.

The determination of hydraulic performances (porosity and permeability) of initial materials and formulations. The investigation of chemical element release from materials and blends using standardized percolation test. The use of column test experiment to assess the treatability performance of blend at laboratory scale.

IV. Approach & Methodology

The approach followed in this thesis is summarized in 3 steps. Schema presented below illustrates the main methodologies explored to identify physicochemical and hydraulic properties of materials and formulations.

(1) The study of rheological behavior of initial materials and considered formulations is based on the determination of rheological behavior and the main parameters giving same indications concerning the implementation conditions and the flowability. The interaction between particles is also correlated to the particle surface explaining the attraction or repulsion between particles. However, the effect of interaction influences obviously the stability of matrix that requires chemical interpretations. Particle size and interaction between particles describe the hydraulic performances of formulations.
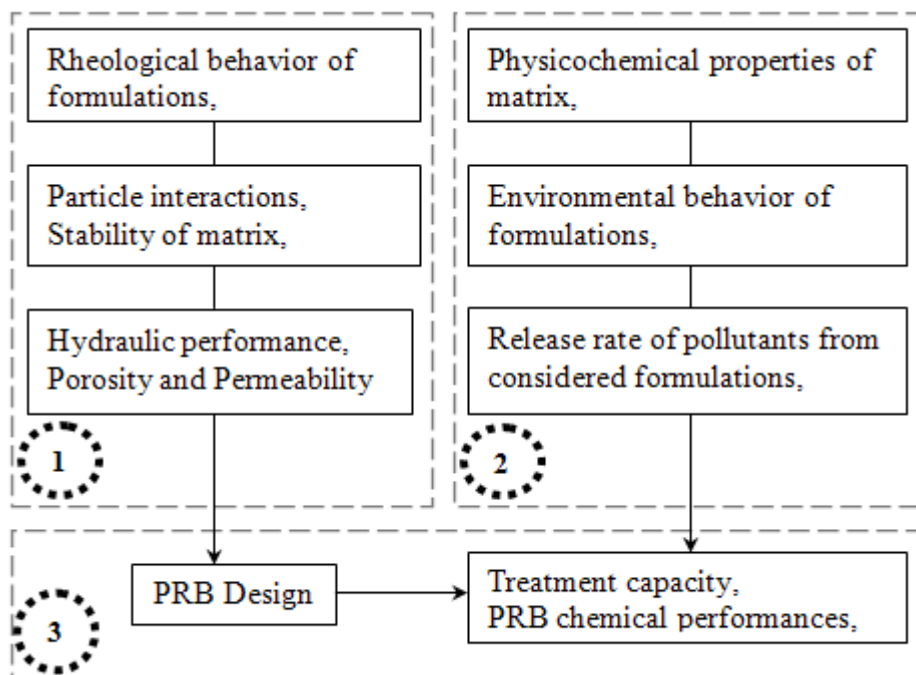
(2) The determination of physicochemical characteristics such as density, surface specific area, pH, conductivity and also the chemical composition of materials and formulations was a step of great interest. This step helps to better understand the different mechanisms governing the release of major elements and heavy metals from materials and considered blends and to study their availability in the effluent. Environmental behavior (leaching and percolation tests) evaluates in this study the possibility of the use of waste in PRB by the evaluation of release rate and facilitates the selection of formulations presenting high stability and homogeneity.

3 Main properties evaluated in the first and second steps may help to select a formulation giving better stability and hydraulic performances and characterized by a certain chemical stability. The selected formulation lead to the assessment of its capacity to treat polluted effluent.

V.   Outline

The present thesis comprises 8 Chapters:

Bibliographic research (Chapter I) presents briefly the Permeable Reactive Barrier (PRB) technique used to treat groundwater and the main criteria leading to reactive material selection. Reactive material such as calcium phosphates (Apatite) may be introduced in PRB for thin high capabilities to treat wastewater, hence the definition of its crystalline structure, physicochemical characterizations and mechanisms facilitating the removal of heavy metals which where illustrated and discussed in the second section (Calcium phosphates). Third section presents calcium sulfate, its fabrication with different forms and reactivity with water. Porous media and permeability determination were presented in fourth section.

The second chapter entitled "Materials & Characterization procedures'" presents the main techniques to determine the physicochemical characterization and properties related to particle surface such as the charge and the procedure used to determine the rheological behavior and fluidability.

Physicochemical and mineralogical properties of materials chapter focuses on the characterization of materials by application of different procedures described in "Materials & Characterization procedures'". Density, particle size distribution, chemical composition and the mineralogical phases present in the samples of calcium phosphate and calcium sulfate were presented.

Formulations destined to the evaluation of rheological behavior are summarized in Chapter IV. Two series of formulations were proposed, binary (calcium sulfate with water, calcium phosphate with calcium sulfate) and ternary blends (calcium

phosphate blended with calcium sulfate and water). Materials consisted in formulations with different proportions to determine the adequate blend revealing the stability and to study the interaction between particles.

The results of rheological behavior of binary and ternary blends are discussed in Chapter V and VI. This chapter presents the rheological properties of synthesized hydroxyapatite under its gel form using steady and dynamic procedures. Rheological properties of binary blends were interpreted as a function of viscosity and applied strain parameters and chemical point of view.

Chapter VII discusses the chemical behavior of blends formulated from rheological behavior and interaction between particles results. Considered blends were mineralogically characterized. Chemical behavior was assessed using standardized leaching behavior. Another interest of leaching test was to study the stabilization of calcium sulfate by-product using synthesized hydroxyapatite-gel (Ca-HA$_{Gel}$). Hydraulic and chemical properties are presented in Chapter VIII. The selection of formulation destined to PRB application was based on the hydraulic performances (porosity and permeability), the release rate of elements such as sulfur, strontium and heavy metals from calcium sulfate by-products and the capacity of hydroxyapatite proportion in the stabilization of released elements. Selected blends were studied using column test assimilated to PRB to evaluate the performance of blend to remediate wastewater containing lead and cadmium.

Chapter 1
Literature review

I.   Permeable Reactive Barrier

1.   Introduction

Permeable Reactive barrier (PRB) is a technique used for the remediation of soil and groundwater. Using this concept in large-scale facilities remains of major interest. PRB can be applied to the treatment of groundwater resources containing different toxic pollutants such as hexavalent chromium, dissolved components (SO_4, Fe, Ni, Co, Cd and Zn) and dissolved nutrients such as nitrate. It should be noted that the reactive material widely used in the world for reactive barrier is the zero-valent iron (ZVI) (near 120 applications within 83 are large scale [1]). Therefore, this reagent has great purification power resulting from the substances reduction of toxic metals by transforming them to inert or less dangerous substances. In recent years, reagents for groundwater remediation which have attracted attention for their adsorption capacity of species include activated carbon [2], apatite [3], fly ash and zeolites [4-5], the atomized slag [6] and limestone [7]. Precipitation, adsorption and immobilization process such as nucleation by inclusion and substitution reactions are considered to be the main physicochemical mechanisms promoting mitigation of the contamination level in the barrier. But the main issues that arise in PRB technology are the reactive media durability characterization and the hydraulic performances of the barrier.

2.   PRB Notions

2.1.   Definition

Permeable reactive barrier is an innovative and passive (without energy input) concept, based on the location of a reactive material perpendicular to the flow of groundwater in an aquifer. **Figure 1** shows a simplified schema of the groundwater purifying process using PRB technology. In terms of efficiency, the barrier allows the passage of a volume of water (proportionally to the hydraulic conductivity) resulting in the ability of the reactive material used to trap and intercept a plume of pollutants

by different immobilization agents limiting the leachability of the barrier. Treatment efficiency is a function of residence time and mechanical characteristics that facilitate preferential flow water through the barrier following a natural hydraulic gradient.
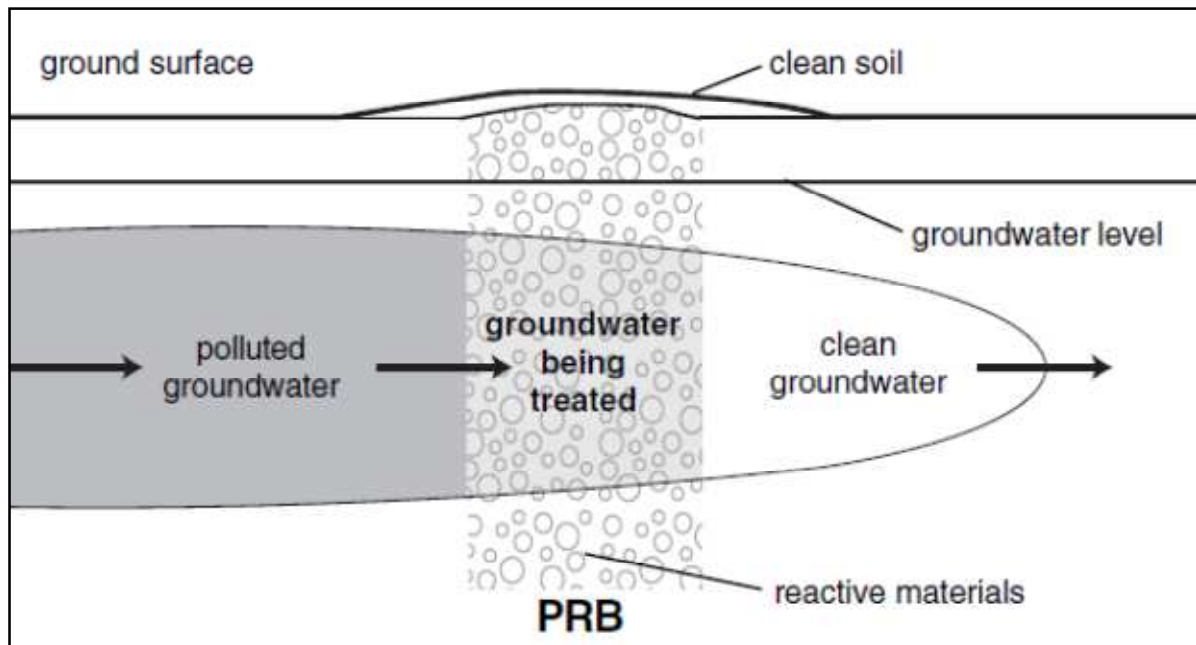
Figure 1: PRB general concept [8]

Furthermore, the reduced cost due to the semi-permanent installation, lack of external energy supply, monitoring and productive use of the site after installing are the principal advantages of PRB project. Obviously, the transformation of groundwater contaminants to acceptable and inert forms regarding the environment is the major purpose to reach by using an adequate reactive material. Traditional methods such as "pump-and-treat" technology and microbiological processes are not favorable for a number of chemical harmful contaminants [9] and operating costs of PRB is 50% lower than the costs of pump-and-treat method used so far [10].

Performance reduction of PRB depends primarily on common problems associated to the regression of the porosity of the reactive material followed by a clogging and blockage of the flow in the upstream of the barrier, resulting in the failure of potential reactive and hydraulic properties. System development of reactive barriers for heavy metals and radionuclides removal in groundwater requires a comprehensive understanding of elementary processes that control the interactions

between dissolved contaminants and reactive materials. Schneider et al. studied the feasibility test on landfill SRB using Fe0, apatite and alkali hydroxide (Ca(OH)$_2$ and Ba(OH)$_2$) to prevent the infiltration of contaminants in an acid medium, which attracted attention [11].

2.2. Models and conventional system

Currently, most widely used PRB systems for in-situ groundwater treatment are Continuous PRB and Funnel-and-Gate PRB. Indeed, each of these configurations is characterized by its own influence on the flow and a perfect hydrodynamic modeling of the barrier emplacement milieu may be required to help the selection of the appropriate system for the treatment of polluted plumes.

2.2.1. Continuous PRB

The first application of this type of barrier in France was in 1994 in NEUVILLE in Ferrain (A22 road site) to intercept plumes loaded by Chrome VI using ECOSOL granules as reactive media. The continuous barrier is a trenched system filled with a reactive material. **Figure 2** schematizes the concept of continuous barrier where the contaminated plume moves unimpeded through the reactive zone.
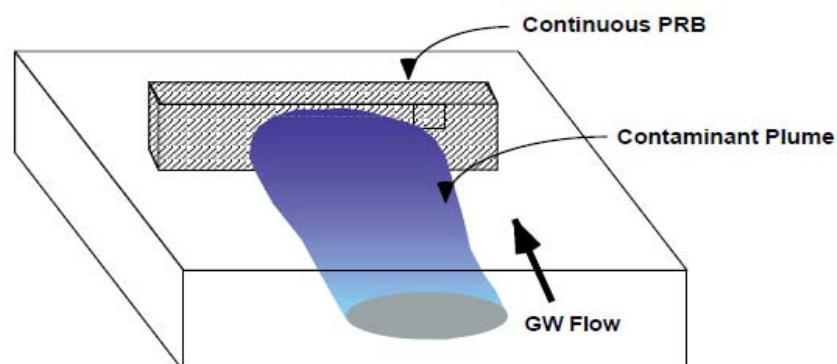
Figure 2 : Continuous PRB trenched system [12]

It plays a fundamental role on the minimization of hydraulic disturbances by mitigating the impact on the groundwater flow conditions through the barrier, according to a hydraulic gradient that generates a natural flow velocity. However,

adequate implementation of the barrier is sufficient to cover and pick up a comparable volume in the cross section of the plume. The continuity of the barrier should ensure an easy drainage of groundwater. The residence time depends on the groundwater velocity in the aquifer and natural slope. However, to avoid overflow problem of contaminated groundwater, it is preferable that the hydraulic conductivity of the aquifer be less than that of the installed barrier and the thickness or reactive volume should be overdesigned and sufficient to ensure an effective treatment.

2.2.2. Funnel and Gate system

The Funnel-and-Gate technology allows the interception of groundwater and the direction of plume flow to the reactive medium. This barrier consists of two impermeable screens (clay, rock, etc) embedded in the rock layer (substrate); forming a funnel that plays a major role in flow changing and direction of the plumes to the permeable reactive gate (i.e. Sheet piling funnels direct the plume through the reactive gate). **Figure 3** shows a prototype of Funnel-and-Gate system. In France, this type of treatment system was installed at AUBY in 1998 (COKERIE site) for the interception of Polycyclic Aromatic Hydrocarbons (PAHs) using activated carbon. The last PRB installation was at BREST (2002) to rehabilitate a hydrocarbon lagoon (Ballast lagoon) using activated carbon to prevent groundwater contamination by infiltration of heavy metals, phenol compounds and THC. The flow of groundwater with impermeable walls accelerates the flow of plume toward the reactive media. In addition, to minimize the restriction of water flow, the permeability of the reactive material must be equal or greater than the permeability of the aquifer. The large thickness of the reactive medium ensures complete purification of contaminated plume by the surface of contact and sufficient residence time.
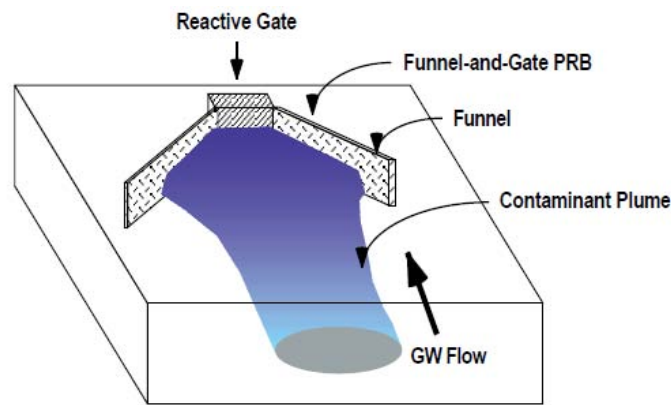
Figure 3 : Funnel and Gate configuration [12]

Residence time, thickness of the reactive media and hydrological modeling are very important parameters in the choice of implantation milieu, configuration and design of the barrier. Clogging and saturation of the reactive media by precipitation of pollutants reduce the hydraulic performance (decreased permeability) and chemical performance (limited reactivity), and replacement, restoration or reconstruction of the barrier can be applied to make efficiency treatment of that system. A new process for groundwater treatment is based on the collection of polluted groundwater (filters made of removable cartridges connected in series or in parallel) located at the permeable barrier. This process which is called Panel-Drain® (patented by Soletanche Bachy) has shown a great ability to decontaminate groundwater by the introduction of reactive materials in cartridges that target the retention of a specific pollutant. For comparison, the depth of the barrier is 15 to 20m, while the depth of the Panel-Drains is more than 50m [13].

2.3. PRB design

The design of the reactive barrier depends on the nature of pollutants, the levels of contaminant concentrations and residence time [14]. It is often initiated by using a quantitative directed exploration (QDE) approach for the prediction of conditions for the placement, location and evaluation of performance of PRB [15]. It seems important to highlight the different physicochemical parameters helping to design a barrier such as evaluation of the contact time of polluted water depending on the specific surface area of reactive material and the rate of contaminants degradation.

25

The hydraulic parameters affecting the performance of the permeable barrier such as variations in the concentrations of pollutants in the upstream, the hydraulic gradient, direction of flow and hydraulic conductivity must be taken into account in PRB conception [16]. The velocity of groundwater through the reactive cell must always be greater than in an aquifer, i.e. hydraulic conductivity of the cell must be very uniform to ensure distribution of flow into reactive media. Performance evaluation treatability seems an important step in the analysis and selection of the reactive medium. Treatability tests provide information on the estimated half-life of degradation reaction and the evaluation of the lifetime of the barrier.

The batch tests allow the choice of processing system. They rely on the contact of the reactive material with de-ionized water to analyze the compound concentrations as a function of time under defined conditions. However, these tests are used to detect the properties of heavy metals trapping by the reactive material; they can be faster and cheaper to carry out. Taking precautions in the extent of analysis for the interpretation and extrapolation of the results in terms of flow dynamics is needed to assess the reactive capacity. On the other hand, the evaluation of geochemical parameters is performed by the laboratory column tests.

Figure 4 illustrates the typical system of column test. Column test is used to choose the design of PRB system under dynamic flow conditions. Highlighting the change in contaminant concentrations and inorganic compounds is based on the distance traveled through the reactive cell. The determination of specific concentrations at different point in the column is made by extracting volume samples across the different sampling ports present on the length of the column. To ensure good flow distribution through the reactive media, the establishment of a loose layer of sand or gravel at the top and bottom of the column is acceptable. Interpretation of results is done by analyzing the major inorganic cations such as Ca, Mg, Na, Fe, Mn and K, the major anions such as Cl, SO_4, NO_3 and NO_2 and alkalinity (bicarbonate and hydroxide) influent and effluent.
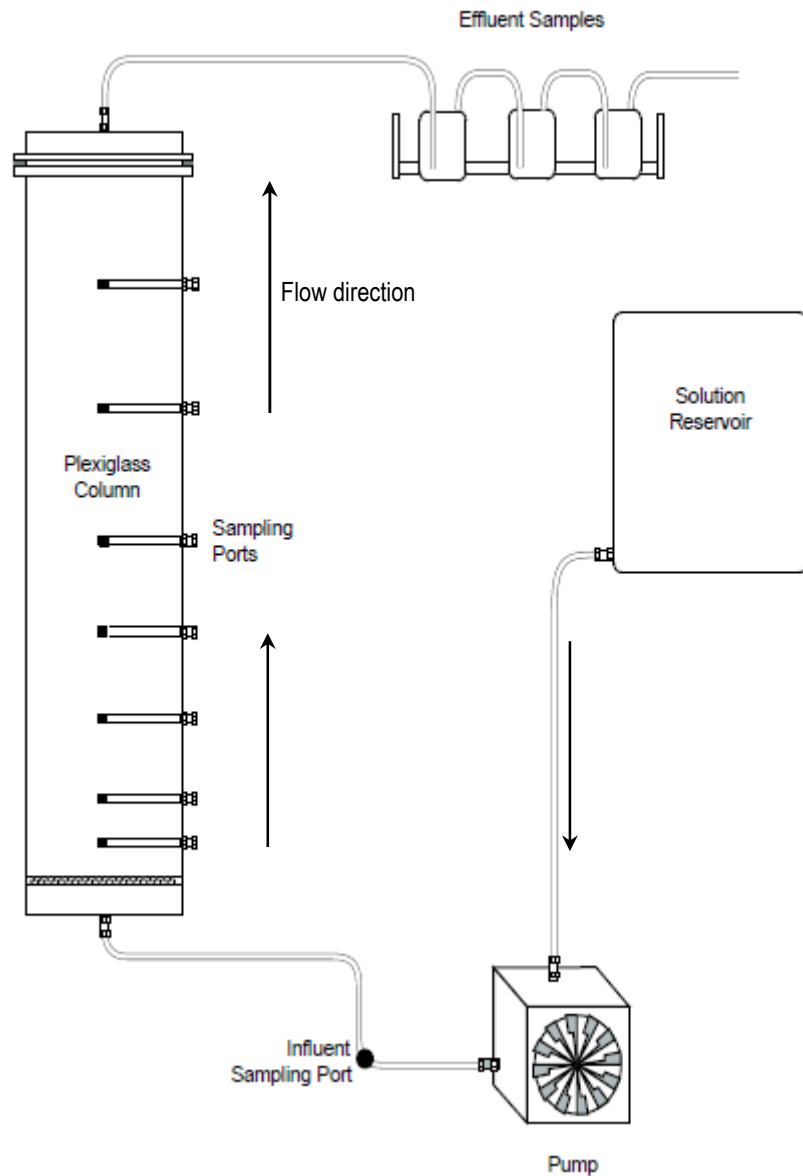
Figure 4 : Schematic of the column-test

The kinetic study of pollutants capture can be used for barrier designing and analyzes preliminary data of column test determines the degree of retention of reactive media versus residence time. The kinetic used for this assessment is first-order kinetic:

$$C_f = C_0 \, e^{-kt} \qquad \text{[Eq.1]}$$

With C_f is the final concentration (mg.l^{-1}), C_0 is the initial concentration of the pollutant in question (mg.l^{-1}), k is the degradation rate (rate of reaction, h^{-1}) and t is

the time (h). From this relationship, we can deduce the time required to reduce two fold the concentration of a pollutant to acceptable levels as follows:

$$t = \frac{\log\frac{C_0}{C}}{k}$$

[Eq.2]

The evaluation of the half-life represents the period required to reduce the average concentration of a contaminant can be estimated by the following equation [3]:

$$t_{1/2} = \frac{\ln(2)}{k} = \frac{0.693}{k}$$

[Eq.3]

The comparison between the half-lives allows the selection of the appropriate reactive material. The selection of reactive material must have a shortest half-life. The half-life can be estimated by batch or column tests. Determining the rate of reaction is based on the phenomenological Arrhenius law that takes into account two parameters independent of temperature, the activation energy E_A expressed in kJ.mol^{-1} (initiate chemical reaction) and A is the frequency factor whose unity is that of k (h^{-1}). The rate of reaction to an absolute temperature T (°C) is:

$$k = A.e^{\frac{E_A}{RT}}$$

[Eq.4]

It should be noted that the residence time increases at low temperatures and the rate of degradation can be written in a different way depending on the velocity and depth of the barrier. Indeed, the study by LUCEY (2006) [17] for the evaluation of dynamic properties of the permeable barrier proposes the use of the follow relationship to calculate the rate of reaction in PRB.

$$k = \frac{Q}{P} (C_0 - C_f)$$

[Eq.5]

Where k is the rate of reaction in mmol.l^{-1}.day^{-1}, Q is the flow in the barrier in m.d^{-1}, P is the depth (height) (m); C_f is the final concentration in mmol.l^{-1} and C_i is the initial concentration (mmol.l^{-1}). The width of the barrier can be defined as follows:

$$W_b = \frac{1.0\ m^2 ml^{-1}}{\rho_a} \frac{Log\frac{C_f}{C_e}}{3} W_{ref}$$

[Eq.6]

Where W_b is the width of the barrier in m; ρ_a is the surface concentration of the solution in m².l⁻¹; C_i is the concentration of the influent; C_f is the concentration of the effluent and W_{ref} is the reference width (it depends on the velocity of groundwater and studied pollutant). This relationship was developed for determining the width of a permeable reactive barrier based on ZVI [18]. The determination of the thickness of the barrier takes into account the determination of residence time and velocity of contaminated plume and groundwater. It is done either by column-test or by the hydrological modeling of the configuration. The length of the barrier depends on the depth of the aquifer and the expression of the thickness of the barrier that is as follows [19]:

$$E_b = V.\ t.\ SF \qquad\qquad\qquad\qquad\text{[Eq.7]}$$

Where E_b is the thickness of the barrier (m), V is the velocity through the reactive cell (m.d⁻¹); t is the residence time and SF is the safety factor depends on the seasonal variation in the flow, changes in concentrations, groundwater velocity and flow direction. SF is determined by modeling the barrier taking into account the parameters mentioned above.

2.4. Performance & monitoring

The performance of PRB depends on two major factors that can lead to the type and amount of pollution present in the groundwater, flow velocity and hydraulic properties of the barrier. Hydraulic flow conditions that require further characterization of water regimes and adequate modeling of the aquifer level for the interception and perfect treatment of plumes of contaminated groundwater are the major factors influencing the hydraulic properties of the barrier. Moreover, performance evaluation of PRB is realized by determining the hydrological parameters such as hydraulic conductivity and geochemical parameters such as redox potential, pH, dissolved oxygen, alkalinity and heavy metals content on both sides of the barrier. The numerical simulation interpretation of geochemical parameters in advance at the laboratory scale is a major step in facilitating the design

of the barrier and optimizing processing performance. Sometimes these parameters are identified by performing tests on the body core of the barrier obtained by coring. Furthermore, the chemical parameters can be measured by the technique of piezometers analyzing water samples in the upstream and downstream of the barrier.

The strategy for PRB monitoring includes evaluation of the potential of contaminants and harmful environmental by-products through reactive cell and potential effects on groundwater quality caused by the reactive media itself [16]. Indeed, studies in this direction show that biogeochemical conditions within the cell have a reactive role in determining the effectiveness of the barrier [20]. Nevertheless, the effectiveness of the barrier seems an important indication that changes over time, in other words, it is impossible to predict the durability and life cycle of reactive media without considering biogeochemical processes. Performance affectations of PRB by geochemical processes result in anaerobic corrosion (higher pH), the accumulation of carbonates (precipitation) and biological phenomena. These biogeochemical phenomena contribute explicitly to the progressive reduction of hydraulic conductivity, especially the growth of bacteria and the accumulation of gases (nitrogen and methane) in the pore volume of reactive material, which causes the decrease in available porosity and hydraulic performance and system deterioration by increasing the head loss. Obviously, the durability reduction of the barrier performances depends primarily on the mass flux of certain dissolved solids and secondly the recovery of reactive particles by dissolved precipitate solids. Moreover, technical analysis has often shown that the reduction in porosity is attributed to the precipitation of the hydroxides and carbonates at the surface of the reactive material in permeable barrier [21][22]. As a result, the life of a barrier depends on the reaction rates of reactive contaminants over time [23]. Hence, it seems important to regenerate and replace the exhausted reactive material, for the decontamination process to continue. The performance of the PRB is related to the different physicochemical events promoting the decrease in porosity, the change of flow direction and the preferential loss of hydraulic head control. The effects of geochemical parameters

and aquifer parameters on the reduction of barrier porosity are directly dependent on the type of reactive material used, influence of the concentration, velocity coefficients, uniformity and heterogeneity of aquifer and hydraulic conductivity of the barrier. However, the heterogeneity of the aquifer and the permeability of the barrier influence also the penetration of suspended solids and the formation of chemical compounds that precipitate later. Therefore, at a permeable barrier, reducing the pore volume caused by the precipitation of secondary minerals is generally estimated by the volume of these minerals based on stoichiometric calculations to assess the change in the concentrations on both side of the barrier [21]. It should be noted that the main objective of a monitoring program and performance monitoring of PRB is to ensure that the plumes are collected correctly and treated so that contaminant concentrations downstream were below the thresholds of toxicity.

2.5.   Advantages and disadvantages

Table 1 summarizes the main advantages and disadvantages of permeable reactive barriers already worldwide installed. The main advantage of PRB relative to other conventional methods of treatment is to reduce operating costs and maintenance [24]. In addition, the major drawback of the PRB is the difficulty to estimate and determine the lifetime of the reactive material.

Table 1 : Advantage and disadvantage of PRB

Advantages	Drawbacks
In-situ and passive treatment, limited maintenance after installation;	Limited to shallow plumes about 15m below the subsurface;
No surface structure;	Plume must be defined and well characterized despite the limited data on life cycle of the barrier;
Contaminants treated in subsurface, Minimizing exposure to heavy metals ;	Hydraulic heterogeneity around the barrier creates insecurity in passive treatment;
Potentially cheaper than pump-and-treat system;	Pore clogging and fouling of reactive media; (Loss of permeability and hydraulic performances);
Natural slope allows the flow of plume ;	
No influence on groundwater regime flow;	Need to replace the reagent after the exhaustion

	of retain pollutants ability;
Operating costs offset the construction cost , i.e. acquisition costs and monitoring operations are low;	Contaminated groundwater is treated, while the contaminated soil is not treated;
Applicability in urban areas;	Need to know the different hydrological information in the aquifer;

3.   Reactive materials versus contaminants

The diversity of pollution of groundwater sources complicates the choice of suitable reactive media. In this second part we will talk at first, the main sources of pollution of natural environments that affect groundwater seepage through the soil. In a second step, we will discuss the different selection criteria and selection of the reactive media based on the descriptive parameters indicating the reactive capacity, the hydraulic performance and durability.

3.1.   Groundwater pollution

3.1.1. Contaminant sources

Pollution of groundwater by the different sources of pollutants is related to two categories identified as point sources and diffuse sources. Point sources are located in municipal landfills, sites of industrial waste disposal and environmental accidents or leaks in harmful products storage tanks, such as gas and oil derivatives. While diffuse sources target a large volume of groundwater through the use of fertilizers on the fields of agriculture and green spaces. In Europe, as the consequence of vast area of agriculture plains, distribution of pollution caused by a source distribution appears to be the first factor of groundwater contamination by dissolved nutrients such as nitrates and perchlorates [25]. Sources of perchlorate contamination in water are ammonium perchlorates recently identified by the Environmental Protection Agency (EPA). However, contamination of groundwater is caused by the infiltration of urban wastewater (domestic and/or industrial) loaded with heavy metals (Al, Fe, Mn, Co and Mo), and pollution by Pb, Zn, Cd , Cr and Ba can be attributed to uncontrolled dumping of industrial wastes [24].

3.1.2. Common polluants

In the literature, several authors have investigated contaminant capture and purification of groundwater by the in-situ PRB process, or by testing at the laboratory scale. Among the contaminants commonly found in groundwater and where the treatment was designed by PRB, uranium [26], chromium [27], arsenic [28], Selenium [29], fluoride [7], cadmium [30], heavy metals such as Pb, Cd and Zn [31][3], Volatile Organic Compounds (VOCs), Chlorinated Aliphatic Hydrocarbons (CAH) [32] and Polycyclic Aromatic Hydrocarbons (PAHs) [33] like MTBE (Methyl Tertio-Butyl Ether) and monocyclic (HAM) like BTEX (Benzene, Toluene, Ethyl and Xylene). Human activities, mining and nuclear military operations contribute in a direct contamination of groundwater resources at very harmful magnitudes and dangerous radioactivity, especially uranium, strontium and their derivatives [34][35]. Groundwater can be contaminated by chromium in both forms Cr (VI) or Cr (III). Cr (VI) is the most soluble, mobile and toxic (mutagenic and carcinogenic effects). However, the Chrome in its trivalent state is much less soluble and almost immobile, and the elimination of this pollutant can be done by implementing a PRB-ZVI based [36].

As known, arsenic ion is present in two oxidation states, As (III) and As (V), and its elimination at the level of groundwater may be applied by the installation of a PRB-ZVI [37] cited by [27]. Moreover, studies by BEAK et al. (2009) [28] show that the oxidation of As (III) to As (V) causes corrosion of the reactive iron grains reducing the degree of retention. Due to health effect of Arsenic presence in groundwater, the USEPA lowered the admissible ecotoxicity threshold to $0.01ml.l^{-1}$ in 2006.

Chlorinated hydrocarbons such as trichloroethene (TCE), perchloroethylene (PCE) and 1,2 dichloroethylene (1,2-DCE) [20] are especially commercial solvents [8] and PAHs that can be eliminated by the bio-barrier based on the aerobic degradation and the first installation of PRB-ZVI to intercept plumes of VOC was conducted in 1996 in Colorado (United States) [38]. Studies by Skinner et al. (2006) have shown that the use of PRB consisting of anionic limestone drain and a bed of limestone supports the

reduction of sulfates and nitrates by denitrification mechanisms and bacterial processes such as the use of sulfur-reducing bacteria [39]. The experiments conducted by Guerin et al. (2002) and his colleagues on the interception of oil compounds using the system Funnel-and-Gate was based on the use of peat. It has been shown that biomass can ensure effective treatment of water contaminated with BTEX [40].

3.2.   Selection criteria of the reactive medium

The choice of suitable reactive material is based on the chemical description and extent of pollutants in the environment. **Table 2** classifies different reactive materials based on their reaction mechanisms to trap pollutants. The importance of the chemical composition and the degree of harmfulness prove to be quite important parameters to consider when selecting reactive media. The compatibility of the reactive media with the environment is paramount. Furthermore, the chemical description should highlight the repercussions of reactive materials such as undesirable chemical reactions and by-products generated by the different interaction between reactive material and pollutants. The criteria in the selection of reactive material are:

♣ Reagent showing no source of contamination of soil and groundwater;
♣ Reagent with a large capacity and efficiency;
♣ Stable Reagent, less soluble and available at low and reasonable costs;
♣ Reagent promoting hydraulic performances (porosity and permeability);

Table 2: Classification of reactive materials according to the mechanisms of interaction [41]

Mechanisms	Reactive matters
Adsorption or substitution (Inorganic compounds)	Activated carbon, Activated alumina, bauxite, Exchange resin, Ferric oxide and hydroxide, magnetite, Phosphate, Zeolite.
Precipitation (Inorganic compounds)	Zero Valent Metal (ZVM), Limestone, Ferrous hydroxide, Ferrous carbonates, Ferrous sulfide, Lime, Fly ash, Biota, [$Mg(OH)_2$, $MgCO_3$, $CaCl_2$, $CaSO_4$, $BaCl_2$],
Degradation (Inorganic compounds)	Biota, ZVM
Adsorption (Organic compounds)	Zeolite, Activated carbon, Clay…

Degradation (Organic compounds)	Ferrous minerals, ultra-micro-bacteria, ZVM, Aerobic environment

Generally, the reactive media must meet the selection criteria mentioned above and enhance any of the decontamination processes yield. Main decontamination process adsorption, absorption, cation exchange (Activated Carbon, Zeolite, ...), precipitation and degradation. Precipitation process transforms the pollutants into insoluble solids deposited on the surface of the reactive particles and degradation of organic compounds process may be chemical or biological (aerobic or anaerobic).

3.3. Reactive matters widely used

The reactive material commonly used for groundwater treatment in installed reactive barriers has shown a great capacity to retain pollutants. However, it seems interesting to quote briefly the main in-situ used reactive materials, their impacts on groundwater in terms of treatment and efficiency as well as different advantages and inconveniencies.

Globally, most PRB use ZVI material with regard of its efficiency treatment of polluted plumes. Furthermore, the purification of shallow water depends on two processes, reduction and degradation by the precipitation of inorganic compounds. However, ZVI immobilizes perfectly heavy metals such as Cr, Se, Pb, U, Co, Ca, Zn, Cu and Hg, anionic contaminants such as sulfate, nitrate, phosphate and the arsenic and organic compounds [9][20][27]. ZVI can be combined with other reagent such as red mud and fly ash in the treatment of acidic groundwater [42]. The major drawback that must be considered is the high cost of ZVI that can reach $\approx$400€.tonne^{-1}. Granular activated carbon is often used in PRB [2]. It is characterized by a relatively high adsorption capacity for organic and inorganic compounds due to its large specific surface area of about 1000m².g^{-1}. It should be noted that activated carbon can be combined with biological treatment. Despite its effectiveness in polluted water treatment, its cost is relatively high ($\approx$1300€.tonne^{-1}) that minimizes its utilization chances in PRB. Calcite (CaCO$_3$) used in PRB for pollutant elimination

such as fluoride present in groundwater [7] and reduction of acidity (generated by oxidation of sulfated residues and inorganic contaminants [43][44]) has demonstrated a high retention capacity. The peat (humic material) for the implementation of reactive window "Funnel-and-Gate" barrier was beneficial to the retention of petroleum hydrocarbons like HAM, BTEX dissolved phases and alkanes [40]. The addition of organic products such as pecan shells as sources of micronutrients and protein to promote biological treatment by the construction of a multi-barrier can be used to intercept pollutants in groundwater.

4.   Conclusion

The PRB is currently considered as the most widely used passive technique for the treatment of polluted groundwater. The choice of the reactive media and the description of its performance to retain pollutants is an essential step for the design of a PRB. The ability, efficiency and longevity of the reactive material are essential parameters to master for the decontamination process to continue, and the exhaustion of the reactive power purification media which generates lower hydraulic performance requires rejuvenation and regeneration.

Calcium phosphates have shown a great aptitude for the treatment of effluents and waste stabilization. This material will be considered in this study.

II.   **Calcium phosphate (Apatite)**

1.   Introduction

Calcium phosphates are products widely used in many fields such as medicine, agriculture and food industries, and can also be used to trap and immobilize heavy metals and other pollutants. The first identification of the structure of calcium phosphates (apatite structure) as the minerals of human origin was revealed in 1926, based on XRD analysis. Indeed, calcium phosphates are extremely stable and have a significant useful life between 1000 to 100.000 years in different geological conditions. Moreover, specifically the apatite group is often composed of three forms,

hydroxyapatite, fluorapatite and chloroapatite, who are able to add half of the periodic table of elements in their atomic structures (i.e. trapping more than 99% of uranium [45], and immobilization of about 60 to 99.9%, 20-98% and 29-98% Pb, Cd, and Zn, with a retention capacity of 73 and $41mg.g^{-1}$, respectively [46]). Hence their interest and suitability for use in decontamination processes and wastewater treatment or contaminated groundwater. In addition, apatites can be used in permeable reactive barriers or mixed with soil or contaminated waste, and is intended also for heavy metals stabilization.

The first application in a permeable reactive barrier (PRB) by introducing the Apatite II [$Ca_{10-x}Na(PO_4)_{6-x}(CO_3)_x(OH)_2$, where x < 1] (Apatite II^{TM}(commercial apatite) about 100 tons) as reactive material was carried out in 2001 in Idaho [47][48]. Interest in the use of apatite in the PRB is due to its ability to admit a large number of ions in the crystal structure, chemical stability and low solubility in water ($K_{sp}<10^{-20}$) depending on environmental conditions ($K_{sp}<10^{-48}$, under alkaline conditions) [49][50]. Hydroxyapatite synthesis can be done by several methods based on the addition of a chemical compound containing calcium and other compounds containing adequate amounts of phosphate.

2. Calcium phosphate

Apatite compounds are commonly identified under the stoichiometric system $M_{10}(XO_4)_6Y_2$, which has the general formula of apatites, where M is a divalent cation such as Ca^{2+}, Cd^{2+} and Pb^{2+}, XO_4 is a trivalent anionic group (PO_4^{3-}, MnO_4^{3-} and AsO_4^{3-}) and Y is a monovalent anion (OH^-, F^- and Cl^-). Moreover, they show a great fixation capacity of contaminants under different immobilization modes. **Table 3** shows the molar rate Ca/P for different groups of calcium phosphate and their structures. In this regard, the stoichiometric ratio Ca/P of 1.67 reveals the crystalline apatite structure from the chemical formula of calcium phosphates, the crystal structure of non-stoichiometric (non-apatitic) calcium phosphate complex is assigned to the Ca/P <1.67 for more soluble phosphate minerals.

In addition, the purity of hydroxyapatite depends on the ratio Ca/P. It must be greater than or equal to 1.67 and is a key indicator for predicting crystal properties (ie, uniform distribution of atoms in the crystal lattice) and characteristics of insolubility. **Figures 5** and **6** refer to different forms of calcium phosphate and the change in Ca / P ratio as a function of time, temperature and solubility [51][52] during their synthesis or formation.

Table 3: Apatitic and non-apatitic calcium phosphates

Abbreviation	Calcium phosphate	Chemical formula	Structure	Ca/P
MCP	Monocalcium phosphate hydrate	$Ca(H_2PO_4)_2, H_2O$	non-apatitic	0.50
MCPA	Monocalcium phosphate anhydrous	$Ca(H_2PO_4)_2$	non-apatitic	0.50
DCP	Dibasic calcium phosphate	$Ca(HPO_4)$	non-apatitic	1.00
DCPD	Dicalcium phosphate hydrate	$Ca(HPO_4), 2H_2O$	non-apatitic	1.00
DCPA	Phosphate dicalcique anhydre	$CaHPO_4$	non-apatitic	1.00
γ-CPP	γ-Calcium pyrophosphate	$Ca_2P_2O_7$	non-apatitic	1.00
CPPD	Calcium pyrophosphate dihydrate	$C\,a_2P_2O_7, 2H_2O$	non-apatitic	1.00
OCP	Octacalcium phosphate	$Ca_3H_2(PO_4)_6, 5H_2O$	non-apatitic	1.33
α-β-TCP	Tricalcium phosphate	$Ca_3(PO_4)_2$	non-apatitic	1.50
ATCP	Apatitic tricalcium phosphate	$Ca_9(HPO_4)(PO_4)_5(OH)$	Apatitic	1.50
ACP	Amorphous tricalcium phosphate	$Ca_9(PO_4)_6, nH_2O$	non-apatitic	1.50
CDA[1]	Calcium-deficient apatite	$Ca_{10-x_\square x}(HPO_4)_x(PO_4)_{6-x}(OH)_{2-x_\square x}$	Apatitic	1.58
Ca-HA	Hydroxyapatite	$Ca_{10}(PO_4)_6(OH)_2$	Apatitic	1.67
Ca-HA$_T$	Tribasic calcium phosphate	$Ca_5(PO_4)_3(OH)$	Apatitic	1.67
TCPM	Tetracalcium phosphate monoxide	$Ca_4(PO_4)_2O$	Apatitic	2.00

[1] Chemical formula: □ lacuna and $0 < x < 2$

Different calcium phosphate phases such as OCP, CPPD and γ-CPP do not exist as geological mineral [53], and can be synthesized from carbonates and phosphates, by different methods detailed thereafter. The DCPD is present at low pH and the compound TCPM does not form in aqueous solution and, it transforms to Ca-HA by simple hydrolysis. Of course, hydroxypatite and phosphocalcic hydroxylapatite are the most stable phases in the calcium phosphate family. Their crystal structures allow the ionic substitution with heavy metals and radionuclides, and subsequently promote the different mechanisms of stabilization and trapping.
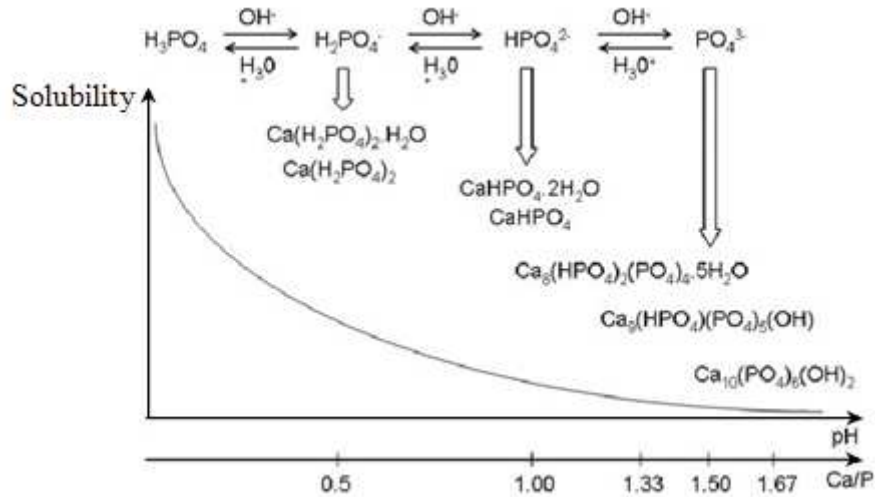
Figure 5: Calcium orthophosphate obtained by neutralization of phosphoric acid [51]
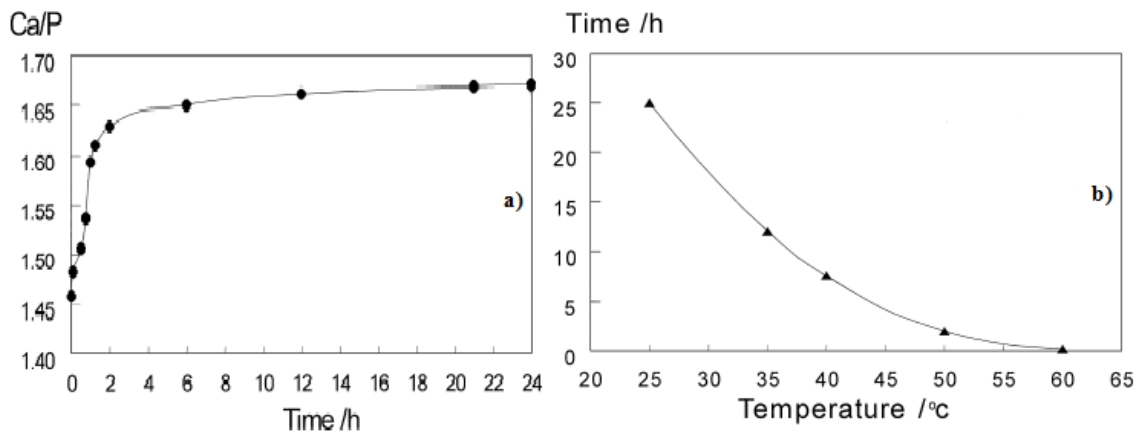
Figure 6: a) Variation of the ratio Ca/P as a function of reaction time at 35°C, *b)* Formation time of pure Ca-HA as a function of temperature according to *Lui et al (2001)* [52]

Formation of stable Ca-HA obeys to two main factors: time and temperature. From the first seconds of the synthesis reaction, the formation of MCP (more acidic and soluble compound) is obviously pronounced following the synthesis procedure (i.e. synthesis by neutralizing orthophosphoric acid described later), it crystallizes in the triclinic structure and turns into MCPA at a temperature of about 80°C under acidic pH conditions. DCPD precipitation occurs at room temperature in an acidic pH (4<pH<5.5) aqueous solution, and it crystallizes in the monoclinic structure. At temperatures above 80°C, it becomes DCPA triclinic structure, which plays a fundamental role in the synthesis of the intermediate phase, called calcium-deficient apatite (CDA).

OCP-like intermediate form during the precipitation of CDA is often characterized by an atomic arrangement similar to that of hydroxyapatite. It is an unstable compound with a Ca/P=1.33. Therefore, heat treatment allows the rapid decomposition of CDA to β-TCP with a ratio Ca/P=1.58, which in turn quickly transforms into ACP in water (amorphous tricalcium phosphate) with a Ca/P=1.50. The ACD is a transition phase arising during the precipitation of calcium phosphates in aqueous solution; it is characterized by a smaller surface area comparing it with that of OCP and hydroxyapatite crystal characterized by a more stable arrangement.

The next step of the reaction results in the transformation of ACP in calcium-deficient hydroxyapatite ($Ca_{10-z}(HPO4)_6(PO_4)_{6-z}(OH)_{2-z}, nH_2O$ where $0 \leq z \leq 1$) in the presence of inhibitors such as carbonates and pyrophosphates. It is characterized by a poor crystalline structure, submicron size and specific surface area of about 25-100$m^2.g^{-1}$. The compound β-TCP (it does not precipitate in an aqueous solution) obtained by calcination of the CDA, can be transformed into α-TCP at a temperature above 1125°C, while the product α-TCP precipitates rapidly in an aqueous solution under calcium-deficient hydroxyapatite form. From 22h of reaction time at room temperature, precipitation and stabilization of DCP led to the formation of a stable Ca-HA stochiometrically equilibrated with a molar ratio Ca/P of 1.67. To conclude, we can say that when the reaction time reaches values above 24h or the temperature reaches over 600°C, the ratio Ca/P stabilizes (**Figure 6**). The temperature increase during the reaction could shorten the time of the formation of a pure Ca-HA. This is explained by the change in grain size which increases with temperature. To summarize, the process of precipitation at pH 10 to 11 of hydroxyapatite is as follows, OCP $\xrightarrow{rapidly}$ ACP→ Ca-HA [52].

The synthesized Ca-HA may be used for decontamination processes. Furthermore, the performance of apatite to stabilize and immobilize the metal ions were assessed by analysis taking into account the influence of pH, hardness, alkalinity and salinity of the interstitial solution. This has been widely reported in the literature. Indeed, several applications have been proposed to integrate the calcium phosphates in the

decontamination methods. In addition, the apatites can be used in the treatment of soil and/or groundwater. **Figure 7** illustrates the different methods of application as a reagent using the calcium phosphate.
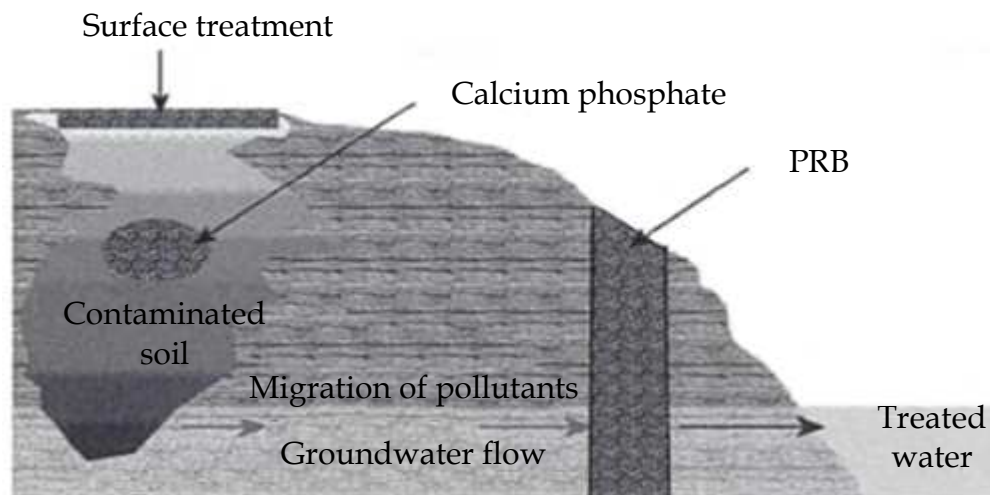
Figure 7: Contaminated soil treatment methods using calcium phosphate [50]

These methods result in the implementation of calcium phosphates in the soil surface to prevent infiltration of contaminants through the soil, direct injection by mixing them with soil and/or the formation of a PRB [50]. Moreover, the implementation can be done by injecting a solution containing sodium citrate, calcium chloride, calcium phosphate, ammonium nitrate and sodium fluoride in controlled conditions: pH (basic of about 8), concentration (the reaction between calcium and phosphate at a concentration below 10 mM), temperature and soil physicochemical properties. The analysis of the precipitate after separation of soil particles by using X-ray diffractometry (XRD) shows that it corresponds to hydroxyapatite [54]. For example, the injection of a solution of calcium citrate and a solution of sodium phosphate in soil gives the formation of apatite particles that form a thin layer on soil particles to react as an adsorbent for heavy metals [55]. Advantages promoting the use of calcium phosphates in the treatment of polluted areas are their availability in the environment and/or their ease of preparation, low cost ($\approx$350€.ton^{-1}), their high chemical stability and resistance to degradation in different geological conditions.

3. Properties and characteristics of apatite

3.1. Some chemical characteristics

Calcium phosphate particles characterization can be achieved by various techniques allowing the description of crystalline phases and the evaluation of thermochemical stability. Methods widely used for this description, X-Ray Diffraction (XRD), scanning electron microscopy (SEM) and Fourier transform infrared analysis (FTIR), have been widely discussed. In this regard, many authors have chosen ionic characterization that includes the identification of the atomic ratio Ca/P and determination of mineral phases and micro and poly-crystalline structure and determination of the amount and chemical nature of apatites.

3.1.1. FTIR Spectrum

Determination of the ionic functional group in the hydroxyapatite can be established by infrared spectroscopy.
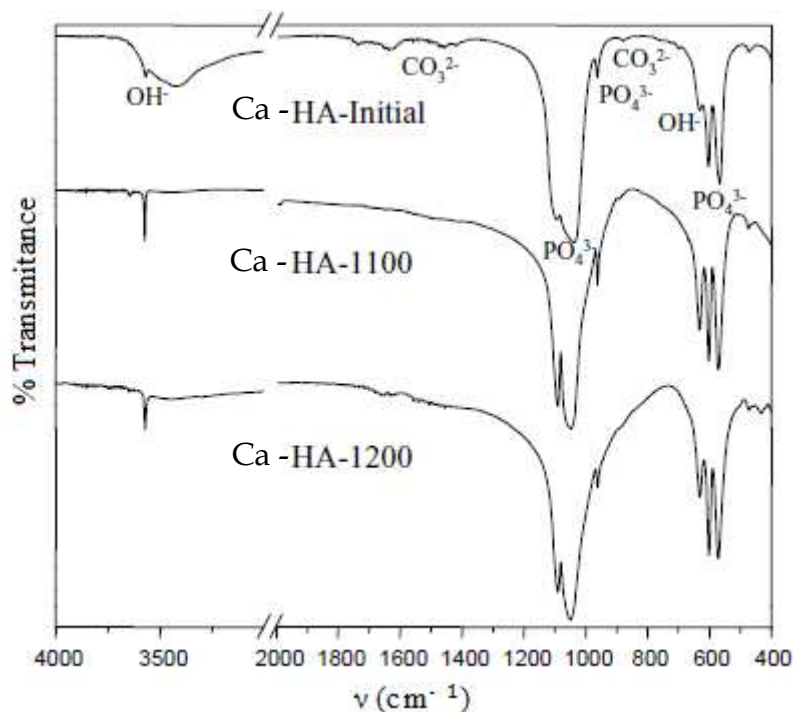
Figure 8: IR spectrum of hydroxyapatite calcined at different temperatures according to PADILLA et al (2005) [56]

Bands corresponding to the absorption frequencies of synthetic hydroxyapatite particles made by precipitation method are shown in **Figure 8**. OH⁻ bands indicate the existence of vibrational modes of libration v_L or symmetric valence v_s, stretching bands PO_4^{3-} group appear as stretching and/or deformation (symmetric or antisymmetric) and CO_3 group vibrations indicate the substitution of phosphate ions. The characteristic bands of calcium phosphates are listed in **Table 4**. Hydroxyapatite calcinations (1100 and 1200°C) induce high crystallization degree. The IR observations showe the absence of CO_3^{2-} ions which decompose as carbon dioxide CO_2. High crystallinity leads to sharper band resolution.

Table 4: IR bands corresponding to vibration modes and ionic arrangements

IR Band (cm⁻¹)	Vibration energy	Intensity	Assignment
3569	v_s	Shoulder	Symmetric stretching vibration of OH⁻ ions
631	v_L	Shoulder	Libration movement of OH⁻ ions
1092	v_3	Strong	Antisymmetric stretching of PO_4^{3-} ions
1040	v_3	Strong	Antisymmetric stretching of PO_4^{3-} ions
962	v_1	Medium	Symmetric stretching of PO_4^{3-} ions
603	v_4	Strong	Antisymmetric deformation of PO_4^{3-} ions
567	v_4	Strong	Antisymmetric deformation of PO_4^{3-} ions
1472	v_3	Low	CO_3 group (occupying PO_4 sites)
1417	v_3	Low	CO_3 group (occupying PO_4 sites)

3.2. Mineralogical properties

From the XRD analysis of hydroxyapatite investigated by different authors under different conditions [56][57][58], we can see that it consists of a crystalline phase composed mainly of Ca-HA, α-TCP and TCPM following the degree of calcination (i.e. calcination at temperature above 900°C). Britel (2007) work show that the XRD of precipitated apatite at room temperature followed by drying at 80°C reveals poorly crystalline apatite structure, while stoichiometric apatite calcined at 900°C for 2h remains in an apatitic structure without any additional phase such as tricalcium phosphate TCP or α β [59]. **Figure 9** shows the diffractogram of the hydroxyapatite product obtained by the introduction of reactive phosphate (MCP purity 92% β-TCP obtained from apatite after calcination at 900°C for 3 h, and TCPM) in a hydrothermal reactor (heated in an oven at 200°C for 48 h) with 100 ml of deionized water. The cooling of the reactor was carried out blowing air at room temperature, and the final product obtained was dried in an oven at 50°C. Adding water to the

mixture of calcium phosphates leads to the formation of Ca-HA according to the reaction [R.1] [60]:

$$x.Ca(H_2PO_4)_2, H_2O + (3 - 2x)Ca_3(PO_4)_2 + (1 + 2x)Ca_4(PO_4)_2O \xrightarrow{H_2O} Ca_{10}(PO_4)_6(OH)_2 \qquad [R. 1]$$
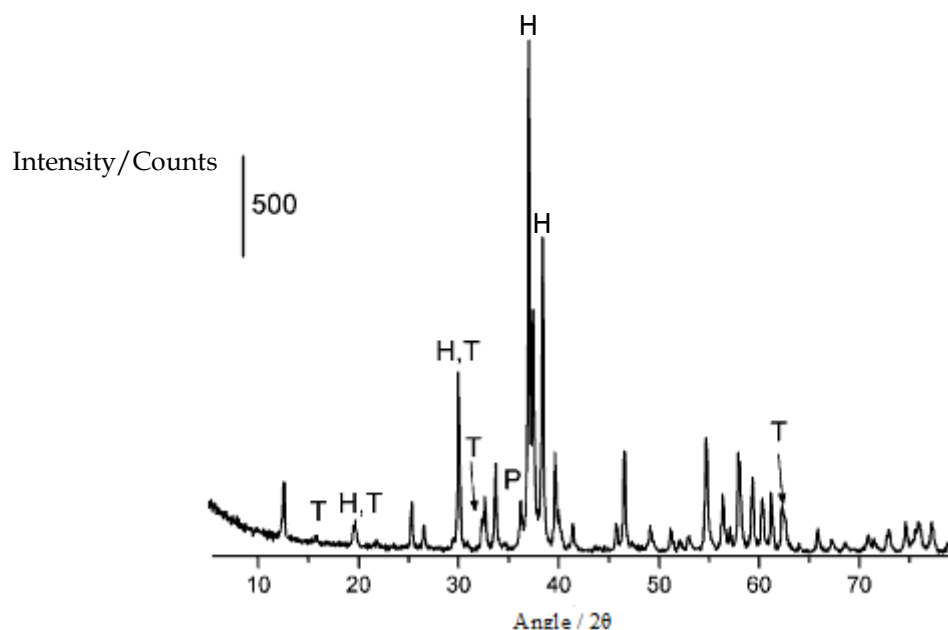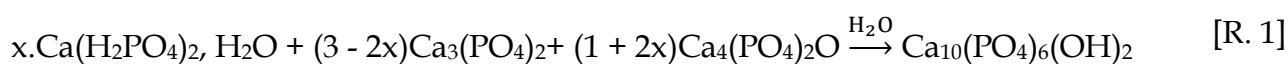
Figure 9: Diffraction pattern of hydroxyapatite after heat treatment [60]
H is the tribasic calcium phosphate (Ca-HA), Ca_5(PO_4)_3(OH), T corresponds to tricalcium phosphate (a-TCP), Ca_3(PO_4)_2 and P is the tetracalcium phosphate (TCPM), Ca_4(PO_4)_2O.

3.3. Apatite dissolution

The dissolution of apatite is controlled by transport of ions until the equilibrium between the substance and the solution is reached. It is considered among the factors predisposing pollutant removal during contact of an apatite particle with an aqueous solution.

Table 5: Solubility of some apatite-metals

Metal	Solid	Chemical form	K_{sp}	Reference
Ca	Hydroxyapatite	$Ca_{10}(PO_4)_6(OH)_2$	10^{-120} (30°C)	[61]
	Fluorapatite	$Ca_{10}(PO_4)_6(F)_2$	10^{-120} (25°C)	[51]
Pb	Pyromorphite	$Pb_5(PO_4)_3(OH)$	$10^{-76.5}$	[62]
	Hydroxypyromorphite	$Pb_{10}(PO_4)_6(OH)_2$	$10^{-62.8}$	[63]
	Fluoropyromorphite	$Pb_{10}(PO_4)_6(F)_2$	$10^{-71.6}$ (25°C)	[64]
	Chloropyromorphite	$Pb_{10}(PO_4)_6(Cl)_2$	$10^{-84.4}$ (25°C)	[65]
U	Autunite	$Ca(UO_2)_2(PO_4)_6.10H_2O$	10^{-49}	[64]
Sr	Strontium-apatite	$Ca_6Sr_4(PO_4)_6(OH)_2$	$10^{-118.4}$	[66]
Cd	Cadmium-apatite	$Cd_{10}(PO_4)_6(OH)_2$	$10^{-42.49}$	[63]

Table 5 gathers the values of solubility product of metal-apatites at room temperature, measured by different authors in the literature. Stoichiometric failure of precipitated calcium phosphate product contributes in crystal structure changing and thus leads to solubility apparently more important than the well crystallized substance in thermodynamic conditions. Of course, hydroxyapatite is the most stable phase under physiological conditions defined beforehand. Undoubtedly, the specific surface area of apatite is always related to the dissolution. This solubility product depends on temperature and ionic strength. Furthermore, Ca-HA shows incongruent solubility.

4.   Mechanisms of pollutant retention

The pollutant elimination in aqueous media by the use of calcium phosphates as reactive material proceeds through different physicochemical mechanisms as adsorption, chemical precipitation, ion exchange and substitution. Treatment of waste or contaminated water can be made by putting it in contact with a reactive material capable of maintaining the characteristics of pollutants trapping. Apatite pollutants capture capacity has been largely studied in literature. Main studied cases are the stabilization of heavy metals such as Pb, Cd, Zn, Cu and U through the creation of chemical bonds with phosphate and other minerals with low solubility. However, exchange between the apatite particles and the aqueous solution takes place at the contact interfaces. The reactivity of hydroxyapatite requires the presence of significant amounts of carbonates (carbonate apatite) to improve trapping by substitution and it depends on aptitude purity and crystallinity (nucleation sites). The main purpose of this section is to highlight the different mechanisms associated with apatite to immobilize heavy metals and metalloids. The retention capacity of hydroxyapatite to may be evaluated by different models.

4.1.   Adsorption capacity

The Ca-HA adsorbent surface capacity allows the fixation of pollutants by simple interaction either electrostatic or chemical reaction. It can be manifested by two kinds

of adsorption, physisorption (physical adsorption) attributed to Van-Der-Waals forces, it's a non-specific adsorption, and/or chemisorption (chemical adsorption surface) established by the chemical bonds between the particle and the pollutant, it's a adsorption. Therefore, apatite can adsorb up to 5% of its mass by the mechanism of chemisorption [47]. However, the adsorption depends on the concentration of heavy metals in the solution, surface properties, particle size, degree of crystallinity and ions competing. It also depends on the intrinsic characteristics of the material and its equilibrium in the solution. The chimisorption includes surface complexation and ion exchange. Surface complexation takes place by the attraction of metal cation according to their hydrated radius by attractive forces through the development of electrostatic bonds. In this case, the specific adsorption is the establishment of a chemical bond between the donor electron atoms of the surface ions and acceptor electron atoms. Indeed, adsorption of pollutants by the electrostatic forces is not perfect, by comparing it with the specific adsorption, which forms a compound relatively stable and non-exchangeable. Apatite is an excellent material for non-specific adsorption of cationic metal ions and the amount adsorbed at the surface per unit mass is calculated by the following relationship [66]:

$$q = (C_0 - C_e) \frac{V}{M} \qquad \text{[Eq. 1]}$$

Where C_0 is the concentration of the metal ion in the initial solution (mmol.l^{-1}), C_e is the concentration of the metal ion at the equilibrium, V is the volume of the solution and M is the amount of introduced Ca-HA (g). The model of Langmuir adsorption isotherm is based on the following assumptions: the existence of a finite number of adsorption sites, all sites are equivalent and no interaction between adsorbed ions. This model is as follows:

$$\frac{C_e}{q_e} = \frac{C_e}{q_m} + \frac{1}{bq_m} \qquad \text{[Eq. 2]}$$

Where, C_e is the concentration of the metal at equilibrium (mmol.l^{-1}), q_e is the amount of sorbed metal per unit mass of Ca-HA (mmol.g^{-1}), q_m is the maximum capacity of Langmuir adsorption (mmol.g^{-1}) and b is the constant related to adsorption kinetics linked to energy of the adsorbate to the adsorbent. Several studies have shown the

ability of apatite to trap effectively heavy metals by adsorption [48][66][68]. The capacity of heavy metals retention can be evaluated by Freundlich-Langmuir model, it is a generalized nonlinear empirical equation described as follows:

$$R_{lf} = Q_0 \cdot \frac{K_{FL} C_e^{\frac{1}{n_{FL}}}}{1 + K_{FL} C_e^{\frac{1}{n_{FL}}}} \qquad\qquad \text{[Eq. 3]}$$

Where Q_0 is metal concentration on Ca-HA surface in equilibrium with the initial solution concentration (mg Metal.kg^{-1} Ca-HA), K_{FL} is the adsorption parameter corresponds to the kinetic reaction (mg Metal.kg^{-1} Ca-HA), C_e is the equilibrium concentration of metal (mg.l^{-1}) and n_{FL} is the Freundlich-Langmuir constant.

4.2. Dissolution/Precipitation

Chemical precipitation occurs at saturation of solubility. it is the process by which a soluble substance turns into an insoluble/low soluble form by a reaction with the precipitating agent which can be hydroxide, sulfide, phosphate and carbonate under the conditions of pH, concentration and temperature. It is very beneficial to note that the precipitation of hydroxides occurs when the pH is basic to an optimum level for a specific metal.

Solubility of hydroxides such as hydroxides of Pb, Cd and Ni is minimal when the pH varies between 7 and 9. Indeed, the increase in salinity and pH influence on the sorption of Cd, Co, and Zn by hydroxyapatite [69]. The presence of $H_2PO_4^-$ ions promotes the increase in pH, which alters the balance between the carbonates and bicarbonates and leads to the precipitation of various carbonates materials according to the following overall reaction:

$M^{2+} + HCO_3^- + OH^- \rightarrow M_2CO_3 + H_2O$; where M is a divalent cation   [R. 6]
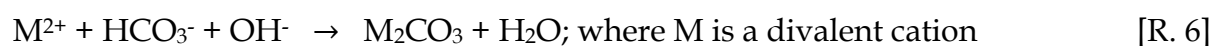
Hydroxyapatite is characterized by rapid kinetics of precipitation above neutral pH values in the presence of heterogeneous nucleation sites suitable for the immobilization of heavy metals. The precipitation requires the formation of stable and insoluble nuclei, for example, precipitation of hydroxypyromorphite is followed

by a crystallization (nucleation and growth of the structure of hydroxypyromorphite). Indeed, nucleation is triggered by a diffusional gradient of dissolved phosphate ions, which enhances the trapping of ions Pb^{2+} by combining with the phosphate ions. In fact, there are two mechanisms of nucleation, homogeneous nucleation in Ca-HA and heterogeneous nucleation, which corresponds to the germination and the intrusion of the nucleus at the particle surface. In addition, the change in the crystalline structure is affected by the precipitation of the nucleated lead-phosphate compound on the surface of crystallized Ca-HA forming nuclei uniform distribution and homogeneous size. Precipitation of Pb^{2+} occurs following the reactions:

$$Ca_{10}(PO_4)_6(OH)_{2(s)} + 14\,H^+_{(aq)} \xrightleftharpoons{\text{dissolution}} 10\,Ca^{2+}_{(aq)} + 6\,H_2PO^-_{4(aq)} + 2\,H_2O \qquad \text{[R. 7]}$$

$$10\,Pb^{2+}_{(aq)} + 6\,H_2PO^-_{4(aq)} + 2\,H_2O \xrightleftharpoons{\text{Pecipitation}} Pb_{10}(PO_4)_6(OH)_{2(s)} + 14\,H^+_{(aq)} \qquad \text{[R. 8]}$$
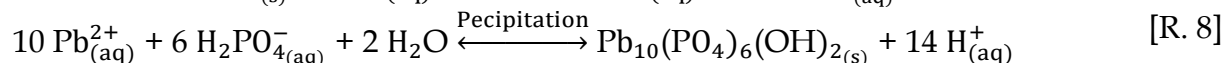
Hydroxyapatite dissolution is strong and quickly established, which explains the presence of ions PO_4^{3-}, OH^- and Ca^{2+} ions. Indeed, the dissolution of Ca-HA increases the pH of the solution, allowing the precipitation of Pb^{2+} and other divalent heavy metals according to the above reactions.

4.3.   Substitution

The substitution results from the replacement of one ion by another of the same sign but different electric charge. At the crystal structure of apatite, substitution occurs by replacing the Ca^{2+}, PO_4^{3-} and OH^- sites. It should be noted that the ionic substitution in the apatite is particularly well illustrated by the geological apatite or in the biological apatite [53]. However, the coupled ion substitution is the major substitution. It takes place by maintaining the neutrality of the ionic charge (i.e. apatite neutralizes acidity by substituting PO_4^{3-}, CO_3^{2-} and OH^-) or either by a second substitution with an opposite ion charge, or either by vacant sites presence in the crystal lattice (substitution of Ca^{2+} by Na^{2+}). In this case, the substitution of carbonate decreases the lattice parameter "a" and increases the lattice parameter "c" in the apatite structure. The substitution sites of phosphate by carbonate is controlled by

the presence of cations (Na$^+$ increases the rate of substitution of phosphates). The major drawback of this substitution is the decrease in crystallinity of the apatite and thus increasing the solubility. Local substitution can occur at high temperatures where the ions OH$^-$, Cl$^-$ and F$^-$ can substitute each other in different chemical forms of apatite (hydroxyapatite, fluorapatite and Chloroapatite).

4.4. Ionic exchange

Ion exchange is based on the adsorption of protons and acid anions from a solution onto the apatite surface. For example, studies by *Corami et al* (2008) [66] on the sorption of heavy metals such as Cd, Pb, Zn, and Cu by hydroxyapatite have shown specifically that the elimination of cadmium by Ca-HA is due to a two-step mechanism. The first step is surface complexation of M^{2+} ions as shown by *BAILLIEZ et al* (2007) [70] for the retention of lead, and the second step depends on the diffusion of metal ions within the Ca-HA particles through ion exchange with Ca^{2+} ions.

5. Conclusion

Calcium phosphate occurs in different phases, the apatitic phase is the more stable stochiometric structure characterized by Ca/P ratio of 1.67 known as hydroxyapatite (Ca$_{10}$(PO$_4$)$_3$(OH). The apatitic crystalline structure is also influenced by physicochemical parameters such as pH, temperature reaction, aging time and reactant concentrations. However, the synthesis of hydroxyapatite can be made by different methods. Stability of synthesized product is controlled by the solubility of product in aqueous solutions. The solubility product (Ksp) value of Ca-HA is around 10^{-120}. In addition, the solubility is also conditioned by pH, chemical composition and saturation index, and on the other hand is related to the morphological structure (particle size and surface structure).

Chemical and physical sorption, surface complexation, dissolution-precipitation, ion exchange and substitution are the main mechanisms governing the heavy metals retention by hydroxyapatite. Many models were proposed to simulate the adsorption

of pollutants by Ca-HA such as Langmuir and Freundlich models. The use of apatite in PRB and soil treatment has gained attention in the last years. Especially, it has high capacities to remediate groundwater and wastewater. The main advantages to use synthetic apatite are the high stability, ease of preparation method and the low cost.

III. Calcium sulfate

1. Introduction

Calcium sulfate is generally present in nature in the form of crystalline rock, is sedimentary gypsum, which is often characterized by a purity exceeding 90%. Industrial processes such as the preparation of phosphoric acid from phosphate rock (phosphogypsum), treatment of gas desulfurization using lime stone (desulfogypsum), the manufacture of hydrofluoric acid from calcium fluoride (fluoranhydrite), etc ... can also produce this material as a byproduct, with grades of mineral impurities (phosphate and other impurities combine with calcium sulfate). Consequently, the gypsum by-product containing levels of heavy metals, raises storage problem and provides a negative impacts on the environment. The valorization of phosphogypsum is an essential process and can be carried out by its use as a hydraulic binder, fertilizer and construction material (added to cement to modify setting properties).

2. Calcium sulfate forms

Calcium sulfate exists in three different forms, calcium sulfate dihydrate ($CaSO_4.2H_2O$, Gypsum, G), calcium sulfate hemihydrate ($CaSO_4.1/2H_2O$, Plaster, P) and calcium sulfate anhydrite ($CaSO_4$). The change in the crystalline form depends on the calcination temperature following the method of dehydration (i.e. in air or water vapor). **Figure 10** summarizes the treatment processes of gypsum for the formation of other phases of calcium sulfate and their crystalline structure.

The firing of gypsum at a temperature of 120°C allows hemihydrates formation. Dehydration under steam in an autoclave (2-7bars) gives α form well-crystalline and compact (monoclinic structure). This is due to the dissolution / re-crystallization of gypsum particles. The dehydration of gypsum in air by firing in kilns leads to the formation of β-hemihydrate form of less-crystalline structure.

Dehydration in water vapor				
Cristalline structure				
Monoclinic	Monoclinic	Hexagonal	Orthorhombic	Cubic
Dihydrate	Hemihydrate α **120°C** / Hemihydrate β **120°C**	Anhydrite III (α, β) **200°C**	Anhydrite II (α) **250°C** / Anhydrite II (β) **400°C**	Anhydrite I **1200°C**
Endothermic	Endothermic	Exothermic		Endothermic
Transformation reaction				
Dehydration in air				

Figure 10: Different phase of calcium sulfate after heat treatment

The conversion reaction of dihydrate to hemihydrate is an endothermic reaction. The reaction of dehydration of gypsum at room temperature ($CaSO_4.2H_2O \rightarrow CaSO_4,0.5H_2O + 1.5H_2O$) is controlled by the pressure of water vapor, which for pressures above 0.1013MPa, plaster formed is P(α) and at a temperature above 100°C and for pressures below 0.1013MPa, plaster β (P(β)) appears at a temperature below 100°C.

At temperatures above 200°C and according to firing mode, the structure of hemihydrate is converted to the anhydrite III following an endothermic reaction. Anhydrite III (α, β) Form is characterized by a hexagonal crystal structure (soluble anhydrite) known under their empirical formula $CaSO_4, \varepsilon H_2O$ with $0.06 \leq \varepsilon \leq 0.11$, and absorbs water vapor easily to form hydrogen bonds and rebuild the hemihydrate structure. Above a temperature of 250°C, anhydrite III is transformed into anhydrite II (α, β) after an exothermic reaction. The crystalline form of anhydrite II (α, β) is orthorhombic; it is the most stable form is a natural anhydrite (molecular weight of 136.1g.mol⁻¹). Anhydrite I is obtained using a high temperature following

an endothermic reaction. Crystalline structure is compact (molar mass of 136.1g.mol^{-1}). The anhydrite is unstable at room temperature. The stability of the phases formed from gypsum depends on the temperature and mode of treatment.

3.   Reactivity of calcium sulfate

Reactivity of calcium sulfate is often illustrated by the hydration of hemihydrated particles which are characterized by a low mixing ratio of P(α) (water/powder ~ 0.4) [71] and anhydrite . Contact of $CaSO_4$ particles with water causes their partial dissolution leading to the supersaturation of the solution by Ca^{2+} and SO_4^{2-}. In addition, ions already present in the pore solution are adsorbed on the surface of the particles to form a covering layer. Once the thickness of the adsorbed layer reaches a limit state, it ends up forming cracks facilitating the passage of water that comes into contact with a fresh surface of the particles, allowing the formation of nuclei of gypsum precipitates on the particle surface [72][73]. Consequently, control of hydration scenario of calcium sulfate is correlated to the dissolution of P(α), the nucleation and growth of gypsum. The hydration of calcium sulfate is assessed by the conductivity of the supernatant solution, or by scanning electron microscopy (SEM) and by analysis of the specific surface area (BET method). However, the conductivity of 2 to 2.5mS.cm^{-1} indicates that the solution is saturated in a steady state with the formation of the solid phase of gypsum, and a conductivity greater than 5.2mS.cm^{-1}, the solution is supersaturated with a metastable gypsum state (gypsum formation is initially incomplete) [74].
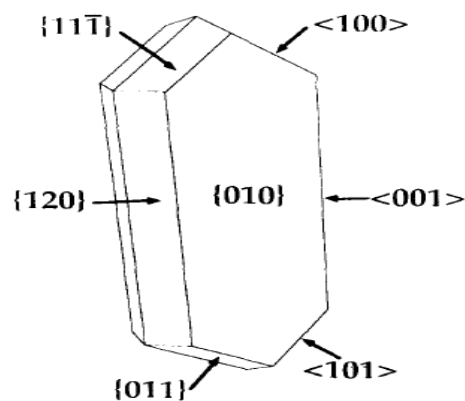
Figure 11 : Crystal morphology of gypsum [75]

Studies by *Finot, et al (1997)* [76] using atomic force microscopy to assess the stability of the different faces of calcium sulfate dihydrated under the influence of relative humidity, show that the precipitation of sulfate calcium is supposed to have the composition of the fraction present in the anhydrite gypsum. However, the formation of gypsum is due to the precipitation on the (010) crystalline face (**Figure 11**). Face (010) is the most responsive and provides guidance on the change in mechanical properties depending on the relative humidity (10-35%). The faces ($\bar{1}$01) are characterized by a neutral and weak attractive links with other faces (-H bonding) attributed to water molecules. The density charge of the sides checks the creation of charged surfaces that characterize the ability of adsorption and varies from one area to another. Following the comparison between the charge densities of the faces references, the face (120) is considered the densest and sticking on easily with the other sides by strong interactive links [77].

4. Conclusion

The calcium sulfate may be found as dihydrated (gypsum) , hemihydrated (plaster) and anhydrite forms. The gypsum and plaster have a monoclinic structure. Their crystalline structure is influenced by dehydration process. Plaster hydration obeys to dissolution/precipitation mechanism and gypsum formation take place by growth of (010) crystalline face.

IV. Hydraulic performances

1. Introduction

Granular and reactive materials have a high capacity to retain dissolved pollutants containing heavy metals. For example, the soil plays a very interesting role in the infiltration and percolation of runoff, leaching of garbage in landfills or industrial processes. These waters are continuing their infiltration in the various soil layers, until reaching groundwater. However, the prediction of the flow rate of polluted water is indispensable to assess the transfer of contaminants from groundwater and

provides information on the hydraulic conductivity that's considered as an essential parameter in the characterization of the infiltration rate.

The geometric factors of the material structure allowing infiltration of fluids through porous media are porosity (pore size), geometry of the pores and thickness of the porous medium. The fluid passing through the porous media obeys to the inlet pressure which allows the passage of a predetermined volume of fluid through the porous sample (capillary forces related to surface wettability). Therefore, the determination of permeability is based on two essential parameters, flow and hydraulic gradient resulting in the ability of the porous material to let through the fluid. The values of permeability allow the classification of permeable materials, semi-permeable and impermeable.

Permeability and porosity parameters are essential to the location of implantation sites, the design of permeable reactive barriers and prediction of its hydraulic performance. In this case, multiple relationships, models and theoretical methods describe the evolution of permeability based on the geometrical structure of macroscopic and microscopic levels (particle size) of the material and on the assimilation at the porous network to cylindrical channels and are related to material properties such as specific surface area. The conditions for the evaluation of hydraulic parameters depend on the state parameters such as pressure (hydraulic head), temperature and viscosity of the fluid used in contact with the porous material.

2.   Porous media characterization

2.1.   Porous structure

Porous material structure has a component that includes three parts, gas (air), liquid (adsorbed or free water) and granular skeleton. The void volume consists of occlude air and water. **Figure 12** illustrates a simplified model of the various components of a porous medium.
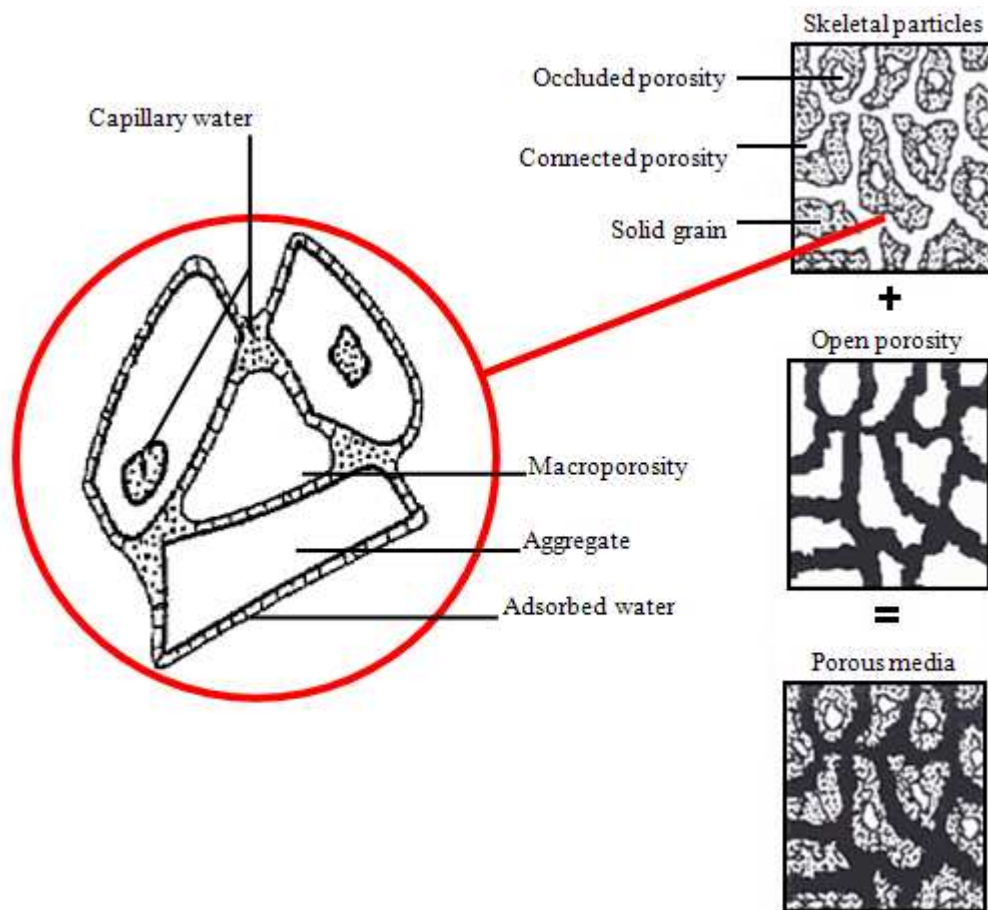
Figure 12 : Main components of a porous solid

The porous medium is formed by the non-empty interconnected open voids, interconnected open voids and closed voids. The continuous space shows the interconnected pores that ensure surface contact and facilitates the transport mechanisms of matter with surrounding environment, unlike connected voids that contribute to fluid diffusion and transport. The category that has closed pores (occluded) porosity is isolated and does not allow access or fluid communication with the external environment, it is the residual porosity. Indeed, the apparent volume brings together solid volume V_s, V_o open void volume and the closed void volume V_f. However, the pore distribution depends to water physical connections between solid grains of porous matrix. Water in the solid interstices may be capillary, gravity or retention and **Figure 12** shows the different phases of water particles in the porous medium.

Porosity classification depends also on the pore water nature present in the pores and mobile water that characterizes the macroporosity (open porosity) by the free flow once porous solid is saturated. Water in the microporous structure is adsorbed water which binds to the surface of grains in the form of thin layers of dipole water. The retention water is attracted by surface tension on article surface. Mobile water is available in the macroporous, it is easily removable and replaceable.

2.2. Porosity

Void geometric complexity requires its decomposition into a single element, the pores, which are used in solid porosity (ϕ) determination. The relationship between the void volume and the volume of the solid is as follows:

V_a: Apparent volume = $V_s + V_v$ and the porosity relationship is: $\phi = \dfrac{V_v}{V_a}$ $\qquad$ [R. 1]

The distinction between different porosities is not only geometric, but refers to contents of void phase. Therefore, the porosity term is distinguished by the volume of fluid occupying the micro and macroscopic and inter-granular interstices. However, the effective porosity term is defined as gravity water volume in saturated porous media reported to its total volume. The effective porosity is also called drainage porosity. The movement of water in interconnected pores following pressure gradient characterizes the filtration ability. Available porosity depends on saturation degree.

2.3. Porosity determination

Porosity calculation or measurements are made by several methods. However, the total porosity is composed of connected porosity and closed porosity. Typical methods for porosity measurement gives total porosity (porosity accessible to water) or microporosity (by gas expansion and mercury injection). Porosity can be quantified by image analysis obtained from the actual scanning electronic microscopy (SEM). Studies carried out by *Wantanaphong et al* (2006) [78] to quantify

pore clogging of PRB test body obtained by coring, shows the possibility to determinate total porosity by SEM and finally to assess barrier life cycle.

2.4. Permeability

The permeability of a material is its ability for a fluid to pass-throughout. It also depends on the macro and microstructural morphology and saturation degree of materials. The hydraulic conductivity K (m.s^{-1}) (coefficient of permeability or kinematic permeability) depends on the intrinsic permeability of the porous medium (permeability geometric) k (m²) and the kinematic viscosity η (m.s^{-1}). The relationship between intrinsic and kinematic permeability is following:

$$K = \frac{k.\rho.g}{\mu} \hspace{4cm} \text{[R. 2]}$$

With μ is the dynamic viscosity of the fluid (Pa.s); g is the gravity (m.s^{-2}) and ρ is the fluid density (kg.m^{-3}). Unit widely used in hydrology field is "Darcy" (DARCY1856), it is the intrinsic permeability of a material when a fluid (μ = 1cPo, water at 20°C) displaces at a velocity of 1cm.s^{-1} according to 1atm.cm^{-1} pressure gradient (1Darcy = 10^{-12}m² = 10^{-5}m.s^{-1}). Darcy's law discussed later allows the calculation of permeability as a function of stationary flow rate and hydraulic head. Existence of factors affecting the permeability such as compaction (i.e. permeability decreases by increasing confining stress) and anisotropy associated to confining stress, increased aggregates, texture and size distribution (heterogeneity of density) do not allow evaluation of a precise value of the permeability at the laboratory scale. However, determination of permeability from the grain size is possible, where the permeability rises as the aggregate size increases. The heterogeneity associated with a confining stress often affects the permeability [79], and permeability decrease is attributed to the reduction of voids caused by compaction when it depends on an isotropic confining stress and large. **Table 6** tabulates the values of the permeability coefficient of different soils. The permeability of clay and silt is less important than the permeability of the sand and gravel; this is due to the size distribution of each material and the inter-granular porosity of solid particles.

Table 6: Soil permeability

Soil	Permeability (m.s^{-1})
Clay	1.0×10^{-7} - 1.0×10^{-6}
Loam	1.0×10^{-6} - 1.0×10^{-5}
Fine sandy	1.0×10^{-5} - 5.0×10^{-5}
Medium sand	5.0×10^{-5} - 2.5×10^{-4}
Coarse sand	2.5×10^{-4} - 1.0×10^{-3}
Gravel	1.0×10^{-3} - 1.0×10^{-2}

Empirical expressions of permeability differ according several parameters such as structural morphology of the material particles, porosity, surface area and water content. Among the models often used for the macroscopic and/or microscopy description of a porous medium and to estimate the in situ permeability of soil, the Hazen formula (1892) based on the size of the material pores [80]. Hazen formula is generally limited to $0.01cm<d_{10}<0.3cm$ [81][82], involving only the grain diameter, is expressed by the following equation 13:

$$k = C{\cdot}d_{10}^2 \qquad\qquad\qquad [Eq. 3]$$

With k is the geometric permeability (cm²); C is a dimensionless constant (Hazen empirical coefficient) and d_{10} is the maximum diameter of the finest grains whose weight 10% of the total weight of the material used (cm). The empirical correlation between geophysical parameters is described below. The permeability can be evaluated from the arrangement and size, by assimilating particles to spherical structure, the relationship established by Schlichter was used to estimate the permeability from the structural geometry of the solid grains by following relationship:

$$k = C.d_{10}^2.\phi^{3.3} \qquad\qquad\qquad [Eq. 4]$$

Where k is the intrinsic permeability; C is a constant; d is the diameter of grains presenting 10% of material total weight and ϕ is the porosity.

Brinkmann model is based on the macroscopic properties of the porous medium. The model considers pore walls as barriers to fluid flow [83]; this model is expressed by the following relation:

$$k = -\frac{1}{18} \left(\frac{3}{4}(1\text{-}\phi)\right)^{2/3} \left(3 + \frac{4}{1-\phi} - 3\sqrt{\frac{8}{1-\phi}}\right), \text{ with } \phi \text{ is the porosity.}$$ [Eq. 5]

3. Microstructural morphology

The pore architecture is a fairly complex structure; it is defined following pores distribution of material volume. Indeed, the pore distribution determines the classes of porosity within the material and provides its ability to be crossed by a fluid according to pore connectivity and total volume of the material. In this section, we describe the main properties and parameters related to porous materials such as pore size, connectivity and tortuosity.

3.1. Pore size

Distribution of pore size depends on the structure of the porous medium in terms of texture correlated with surface area and particle size distribution of grains. However, classification of material pore size includes three categories, macroporosity, microporosity and mesoporosity. **Table 7** classifies pore size following structural morphology. The microporosity has a fundamental role in the flow of water saturated medium.

Table 7 : Classification of pore size

Macroporosity (nm)	Microporosity (nm)	Mesoporosity (nm)
$r_p > 50$	$r_p < 2$	$2 < r_p < 50$

The determination of the pore size distribution can be made by mercury porosimeter and thermoporometry analysis. Pore radius (r_p) determines the class of porosity vis-a-vis pore volume (V_p), it is identified from the curve: V_p = f (r_p). *Thompson-Katz (1987)* [84] relationship consists to evaluate intrinsic permeability k from the critical radius (r_c) corresponding to maximum pore volume by mercury intrusion method. Hydraulic radius (r_h) can be deduced from the spectrum of the pore radius of a sample. The average size of porous medium can be correlated to the physical condition of the fluid entrapped in the pore volume.

3.2. Hydraulic diameter

Average hydraulic diameter is used to describe the tortuosity of a porous material considering that the flow in the pores follows a non-circular dimension. Indeed, it may be a function of porosity and particle diameter and is defined as:

$$d_h = 4\,\frac{V}{A}$$
[Eq. 6]

Where V is the pore volume and A is the wetted surface. The relation $d_h = 4\,(\frac{\phi}{1-\phi})(\frac{1}{a_s})$; with ϕ is the porosity, and a_s is the particle surface relative to volume (in the case of spherical particles of diameter d, $a_s = 6.d^{-1}$), it is used in Kozeny-Carman formula for calculating permeability as a function of porosity thereafter described.

4. Darcy's low

4.1. Definition

Darcy's law (1856) describes the flow of a fluid through a layer of porous material and determines the permeability from the application of a constant hydraulic head at a constant laminar flow (pressure gradient is proportional to the flow velocity in the pores). This law is a differential form in a single direction [85] (vertical or horizontal) and is written as follows:

$$V = -\,K\,\overrightarrow{grad}\,\Psi$$
[Eq. 7]

Where V is the flow velocity (m.s^{-1}), K is the permeability (m.s^{-1}) and Ψ is the hydraulic potential which has the sum of capillary and gravitational components ($\Psi = P + \rho.g.z$) with P is applied pressure (Pa), ρ is the water density, g is the gravity (m.s^{-2}) and z is the traveled distance (m). For vertical flow, Darcy's law is written:

$$\frac{d\theta}{dt} = -\,K\,\frac{d\Psi}{dz}$$
[Eq. 8]

Where θ is the water content (%) and t is the travel time along the z axis (s), the introduction of the expression of Ψ in the equation:

$$\frac{d\theta}{dt} = -K\left(\frac{dP}{dz} + \rho.g\right)$$ [Eq. 9]

Verification of Darcy's law studies by *Vachaud* (1966) [86] show that each material obeys to law for a one-dimensional horizontal flow used for the determination of capillary conductivity. Generalized Darcy's law along the horizontal axis is:

$$q = -K(\theta)\frac{d\psi}{dx}$$ [Eq. 10]

With, q is the unit flow rate of water corresponding to the volumetric water content θ, K is the capillary conductivity coefficient and ψ is the capillary potential (capillary suction). Generalizing Darcy's law in three dimensions is written as follows:

$$\overrightarrow{V_p} = \frac{\mu}{k}\vec{u} + \rho\vec{g}$$ [Eq. 11]

Where $\vec{u}$ is the average velocity of flow, k is the intrinsic permeability of the porous medium and $\overrightarrow{V_p}$ is the pressure gradient on both sides of the porous medium.

4.2. Integral form of Darcy's law

The flow rate q is constant over time in steady state and is written as follows:

$$q = -K(h)\left(\frac{dh}{dz} + 1\right)$$ [Eq. 12]

With K is the hydraulic conductivity (m.s^{-1}), h is the piezometric head (m) and z is the traveled distance (m). The fluid flow rate q traveled a distance L between two points z_1 and z_2 along the vertical axis z, the integration of the relationship gives the traveled distance according to the piezometric head upstream (h_1) and downstream (h_2) of the sample:

$$L = Z_1 - Z_2 = \int_{h_1}^{h_2} \frac{dh}{(1+\frac{q}{K(h)})}$$ [Eq. 13]

4.3. Relationship between porosity and permeability

Granular material description in terms of particle size and pore distribution in porous matrices is based on formula that takes into account the porosity and permeability. The Kozeny (1927) [87] formula is:

$$k = \frac{C \cdot d^2 \cdot \phi^3}{(1-\phi)^2}$$ [Eq. 14]

Where k is the permeability, ϕ is the porosity (%) C is an empirical constant which takes into account the form and tortuosity of the porous channel (0.5 (circle), 0.562 (Square), 0.597 (triangle)) and d is the particle size (diameter) [85]. Experiments conducted by Fair and Hatch (1933) on the assessment of factors influencing the flow of water [85] were based on replacing the parameter d by the factor V/A, where A is the total area of a representative sample of particles whose total volume is V. Developing the formula of Kozeny by *Fair and Hatch* (1933) by assimilating the porous structure to a hypothetical structure such as capillary tubes of radius r [88][89]. The structural formula is based on Poiseuille's equation (1839).

4.3.1. Poiseuille's equation

The cylindrical Poiseuille flow of a fluid through a channel of radius r subjected to a pressure gradient obeying Poiseuille's equation is defined as:

$$Q = \frac{\pi r^4}{8\mu} \frac{\Delta P}{L_e}$$ [Eq. 15]

With Q is the volumetric flow rate ($m^3.s^{-1}$), r is the radius of the channel, ΔP is the pressure gradient (Pa) and L_e is the effective length of the channel. The model of porous structures (n identical straight cylindrical pores) is treated as a network of parallel capillaries of radius r, the modeling of fluid flows in a material of the same characteristics based on flow determination in the material and flow in the porous network.

The flow in the material is: $Q = \frac{k}{\mu} A \frac{\Delta P}{L}$; and flow in a pore is the following: $q = \frac{\pi r^4}{8\mu} \frac{\Delta P}{L}$ and knowing that $Q = n.q$; with n the channel number. The permeability associated to this model is:

$$k = n \frac{\pi r^4}{8A}$$ [Eq. 16]

4.3.2. Tortuous channels model

This model is based on the correction approximate straight-channel model by a tortuous channel through the material with an effective length L_e greater than the total length L of the material. The porosity in the apparent volume of the material (n-channel radius "a" and length L_e) is estimated by the following relation:

$$\phi = n.\pi.a^2.\tau$$ [Eq. 17]

With n is channels number, "a" is channel radius and τ is the tortuosity. Flow in each capillary channel is defined by Poiseuille's equation bellow. Filtration velocity through the porous body taking into account that the porosity is active ($\phi/3$) is following: $v = n.q = \frac{\phi.a^2}{24\mu\tau^2} \frac{\Delta P}{L}$ and permeability associated to this model is:

$$K = \frac{\phi.a^2}{24\mu\tau^2}$$ [Eq. 18]

4.3.3. Kozeny-Carman model

Kozeny-Carman modeling is based on Kozeny (1927) relationship modified by Carman (1937) [90]. The modification considers the porous material as a collection of capillary tubes. Moreover, the relationship between permeability, specific surface area and porosity of the material is as follows:

$$k = \frac{C.g}{\mu_w \rho_w} \frac{\phi^3}{S_s^2 (1-\phi)^2 D_r^2}$$ [Eq. 19]

With, k is the hydraulic conductivity (permeability coefficient) (m.s^{-1}), A is the section of sample, constant C depends on the shape and tortuosity of the pores (often

C=0.2 by considering that the water does not move in straight channels but around irregularly shaped solid particles); μ_w is the dynamic viscosity (Pa.s) ρ_w is the density of water (kg.m^{-3}), ϕ is the porosity, Ss is specific surface area (m².kg^{-1}) and Dr is the specific weight of solid (ρ_s/ρ_w). The Kozeny-Carman model is consistent with the development of *Fair and Hatch* (1933) [85], it is based on four assumptions:

♦ The volume of inter-granular voids is treated as a channel of constant section and length;
♦ The volume of inter-granular voids is equal to the volume of the channel;
♦ The lateral surface of the channel is equal to the outer surface of the grains;
♦ The flow regime is laminar solid particles are relatively compact [89];
♦ The electrochemical reactions between the solid particles and water are negligible,

Kozeny-Carman formula can be used in evaluating the hydraulic conductivity of a permeable reactive barrier to predict the reduction of porosity and hydraulic performances in general. *LI et al*, (2006) [91] have used this model to explain the reduction of permeability as a function of porosity in a PRB-ZVI based, using the following equation:

$$k = \frac{1}{5S_s^2}\left(\frac{\rho_w g}{\mu}\right)\frac{\phi^3}{(1-\phi)^2} \qquad\qquad \text{[Eq. 20]}$$

Where k is the hydraulic conductivity (m.s^{-1}), Ss is the specific surface area per unit volume of reactive material particles (1/m) (ratio of surface area and bulk volume), ρ_w is the water density; g is the gravity (m.s^{-2}), ϕ is the porosity of the material (%) and μ is the absolute viscosity of water. The evaluation of the permeability of a permeable barrier at time t can be performed using the following equation:

$$k_t = k_0 \left[\frac{\phi_0 - \Delta_{\phi_t}}{\phi_0}\right]^3 / \left[\frac{1 - \phi_0 + \Delta_{\phi_0}}{1 - \phi_0}\right]^2 \qquad\qquad \text{[Eq. 21]}$$

Where K_0 is the initial hydraulic conductivity (m.s^{-1}), ϕ_0 is the initial porosity; Δ_{ϕ_t} is the reduction of the porosity at time t. It should be noted that the reduction of the porosity is not linearly related to the reduction of hydraulic conductivity of the barrier [91]. However, these two parameters influence the performance of the flow.

The material is modeled by porous channels of "a" section; the constant flow is given by the following relation:

$$Q = \frac{{r_h}^2}{h_0 \mu} a \frac{\Delta P}{L_e} \qquad \text{[Eq. 22]}$$

Where r_h is the hydraulic radius (ratio of the volume of the pore and the lateral surface of the pore);

$$r_h = \frac{aL_e}{m_s S_s} = \frac{V_v}{m_s S_s} \frac{1}{(V_a - V_v)} = \frac{\phi}{\rho_s S_s (1-\phi)} \qquad \text{[Eq. 23]}$$

$$a \cdot L_e = V_v = \phi.V_a = \phi.A.L; \text{ where: } a = \frac{\phi.A.L}{L_e} \qquad \text{[Eq. 24]}$$

Comparing this relation with Darcy's law relationship, we obtain the expression of the permeability:

$$K = \frac{\phi^3}{(1-\phi)^2} \frac{1}{\rho_s S_s^2} \frac{1}{h} \quad (*) \qquad \text{[Eq. 25]}$$

With: $h = h_0.\tau$, where $h_0 = 2$ is a constant depending on the geometry and tortuosity τ is defined above. Another Kozeny-Carman model is based on the development of the relationship of permeability depending on the specific air tubes and tortuous porosity. Indeed, the specific surface area of tortuous tube is as follows: $A_s = 2\pi.n.a.\tau$ and total porosity of the material of n tortuous tubes is as follows, $\phi = n.\pi.a^2.\tau$, where:

$$A_s = \frac{2\phi}{a} \qquad \text{[Eq. 26]}$$

The expression of the permeability according to (*) is described by the relationship:

$$K = \frac{\phi^3}{6 A_s^2.\tau^2} \qquad \text{[Eq. 27]}$$

5.   Permeability determination

The permeability of materials can be evaluated at laboratory scale and/or in-situ with respect to the soil profile. Therefore, the methods to be applied in the laboratory can be composed with simple devices easy to handle, such as permeameters gas

(oxygen, nitrogen), the constant head permeameter and variable head permeameter. In this case, these methods allow the determination of accurate values of the permeability under controlled conditions of pressure and temperature. In addition, in-situ techniques are carried out by direct field testing, among these techniques is found, the TRIMS permeameter, the GUELPH permeameter and standardized devices such as blower door opened and the double ring type single-ring infiltrometer closed. This section highlights the major parameters related to all the methods mentioned earlier, with emphasis on application conditions and relations for the calculation.

5.1. Laboratory scale

This section highlights the major indices related to the laboratory methods mentioned earlier, with emphasis on application conditions and relations for the calculation.

5.1.1. Constant head permeameter

Constant head permeameter is a device for determining permeability of coarse-grained materials such as sand (permeable materials). **Figure 13** shows the simplified process of permeameter. The calculation of permeability following Darcy's law applied to a thickness L of the sample, limited each side by two porous stones of a higher permeability than that of the sample. The sample and the porous layers are placed in a column section "A" fulfills its part of a greater volume of water.

The column is connected to a tube of radius smaller than that of the water column, infiltrated water through the sample is poured into a graduated tube at time t equal to the given flow rate Q in the system (i.e. flow rate Q through the sample equals the volume collected versus time t for the collection).
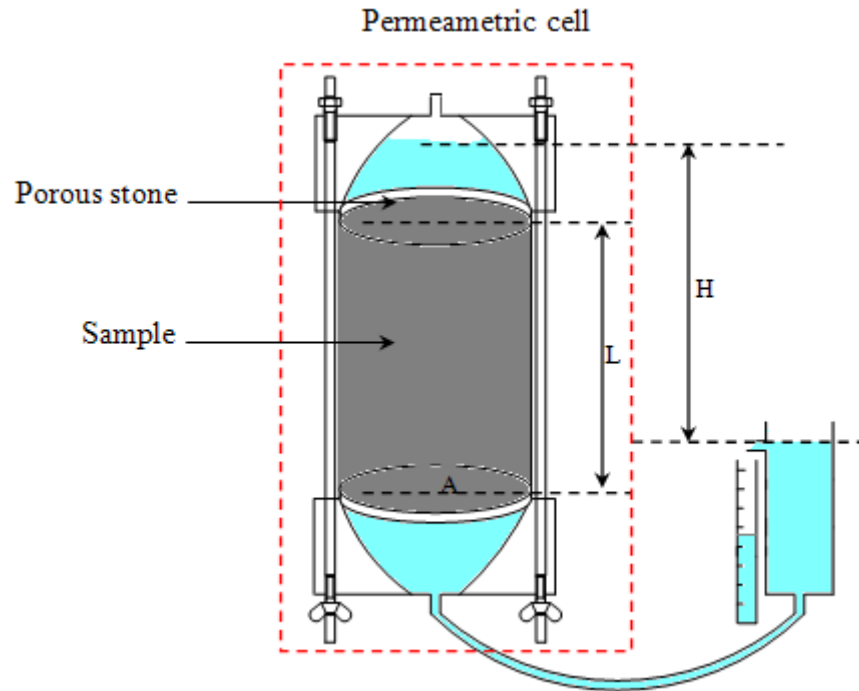
Figure 13: Simplified schema of a constant head permeameter

Flow rate expression is as follows:

Q = A.v.t, with, v = k.i and i=H/L   [Eq. 35]

Where "i" is the hydraulic gradient and H is the piezometric head (m) between the water level in the column and collection tube, the expression of permeability (m.s^{-1}) (hydraulic conductivity) of the sample is as follows:

$$k = \frac{QL}{Aht}$$ [Eq. 36]

5.1.2. Variable head permeameter

This method is used to measure the permeability of fine grained materials such as clays, silt, i.e. it is recommended for materials with low permeability. **Figure 14** shows the schematic device of this permeameter. Therefore, this assessment method for soil permeability is based on the introduction of the sample in a column of section "A", a tube (pipette) of section "a" is brought into contact with the sample to ensure a

steady flow, the transit time of h_1 to h_2 in the water through the pipette used to calculate the flow rate q.
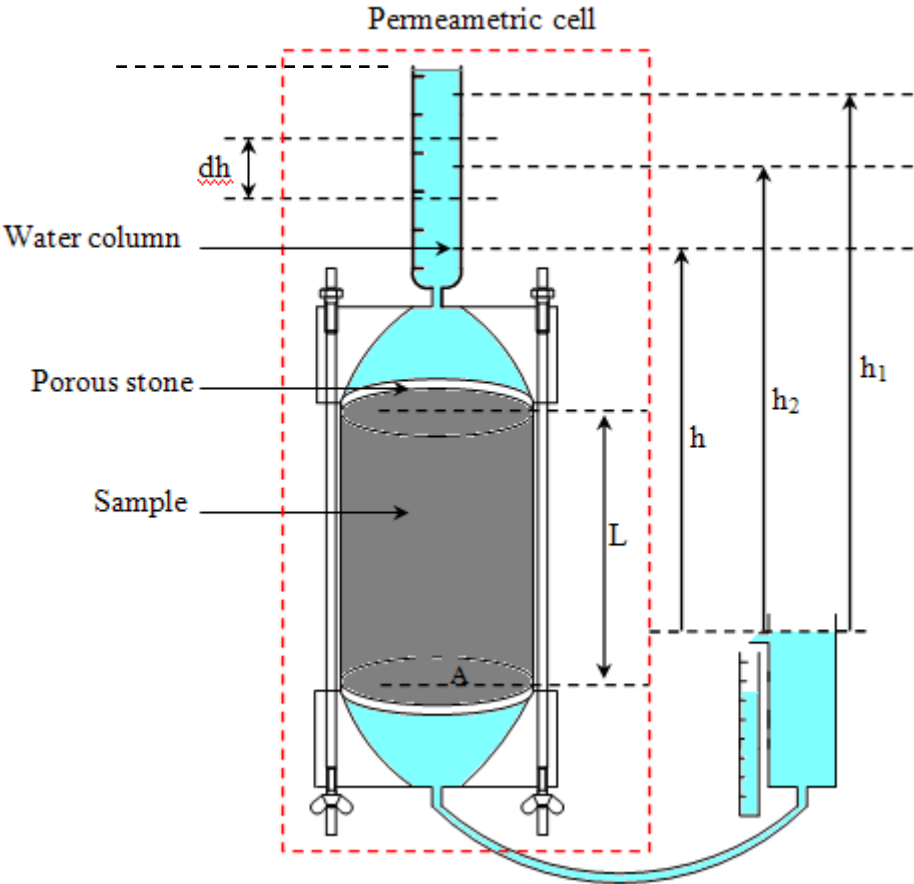
Figure 14: Simplified schema of a variable head permeameter

Flow rate in the column:

$$q = A.v = A.k.i = \frac{A.k.h}{L} = -\frac{a.dh}{dt} \qquad \text{[Eq. 37]}$$

By integrating from h_1 to h_2, the permeability is as follows:

$$k = \frac{a.L}{A.t \ln (h_1/h_2)} \text{ or } k = 2.3 \frac{a.L}{A.t \log (h_1/h_2)} \qquad \text{[Eq. 38]}$$

It should be noted that measures of permeability in laboratory by using the constant head or variable head only provide punctual and unidirectional estimation.

5.2. In-situ permeability calculation

The identification of soil profile led on permeability value is a easy step in geotechnical and civil engineering field. Several developed methods used to evaluate

in-situ permeability mostly permeable layers such as sandy and sandy-loam textures. In addition, in-situ techniques are carried out by direct testing to the field, among these techniques, TRIMS permeameter [92], GUELPH permeameter [93][94] and standardized devices such as double-ring opened infiltrometer [95] and single-ring closed infiltrometer [96].

6.   Conclusion

This chapter has highlighted the main characteristics of PRB. The various chemicals used have been described. A particular focus is made on the determination of the porosity of the formulate PRB. The methods widely used in civil engineering to characterize the porous structure are porosity accessible to water and mercury porosimeter, which give values of total porosity and pore radius of the medium (tortuosity). Nevertheless, porosity is a necessary parameter to evaluate the permeability following the geometry, the grain structure and pore distribution. The fluid flow through the thickness of a material obeys Darcy's law and follows a hydraulic potential at a laminar flow regime (the application of pressure to measure the permeability). However, verification of Darcy's law applies by considering the flow in a material is one-dimensional and depends only on the capillary and the water content. The relationship between porosity and permeability materialized by the Kozeny-Carman model is based on the assimilation of a pore network model to evaluate the theoretical permeability of a material with reference to the specific surface of grains and tortuosity. In general, the assessment of hydraulic performance when designing a permeable barrier (i.e. the reactive material) is performed by percolation tests at constant head and the value of the permeability obtained depends on the supporting environment so that the permeability of the reactive media must be higher than that of the aquifer.

V.   References

[1] ITRC (Interstate Technology & Regulatory Council). 2005. *Permeable Reactive Barriers: Lessons Learned/New Directions*. PRB-4. Washington, D.C.: Interstate

Technology & Regulatory Council, Permeable Reactive Barriers Team. Available on the Internet at www.itrcweb.org.

[2] SNAPE I., MORRIS, C.E., COLE, C.M., 2001. *The use of permeable reactive barriers to control contaminant dispersal during site remediation in Antarctica*. Cold Regions Science and Technology 32; Pp157–174

[3] CONCA J.L., WRIGHT J., 2006. *An Apatite II permeable reactive barrier to remediate groundwater containing Zn, Pb and Cd*. Applied Geochemistry 21; Pp2188–2200

[4] CZURDA K.A., HAUS R., 2002. *Reactive barriers with fly ash zeolites for in situ groundwater remediation*. Applied Clay Science 21; Pp13– 20

[5] KOMNITSAS K., BARTZAS G., PASPALIARIS I., 2006. *Modeling of Reaction Front Progress in Fly Ash Permeable Reactive Barriers*. Environmental Forensics, 7:219–231, Taylor & Francis Group, LLC, ISSN: 1527–5922 print / online DOI: 10.1080/15275920600840552 ; Pp1527–5930

[6] CHUNG H.K., KIM S.K., LEE Y.S., YU J., 2007. *Permeable reactive barrier using atomized slag material for treatment of contaminants from landfills*. Geosciences Journal Vol. 11, No. 2, June 2007, Pp137−145

[7] TURNER B.D., PHILIP J., BINNING B, SLOAN S.W., 2008, *A calcite permeable reactive barrier for the remediation of Fluoride from spent pot-liner (SPL) contaminated groundwater*. Journal of Contaminant Hydrology 95; Pp 110–120

[8] EPA 600/F-97/008, July 1997, *Permeable Reactive Subsurface Barriers for the Interception and Remediation of Chlorinated Hydrocarbon and Chromium (VI) Plumes in Ground Water*. Office of Research and Development; USEPA REMEDIAL TECHNOLOGY FACT SHEET. EPA 542/F-01/005, April 2001. *A Citizen's Guide to Permeable Reactive Barriers*. www.epa.gov/superfund/sites

[9] SIMON F-G., MEGGYES T., 2000. *Removal of organic and inorganic pollutants from groundwater using permeable reactive barriers Part 1. Treatment processes for pollutants*. Land Contamination & Reclamation, 8 (2); Pp103-116

[10] SCHAD H., GRATWOHL P., 1998, Funnel and gate systems for in situ treatment of contaminated groundwater at former manufactured gas plant sites. In: Burmeier, H. (ed.) Treatment Walls and Permeable Reactive Barriers, Vol. 229, NATO CCMS, Vienna. Available on www.books.google.fr Pp56-65

[11] SCHNEIDER P., OSENBRUCK K., NEITZEL K., NINDEL K., 2002, In-Situ Mitigation of Effluents from Acid Waste Rock Dumps Using Reactive Surface Barrier – a Feasibility Study, (Technical Article), Mine Water and the Environment 21: IMWA Springer-Verlag, Pp36-44

[12] POWELL R.M., BLOWS D.W., GULLHAM R.W., et al, 1998, Permeable Reactive Barrier Technologies for contaminant Remediation. EPA/600/R-98/125, Available on: http://www.clu-in.org/download/rtdf/prb/reactbar.pdf. Pp28

[13] COURCELLES BENOIT, 2007, Etude du comportement physico-chimique des filtres de Barrières Perméables Réactives: Modélisation et Expérimentation à l'échelle pilote, Ecole Centrale Paris, Ecole Centrale des Arts et Manufacturations, Thèse soutenue le 22 Janvier 2007, Spécialité Traitement des eaux souterraines, Laboratoire : MSS-MAT, Pp11-12

[14] JIRASKO D., 2004, *Problems connected with use of permeable Reactive Barriers for groundwater treatment*, Proc. Geotechnical workshop of post-gradual students, CVUT, ISBN 80-01-03066-0, Czech Technical University, Prague, Czech Republic
http://www.cgts.cz/5e_journal_documents/jirasko.pdf

[15] LEE J., GRAETTINGER A. J., MOYLAN J., REEVES H. W., 2009, Direction site exploration for Permeable Reactive Barrier design, (ELSEIVIER) Journal of Hazardous Materials 162, Pp22-229

[16] GAVASKAR A., NEERAJ, G., SASS, B., , JANOSY, R., and HICKS, J., 31 Mars 2000, *Design Guidance for Application of PRB for GW Remediation*, Project officer; LUGHTNER ALISON, Air Force Research Laboratory, Tyndall Air Force Base, Florida, Contact No, F08637-95-D-6004, Delivery Order No, 5503, Study Sponsored by SERDP (Strategic Environment Research and Development Program).

[17] LUCEY K.S. 2006, *Permeable Reactive Barriers as Long-Term Solutions for Groundwater Remediation: Dynamics of Groundwater Properties, Methane Concentrations, Dissolved Inorganic Carbon Concentrations, and Rates of Carbon Oxidation Processes, Across the NITREX Permeable Reactive Barrier in Waquoit Bay, Cape Cod.* Wellesley, Massachusetts 02481 USA

[18] TRATNYEK, P.G., JOHNSON, T.L., SCHERER, M.M. EYKHOLT, G.R., 1997, R*emediating Groundwater with Zero-Valent Metals: Chemical Considerations in Barrier Design*. www.info.ngwa.org

[19] GAVASKAR A., et al. 1998, *Permeable Barrier for Groundwater Remediation, Design, Construction and Monitoring*, for additional Bettelle books and Software on Remediation, Treatability Testing. Pp30-35

[20] ZOLLA V., SETHI R., DI MOLFETTA A., 2007. *Performance Assessment and Monitoring of a Permeable Reactive Barrier for the Remediation of a Contaminated Site*. American Journal of Environmental Sciences 3 (3): ISSN 1553-345X © 2007 Science Publications; Pp158-16

[21] LI L., BENSON C.H., LAWSON E.M., 2006. *Modeling porosity reductions caused by mineral fouling in continuous-wall permeable reactive barriers*. Journal of Contaminant Hydrology 83; Pp89– 121

[22] WANTANAPHONG J., MOONEY S.J., BAILEY E.H., 2006. *Quantification of pore clogging characteristics in potential permeable reactive barrier (PRB) substrates using image analysis.* Journal of Contaminant Hydrology 86; Pp299–320

[23] NAVFAC, 2002. *Advances in Permeable Reactive Barrier Technologies.* Tech Data Sheet Naval Facilities Engineering Command Washington, DC 20374-5065, NFESC TDS-2089-ENV

[24] NAVARRO A.J., CHIMENOS M., MUNTANER D., A. INES FERNANDEZ. 2006, *Permeable Reactive Barriers for the Removal of Heavy Metals: Lab-Scale Experiments with Low-Grade Magnesium Oxide.* Ground Water Monitoring & Remediation 26, No. 4; Pp142–152

[25] STRIETELMEIER, B.A., ESPINOSA, M.L., JOSHUA D. ADAMS, LEONARD, P.A., HODGE, E. M., 2001, *Use of a unique bio-barrier to Remediate nitrate and Perchlorate in Groundwater*, In Proceedings of the 2001 International Containment and Remediation Technology Conference and Exhibition, June 10-13-2001, Orlando-FL, www.clu-in.org/perchlorate/downloal/strietelmeier1.pdf
(Or strietelmeier2.pdf)

[26] NAFTZ D. L., FULLER C. C., SNYDER T., STOLP B. J., 2006, Permeable Reactive Barrier: Application to Abandoned Mine Land Reclamation in UTAH, Paper presented at 2006 National of Abandoned Mine Land Programs 28th Annual Conference, September 25-27, Billings MT, Pp1-13

[27] BLOWES D.W., PTACEK C.J., BENNER S.G., McRA C.W.T. 1998. *Treatment of dissolved metals using permeable reactive barriers. Groundwater Quality: Remediation and Protection* (Proceedings of the GQ'98 Conference held at 4g3 Tubingen, Germany, September 1998). IAHS Publ. no. 250, Pp483-490

[28] BEAK D.G., WILKIN R.T. 2009. *Performance of a zero-valent iron reactive barrier for the treatment of arsenic in groundwater: Part 2. Geochemical modeling and solid phase studies*; Journal of Contaminant Hydrology 106; Pp15–28

[29] SASAKI K., D.W. BLOWES B., C.J. PTACEK B., GOULD W.D., 2008, *Immobilization of Se (VI) in mine drainage by permeable reactive barriers: column performance.* Applied Geochemistry 23; Pp1012–1022

[30] NATALE F. D., NATALE M. D., GRECO R., LANCIA A., LAUDANTE C., MUSMARRA D., Groundwater protection from cadmium contamination by Permeable Reactive Barrier, (ELSEVIER) Journal of Hazardous Materials 160, Pp428-434

[31] WRIGHT J., CONCA J.L., RICE K.R., MURPHY B., 2004, *PIMS using apatite II™: how it works to remediate soil & water.* In sustainable Range Management, Proceedings of the Conference on Sustainable Range Management, January 5-8-2004, New Orleans, Available from www.battelle.org/book-store, ISBN 1-57477-144-2, B4-05

[32] MACMAHON P.B., DENNEHY K.F., SANDSTROM M.W. 1999. *Hydraulic and Geochemical Performance of a Permeable Reactive Barrier Containing Zero Valent Iron*, Denver Federal Center; Groundwater, Vol.37, No.3; Pp396-404

[33] LIU S-J., JIANG B., HUANG G-Q., LI X-G., 2006. *Laboratory column study for remediation of MTBE-contaminated groundwater using a biological two-layer permeable barrier*; WATER RESEARCH 40; Pp3401–3408

[34] SIMON F-G., BIERMANN V., SEGEBADE C., HEDRICH M., 2004, *Behavior of uranium in hydroxyapatite-bearing permeable reactive barriers: investigation using* 237_U *as a radioindicator.* Science of the Total Environment 326; Pp249-256

[35] RAICEVIC S., WRIGHT J.V., VELJKOVIC V., CONCA J.L., 2006. *Theoretical stability assessment of uranyl phosphates and apatites: Selection of amendments for in situ remediation of uranium.* Science of the Total Environment 355, ELSEVIER ; Pp13– 24

[36] FLURY B., EGGENBERGER, U., MÄDER, U., 2009. *First results of operating and monitoring an innovative design of a permeable reactive barrier for the remediation of chromate contaminated groundwater.* Applied Geochemistry 24; Pp687–696

[37] MCREA C. W., BLOWES D. W., & PTACEK C. J., 1997, Laboratory-scale investigation of remediation of As and Se using iron oxides. Proceeding Sixth Symposium and Exhibition on Groundwater and Soil Remediation, March 18-21, Montreal, Quebec, Pp167-168

[38] HOCKING G., WELLS S.L., OSPINA R.I., 2001. *Performance of a Deep Iron Permeable Reactive Barrier for Groundwater Remediation of VOCs.* Submitted to 2001 International Containment & Remediation Technology Conference, to be held June 10-13 at Orlando, *FL.* http://www.containment.fsu.edu

[39] SKINNER S.JW., SCHUTTE C.F., 2006, The feasibility of a permeable reactive barrier to treat acidic sulphate- and nitrate-contaminated groundwater. Available on website http://www.wrc.org.za ISSN 0378-4738 = Water SA Vol. 32 No. 2 April 2006, ISSN 1816-7950 = Water SA (on-line); Pp129-136.

[40] GUERIN T.F., HORNER S., MCGOVERN T., DAVEY B., 2002. An *application of permeable reactive barrier technology to petroleum hydrocarbon contaminated groundwater*, Water Research 36; Pp15–24

[41] THIRUVENKATACHARI R. S., VIGNESWARAN R. NAIDU. 2008. *Permeable reactive barrier for groundwater remediation.* Journal of Industrial and Engineering Chemistry 14; Pp145–156

[42] KOMNITSAS K., BARTZAS G., 2004. *Performance evaluation of low cost permeable reactive barriers for the treatment of highly acidic leachates.* (*Evaluation of low-cost materials for the decontamination of acidic leachates using permeable reactive barrier)*, Proceeding of

the International Conference on sustainable Post Mining Land Management, (eds. C. Heberstreit, J. Kudelko, J. Kulczycka), 4-6 Nov. 2004, Krakow, Poland; Pp161-170

[43] AMOS P.W., YOUNGER P.L., 2003. Substrate characterization for a subsurface reactive barrier to treat colliery spoil leachate, Water Research 37(1), PERGAMON, Pp108–120

[44] KOMNITSAS K., BARTZAS G., PASPALIARIS I., 2004. *Efficiency of limestone and red mud barriers: laboratory column studies*. Minerals Engineering 17, ELSEVIER ; Pp183–194

[45] SIMON F-G., BIERMANN, V., SEGEBADE, C., HEDRICH, M., 2004, Behavior of uranium in hydroxyapatite-bearing permeable reactive barriers: investigation using U^{237} as a radioindicator. Science of the Total Environment 326 ; Pp249-256

[46] CHEN X., WRIGHT, J.V., CONCA, J.L., PEURRUNG, L.M., 1997. Evaluation of heavy metal remediation using mineral apatite. Water, Air, and Soil Pollution 98, Kluwer Academic Publishers. Printed in the Netherlands; Pp 57–78

[47] CONCA J. L., WRIGHT J., 2006, An Apatite II permeable reactive barrier to remediate groundwater containing Zn, Pb and Cd. Applied Geochemistry 21, Pp1288-1300

[48] WRIGHT J., BRYONY H., and CONCA J., 2003, PIMS: an Apatite II Permeable Reactive Barrier to Remediate Groundwater Containing Zn, Pb and Cd. Environmental Geosciences (2003) in press.

[49] WRIGHT J., CONCA, J.L., RICE, K.R., MURPHY, B., 2004. PIMS using apatite II™: how it works to remediate soil & water. In sustainable Range Management, Proceedings of the Conference on Sustainable Range Management, January 5-8-2004, NewOrleans, Available from www.battelle.org/book-store, ISBN 1-57477-144-2, B4-05

[50] MOORE R.C., 2005. Stabilization and Solidification of hazardous, Radioactive and mixed Wastes, ROGER, D.Spence, SHI, Caijun, Chapter 6, Available on, http://www.books-google.fr; Pp98-112

[51] LAYROLLE P., DACULSI, G., 2008. Physicochemistry of Apatite and Its Related Calcium Phosphates. B. Leon, J.A. Jansen (eds.), Thin Calcium Phosphate Coatings for Medical Implants, Chemistry and Materials Science. DOI 10.1007/978-0-387-77718-4_2, Springer Science and Business Media, Pp9-24

[52] LIU C., HUANG, Y., SHEN, W., CUI, J., 2001. Kinetics of hydroxyapatite precipitation at pH 10 to 11. Biomaterials 22 ; Pp301-306

[53] WOPENKA B., PASTERIS, J.D., 2005. A mineralogical perspective on the apatite in bone. Materials Science and Engineering C 25, pp131–143

[54] MOORE R.C., 2003. Situ formation of Apatite for sequestering radionuclides and heavy metals. Invention, Patent NO, US-6, 592, 294, B1

[55] MOORE R.C., SANCHEZ, C., HOLT, K., ZHANG, P., XU, H., CHOPPIN, G.R., 2004. Formation of Hydroxyapatite in soils using calcium citrate and sodium phosphate for control of strontium migration, Radiochemical. Acl, Vol.92, Issue 9-11/2004; Pp719-723

[56] PADILLA S., VALLET-REGI M., GINEBRA M. P., GIL F. J., 2005, Processing and mechanical properties of hydroxyapatite pieces obtained by the gelcasting method, Journal of the European Ceramic Society 25, Pp375-383

[57] VARMA, H.K., SIVAKUMAR, R., 1996, Dense hydroxy apatite ceramics through gel casting technique. Materials Letters 29 ; Pp57-61

[58] YANG, L., NING, X-S., CHEN, K., ZHOU, H,. 2007. Preparation and properties of hydroxyapatite filters for microbial filtration. Ceramics International 33 ; Pp483–489

[59] BRITEL Ouafae, Modelisation et Optimisation par la Methodologie des plans d'experiences de la Synthese : - de l'hydroxyapatite phosphocalcique, - du phosphate tricalcique apatitique, - du phosphate de calcium apatitique carbonate, Thèse soutenue le 17 Janvier 2007, Université Mohamed V Agdal, Faculté des Sciences Rabat, Spécialité : Chimie-Physique. Pp27-30

[60] DOMINGUEZ, M.I., CARPENA, J., BORSCHNEK, D., CENTENO, M.A., ODRIOZOLA, J.A., ROSE, J., 2008, Apatite and Portland/apatite composite cements obtained using a hydrothermal method for retaining heavy metals. Journal of Hazardous Materials 150; Pp99–108

[61] MARCHAT, D., 2005. Fixation du Caldmium par une Hydroxyapatite phosphocalcique – Etude cinétique et thermodynamique. Université de Limoges, Thèse disponible en ligne sur, http://www.unilim.fr/these/2005/sciences/2005limo0062/marchat_d.pdf, Pp182

[62] WRIGHT, J. V., CONCA, J. L., 2003, Remediation of Groundwater Contaminated with Zn, Pb and Cd using Apatite II. Acta Mineralogica-Petrographica, Abstract Series 1, Szeged, 2003.

[63] CRANNELL, B.S., EIGHMY, T.T., KRZANOWSKI, J.E., EUSTEN, J. D., SHAW, E.L., FRANCIS, C.A., 2000, Heavy metal stabilization in municipal solid waste combustion bottom ash using soluble phosphate. Waste Management 20, Pp135-148: In VIELLARD, P., TARDY, Y., Thermochemical properties of phosphates (NRIAGU,

J.O., MOORE, P.B., editors. 1984, Phosphate minerals. Berlin: Springer-Verlag, Pp171-98: In NRIAGU, J.O., 1976, Phosphate-clay mineral in soil and sediments. Can J Earth Sci, 13:717:

[64] NRIAGU, J.O., 1973. Lead Orthophosphate – III. Stabilities of fluoropyromorphite and bromopyromorphite at 25°C. Geochimica et Cosmochimica Acta, ELSEVIER, Volume 37, Issus 7 July 1973; Pp1735-1743

[65] NRIAGU, J.O., 1973. Lead Orthophosphate – II. Stabilities of chloropyromorphite at 25°C. Geochimical et Cosmochimical Acta, ELSEVIER, Volume 37, Issus 3 March 1973; Pp367-377

[66] CORAMI, A., MIGNARDI, S., FERRINI, V., 2008, Cadmium removal from single- and multi-metal (Cd , Pb , Zn, Cu) solutions by sorption on hydroxyapatite. Journal of Colloid and Interface Science 317; Pp402–408

[67] HESLOP, D.D., BI, Y., BAIG, A.A., OTSUKA, M., HIGUCHI, W.I., 2005. A comparative study of the metastable equilibrium solubility behavior of high-cristallinity and low-cristallinity carbonated apatite using pH and solution strontium as independent variables. Journal of Colloid and Interface Science, Vol.189, Issue 1; Pp14-25

[68] MARTIN W. A., LARSON S. L., FELT D. R., WRIGHT J., GRIGGS C. S., THOMPSON M., CONCA J. L., NESTLER C. C., 2008, The effect of organics on lead sorption onto Apatite II™, Applied Geochemistry 23, Pp34-43

[69] DELRIO J. G., SANCHEZ P., MORANDO P. J., CICERONE D. S., Retention of Cd, Zn and Co on Hydroxyapatite filters, Chemosphere 64, Pp1015-1020

[70] BAILLIEZ Sandrine, 2003, Adsorption du plomb sur des hydroxyapatites et frittage thermique : processus cinétiques et transfert thermique, Institut National des Sciences Appliquées de Lyon, Thèse soutenue le 20 Février 2003, Spécialité : Génie des Procédés

[71] JAFFEL HAMOUDA., 2006, *Caractérisation multi-échelle de matériaux poreux en évolution : cas du plâtre*. Thèse soutenue le 08 Décembre 2006, Ecole polytechnique, Palaiseau, Pp16

[72] SIEVERT T., WOLTER A., SINGH N.B., 2005, *Hydration of anhydrite of gypsum (CaSO4.II) in a ball mill*, Cement and Concrete Research 35, Pp623-630

[73] KONTREC J., KRAJLJ D., BRECEVIC L., 2002, *Transformation of anhydrous calcium sulphate into calcium sulphate dihydrate in aqueous solutions*, Journal of Crystal Growth, Pp203-211

[74] BOISVERT J-P., DOMENECH M., FOISSY A., PERSELLO J., MUTIN J-C., 2000, *Hydration of calcium sulfate hemihydrate (CaSO$_4$,1/2H$_2$O) into gypsum (CaSO$_4$,2H$_2$O). The*

influence of the sodium poly(acrylate)/surface interaction and molecular weight, Journal of Crystal Growth, Pp579-591

[75] BOSBACH D., JUNTA-ROSSO J. L., BECKER U., HOCHELLA JR., M. F., 1996, Gypsum growth in the presence of background electrolytes studies by Scanning Force Microscopy, Geochimica and Cosmochimica Acta, Vol. 60, No. 17, Pp3295-3304

[76] FINOT E., LESNIEWSKA, E. MUTIN, J.-C, GOUDONNET, J.-P, 1997. *Reactivity of gypsum faces according to the relative humidity by scanning force microscopy*, surface science 384, Pp212-217

[77] FINOT E., LESNIEWSKA, E. MUTIN, J.-C, GOUDONNET, J.-P, MUTIN, J-C., DOMENECH, M., AIT KADI, A., 2001. *Correlation surface forces with surface reactivity of gypsum crystals by atomic force microscopy. Comparison with rheological properties of plaster*, Solid State Ionics 141-142, Pp39-46

[78] WANTANAPHONG J., MOONEY, S.J., BAILEY, E.H., 2006, Quantification of pore clogging characteristics in potential permeable reactive barrier (PRB) substrates using image analysis. Journal of Contaminant Hydrology 86; Pp299–320

[79] SHAFIEE, A., 2008, Permeability of compacted granule-clay mixtures, Engineering Geology 97, Elsevier, Pp199-208

[80] SHEPHERD, R.G., 1989, Correlation of permeability and Grain Size; Vol. 27, No. 5-GROUNDWATER-Spetember-October 1989; Pp633-638

[81] HAZEN, A., 1892, Some physical properties of sands and gravels, with special reference to their use in filtration, 24th Annual Rep., Massachusetts State Board of Health, Pub. Doc. No. 34, Pp539-556

[81] HAZEN, A., 1911, Discussion of Dams on sand foundation by A. C. Koenig. Trans. Am. .Soc. Civ. Eng., 73, Pp199-203

[83] Le GALLO, Y., BILDSTEIN, O., BROSSE, E., 1998, Coupled reaction-flow medeling of diagnostic changes in reservoir permeability, porosity and mineral compositions, J. Hydrol. 209, Pp366-388

[84] KATZ, A. J., and THOMPSON A. H., 1987, Prediction of rock electrical conductivity from mercury injection measurements: Journal of Geophysical Research, v. 92, Pp599-607

[85] CHILDS, E. C. SC.D. COLLIS-GEORGE, N., 1950, The permeability of porous materials. Proceedings of the Royal Society of London. Series A, Mathematical and Physical Sciences, Vol. 201, No. 1066 (Apr. 26, 1950); Pp392-405

[86] VACHAUD, G, 1966, Vérification de la loi de Darcy généralisée et détermination de la conductivité capillaire à partir d'une infiltration horizontale,

Symposium on Water in the Unsatured Zone, Wageningen, Pays-bas, IASH/AIHS, UNESCO, vol1 ; Pp277-287

[87] KOZENY, J. 1927, Ueber Kapillare Leitung des Wassers im Boden, Wien, Akad. Wiss., 136(2a), 271

[88] FAIR, G. M., HATCH, L. P., 1933, Fundamental factors governing the stream-line flow of water through sand, J. Am. Water Works Assoc., 25, Pp1551-1565

[89] CARRIER, W.D. 2003. Goodbye, Hazen; Hello, Kozeny-Carman. Journal of Geotechnical and Geoenvironmental Engineering. Pp1054-1056

[90] Carman, P. C. (1937). Fluid flow through granular beds. *Transactions of the Institution of Chemical Engineers (London)*, *15*, Pp150-166.

[91] LI, L., BENSON, C.H., LAWSON, E.M., 2006, Modeling porosity reductions caused by mineral fouling in continuous-wall permeable reactive barriers. Journal of Contaminant Hydrology 83; Pp89– 121

[91] INRA Avignon, Conductivité hydraulique proche de la saturation par la méthode de l'infiltromètre à disque sous succion, Unité de Science du Sol, Fiche de protocole.
http://www.avignon.inra.fr/content:download/4460/72431/file/trims_prot.pdf

[93] AMOOZEGAR, A., 1989, Comparison of the Glover solution with the simulaneous-equations approach for measuring hydraulic conductivity, Soil Sci. Soc. Am. J. 53, Pp 1362-1367

[94] ELRICK, D. E., REYNOLDS, W. D., 1992. Methods for Analyzing Constant head well Permeameter data. Dep. of Land Resource Science, Univ. of Guelph, Guelph, ON, Canada NIG 2W1; and W.D. Reynolds, Land Resource Research Centre, Agriculture Canada, Ottawa, ON, Canada K1A OC6. Received 7 Nov. 1990, Soil Sci. Soc. Am. J. 56; Pp320-323

[95] AFNOR, NF X30-418, (Juillet 2007), Détermination de la perméabilité d'une formation géologique en place, de matériaux rapports, ou artificiellement reconstitués (Infiltromètre à double anneau, de type ouvert).

[96] AFNOR, NF X30-420, (Aout 2007), Détermination de la perméabilité d'une formation géologique en place, de matériaux rapports, ou artificiellement reconstitués (Infiltromètre à simple anneau, de type fermé), Essai à charge constante et essai à charge variable

Chapter II
Materials & Characterization procedures

This chapter focuses on the main techniques to determine physical and chemical properties of calcium sulfate (support material) and calcium phosphate (hydroxyapatite, Ca-HA). Material characterization procedures were described in detail and were based on the use of different techniques aiming at the determination of the density, the surface area and particle size distribution as well as the mineralogical phases present in the samples of calcium phosphate and calcium sulfate.

I.   Materials

1.   Calcium sulfate

This study was performed on calcium sulfate dihydrated (G) and hemihydrated P(α) provided by PRAYON® (Belgium). Calcium sulfate was obtained by a hemihydrates process 2 (HP2) as shown in **Figure 15**. The process is based on the production of phosphoric acid by mixing sulfuric acid (H_2SO_4, 98%) and phosphate. α-Hemihydrated particles was produced by precipitation in the first step of process.
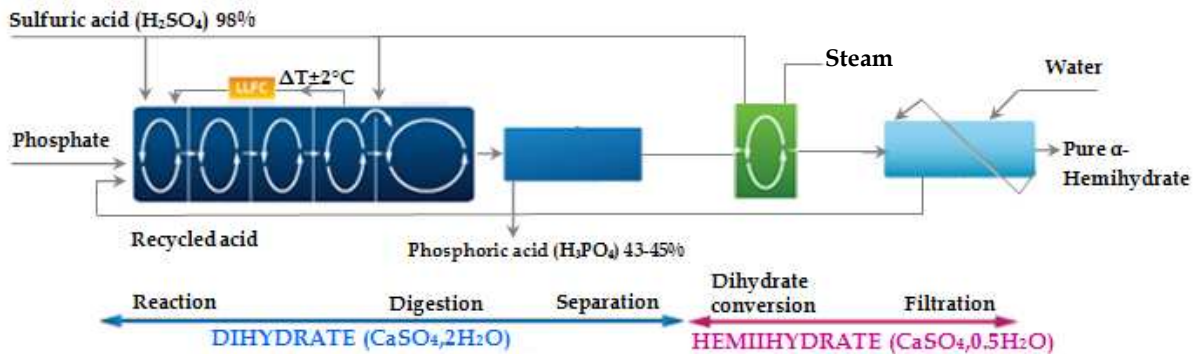
Figure 15: Calcium sulfate (α-hemihydrates and gypsum) manufacturing process (PRAYON®)

The second step consists in the rehydration of produced calcium sulfate hemihydrated to obtain calcium sulfate dihydrated (i.e. this operation purify the hemihydrated particles by reducing the content of the unreacted P_2O_5 acid and co-crystallized in gypsum. The last step describes the conversion of gypsum to plaster under steam followed by filtration and washing to get a pure product.

2.   Calcium phosphate (Hydroxyapatite Gel, Ca-HA$_{Gel}$)

Calcium phosphate was prepared from calcium carbonate ($CaCO_3$, 98% purity) and calcium phosphate ($NH_4H_2PO_4$, purity 99.4%) by wet process. The reaction between the two compounds is stoichiometric with a Ca/P molar ratio of 1.67, and the amount of distilled water added is three times higher than the amount of calcium carbonate. Ca-HA particles synthesis was produced by the ammonium phosphate ($NH_4H_2PO_4$) dissolution in de-ionized water by preliminary stirring (helical ribbon Stainless Steel) of 350rpm for 30 minutes in an open Pyrex® reactor (working volume 1L and inner diameter 10cm). After $NH_4H_2PO_4$ solution has been prepared, calcite was added. The reaction was maintained for 48 hours to ensure homogenization under room conditions of temperature and pressure to obtain Ca-HA$_{Gel}$ as follows:

$$10CaCO_3 + 6NH_4H_2PO_4 \rightarrow Ca_{10}(PO_4)_6(OH)_2 + 10CO_2 + 2H_2O + 6NH_4OH \qquad [R.1]$$
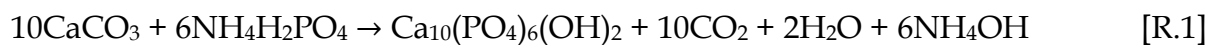
Compounds reaction is accompanied by a release of CO_2 and the Ca-HA product precipitates at a basic pH of 8.3. For example, production of 1kg of Ca-HA, over 438g of CO_2 is released. *Verwilghen et al* (2009) [1] have reviewed that the reaction and maturation time are correlated to temperature. Ca-HA to be characterized was rinsed with distilled water to eliminate unreacted phosphate.
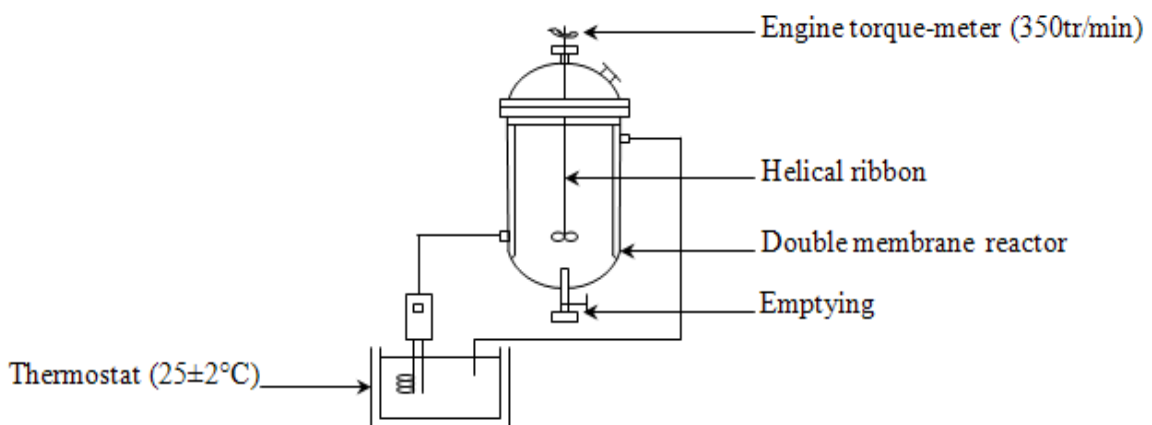
Figure 16: Ca-HA$_{Gel}$ synthesis process

Ca-HA$_{Powder}$ was obtained by drying Ca-HA$_{Gel}$ at temperature of 105±0.5°C during 24 hours in accordance with EN 14346 [2]. **Figure 16** shows the experimental set up developed for the synthesis of Ca-HA$_{Gel}$.

II.   Characterization techniques

1.   Physicochemical properties

1.1.   Helium Pycnometer (bulk mass)

Sample densities were measured using Micrometrics ACCUPYC 1330 helium pycnometer. This kind of pycnometer provides a more accurate determination of density in comparison with the liquid pycnometer (risk of swelling of the material). The principle of this apparatus is based on measuring the volume of sample from a known mass. The sample is introduced into a cell which consists of a sample holder (3.5cm^3 or 1cm^3) and a given volume calibrated chamber. A known sample mass of about 3g is introduced into a cell of 3.5cm^3 inserted into the sample chamber. Helium explores the pores of the material at a pressure, which determines the volume of the vacuum in the sample compared to the pressure in the chamber calibrated. The measurement takes about 30 min and the value of density was obtained after five repetitions of the automated measurement until the results reach indicative average values (g.cm^3).

1.2.   Specific surface area (BET method)

BET method (Brunauer, Emmett and Teller) is a technique for measuring powders specific surface area (S$_s$) by assuming that the adsorption of gases takes place in multimolecular layers. In this thesis, the specific surface area of materials was determined using a device GEMINI (MICROMETRICS). The general principle of the method involves the adsorption of nitrogen at its liquefaction temperature (-196°C) on the surface of a material to be studied by keeping a cell adsorption. A sample mass of about 300mg was introduced into a tube and degassing is carried out for 6 hours at 105°C under vacuum. The sample is subjected to five different pressures of

nitrogen at the temperature of liquid nitrogen. The adsorption isotherm is identified by the nitrogen pressure, which allows deducing the volume of adsorbed gas from the gas pressure P and its saturated vapor pressure P0 and so deducing the specific surface $m^2.g^{-1}$.

1.3.   Particle size distribution

Granular material extent used in this study was determined by a laser particle sizer Mastersizer Hydro 2000-2000 (Malvern Instruments) at size interval of 0.02-2000µm. Determining the sample size using the laser particle size is based on the introduction of particles in ethanol as a dispersant. The suspension is subjected to ultrasonic shacking for one minute and the analysis is performed after stopping ultrasound The suspension is introduced into a cell with a circulation pump. Within the cell, a laser beam passes through the suspension before being projected onto the photodiode measurement result of the interaction between the laser and particles. The results are discussed based on the Mie theory assimilating particles to spheres of equivalent volumes. This method allows the identification of the particle mean diameter compared to a mass percentage. For example, the mean diameter d_{10} corresponding to the particle size whose mass represents 10% of the total mass of the sample. From a geotechnical standpoint, the determination of diameters such as d_{50} (average diameter), d_{60} and d_{30} facilitates the description of the material composition and the determination of physical properties.

2.   Microstructural analysis

Scanning electron microscope (SEM) is used to characterize the morphology and chemical compounds of materials. The apparatus used is Philips XL 30 ESEM FEG. The observations was coupled to EDX chemical microanalysis to analyze the composition of materials. The samples were metalized with gold by vacuum evaporation with sputter coater Polaron Range.

3. Chemical properties

Preparation of solutions for element concentrations analysis in the various materials is a preliminary and important step.

3.1. Mineralization

Mineralization according to NF X31-151 [3] is one of the methods often used in the chemical characterization of material composition. It applies by the dissolution of particles by adding a mixture of hydrochloric acid (HCl) and nitric acid (HNO_3) (aqua regia) with a concentrated ratio (volume) of $HCl/HNO_3 = 3$ (3.75ml of HCl and 1.25ml of HNO_3). The dissolution of particles was done on SCP DigiPREP Jr mineralization device by heating samples on heating block (coated graphite Teflon®) at temperature of 90°C.

3.2. Leaching test

Leaching test standardized method allows the characterization of soluble ionic elements removable by dissolution in contact with a solvent at a given time. The standard for leaching test (EN 12475-2) [4] is widely used for identification of environmental impacts of a raw material. This is a test with a unique batched with a liquid/solid ratio (L/S) of 10; the leaching solution was de-ionized water (100ml) and the solid aggregate of less than 4mm (10g) was used. The contact duration between solid and solvent is 24 hours under rotary stirring of 120rpm at room temperature. After stirring, the suspension was filtered using a filtration system average pore diameter of 0.45mm and analyzed using ICP-AES and ion chromatography. The soluble fraction was determined by drying of about 40ml of eluate solution at 103±2°C filtered at 0.45mm and weighing the dry residue.

3.3. Hydrogen potential (pH) / particle surface charge

Hydrogen potential of the materials was determined using the French standard X31-103 [5]. The principle of pH measurement was based on the dissolution of 10g of

material in 25 ml of de-ionized water by stirring suspension during 60min in an ambient temperature of $20 \pm 5°C$. After stirring, the mixture was left at rest for 2 hours and the measurement was performed using a pH meter.

The charge of the particle surface was characterized by evaluating the pH point of zero charge pH_{pzc}. This is the pH of a material in aqueous solution in a neutral electric potential and its determination is based on electrochemical titration and involves placing $50cm^3$ of NaCl solution (0.01M) as electrolyte in closed vials and adjust initial pH following values between 2 and 12 by adding NaOH or HCl (0.1M). A mass of 0.15g of material was added to each vial (the vials were closed to avoid CO_2 absorption) and final pH was measured after stirring for 48h at room temperature. The value of pH_{pzc} was obtained when initial pH is equal to final pH (the intersection between the bisector curve without adding material and $pH_{final}=f(pH_{initial})$ curve). Mass titrations were carried out by suspending amount of material in 50ml of KNO_3 0.01M solution under N_2 atmosphere at lab temperature. The pH measurements were done after equilibration and pH_{pzc} values were evaluated by plotting the pH as a function of the added amount of material.

3.4. Metal element analysis

Inductively Coupled Plasma (ICP) has been used for metal element analysis. This technique is based on the separation and ionization of atoms by ions in a hot flame (injection into argon plasma), the identification and quantification of ionic elements that constitute a sample is done according to their mass. In this research project, we will focus on the determination of major and minor elements in the eluates liquids such as Al, Ca, Cd, Cr, Cu, Fe, K, Na, Pb, Si and Zn with a detection limit in $mg.l^{-1}$ (ppm or ppb). For sample preparation, 20ml of distilled water are introduced to the leachate. This corresponds to the dilition rate of 3. The apparatus used is our ULTIMA-2 (HORIBA Jobin Yvon).

3.5. Ion analysis

Anion (PO_4^{3-}, SO_4^{2-}, Cl^- and F^-) concentrations in solution was performed using the ionic chromatography (DIONEX ICS 3000 device with a AS19A anion column (4mm) connected to a AG19A pre-column (the self-suppression is provided by a ASRS-II suppressor). The analysis protocol relies on the injection of the solution (prepared by mineralization or leaching) to be analyzed in a 10µl injection loop at a flow rate of 1mL.min^{-1}. The unit is led by a self-generator eluent KOH to a concentration gradient between 18 and 40mmol.l^{-1} for about 23min, to keep the pH constant at 13.

3.6. Loss on ignition (LOI)

Loss on ignition was determined following the EN196-2 standard [6]. Materials calcination was carried out in oxidant atmosphere (air) in an oven at 975±25°C during 24hours by introducing 5.0g of material into alumina crucible. LOI was calculated by mass difference before and after treatment. Water and carbonic gas were eliminated and oxidisable elements eventually present were oxidized.

4. Rheological behavior

The rheological tests were used to determine elasticity and viscosity of the materials. The viscosity and elasticity of the samples were determined using a rheometer. The rheometer used in this study is a Rheo RheoStress RS 150 (Haake). Two kinds of tests were performed, a simple flow testing on the Ca-HA$_{Gel}$ and on all the formulations; and dynamic oscillatory tests for the Ca-HA$_{Gel}$ at different stages of synthesis. The tests were performed by varying the shear rate from 0.01 to 500s^{-1} at a constant temperature of 20±5°C for 300s. The measurement was made after an homogenization by recording three successive tests to ensure the reproducibility of the measurements. As for the tests in oscillatory mode, we set the shear stress at 50 Pa and vary the frequency from 1 to 50Hz at a temperature of 20±5°C during 300s.

5. Zeta potential

Zeta potential (ζ-potential) is an essential parameter for the interpretation of the interactions between particles and the prediction of their stability. The general notion of ζ-potential measurement is summarized in the determination of a potential difference between the boundaries of the diffuse layer. The value of ζ-potential is derived by measuring the electrophoretic mobility μ_e. The assumption made is that the particles are spherical and non-conductive, the charge q of the solvent is considered as a uniform charge. Electrophoretic mobility is based on the electrophoresis technique of measuring the movement of charged particles suspended in a liquid under the influence of an electric field. Electrophoretic mobility μ_e is calculated from the following relationship:

$$\mu_e = \frac{v}{E} \text{ et } E = \frac{U}{L} \quad\quad\quad\quad\quad\quad [Eq.1]$$

With, v is the average velocity of particles (m/s); E is the electric field ($V.m^{-1}$), U is the potential difference (V) and L is the length of the cell (m). The ζ-potential measurements were performed with a micro-electrophoresis apparatus Zetasizer 3000 HSA (Malvern Instruments Ltd). Test samples were dried and the suspension was prepared by the introduction of about 5g of sample mixed in 25ml of distilled water with a syringe in the measuring cell. The apparatus is equipped with a helium-neon laser (He-Ne) of 10mW emitting a polarized light beam of wavelength 633nm, and an avalanche photodiode as a receiver. The electrodes apply an alternating voltage of the suspension in the measuring cell, allowing the movement of particles along a gradient of potential. Particle velocity is evaluated by measuring the temporal fluctuation of the intensity scattered by the particles moving in the network interference (detection of electrophoresis is performed by a laser Doppler).

6.   Thermo-gravimetric analysis (ATG-DSC)

Thermo-gravimetric technique is based on the determination of mass changes of a material due to changes in chemical phases by thermal and physicochemical transformations during heat treatment. It consists in the introduction of a few milligrams of powder sample in the process chamber by keeping in platinum crucibles or alumina. The heat rate used is $20°C.min^{-1}$. The temperature was programmed between ambient and 1000°C. Differential thermal analysis shows the nature of the physical or chemical transformation by quantifying the energy absorbed or released by the material during processing. Thermogravimetric and calorimetric data were collected in a dynamic air atmosphere (flow rate of $10cm^3.min^{-1}$). The apparatus used in this study was SDTQ600 and the masses of samples were of about 20mg.

7.   Phase determination – X-ray diffraction

X-ray diffraction is a basic technique for characterization of mineral phases and crystalline materials. The sample is placed between an X-ray source and detector. The general method involves bombarding the sample with x-rays and watching the X-ray intensity is distributed according to the orientation in space and following the diffractograms between 10 and $80°2\theta$ with a step of counting of $0.02°2\theta$ and a counting time per step of 3s. The detection intensity is recorded as a function of the deflection angle of the beam 2θ. The device used was a SIEMENS D5000 diffractometer (Power 40mA, 45kV, Copper anticathode Cu, K_α (λ = 1.540Å) and a nickel filter to remove the K_β line of Cu).

8.   Raman spectroscopy analysis

The analysis principle of Raman spectroscopy is based on scattering of a laser photon by a sample molecule and loses (or gains) of energy during the process. The amount of energy lost is seen as a change in energy (wavelength) of the irradiating photon. This energy loss is characteristic for a particular bond in the molecule. This technique

can even provide information on physical characteristics such as crystalline phase and atoms orientation. The Raman spectroscopy was used to analyze the Ca-HA under its gel and solid forms, as well as gypsum and plaster for comparison. The analysis method was a punctual analysis where the sample was placed in platinum crucible of 90µl and the analysis was carried out under 400mW external cavity stabilized by Invictus NIR diode laser at 785nm is used for sample illumination by scattering the laser photon.

9.   Infrared Analysis (FTIR: Fourier Transformed Infrared)

Infrared spectroscopy is a characterization technique based on the absorption of infrared rays by the material to be analyzed. The principle is based on the absorption of molecules of a light beam as energy with a wavelength close to their energy vibration. Consequently, the intensity of reflected or transmitted by the molecules decreases. The absorbed energy is illustrated by absorption bands which depend on the electronegativity of atoms and mass. The field of vibrational energy between molecules is 4000 and 400cm^{-1} and the apparatus used is FITR-8400 (SHIMADZU).

References

[1] VERWILGHEN, C., CHKIR., M., RIO, S., NZIHOU, A., SHARROCK, P., DEPERLSENAIRE, G., 2009, Convenient conversion of calcium carbonate to hydroxyapatite at ambient pressure, Materials Sciences and Engineering C29, Pp771-773

[2] EN 14346, December 2006, Characterization of waste — Calculation of dry matter by determination of dry residue or water content

[3] AFNOR, 1993, French standard NF X31-151, *Sols, sédiments, boues de station d'épuration - Mise en solution d'éléments métalliques en traces* (Cd, Co, Cr, Cu, Mn, Ni, Pb, Zn) par attaques acides.

[4] AFNOR, EN 12457-2, 2002, *Characterization of waste – leaching – compliance test for leaching of granular waste materials and sludges*. Part 2. One stage batch test at a liquid to solid ratio of 10 l/kg for materials with particle size below 4 mm, European Standard NF, December 2002.

[5] AFNOR, 1996 NF *X31-103* (1988) Détermination du *pH* dans l'eau - Méthode électrométrique. In Qualité des sols

[6] AFNOR, EN196-2, Avril 2006, Méthodes d'essais des ciments, détermination de la perte au feu

Chapter III
Physicochemical and mineralogical properties of initial materials

This chapter is focused on the characterization of materials by application of different procedures described in chapter II.

Introduction

The first section of this chapter was devoted to the physicochemical characteristics of materials. Morphological characterization gives indications concerning sample structure such as bulk density, specific surface area, particle size and textures. Chemical characterizations may allow identification of chemical nature and chemical environment of elements present in hydroxyapatite and calcium sulfates samples. Surface charge of particles has been studied in detail and results are summarized. Mineralogical properties were investigated by using X-ray diffraction. Raman spectroscopy and Infrared techniques have been used to improve the understanding of the chemical structure; a comparison between methods used is also proposed.

I.   Physicochemical characterization

1.   Bulk density and specific surface area

Table 8 summarizes the various results of physical characterizations. The density of the plaster is slightly greater than that of gypsum and the specific surface area of hydroxyapatite particles is higher. This indicates the reactive capacity to integrate a large number of pollutants. Difference in calcium sulfates specific surface area values can be due to the hydration process that influences particle size.

Table 8: Physical properties of materials

	P_α (Powder)	G (Powder)	Ca-HA (Powder)	Ca-HA(Gel)
Bulk density (g.cm^{-3})	2.81	2.25	2.58	1.23
Specific surface area* (m².g^{-1})	72.81	26.27	138	-

* BET method

From the density of calcium sulfate particles, it is possible to determine the content of gypsum and plaster by volume in the samples compared to the density of pure gypsum and pure plaster (α) (ρ_G = 2.32g.cm^{-3} and ρ_P =2.80g.cm^{-3} respectively) by the following relationships:

$$G = \frac{\rho_G^c - \rho_P}{\rho_G - \rho_P} \text{ and } P = \frac{\rho_P^c - \rho_G}{\rho_P - \rho_G} \hspace{2cm} \text{[Eq.1]}$$

Where ρ_G^c is the measured density of gypsum (g.cm^{-3}) and ρ_P^c is the measured density of plaster (α) (g.cm^{-3}). We found that plaster is partially hydrated; it contains 11% v/v of gypsum. The bulk density of Ca-HA$_{Gel}$ was calculated as a function of volume of powder mass.

2.   Particle size distribution (PSD)

Material PSD was illustrated in **Figure 17**. Materials geotechnical designation allows the texture classification and identification (**Table 9**). The class of grains of plaster and Ca-HA$_{Powder}$ seems to have the silty sand texture and for gypsum particles having a diameter less than 1 mm have a sandy-loam texture. Ca-HA$_{Gel}$ is identified as silty texture.
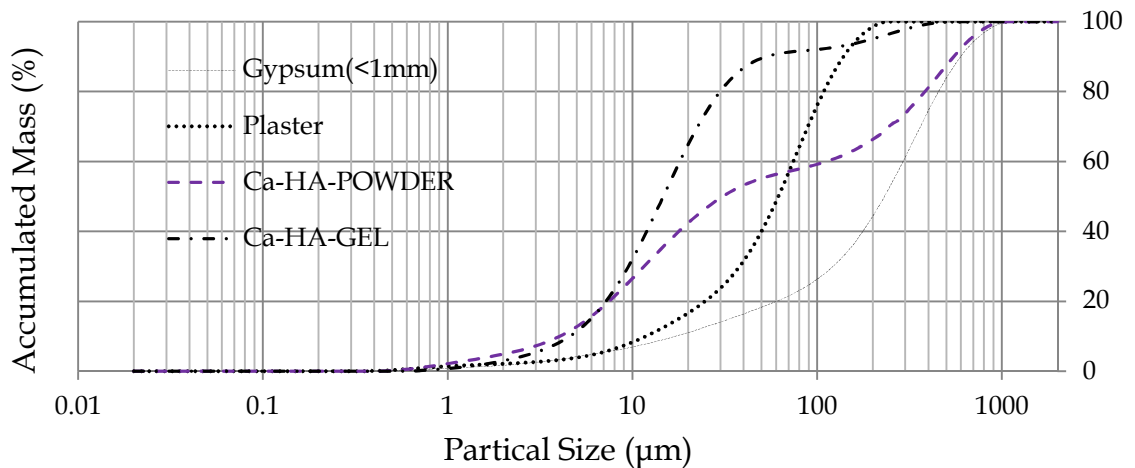
Figure 17: Particle size distribution of gypsum (<1mm), plaster, Ca-HA$_{Powder}$ and Ca-HA$_{Gel}$

Table 9: Granulometric and textural classification

	Granulometric distribution (μm)			Granulometric fraction (%)		
	d(0.1)	d(0.5)	d(0.9)	Sand	Silt	Clay
Gypsum(<1mm)	6.5	27.74	246.59	79.6	18.7	1.7
Plaster(α)	11.86	61.69	138.99	48.9	49.0	2.1
Ca-HA$_{Powder}$	4.05	30.82	548.62	43.4	51.7	4.9
Ca-HA$_{Gel}$	4.59	14.69	52.92	9.0	88.0	3.0

3. Microstructural analysis

Crystalline morphology were identified by Scanning Electron Microscopy (SEM). This section is focused on the description of the microstructure of calcium sulfate α-hemihydrates (plaster), calcium sulfate dihydrate (gypsum) and hydroxyapatite dried and heated at 105°C and 1000°C (10h), respectively. SEM (Energy Dispersion Analysis by X-rays, EDAX) was used to analyze crystalline and morphology of hydroxyapatite particles dried at 105°C. Environmental SEM (ESEM) was exploited to observe the chemical structure of studied materials and morphological data was analyzed conventionally to recorded images. Ca-HA samples were observed indirectly after thermal treatment.

3.1. Plaster microstructure

Crystalline structure of α-plaster is monoclinic with microscopic needle-like crystals. **Figure 18** represents images of calcium sulfate hemihydrates obtained by SEM. Pictures were analyzed at an accelerating voltage of 8 kV and elemental composition was made using EDAX. Calcium sulfate hemihydrates (α) consist of well formed transparent idiomorphic crystals with sharp crystal edges [1]. Scanning electron microscopy pictures illustrated in **Figure 18**, show that α-plaster consists of two forms of crystallographic structures. The first one (**Figure 18**, a) - point A)) is assimilated to flower-like arrangement structured by crystalline sheets interrelated

together to form a spherical geometry. The second one (**Figure 18**, a) - point B)) presents an irregular structure characterized by elongated needle readily cleavable and plate shaped prismatic crystals with variable slenderness that fit around sites of heterogeneous nucleation leading to gypsum crystals entanglement. SEM chemical analysis carried out on plate shaped surface crystals shows the presence of basic compounds and impurities such as strontium.

	Wt(%)	At(%)
C	06.38	12.98
O	28.37	43.34
S	29.48	22.47
Sr	01.87	00.52
Ca	33.91	20.68

Full Scale 1837Cts, Cursor 6.68keV
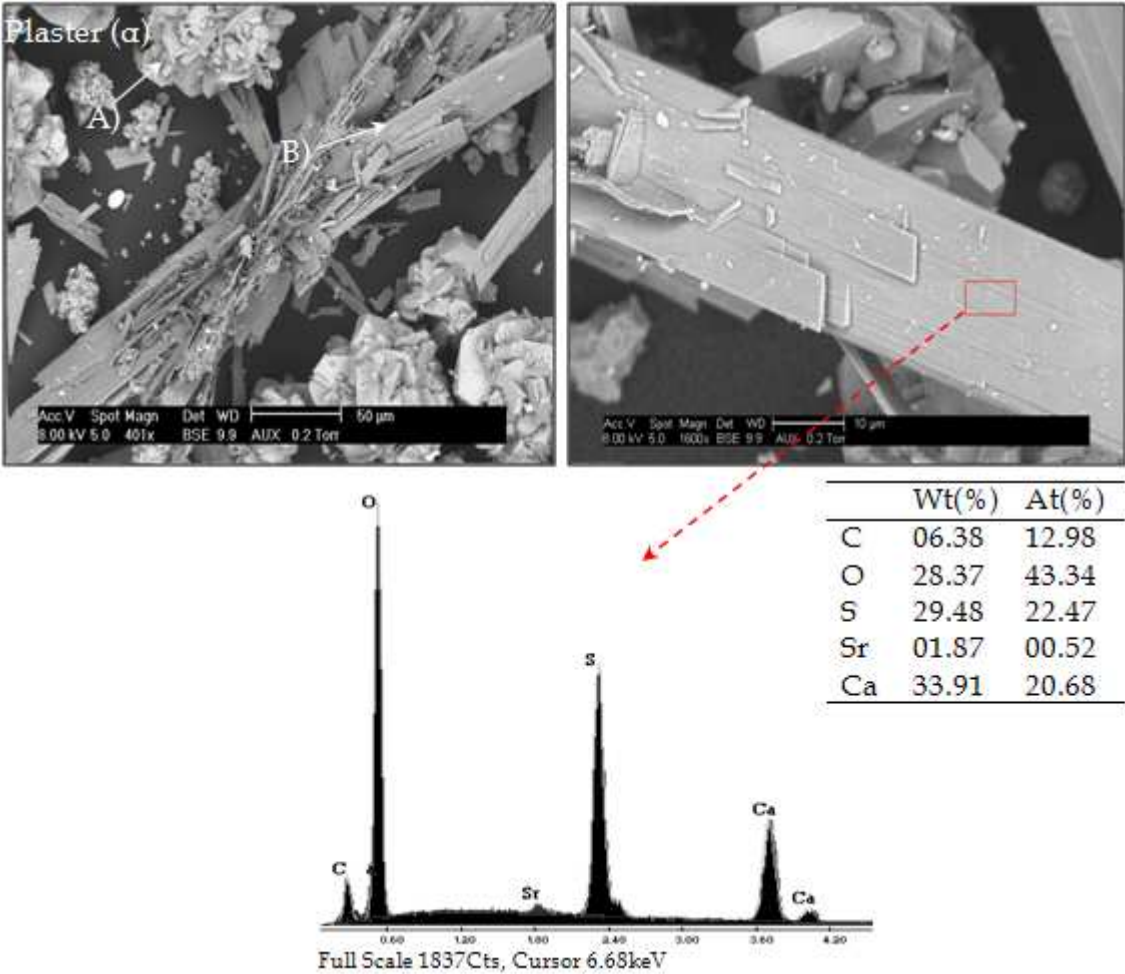
Figure 18 : SEM pictures of plaster (α) (10-50µm)

From EDAX spectra, it can be observed a quite few carbon element coming from organic emulsion on the crystal surface. Atomic Ca/S ratio of plaster is about 0.92, it is the same ratio that have been obtained in the case of gypsum indicating that the calcium sulfates elemental composition is homogeneous.

3.2. Gypsum microstructure

Gypsum contains hydrated particles less than 1mm size consisting of two Ca^{2+}/SO_4^{2-} layers. These layers are bounded by ionic interaction forming growth slice separated by H_2O layers [1]. **Figure 19** represents a SEM analysis of gypsum at an accelerate voltage of 30kV.

	Wt(%)	At(%)
C	30.76	12.98
O	19.81	43.34
S	20.60	22.47
Ca	33.91	20.68

Full Scale 2761Cts, Cursor 18.06keV
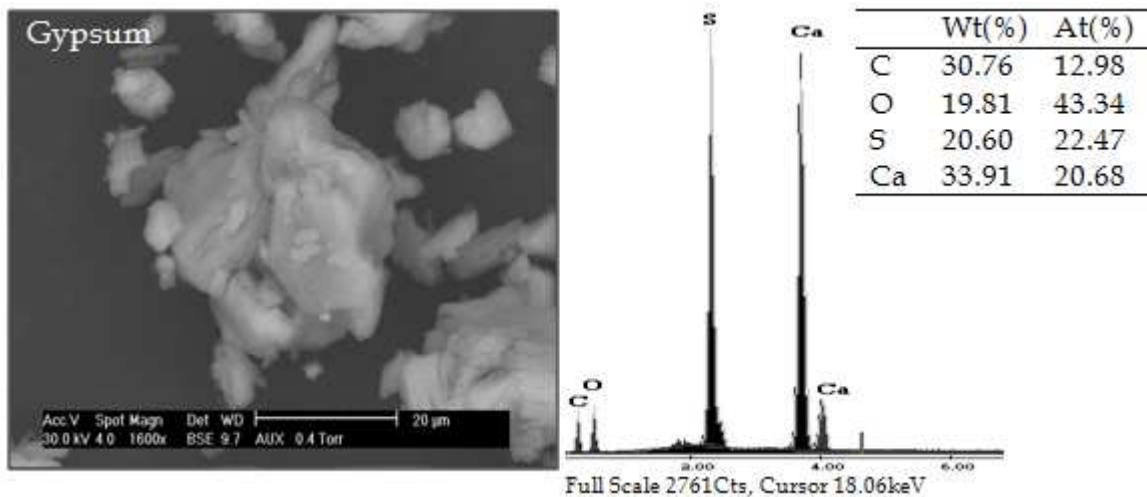
Figure 19 : SEM picture and EDS analysis corresponding to gypsum (<1mm) (20µm)

From **Figure 19**, the disappearance of crystalline needle shape can be observed, this can be explained by dissolution of crystals due to the second filtration according to HP2 process (Chapter IV, § I.1. Calcium sulfate). Gypsum particles behave as massive deposit and have a roughly spherical morphology which clusters together into large units.

3.3. Ca-HA microstructure

Morphology of Ca-HA particles is pseudo-spherical. SEM analysis were carried out by applying an accelerating voltage of 20kV. **Figures 20** and **21** show microstructure of Ca-HA dried at 105°C for 24h. SEM picture obtained at 2µm provides that Ca-HA particle are recovered by superimposed crystalline layers as can be seen through **Figure 20** b).
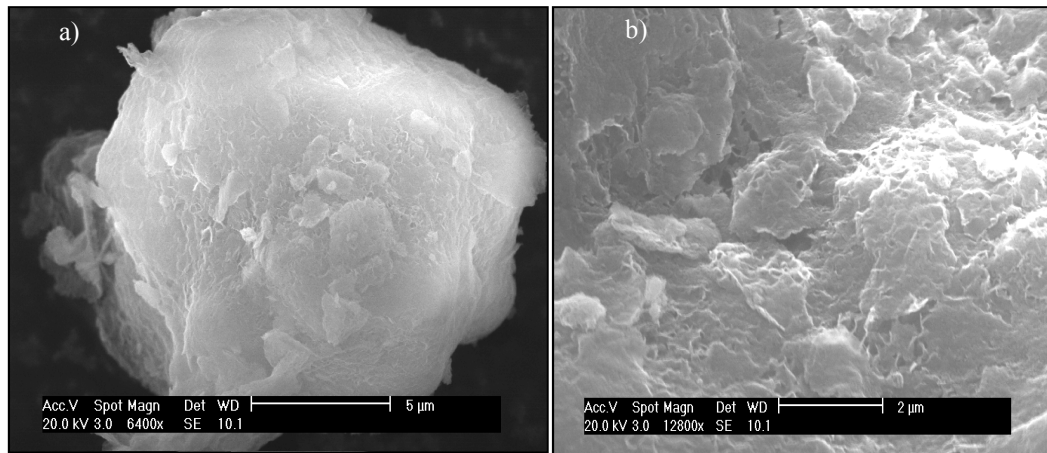
Figure 20: SEM images of Ca-HA dried at 105°C for 24h

	Wt(%)	At(%)
C	13.00	25.27
O	23.53	34.34
P	19.94	15.03
Ca	43.53	25.36

Full Scale 1891Cts, Cursor 9.09keV
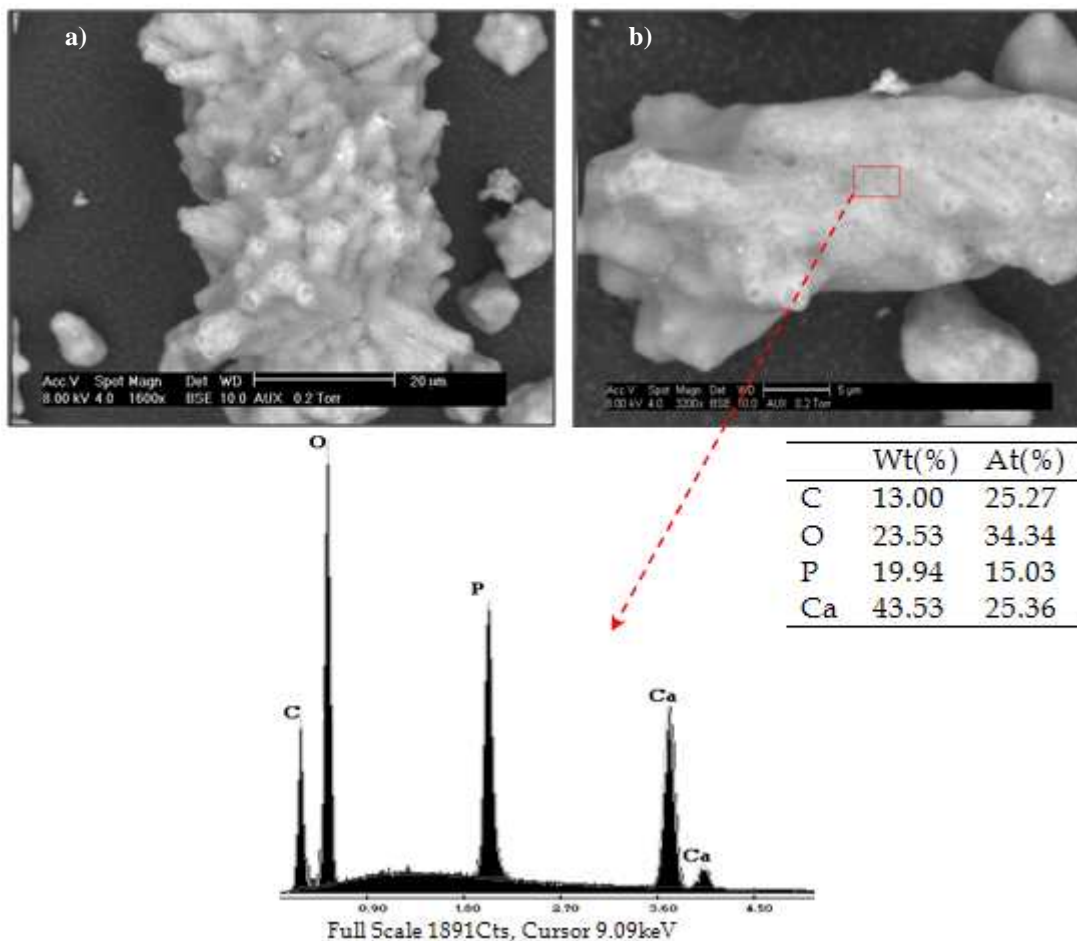
Figure 21 : ESEM of Ca-HA dried at 105°C (5-20µm)

Figure 21 and **22** illustrate both dried and calcined Ca-HA recorded using SEM and environmental SEM. The pictures show that the surface texture of calcined Ca-HA is rough as can be seen in **Figure 22** a). Environmental SEM analysis of Ca-HA particles

reveals a structure characterized by a porous cylindrical structure. Pores are distributed on surface with different slenderness. Comparing SEM micrograph of Ca-HA dried at 105°C (**Figure 21** a)) and that of Ca-HA calcined at 1000°C (**Figure 22** a)), change in the surface of Ca-HA particles due to the high temperature treatment can be observed. Analysis by Environmental SEM has revealed the porous structure of calcined Ca-HA (**Figure 22** b)). EDS surface chemical analysis marked in red illustrated in **Figures 21** and **22** showed that the major elements for both Ca-HA dried and/or calcined were Ca, P, C and O and Ca/P molar ratio is around 1.68 and 1.61 respectively.

	Wt(%)	At(%)
C	10.83	20.93
O	27.61	40.04
P	19.94	14.93
Ca	41.63	24.10

Full Scale 2363Cts, Cursor 9.09keV
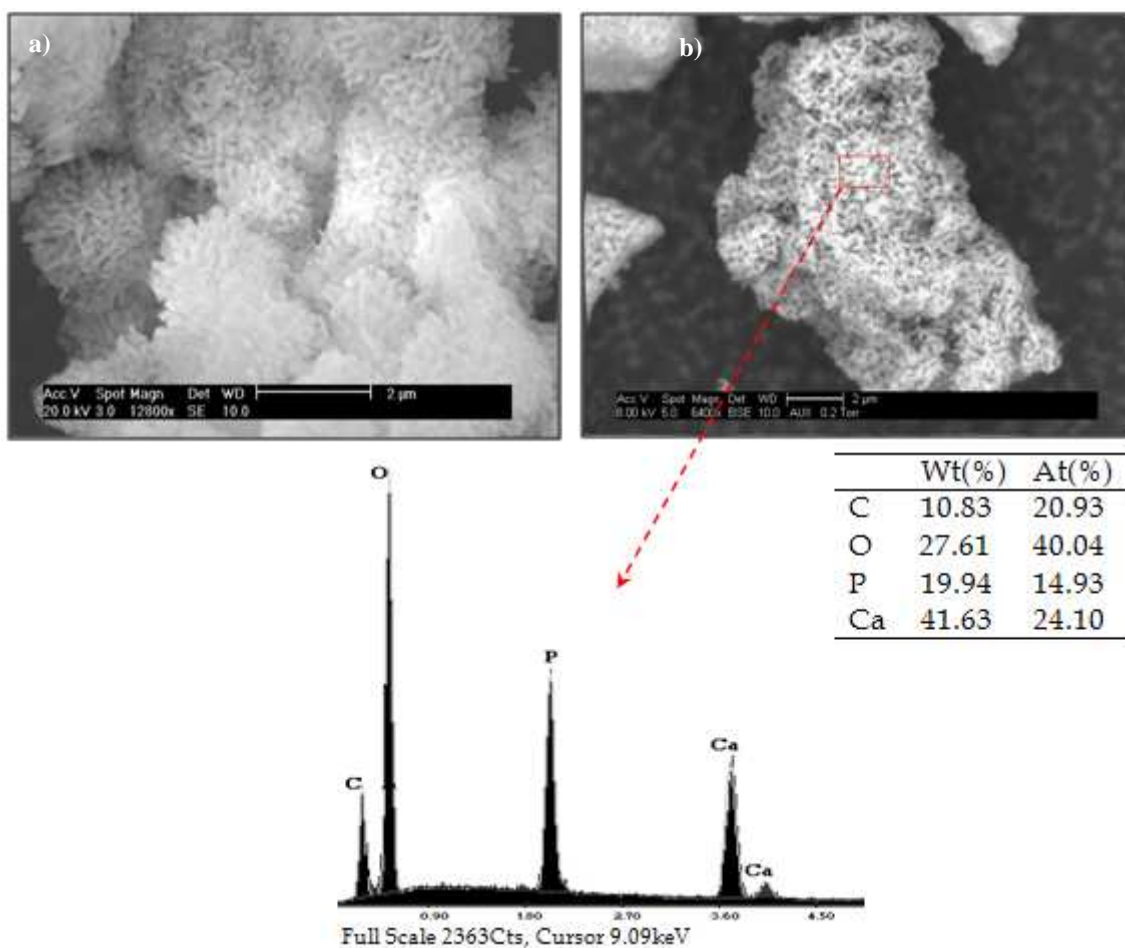
Figure 22 : ESEM micrograph of Ca-HA particles calcined at 1000°C from 10h and the respective Energy Dispersion Spectroscopy (EDS) spectrum

EDS analysis of calcined Ca-HA corroborate the results of Ca/P stochiometric ratio obtained by ICP as discussed in the second section (II. Chemical properties). It

should be noted that the EDS chemical analysis depends on the analyzed surface and Ca/P molar ratio that may change by changing the surface topography.

II.   Chemical properties

1.   Elemental analysis

The chemical analysis of materials done using ICP-AES and ion chromatography showed that calcium sulfates contain non-negligible amounts of ores basic heavy metals. Plaster pH is very acidic (pH=2.88). This is due to the high amount of leached phosphorus (15%) in the solution, which provides an indication of the presence of a phosphoric acid fraction in leached solution. Ca/P stochiometric ratio was assessed for Ca-HA dried and calcined, and results are listed in **Table 10**. For both dried and calcined Ca-HA, Ca/P ratio is about 2.27 and 2.07, respectively, indicating that the Ca-HA synthesized is apatitic with calcium excess since the obtained values are higher than the stoichiometric rate of Ca/P = 1.67.

Table 10: Ca/P ratio of dried and calcined Ca-HA

	Ca-HA dried at 105°C for 24 hours			Ca-HA calcined at 1000°C for 10h		
Ca/P ratio	2.25	2.28	2.28	2.07	2.08	2.07
Average	2.27±0.02			2.07±0.01		

The main difference between dried and calcined Ca-HA was that the later showed higher Ca/P ratio than the dried Ca-HA. The Ca/P molar ratio remains approximately constant when Ca-HA was calcined at 1000°C for 10 hours. The calcination of Ca-HA transforms the calcium phosphate phases from amorphous to crystalline. **Figure 23** presents the Ca/P molar ratio in function of time and pH. The Ca/P molar ratio was followed during 6 months after Ca-HA synthesis. After 48h, Ca/P molar ratio is 2.4. The maturation time influence on the Ca-HA synthesis without stirring.
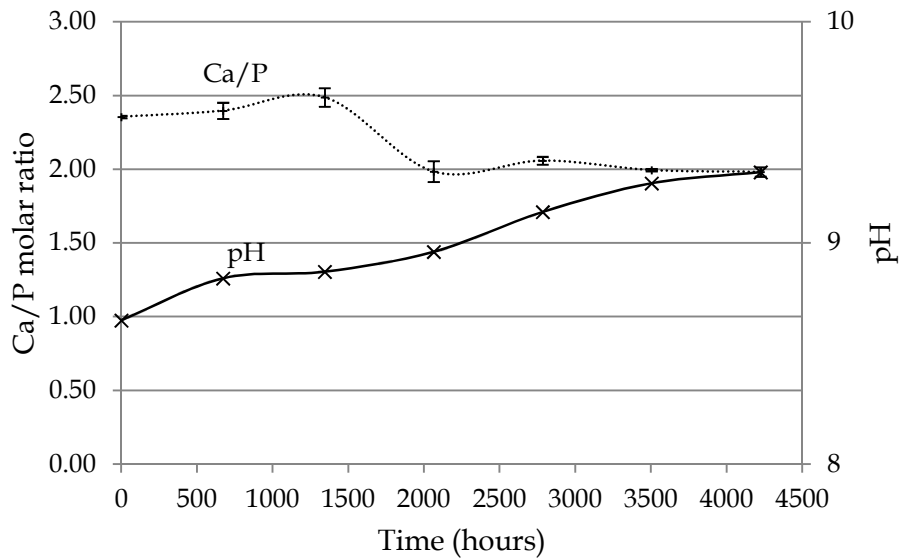
Figure 23: Maturation of Ca-HA after 48h of synthesis

The decrease of Ca/P molar ratio versus of time indicates that the apatitic Ca-HA synthesis reaction continues. The Ca/P molar ratio decreases as pH increases (**Figure 23**). The increase in pH justifies the precipitation of calcium phosphate phases.

Gypsum pH is basic (pH=8.44). Hydration that fixes 1.5 of constitution water molecules, is the main cause of the basicity indicating the presence of precipitated alkalis such as hydroxides and carbonates. Hydroxyapatite pH is basic, 7.85 and 8.41 for Ca-HA$_{Powder}$ and Ca-HA$_{Gel}$, respectively. The difference in Ca-HA-pH values can be attributed to the preparation procedure of powder, and pH value of gel is related to the presence of unreacted phosphate. The Point of Zero Charge (PZC) was assessed by titration as previously described (Chapter IV, § II-1-1.3). **Figure 24** represents the titration curves of the particles of calcium sulfate (gypsum plaster) and hydroxyapatite powder.
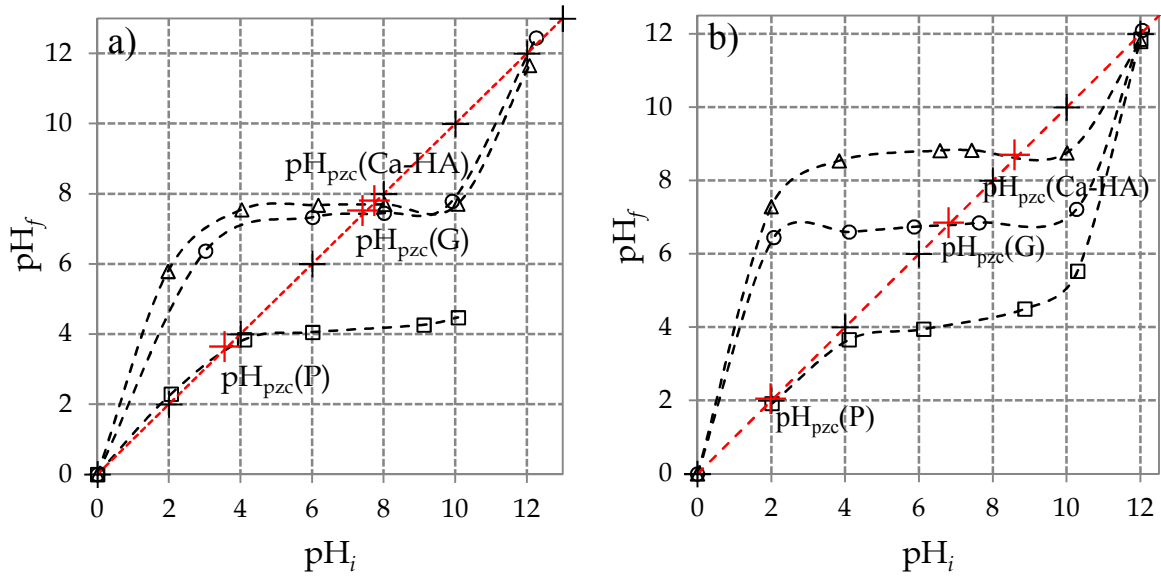
Figure 24: Hydrogen potential at point of zero charge of different materials, a) NaCl 0.01M as supporting electrolyte, b) KNO₃ 0.01M as supporting electrolyte, (--+-- bisectrix curve (pH$_i$=pH$_f$), --□-- Plaster, --○-- Gypsum, --Δ-- Hydroxyapatite)

As shown in **Figure 24**, the pH at the end of the titration increases by increasing initial adjusted pH of supporting electrolyte (NaCl 0.01M solution). The interest to determine pH at point zero charge (pH$_{pzc}$) was to evaluate the net neutral surface charge of particles. Hydroxyapatite and gypsum are characterized by a pH region (natural equilibrium pH) approximately between 6 and 10 where the final measured pH remained constant. The stabilization of pH is related especially to H⁺ consumption due to dissolution reaction and to neutralization effects. At lower initial pH values (below *pre-neutralization region)* a sharp increase of final measured pH was observed. The increase in pH is due to the sharp decrease of H⁺ ions which reacts with the dissolved ions in the bulk solution. In fact, H⁺ consumption results particularly to the enrichment of particle surface due to adsorption-fixation revealing a positively charged surface. For pH values above 10, final measured pH indicating the deprotonation of hydroxyapatite and gypsum particles accompanied by H⁺ release (i.e. pH decrease shows the presence of OH⁻ on the surface with release of H⁺).

Plaster has shown a particular case; not characterized by a neutralization region, this can be directly related to the presence of phosphorous compounds which tend to acidify the suspension. Through **Figure 24**, pH$_{pzc}$ corresponds to the intersection of

bisector straight line with titration curves. The pH_{pzc} values of hydroxyapatite, gypsum and plaster were estimated equal to 7.6, 7.4 and 3.4, respectively, when using NaCl as supporting electrolyte. The acid-base properties in case of KNO_3 selection as supporting electrolyte of materials were investigated at lab conditions. The PZC of plaster, gypsum and Ca-HA are about 2.0, 6.8 and 8.6, respectively. Those results may be interpreted by the fact that the surface of hydroxyapatite and gypsum particles was protonated leading to H^+ ions adsorption. Point zero charge of hydroxyapatite changes by changing supporting electrolyte solution. Surface exchange of Ca^{2+} by Na^+ does not cause any surface charge modification leading to pH_{pzc} lowering. Surface of gypsum and plaster particles are negatively charged as $pH<pH_{pzc}$, in the other side, hydroxyapatite surface is positively charged as though $pH>pH_{pzc}$.
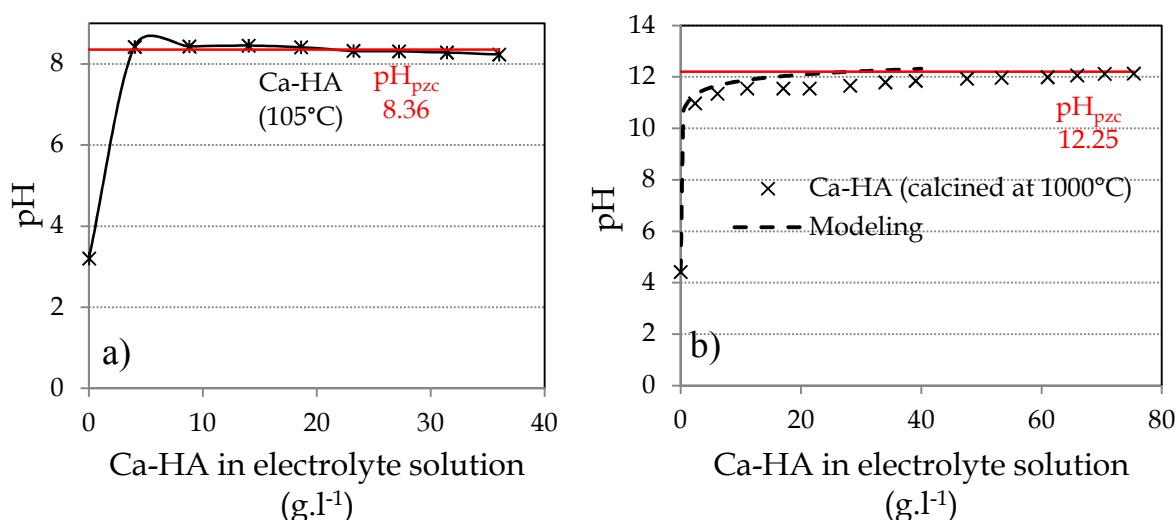
Figure 25: pH as a function of the added amount of Ca-HA (KNO_3 0.01M as supporting electrolyte), a) case of dried Ca-HA (105°C), b) case of calcined Ca-HA (1000°C), **– – –** Modeling was assessed by PHREEQC code software using stochiometric hydroxyapatite ($Ca_5(PO_4)_3OH$).

The substitution of Ca^{2+} by Na^+ on the particle surfaces (in the supporting electrolyte bulk solution) can be considered the main cause of the surface charge. Adsorption of H^+ and Ca^{2+} substitution lead to the formation of species such as HPO_4^{2-} and $NaHPO_4^-$ following the hydrolytic reactions described below. Bell et al. (1973) have reported that the point zero charge of synthesized hydroxyapatite is about 8.5 using

titration method and PZC value is unaffected by the surface area. This result is in accordance with (Ca-HA)-PZC value obtained in this study.

Figure 25 shows titration curves of Ca-HA, gypsum and plaster particles. Ca-HA particles in electrolyte solution are not influenced by added H^+ when pH ranges from 6 to 10. Dissolution and hydrolytic reactions occurring in Ca-HA particle suspension electrolyte aqueous solutions, i.e. NaCl or KNO_3 (0.01M) are as follows:

$$Ca_5(PO_4)_3(OH) \leftrightarrow 5Ca^{2+} + 3PO_4^{3-} + OH^- \qquad [R.1]$$

$$Ca^{2+} + OH^- \leftrightarrow CaOH^+ \qquad [R.2]$$

$$CaOH^+ + OH^- \leftrightarrow Ca(OH)_{2(aq)} \qquad [R.3]$$

$$Ca^{2+} + PO_4^{3-} + 2H^+ \leftrightarrow CaH_2PO_4^+ \qquad [R.4]$$

$$Ca^{2+} + PO_4^{3-} + H^+ \leftrightarrow CaHPO_4 \qquad [R.5]$$

$$Ca^{2+} + PO_4^{3-} \leftrightarrow CaPO_4^- \qquad [R.6]$$

$$Na^+ + PO_4^{3-} \leftrightarrow NaPO_4^{2-} \qquad [R.7]$$

$$Na^+ + PO_4^{3-} + H^+ \leftrightarrow NaHPO_4^- \qquad [R.8]$$

$$Na^+ + PO_4^{3-} + 2H^+ \leftrightarrow NaH_2PO_4 \qquad [R.9]$$

$$K^+ + PO_4^{3-} \leftrightarrow KPO_4^{2-} \qquad [R.10]$$

$$K^+ + PO_4^{3-} + H^+ \leftrightarrow KHPO_4^- \qquad [R.11]$$

$$K^+ + PO_4^{3-} + 2H^+ \leftrightarrow KH_2PO_4 \qquad [R.12]$$

$$PO_4^{3-} + H^+ \leftrightarrow HPO_4^{2-} \qquad [R.13]$$

$$PO_4^{3-} + 2H^+ \leftrightarrow H_2PO_4^- \qquad [R.14]$$

$$PO_4^{3-} + 3H^+ \leftrightarrow H_3PO_4 \qquad [R.15]$$
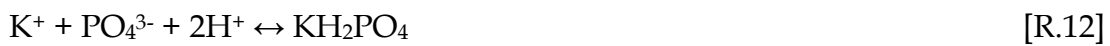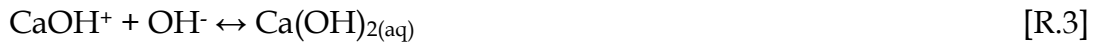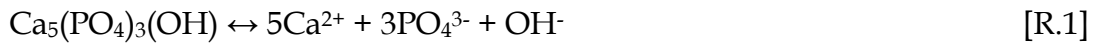
Skartsila et al (2007) [3] have reported that it is possible to quantify the number of H^+ ions reacted noted henceforth $H^+_{dissolution}$ with the dissolved species in the bulk supporting electrolyte KNO_3 0.01 M solution from reactions [R. 1], [R. 2], [R. 4], [R. 5] and equilibria for [R. 11] to [R. 15]. Through reactions, calculation of $H^+_{dissolution}$ may be performed by summing the number of H^+[R.4, R.5, R.(11-15)] ions consumed for the formation of $CaH_2PO_4^+$, $CaHPO_4$, $H_2PO_4^-$ and H_3PO_4, H^+[R.2] ions consumed for the neutralization of the OH^- ions released from the dissolution of the $CaOH^+$ species

and $H^+_{[1]}$ ions consumed for the neutralization of the OH^- ions released in the bulk solution in the case of dissolution of hydroxyapatite. Determination of all H^+ ions consumed requires a good identification of species at the equilibrium and can be calculated by the following relationships [3]:

$$H^+_{[R.1]} = 1/5 \, (C_{Ca_t,f} - C_{Ca_t,in})V \qquad \text{[Eq. 2]}$$

$$H^+_{[R.2]} = (C_{CaOH+,in} - C_{CaOH+,f})V \qquad \text{[Eq. 3]}$$

$$H^+_{[R.4, R.5, R.(11-15)]} = \sum_i (C_{i,f} - C_{i,in})V.y_i \qquad \text{[Eq. 4]}$$

Where $C_{Ca_t,f}$ is the final concentration of calcium at equilibrium, $C_{Ca_t,in}$ is the initial concentration of calcium, V and y_i are the volume of the suspension and the stoichiometric coefficient of H^+ at the respective equilibrium. From results showed in **Figure 25** of dried and calcined hydroxyapatite mass titration, we have found that the obtained pH_{pzc} values are different. This can be explained by the fact that Ca-HA dried at 105°C contains amounts of non-apatitic phases such as Brushite ($CaHPO_4.2H_2O$) and Monetite ($CaHPO_4$); precipitation of acidic calcium phosphates is considered the major mechanism that influences the Ca-HA surface and then neutral charge value modification. Ca-HA heated at 1000°C corresponds to stable apatitic structure with Ca/P=1.67 ratio characterized by high pH value that can reach 12.10. A Phreeqc model can have been used to explain the experimental value of PZC obtained. The model allows the calculation of pH in function of added amount of stochiometric Ca-HA. The model gives 12.25 as PZC value corresponding to pH stabilization. Higher pH values prove the absence of species like H_3PO_4, $H_2PO_4^-$ and non-apatitic phases content are negligible. It seems probable that the release of H+ indicates only pure hydroxyapatite precipitation. In this case, number of $H^+_{dissolution}$ can be concluded from relationships 2 and 3.
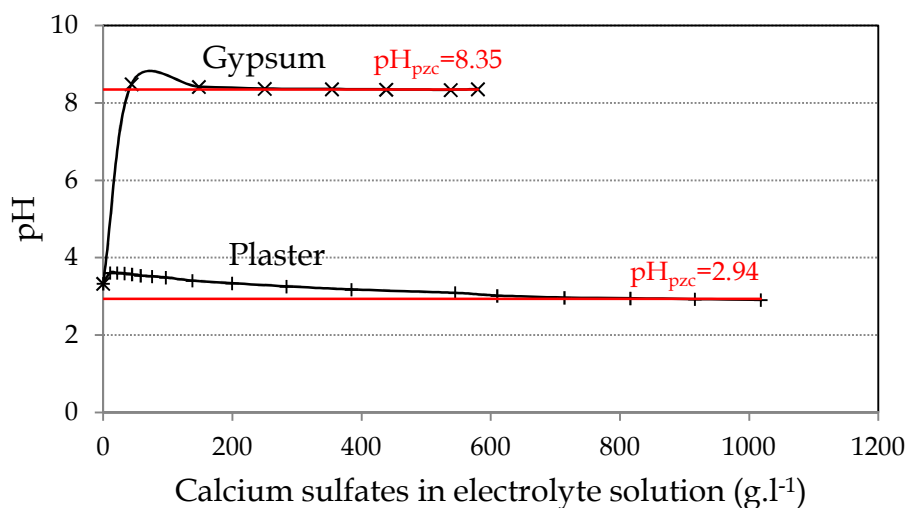
Figure 26: The pH as a function of the added amount of gypsum and plaster (KNO_3 0.01M as supporting electrolyte)

Figure 26 represents PZC values of gypsum and plaster obtained by mass titration method. PZC values correspond to the plateau where pH was remained constant. Mass titration reveals that pH_{pzc} of gypsum is about 8.35 and pH_{pzc} of plaster is 2.94. Dissolution and hydrolytic reactions occurring in gypsum suspension in supporting electrolyte (NaOH or KNO_3 0.01M) aqueous solutions are as follows:

$$CaSO_4.0.5H_2O \leftrightarrow Ca^{2+} + SO_4^{2-} + 0.5H_2O \qquad [R.20]$$

$$CaSO_4.2H_2O \leftrightarrow Ca^{2+} + SO_4^{2-} + 2H_2O \qquad [R.21]$$

$$SO_4^{2-} + H^+ \leftrightarrow HSO_4^- \qquad [R.22]$$

$$SO_4^{2-} + 2H^+ \leftrightarrow H_2SO_4 \qquad [R.23]$$

$$Na^+ + SO_4^{2-} \leftrightarrow NaSO_4^- \qquad [R.24]$$

$$K^+ + SO_4^{2-} \leftrightarrow KSO_4^- \qquad [R.25]$$
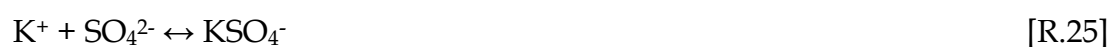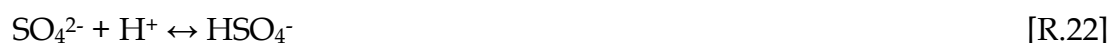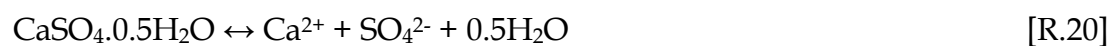
The point zero charge values are different in analyzed material and could be correlated to the nature of supporting electrolyte and solid purity. **Table 11** summarizes PZC values of Ca-HA, plaster and gypsum and those obtained in literature.

Table 11: PZC values of materials

Material	Supporting electrolyte	Equilibration time (hr)	PZC	PZC (MT)
Ca-HA	NaCl	48	7.6	-
	KNO$_3$	48	8.6	8.36[a], 12.30[b]
Gypsum	NaCl	48	7.4	-
	KNO$_3$	48	6.8	8.35
Plaster	NaCl	48	3.4	-
	KNO$_3$	48	2.0	2.94

[a] Ca-HA dried at 105°C for 24h, [b] Ca-HA calcined at 1000°C for 10h, MT mass titration

Table 12: Carbon amount in Ca-HA, gypsum and plaster (g)

	Total carbon (TC)	Inorganic carbon (IC)
Ca-HA*	1.29±0.06	1.28±0.03
Gypsum	n.d	n.d
Plaster (α)	n.d	n.d

* Dried at 105°C for 24h, n.d non-detected

Table 12 summarizes total carbon (TC) and inorganic carbon (IC) present in calcium sulfate material and in Ca-HA$_{Powder}$. Obtained results prove the absence of carbon in both calcium surface structures, even ATG-DSC analysis discussed later justifies these results.

1.1. Composition of calcium sulfates

Plaster and gypsum wastes mineralization reveal the presence of a significant amount of heavy metals. **Table 13** summarizes the anionic metals occurring in plaster and gypsum by-product. The total amounts of sulfate present in plaster and gypsum are 73% and 70% respectively in regards to the total mass. The total amounts of phosphate present in plaster and gypsum are similar and do not exceed 1.2%. **Table 14** tabulates the cationic elements present in plaster and gypsum wastes. The alkaline elements (Al, Ca, Fe, K, Mg and Na) present in plaster and gypsum samples have a total percentage amount of 32.42% and 39.02% respectively. The total minor elements (Cd, Cr, Cu, Pb and Zn) represents 3.19% and 2.79% regarding to the

elements presents in gypsum and plaster respectively. The percentage of Ba, Ni and Sr in gypsum and plaster is higher than 2%. These metals may be present in the gypsum as Barite ($BaSO_4$), Celestine ($SrSO_4$) and Nickel sulfate ($NiSO_4.6H_2O$).

Table 13: Anionic metals present in calcium sulfates by-product

	Hemihydrated calcium sulfate (Plaster)	Dihydrated calcium sulfate (Gypsum)
Elements	mg.kg^{-1}	mg.kg^{-1}
SO_4^{2-}	766237	846295
PO_4^{3-}	11600	14022

Table 14: Elementary composition analysis of both industrial calcium sulfates

Elements	Hemihydrated calcium sulfate (Plaster) mg.kg^{-1}	(%)	Dihydrated calcium sulfate (Gypsum) mg.kg^{-1}	(%)
Al	5055±110	0.95	4984±81	0.78
As	14±8	0.00	64±7	0.01
Ba	31304±481	5.88	30824±299	4.85
Ca	134772±25569	25.33	214543±2151	33.75
Cd	3810±149	0.72	3956±84	0.62
Co	5021±197	0.94	5222±105	0.82
Cr	4714±168	0.89	4977±100	0.78
Cu	2102±97	0.40	2188±42	0.34
Fe	5119±116	0.96	5627±111	0.89
K	6772±372	1.27	7016±117	1.10
Mg	15978±14152	3.00	10706±134	1.68
Mn	5137±202	0.97	5332±111	0.84
Na	4840±406	0.91	5242±1829	0.82
Ni	14229±470	2.67	15455±316	2.43
P	3783±81	0.71	4573±26	0.72
Pb	2442±104	0.46	2691±51	0.42
S	255752±17860	48.07	282474±4852	44.43
Sb	25±15	0.00	84±8	0.01

Se	515±36	0.10		696±22	0.11	
Si	129±27	0.02		746±300	0.12	
Sr	26571±2822	4.99		24269±4437	3.82	
V	52±10	0.01		79±7	0.01	
Zn	3849±128	0.72		3994±83	0.63	
Total	531995	100.00		635752	100.00	

1.2. Leaching analysis (French standard)

The leaching tests were carried out according to European standard EN 12457-2 [4]. Leached quantity obtained by extraction after 48 hours was analyzed using ICP-AES. Therefore, leached samples were compared to thresholds of waste acceptance criteria (WAC) summarized in Appendix 3. **Table 15** presents the results during the leaching test of calcium sulfates by-products (Gypsum and Plaster). Solubility products of plaster and gypsum are $K_{Plaster}=6.22\times10^{-4}$, $K_{Gypsum}=2.0\times10^{-3}$ respectively. The plaster leaching test reveals that the Pb amount is very high comparing to the WAC. The leaching test carried out on gypsum shows that the behavior of Cadmium, Nickel, Antimony and Selenium are hazardous.

Table 15: Amount of leached elements from gypsum and plaster according to EN 12457-2 standard

	Gypsum <1mm			Plaster		
Elements	mg.kg^{-1}	(%)	Rate of release (%)	mg.kg^{-1}	(%)	Rate of release (%)
Al	98±3	0.54	1.97	574±1	2.75	11.36
As	18±0	0.06	28.64	10±0	0.05	70.20
Ba	25±0	0.07	0.08	3±0	0.01	0.01
Ca	6754±345	48.99	3.15	8939±28	42.85	6.63
Cd	33±0	0.08	0.85	2±0	0.01	0.06
Co	34±0	0.07	0.67	N.A	—	—
Cr	38±0	0.11	0.78	3±0	0.02	0.07

Cu	48±0	0.10	2.22	2±0	0.01	0.06
Fe	40±0	0.07	0.72	9±0	0.05	0.45
K	440±9	1.40	6.28	244±0	1.17	3.62
Mg	122±1	0.19	1.15	85±0	0.41	0.54
Mn	40±0	0.11	0.75	N.A	—	—
Na	1040±42	6.07	19.85	1077±3	5.16	22.25
Ni	100±0	0.09	0.65	0±0	0.00	0.00
P	40±1	0.18	0.89	1528±4	7.33	40.40
Pb	28±3	0.56	1.06	61±0	0.29	2.51
S	14670±278	39.45	5.19	7959±25	38.15	3.11
Sb	21±1	0.14	25.52	2±0	0.01	10.09
Se	51±0	0.12	7.35	9±0	0.05	1.87
Si	21±4	0.65	2.86	95±0	0.46	73.26
Sr	312±5	0.76	1.29	243±0	1.17	0.92
V	5±0	0.06	7.42	N.A	—	—
Zn	33±0	0.11	0.85	4±0	0.02	0.12
Total	24025	100	120	20797	100	247

III. Mineralogical analysis

1. TG-DSC

Thermogravimetric analysis (TGA) was intended to quantify the content of impurity, gypsum, and plaster in industrial calcium sulfate samples during treatment process, and to evaluate the mass loss due to dehydration of hydroxyapatite particles (dried at 105°C for 24 h). Differential scanning calorimetry (DSC) allowed the identification of thermal transition of materials. Heating treatments were performed at 5°C.min^{-1} from ambient temperature to 1000°C in air with flow rate of 100cm^3.min^{-1}. Residual moisture present in calcium sulfates products are about 5.0 and 20.0% in plaster and gypsum respectively. **Figure 27** shows the heat flow versus temperature. Platinum crucibles (90µl) were used and calcium sulfate samples were introduced as received

without prior treatment using sample of 32.098mg, 34.344mg and 19.012mg of gypsum, plaster and hydroxyapatite, respectively.
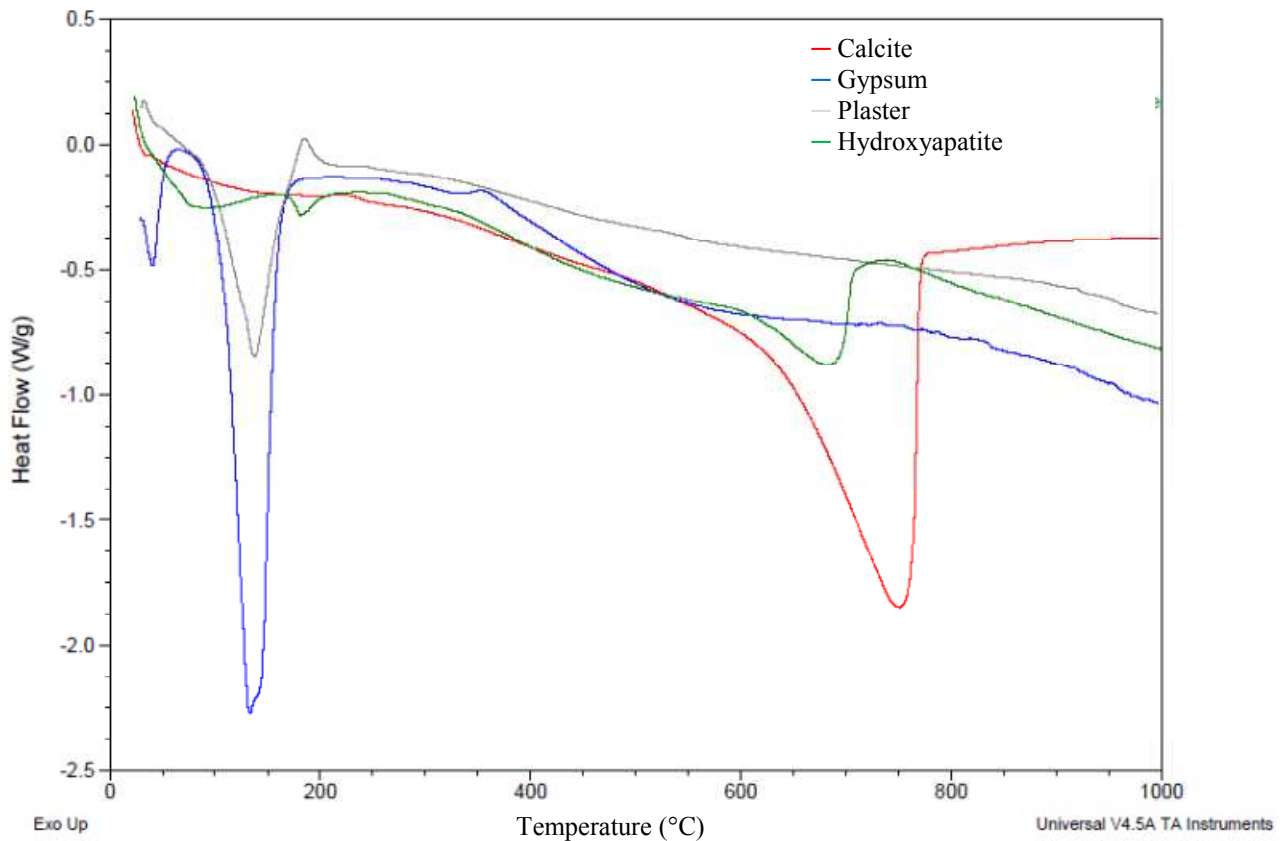
Figure 27 : Differential scanning calorimetry of calcite, gypsum, plaster and Ca-HA$_{Powder}$

The DSC curves (**Figure 27**) for the dehydration of gypsum show two peaks, the first one is located at ≈60°C due to initial gypsum transformation, the second endothermic peack is observed at 133.02°C indicating gypsum dehydration. Gypsum transformation begins at ~60°C with apparition of a very small quantity of hemihydrates ($CaSO_4.0.5H_2O$) which corresponds to the mass loss of 1.23mg of water molecules. At 180°C, the amount of hemihydrates increases and is accompanied by anhydrite apparition. Above 200°C, anhydrite mass seems to be constant, as it can be seen from **Figure 28**.
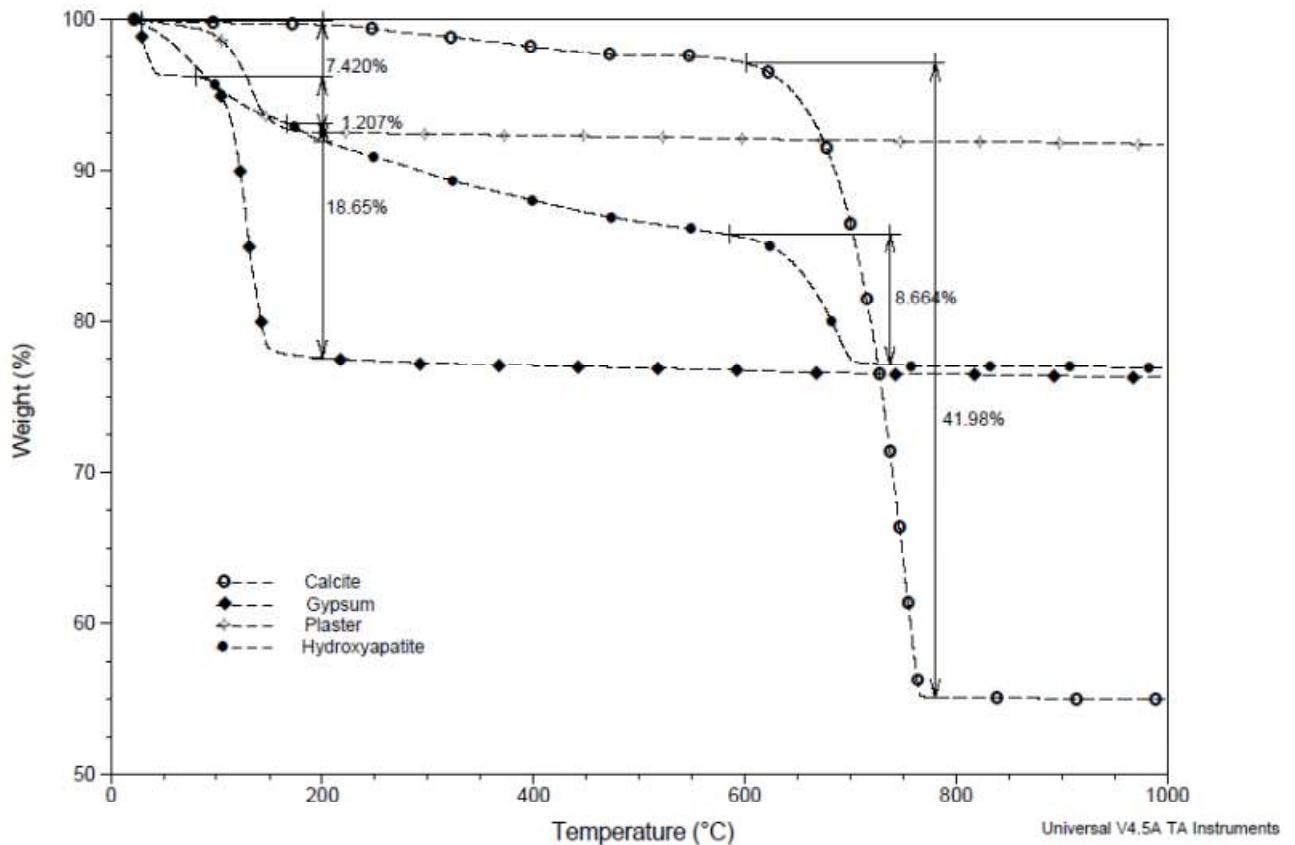
Figure 28: Thermogravimetric analysis of calcite, gypsum, plaster (α) and Ca-HA$_{Powder}$

Industrial gypsum product is characterized by a dehydration heat of 987.8J.g^{-1} concluded from the gypsum DSC curve. Studies by Hudson-Lamb et al. (1996) have investigated that the heat of dehydration of natural gypsum is 147-205J.g^{-1} and 394-500J.g^{-1} for pure calcium sulfate dihydrate. Difference in heat of dehydration values obtained in the present study is higher than those reported by *Hudson-Lamb* [5]. This can be explained by the presence of a non negligible amount of impurities in gypsum. Plaster DSC pattern exhibits that particles belong to α-form, this can be highlighted by the fact that the presence of the endothermic peak at 137.52°C (544.2J.g^{-1}) followed by an exothermic peak at 184.70°C. **Figure 28** illustrates the mass loss of samples after heat treatment (5°C.min^{-1}. 0-1000°C). For calcium sulfate samples, the mass loss describes the change in the structure due to the extraction of crystal water molecules at the beginning of the heat treatment. In addition, the transformation of dihydrated particles to anhydrite is correlated to the mass loss of 18.7% at a temperature of ≈200°C; and the transformation of hemihydrated particles

to anhydrite is characterized by a mass loss of 7.4%. Natural gypsum is characterized by a mass loss of 7.39% and the mean weight loss for calcium sulfate dihydrate is 19.2% [5], and calcium sulfates mass loss obtained in this work are in accordance.

In general, gypsum dehydration proceeds via two mass loss stages. The first mass loss (ML_1) is a partial dehydration of a small amount of gypsum leading to hemihydrates formation. The second mass loss (ML_2) corresponds to the complete dehydration of plaster according to the following stoichiometric endothermic reactions:

$$CaSO_4.2H_2O \xrightarrow{\sim 100°C} CaSO_4.0.5H_2O + 1.5H_2O \text{ (mass loss of 15.70\%)} \qquad \text{[R.26]}$$

$$CaSO_4.0.5H_2O \xrightarrow{200°C} CaSO_4 + 0.5H_2O \text{ (mass loss of 6.2\%)} \qquad \text{[R.27]}$$

$$CaSO_4.2H_2O \xrightarrow{200°C} CaSO_4 + 2H_2O \text{ (mass loss of 20.93\%)} \qquad \text{[R.28]}$$
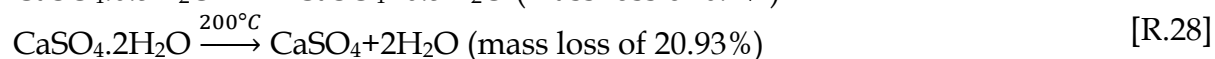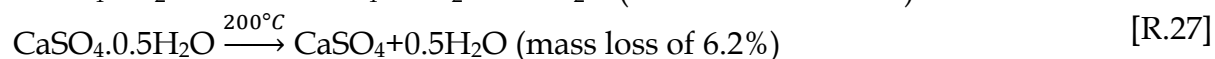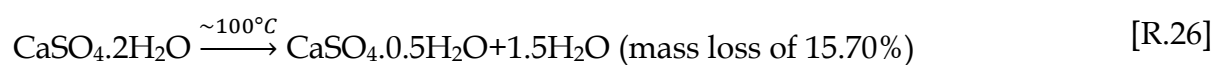
Apparent inert content I corresponds to residue percentage present in calcium sulfates. Gypsum contains ~89% of the total calcium sulfate hemihydrates corresponding to apparent inert content. The same content was obtained from gypsum and plaster densities relationships (§ I.1.). The percentages of formed products during heat treatment by the following relationships [6]:

$$G = ML_1/0.1570 \qquad \text{[Eq.5]}$$
$$P = ML_2/0.062 - G \qquad \text{[Eq.6]}$$
$$I = 100 - (G + P) \qquad \text{[Eq.7]}$$

With G and P are the weight percentages of calcium sulfate dihydrated and hemihydrated respectively in the sample and I is the mass percentage of inert residues in the sample. The mass loss during the thermal analysis is: $ML = (0.062 \times P + 0.2093 \times G)$ [6]. **Table 16** summarizes the percentages of the compounds. Purity of gypsum is about 96.45%.

Table 16: Percentages of products in Gypsum

%Gypsum	%Plaster	%Impurity	%ML
7.83	88.62	3.55	21.8

After calcium sulfates heat treatment, the hydration degree (α) can be calculated as follows:

$$\alpha = w_0/(w_1-w_0)\times100\% \hspace{4cm} [Eq.8]$$

Where w_0 and w_1 are the non-evaporable water contents of plaster and calcium sulfate dihydrate (gypsum), respectively. The hydration degree of hemihydrated calcium sulfate is about 74.12%.

Calcium phosphates are characterized by two mass losses due to evaporation of bound water molecules present in the Brushite compounds ($CaHPO_4.2H_2O$, 0.23mg) and to the decomposition of carbonate above 600°C. This analysis would allow evaluating the conversion rate of carbonate by referring to the thermogravimetric analysis of calcium carbonate (purity 98%). The calculation of the conversion rate of carbonate was evaluated by quantification of the initial and final mass of calcium carbonate in the Ca-HA sample. Knowing that the calcite (calcium source) exhibits a mass loss characterized by endothermic peak localized at 753°C (1238J.g^{-1}) corresponding to its decomposition (decarbonatation) between 600-800°C temperature of 42% (10.83mg). Ca-HA decarbonatation occurs at decomposition temperature between 600 and 750°C with endothermic peak at 688°C (231J.g^{-1}) exhibiting a loss mass of about 8.6% (1.647mg); the decrease in mass loss reveals calcite reaction with ammonium phosphate leading to carbonate conversion rate of ≈85%.

2.   X-ray diffraction

Analysis by X-ray diffraction on Ca-HA particles after heat treatment (calcination at 1000°C during 10hours) shows the existence of the crystalline phase illustrated by stoichiometric hydroxyapatite (Ca/P=1.67). **Figure 29** includes the analysis of Ca-HA by XRD. Synthesized Ca-HA is characterized by ten main peaks (interrecticular distance) similar to the peaks of a synthesized Ca-HA product [7].

The X-ray diffraction patterns of gypsum and plaster reveal the presence of five characteristic peaks corresponding to diffraction angles 11.62°, 20.72°, 28.98°. 31.09° and 33.26° 2θ with respect to the crystal structure of gypsum, and 14.68°, 25.67°, 29.56°, 31.81° and 49.29° 2θ for α-plaster. The presence of a peak of anhydrite (25.67° 2θ position: 3.47Å) in the hemihydrated sample shows his first appearance following an endothermic reaction at the beginning of heat treatment.
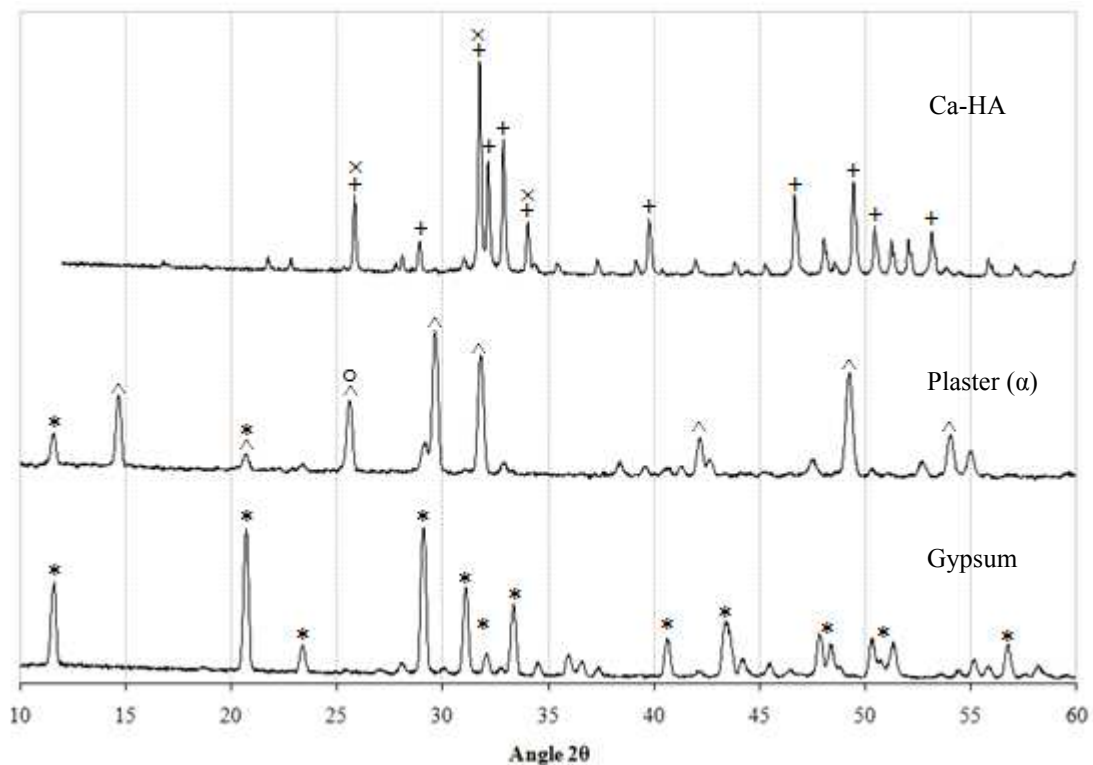
Figure 29: X-ray diffraction of gypsum (*), plaster (^), Anhydrite (°) and Ca-HA calcined at 1000°C (10h) (Ca-HA, Hydroxylapatite (+) and Hydroxyapatite (×))

Study by Mandal et al. (2002) [8] shows that heat treatment of the gypsum at 90°C and 350°C for 10 h indicates the presence of two types of water molecules, loosely held water molecules and strongly held water molecules. This difference is well illustrated by analyzing the infrared spectra of both materials (see **Figure 33**). Heat treatment influence on the monoclinic crystal structure of gypsum (172.2g.mol^{-1}) a loss of 3/2 of water molecules so that it can turn into hemihydrate (145.1g.mol^{-1}) characterized by hexagonal structure.

3.   Raman spectroscopy analysis

The Raman spectra of both plaster and gypsum show differences that suggest structural variations. Difference and systematic shifts in Raman peaks of both gypsum and plaster can be interpreted by the variation in the structure of covalent bounded ion group and its environment. The fundamental vibration modes of gypsum and plaster (α) were assigned to the peaks in Raman spectra and were illustrated in **Figure 30**. Strongest peaks in Raman spectra of plaster (α) by-product analyzed as received, were observed at 1230, 1313, 1603 and 1705cm^{-1} which indicate no identical intensity as those from natural product. Consequently, high intensities at 1200-1800cm^{-1} Raman-shift region can be explained by the presence of impurities where a considerable band broadening meaning incorporation of *foreign anions* leading to crystalline lattice disorder causing by substitution and vacancies, and in the other side to the decrease of hydration degree regarding to gypsum.
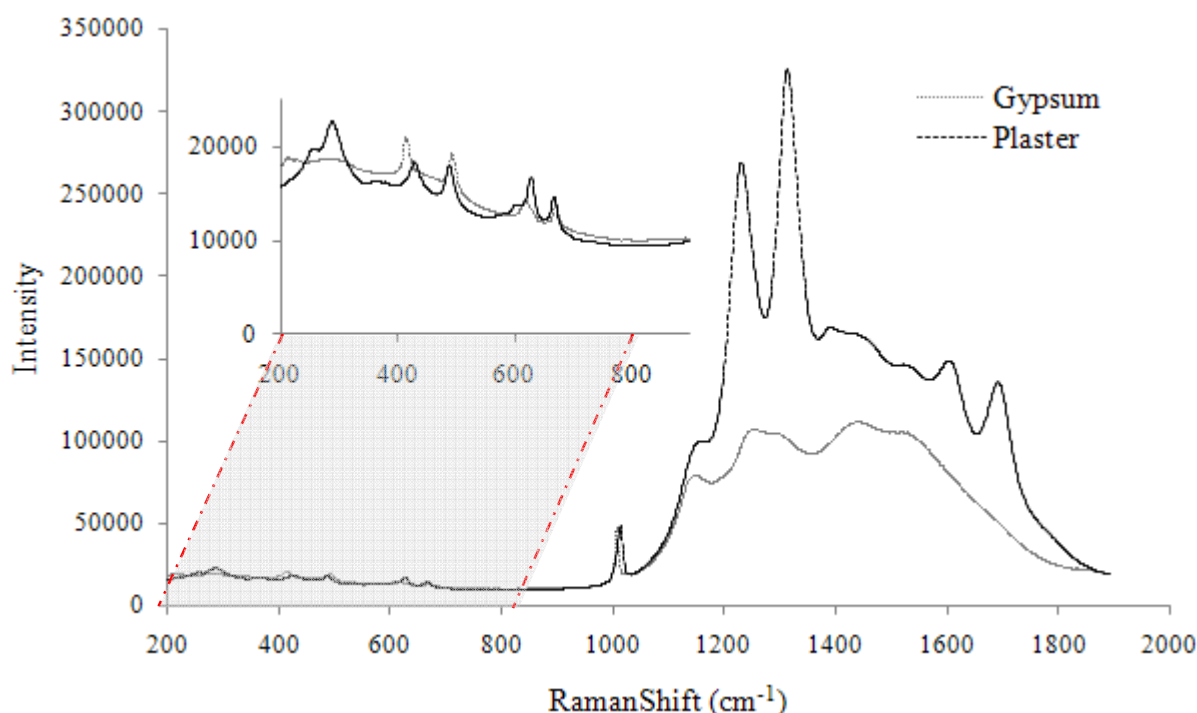
Figure 30 : Raman spectra of gypsum and plaster (α) under ambient conditions

As can be seen from gypsum spectra (**Figure 30**), broadening and non distinguishable bands reveal amorphous and poor crystallinity structure. Crystallinity is more correlated to the atoms arrangements and compact structure.

Water anion bounding with sulfate anions lowered the symmetry. **Table 17** tabulates the main Raman peaks revealing detected sulfate groups.

Frequency of Raman band of gypsum corresponding to sulfate tetrahedron (SO_4^{2-}) symmetric stretch (v_1) found at $1007cm^{-1}$ is less than Raman band of plaster found at $1014cm^{-1}$, this can be explained by the decreasing of hydration degree. Sulfate groups corresponding to v_2 are characterized by doublet exhibiting symmetric bending and detected at ($415, 493cm^{-1}$) and ($428, 488cm^{-1}$) for gypsum and plaster respectively. The peaks at $1152cm^{-1}$ in gypsum and $1164cm^{-1}$ in plaster are assigned to v_3 antisymmetric stretch vibration modes. The doublet peaks at ($620, 670cm^{-1}$) and ($628, 667cm^{-1}$) of gypsum and plaster respectively are assigned to v_4 antisymmetric bend vibration modes. Calcium sulfate peaks are consistent with those listed in literature [9]. Raman analysis carried out by PRASAD et al. (2001) [9] reveal doublet presence ($1152, 1174cm^{-1}$) in plaster Raman spectra. Comparing this result with doublet peak obtained in this work, it was a shift meaning that sulfate ion in hemihydrates is bounded to anionic water by hydrogen bonding leading to the formation of small quantity of gypsum. This explanation may be corroborated by X-ray diffraction analysis, where gypsum is detected in plaster XRD spectra.

Table 17 : Observed Raman band position (cm^{-1}) of sulfate group in calcium sulfate products

Calcium sulfates	v_1	v_2	v_3	v_4
Gypsum [a]	1007	415; 493	1152	620; 670
Gypsum [b]	1008	420; 494	1141	623
Plaster [a]	1014	428; 488	1164; 1230	628; 667
Plaster [b]	1014	421; 490	1152; 1174	630; 680

[a] Present study, [b] From PRASAD et al. (2001) [9]

As shown in **Figure 31**, strongest observed peak in hydroxyapatite at 958 and $960cm^{-1}$ for gel and powder respectively. Principal peaks observed in this study are consistent with those in previous literature [10][11]. However, higher intensity of principal peaks is attributed to (v_1) symmetric stretch corresponding to PO_4^{2-}. In both

hydroxyapatite spectra, very strong vibration mode appears at 1085cm^{-1} attributed to v_3 phosphate mode which is related to symmetric bend. **Table 18** summarizes found Raman band position of phosphate group occurring in Ca-HA samples.
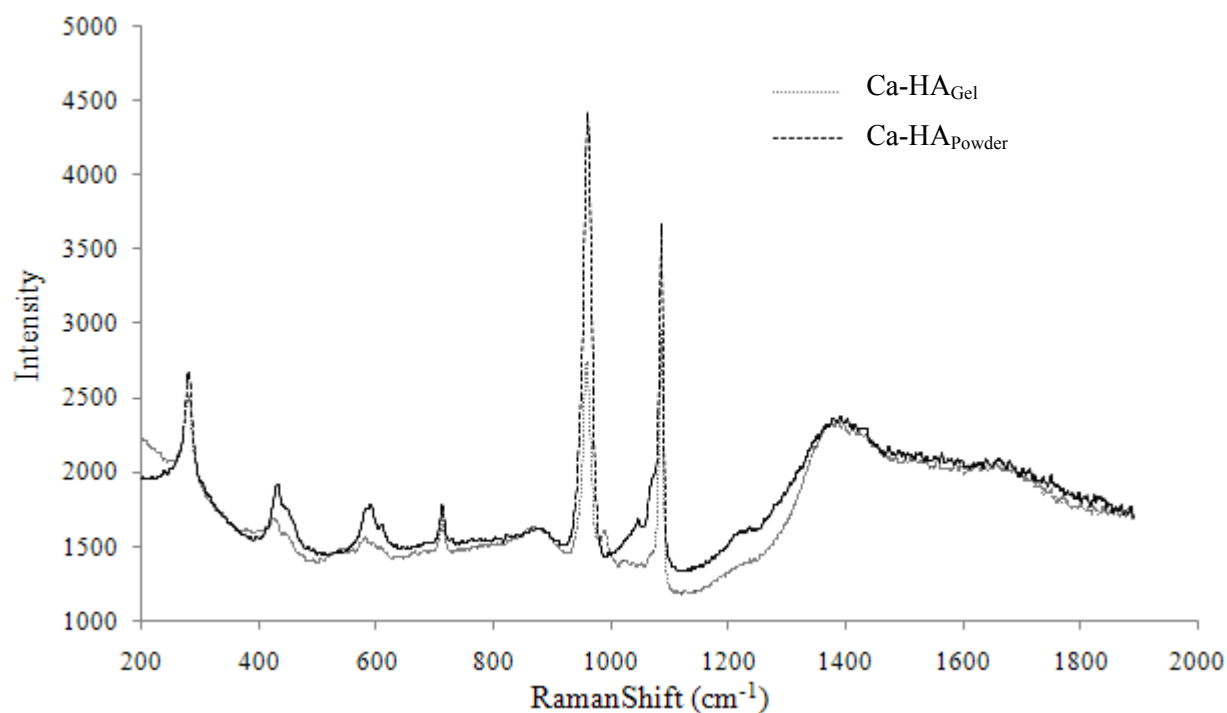
Figure 31 : Raman spectra of both hydroxyapatite gel and powder (heated at 105°C)

Energy bands of both synthetic hydroxyapatites (powder and gel form) are observed at 280cm^{-1} in both cases and assigning Ca-PO$_4$ lattice modes and due to local impurities [11]. Peaks observed at 424 and 431cm^{-1} from Ca-HA Raman spectra corresponds to v_2 PO$_4$ bending mode. Common strong peaks appeared at 712 and 864cm^{-1} are due to the carbonate substitution and local impurities can be assigned to the $v4$ CO$_3$ and HPO$_4^{2-}$. The band at 280cm^{-1} is attributed to the Ca-OH and Ca-PO$_4$ lattice modes [12].

Table 18 : Observed Raman band position (cm^{-1}) of phosphate group in synthesized-Ca-HA

Calcium phosphate	v_1	v_2	v_3	v_4
Ca-HA$_{Gel}$ [a]	985	424	1085	580
Ca-HA$_{Powder}$ [a]	960	431	1085	582
Carbonated Ca-HA [b]	962	431; 440; 449	1031; 1048; 1076	581; 592; 608
Commercial Ca-HA [c]	954; 963	448; 489; 550	1092	574; 601

[a] Present study, [b] From de MUL et al. (1986) [10], [c] From ANTANOKOS el al. (2007) [11]

Raman shift region between 1300 and 1800cm^{-1} is characterizing by asymmetric broad band and ascribed to the presence of carbonate corresponding to the υ_3 CO$_3$ mode.

4.   Infrared analysis

Interpretations of infrared spectra of materials have allowed us to identify the phases and the arrangements of anionic constituent crystal lattices. The products of calcium sulfates are characterized by absorption bands of water in two distinct regions. **Figure 32** illustrates a proposed skeleton of gypsum structure representing bounds between calcium, sulfate and water. **Figure 33** shows the infrared spectra of Ca-HA (Powder), plaster and gypsum.
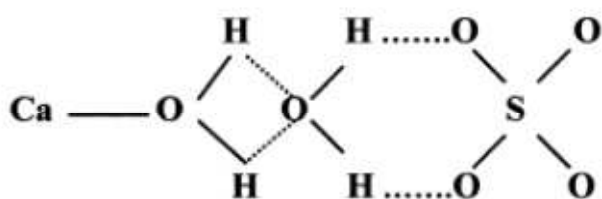
Figure 32 : Proposed structure of gypsum according to Mandel et al. (2002) [9]
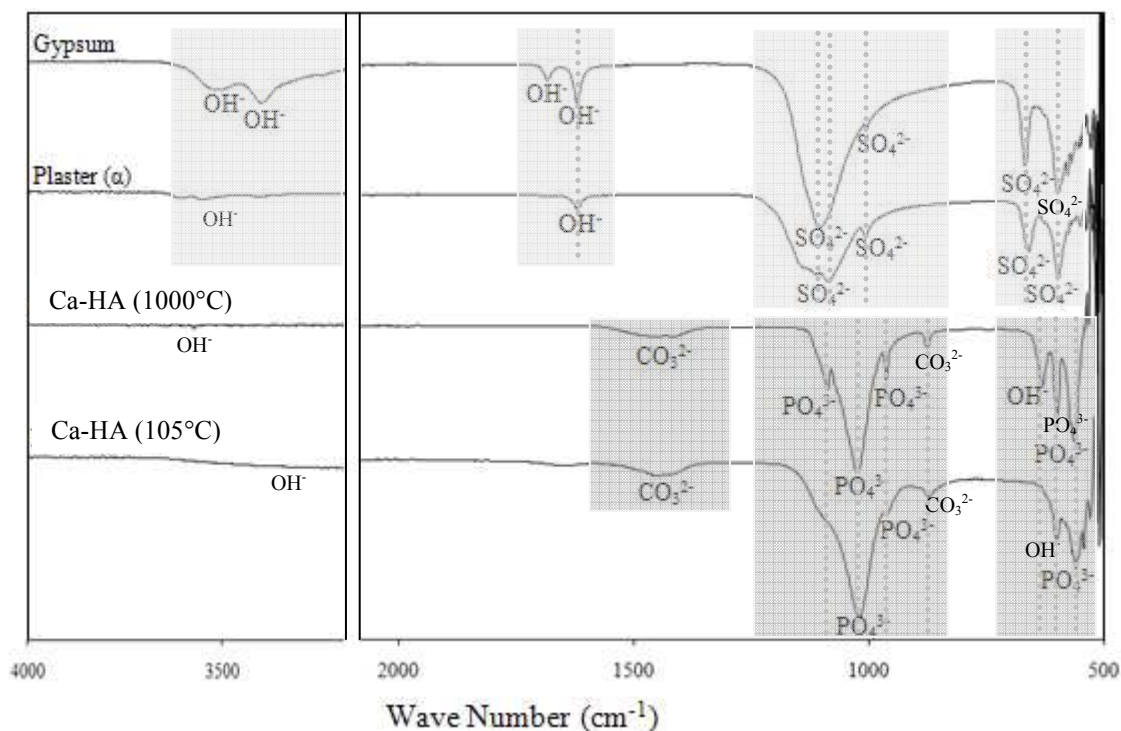
Figure 33: FTIR of gypsum, plaster, Ca-HA dried at 105°C (24h) and Ca-HA calcined at 1000°C

The water in the gypsum is detected at 1620 and 1680cm^{-1} and 3350, 3397 and 3516cm^{-1}. The first region is explained by the presence of deformation modes of shear type which indicates the existence of two types of water molecules, loosely held water molecules at 1680cm^{-1} and strongly held water molecules at 1620cm^{-1} [9]. Consequently, water molecules in calcium sulfates are asymmetric. In the other side, spectral region between 1600 and 1800cm^{-1} indicates H−O−H bending vibration. From proposed gypsum structure, loosely held water molecule is identified as attached to calcium and strongly held water molecule is characterized by hydrogen bounding with sulfate. The low intensity absorption band observed at 1620cm^{-1} corresponds to anionic water present in the plaster. Indeed, plaster got only strongly held water. In addition, the absence of water molecules in the absorption region (3800-3100cm^{-1}) in the hemihydrate samples is due to heat treatment.

The sulfate group determines the symmetry with respect to the water molecules and is a high symmetry tetrahedral structure. In the case of gypsum, sulfate fundamental peak is detected at 1105cm^{-1} and for the hemihydrate it is detected at 1088cm^{-1}; both absorption bands are symmetric stretching bands (v_3). Doublet peaks appearing at

598 and 660cm^{-1} and at 600 and 667cm^{-1} in IR-spectra of plaster and gypsum respectively are assigned as bending vibrations (v_4). The difference between the two intensities indicates that the symmetry is weakened by bounds with the water molecules.

From the Ca-HA spectrum (**Figure 33**), the absence of OH$^-$ bands at high frequencies (3571cm^{-1}). Bands PO$_4^{3-}$ occurring in dried and calcined HAP are detected at 1020cm^{-1} and at 1024cm^{-1} respectively; these bands characterize phosphate structure and are attributed to symmetric stretching (v_3). **Table 19** tabulates observed IR modes of calcium phosphate and their assignments. The presences of broad band at 1450cm^{-1} and at 1456cm^{-1} in both Ca-HA samples indicate the substitution of PO$_4^{3-}$ by CO$_3^{2-}$ ions. Peaks located at 872 and at 877cm^{-1} of dried and heated HAP respectively indicate hydroxide and/or phosphate substitution. IR studies conducted by *Verwilghen* (2006) [7] on the characterization of carbonated Ca-HA calcined at 1000°C for 15h reveal the presence of carbonates groups at 1414cm^{-1}.

Table 19 : Observed IR band position (cm^{-1}) of phosphate group in synthesized-Ca-HA

Calcium Phosphate	v_1	v_2	v_3	v_4
Ca-HA$_{Powder}$ [a]	962	N.O	1020	552
Ca-HA$_{Powder}$ [b]	962	N.O	1024; 1088	563; 598
Ca-HA$_{Powder}$ [c]	961	N.O	1042; 1090	569; 602
Ca-HA$_{Powder}$ [d]	965	473	1044; 1095	575; 603

[a, b] Present study, [c] From VERWILGHEN (2006) [7], N.O No observed
[a] Powder dried at 105°C for 24h,
[b] Powder heated at 1000°C for 10h,
[c] Powder heated at 1000°C for 15h, [d] Powder heated at 900°C for 2h,

Substitution of phosphate by carbonate leads to the formation of calcium carbonate hydroxyapatite. In addition, heat treatment may influence the crystal structure of Ca-HA particles by the decomposition of CO$_3^{2-}$ ions and the release of CO$_2$, arrangement of PO$_4^{3-}$ ions which has the main band with a very high intensity. This can be observed from Ca-HA (1000°C) IR-spectra, apparition of phosphate group indicates the carbonate ions substitution. The substitution of CO$_3^{2-}$ sites by the PO$_4^{2-}$ group

causes the symmetry decreases what consequently decrease the of the apatite structure stability [13].

Conclusion

This chapter describes the physico-chemical and mineralogical characteristic of hydroxyapatite and calcium sulfate dihydrate and hemihydrate. The particle size classification showed that the hydroxyapatite particles have a loamy gel texture. Calcium sulphate hemihydrate (plaster) texture is identified as silty-sand and calcium sulfate dihydrate (gypsum <1 mm) is characterized by a sandy-loam texture.

The heat treatment have shown that calcium phosphate and calcium sulfate dihydrate are characterized by two mass loss due to endothermic reactions indicating the presence of hydrated calcium phosphate and the dehydration of calcium sulfate respectively. Analyses by X-ray diffraction and infrared Fourier transformed carried out on materials have revealed the presence of peaks and characteristic bands of apatite and calcium sulfates. Fundamental vibration modes of both dihydrated and hemihydrated calcium sulfates were assigned to the peaks in Raman and FTIR spectra; the assignment of main peaks of sulfates revealed symmetric stretch. Leaching according to EN 12457-2 shows that by-products of calcium sulfate is in compliance with the admission requirements and acceptation waste criteria.

References

[1] SINGH N. B., MIDDENDORF B., 2007, *Calcium sulfate hemihydrates hydration leading to gypsum crystallization*, Progress in Crystal Growth and Characterization of Materials 53, Pp57-77

[2] BELLI L.C., POSNER A. M., QUIRK J.P., 1973, *The Point of Zero Charge of Hydroxyapatite and Fluoroapatite in Aqueous Solution*, Journal of Colloid and Interface Science, Vol. 42, No. 2, Pp250-261

[3] SKARTSILA, K., SPANOS, N., 2007, Surface characterization of hydroxyapatite: Potentiometric titrations coupled with solubility measurements, Journal of Colloid and Interface Science 308, Pp405-412

[4] AFNOR, EN 12457-2, 2002, *Characterization of waste – leaching – compliance test for leaching of granular waste materials and sludges*. Part 2. One stage batch test at a liquid to solid ratio of 10 l/kg for materials with particle size below 4 mm, European Standard NF, December 2002.

[5] HUDSON-LAMB D.L., STRYDOM C.A., POTGIETER J.H., 1996, *The thermal dehydration of natural gypsum and pure calcium sulfate dihydrate (gypsum)*, Thermochimica Acta 282.283, Pp483-492

[6] DWECK J., LASOTA E. I. P., 1998; *Quality control of commercial plasters by thermogravimetry*. Thermochimica Acta 318. Pp137-142

[7] VERWELGHEN C., 2006. *Fixation des métaux lourds par des phosphates de calcium dans le traitement des fumes d'usines d'incinération d'ordures ménagères*. Thèse soutenue le 13 décembre, 2006, Université Paul Sabatier de Toulouse III. Pp47-60

[8] MANDAL P.K., MANDAL T.K., 2002, *Anion water in gypsum (CaSO₄.2H₂O) and hemihydrates (CaSO₄.1/2H₂O)*; Cement and Concrete Research 32. Pp313-316

[9] PRASAD P. S. R., PRADHAN A. and GOWD T. N., 2001, *In situ micro-Raman investigation of dehydration mechanism in natural gypsum*, CURRENT SCIENCE, VOL. 80, NO. 9, 10 MAY 2001, Pp1203-1207

[10] De Mu, F.F.M. l., HOTTENHUIS, M.H.J., BOUTER, P., ARENDS, J., Ten Bosch, J.J., Micro-Raman Line Broadening in synthetic carbonated hydroxyapatite, J DENT RES Mars 1986 65: Pp437-440

[11] ANTONAKOS A., LIAROKAPIS E., LEVENTOURI T., 2007, *Micro-Raman and FTIR studies of synthetic and natural apatites*, Biomaterials 28, Pp3043-3054

[12] PENEL G., LEROY G., REY C. SOMBRET B., HUVENNE J. P., BRES E., 1997, *Infrared and Raman microspectrometry of fluor-fluor-hydroxy and hydroxyapatite powders*, Journal of Materials Science: Materials in Medecine 8, Pp271-276

[13] VEIDERMA M., TONSUAADU K., KNUBOVETS R., PELD M., 2005, *Impact of anionic substitutions on apatite structure and properties*, Journal of Organometallic Chemistry, Pp2638-2643

Chapter IV
Ca-HA$_{Gel}$ – Gypsum and Ca-HA$_{Gel}$ – Plaster formulations

I.   Introduction

The main purpose of this chapter are threefold:

- The formulation of binary (water/plaster, water/gypsum, Ca-HA/plaster, Ca-HA/gypsum) and ternary (Ca-HA/(water/plaster) and Ca-HA/(water/gypsum) blends.

- The study of their physicochemical characteristics.

- The investigation of the interaction between the calcium sulfate and calcium phosphate.

II.   Binary formulations

1.   Water/Plaster – Water/Gypsum blends

The water/plaster (W/P) and water/gypsum (W/G) (gypsum used in this study has particle diameter less than 1mm) blends were made by mixing either plaster or gypsum with de-ionized water following L/S (liquid/solid) ratio ranging from 0.2 to 1.4. The calcium sulfate amount added was about 100g for all mixtures. Mixing procedure was carried out according to following steps:

♦ Calcium sulfate was powdered into water during 30 s;

♦ Mixture was left 1 min at rest to ensure perfect particle wetting;

♦ The blend was stirred during 30 s with helicoidal stirrer;

♦ Blend was maintained at rest 30 seconds;

Mixtures were used in rheological tests whose results are discussed in the Chapter V. **Table 20** summarizes the added amount of water, gypsum and plaster in W/G and W/P blends and their density and solid concentration. The solid concentration Γ_{B1} of blends was calculated using the following relationships:

$$\Gamma_{B1} = \frac{V_s}{V_{s+} V_w} \quad ; \quad \frac{W}{G} = \frac{1 - \Gamma_B}{\rho_G \Gamma_B} \quad ; \quad \frac{W}{P} = \frac{1 - \Gamma_B}{\rho_P \Gamma_B} \qquad \text{[Eq. 1]}$$

Where V_s is the volume of solid phase, V_w is the volume of water and ρ_G and ρ_P are the densities of gypsum and plaster respectively.

Table 20 : Concentrations of blends based on Water/Gypsum and Water/Plaster

W/G Blends	Water(ml.cm^{-3})	Gypsum (g.cm^{-3})	Density (g.cm^{-3})	Γ_{B1} (Gypsum)
0.4	47	53	100	0.53
0.6	66	51	117	0.44
0.8	100	56	156	0.36
1.0	107	47	154	0.31
1.2	145	54	199	0.28
1.4	146	46	192	0.24
W/P Blends	Water(ml.cm^{-3})	Plaster (g.cm^{-3})	Density (g.cm^{-3})	Γ_{B1} (Plaster)
0.4	51	46	97	0.48
0.6	82	49	131	0.38
0.8	97	43	140	0.31
1.0	121	43	164	0.26
1.2	134	40	174	0.23
1.4	160	41	201	0.21

The solid concentration of both blends increases by decreasing the amount of water in the blends. Thereafter, the influence of solids were investigated in the rheological trails by measuring the viscosity. Added water to plaster leads to the hydration of plaster particles and has otherwise no influence on gypsum (almost hydrated particles). The properties of plaster as binder material used in this study to stabilize Ca-HA$_{Gel}$ structure (for different formulations) have been studied.

2.   Plaster hydration

The contact of plaster particles with water molecules leads to their hydration. The hydration follows the stoichiometric reaction:

$$CaSO_4, 0.5H_2O_{(solid)} + 1.5H_2O_{(aqueous)} \rightarrow CaSO_4.2H_2O_{(solid)} \qquad \text{[R. 1]}$$

The plaster hydration obeys to the *dissolution-crystallization* model, where plaster particles transforms to gypsum. Plaster hydration occurs at an alkaline pH.
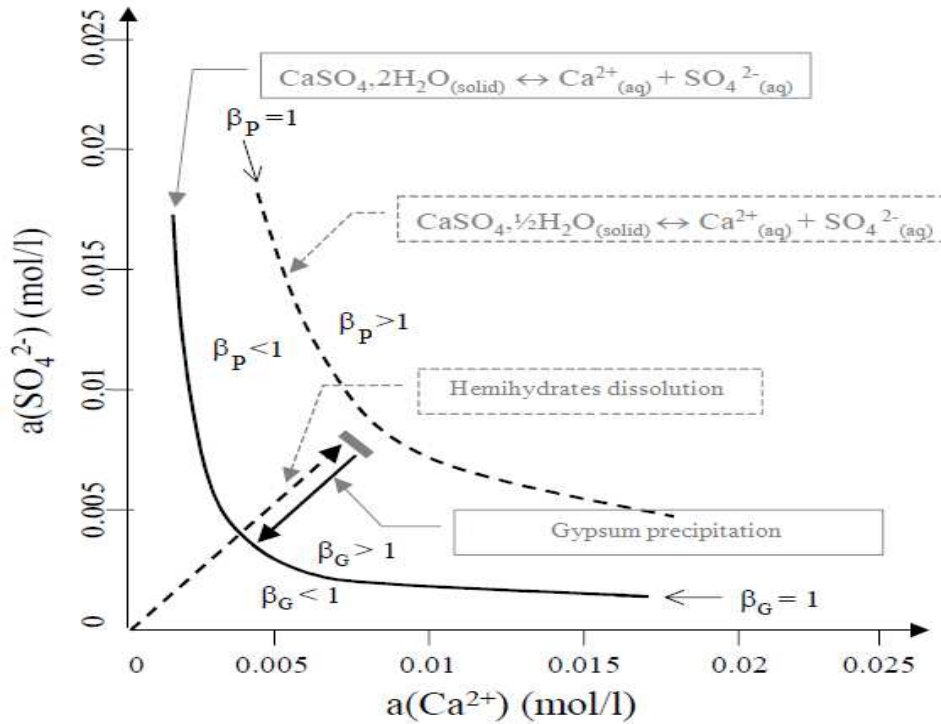
Figure 34: Diagram of calcium sulfate solubility [1]

Hydration mechanisms depend to thermodynamic and kinetic reactions. However, plaster hydration begins in such a way that the free enthalpy of the system is always kept negative during the reaction. **Figure 34** shows the equilibrium phases between plaster dissolution and gypsum precipitation. The curve of hemihydrate solubility curve is illustrated by dotted line (β_P=1) and gypsum solubility curve illustrated by continuous line (β_G=1). Hemihydrates particles equilibrium solubility is defined the following reaction:

$$CaSO_4. \, 0.5H_2O_{(solid)} \leftrightarrow Ca^{2+}_{(aqueous)} + SO_4^{2-}_{(aqueous)} + 0.5H_2O_{(aqueous)}$$ [R. 2]
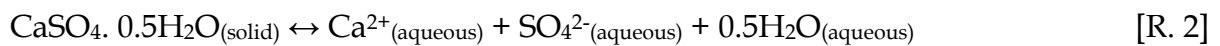
Apparent solubility product of plaster dissolution is:

$$K_P = a(Ca^{2+}). \, a(SO_4^{2-})$$

Where $a(Ca^{2+})$ and $a(SO_4^{2-})$ are the apparent activities of calcium and sulfate ions respectively. Ionic concentration of hemihydrates is more important that gypsum dissolution. **Figure 34** represents different zones of solution state based on saturation degree and evolution of calcium and sulfate ions activities. Saturation degree β corresponds to the variation of dissolution free enthalpy is described as follow:

123

$$\beta = \frac{K_p}{K_G} \quad \text{with } K_G = a(Ca^{2+})_{equilibrium} . \; a(SO_4^{2+})_{equilibrium} \qquad \text{[Eq. 2]}$$

Where K_G is the solubility constant of gypsum and, $a(Ca^{2+})_{equilibrium}$ and $a(SO_4^{2+})_{equilibrium}$ are activities of calcium and sulfate ions in equilibrium phases with gypsum respectively. Plaster or gypsum saturation index delimits three zones defined as shown in **Figure 34**:

- ♦ *β_G < 1, under-saturated solution with respect to gypsum*
- ♦ *β_G>1 and β_P<1, supersaturated solution with respect to gypsum and under-saturated with respect to hemihydrates*
- ♦ *β_P>1, supersaturated solution with respect to hemihydrates (hemihydrate apparent solubility is limited, from where the present situation is impossible to achieve)*

3.   Water consumption by plaster

Water consumption decreases by increasing W/P ratio. As shown in **Figure 35**, W/P ratio of 0.2 corresponding approximately to stoichiometric ratio consumes about 90% of water. However, water requirement indicates the non complete hydration of particle where amount of water is below the necessary amount to trigger dissolution of calcium and sulfate ions.
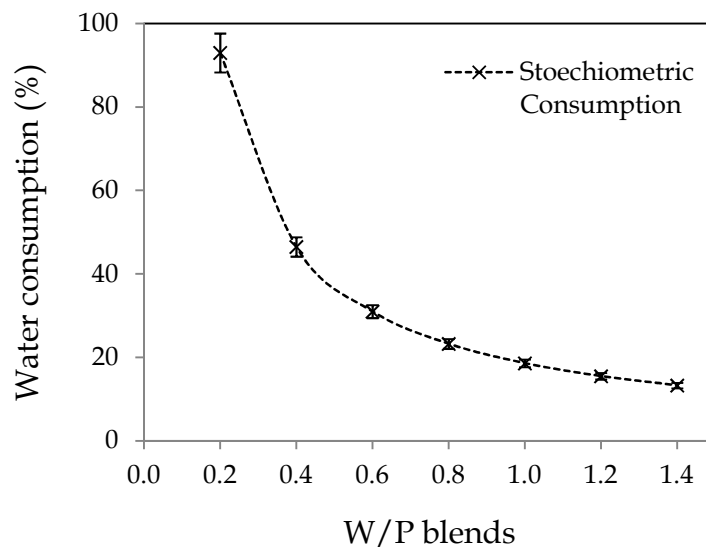
Figure 35: Stoichiometric water consumption of plaster particles

The pastes are difficult to handle due to high viscosity. From 0.4 W/P ratio, water consumption decreases by 50% leading to the beginning of particle hydration. Concerning blends with W/P ratio ranging from 0.6 to 1.4, water consumption decrease seems steady with about 80% of water reduction. Excess water is favorable to start dissolution-precipitation process, and influences particle hydration when crystal are formed by nucleation and/or germination mechanisms. *Jaffel et al [1,2]* have reported that stoichiometric and experimental water consumption (obtained by normalization of magnetization signal NMR (Nuclear Magnetic Resonance) relaxometry) are similar for blends worked according to ratio above 0.8. The difference between stoichiometric and experimental consumption water for blends with W/P ratios below 0.8 is due to the high viscosity of pastes.

4. Porosity of plaster

The porosity is a very important parameter to evaluate the durability for PRB application. It also correlated to the particle's bounds and arrangement. The porosity of plaster after 28 days of dissection was determined according to the accessible water porosity test. The method is based on the saturation of specimen solid body in water (in a vacuum desiccators) under aspiration pressure ensured with a vacuum pump. The experimental set-up is presented in **Figure 36**. This procedure allows the determination of the accessible porosity. The dimension of specimen bodies was of 2cm (diameter) / 5cm (height).
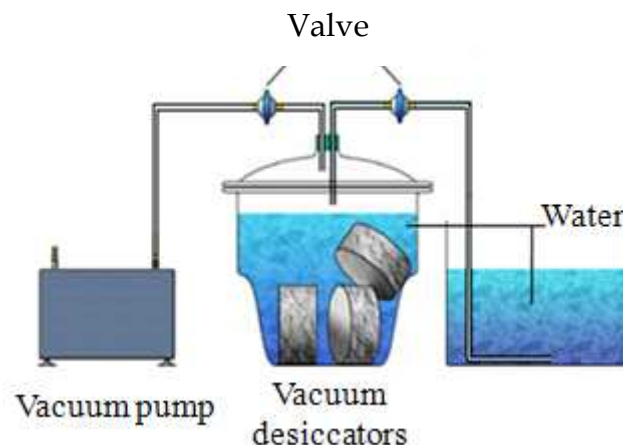
Figure 36 : Water porosity test

The total porosity of plaster was calculated following the relationship:

$$\varnothing_T = \frac{M_a - M_d}{M_a - M_w}$$ [Eq. 3]

Where M_a is the mass in air (g), M_w is the mass in water obtained by hydrostatic weighing (g) and M_d is the dried mass at 105°C (24h) (g). The porosity of plaster paste was calculated by evaluating the compactness of formulations. The compactness Φ relationship is as follows:

$$\Phi = \frac{1}{1 + \rho_P \frac{W}{P}} \text{ with } \varnothing = 1 - \Phi$$ [Eq. 4]

Where $\varnothing$ is the porosity, ρ_P is the bulk density of the plaster (g.cm^{-3}), W is the added water (g) and S is the plaster amount (g). **Figure 37** shows the calculated porosity values of W/P blends before and after dissection. The porosity of plaster increases in function of W/P ratio. The difference between plaster paste and solid plaster corresponds to the free water; the increase of porosity in solid plaster body is explained by the evaporation of free mixing water during dissection period and creation of voids.
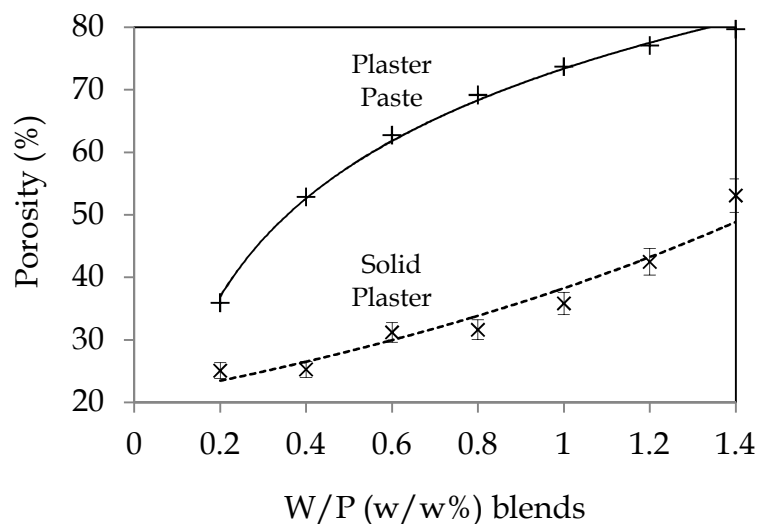
Figure 37 : Porosity of paste and solid plaster after molding

126

5.   Capillary rise

Capillary rise provides indication on the porous structure and capacity of porous solid material to absorb the water. From the total porosity of the solid, the capillary rise capacity can be evaluated. The plaster blended at W/P ratio ranged from 0.4 to 1.4 were used after 28 days of desiccation. The mass of absorbed water was then calculated with the following relationship:

$$M_w = h(t) . \varnothing . A . \rho_w \qquad\qquad [Eq. 5]$$

Where M_w is the mass of absorbed water, h(t) is the height of absorbed water at time t (s), $\varnothing$ is the porosity, ρ_w is the bulk mass of water at lab temperature and A is the section of the specimen solid body. The dimension of sample was 5 cm height and 2 cm diameter. The samples were placed in water and heights of water displacement were recorded. **Figure 38** shows the absorbed mass as a function of time square. The maximum adsorbed mass increases by increasing the W/P mass ratio. The solid bodies blended with 1.2 and 1.4 W/P mass ratio achieve the saturation (approximately 0.05 kg and 0.06 kg of adsorbed mass respectively) after 6 and 8 min.
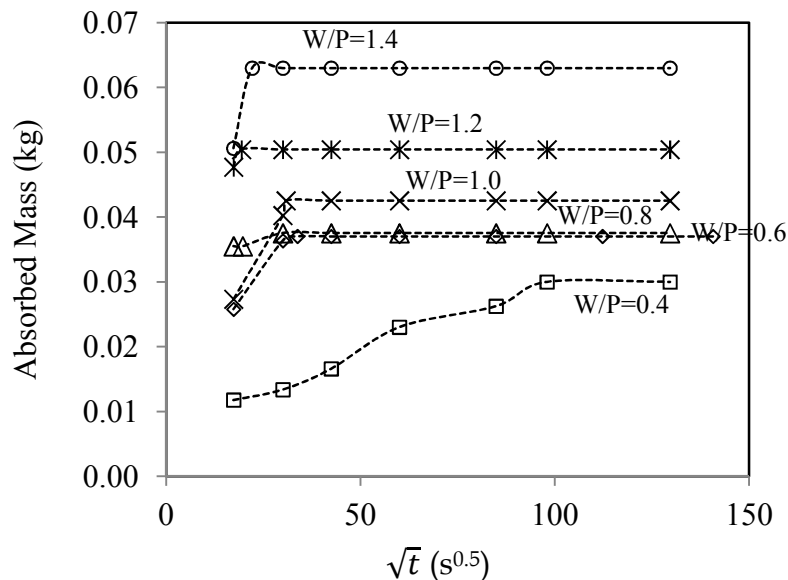
Figure 38 : Adsorbed mass in plaster specimen body as a function of time square

The solid blended with 0.6, 0.8 and 1.0 W/P mass ratio were characterized by an adsorbed mass of about 0.04 kg. Their saturation was observed after 15 to 20 minutes.

Samples with W/P mass ratio ranging between 0.6 to 1.4 may absorb a higher amount of water. This result can be correlated to void and number of capillary radius. Concerning the sample with 0.4 W/P mass ratio, the saturation was achieved after 3 h approximately. The amount of absorbed water at saturation was about 0.03 kg.

6.   Ca-HA$_{Gel}$/Plaster – Ca-HA$_{Gel}$/Gypsum blends

The blends were mixed according to the procedure described for calcium sulfates blends. **Table 21** tabulates the added amount of Ca-HA$_{Gel}$, plaster and gypsum in the Ca-HA$_{Gel}$/(Calcium sulfate) blends. The following Ca-HA$_{Gel}$/(Calcium sulfate) blends were considered: 80%/20%, 70%/30% and 60%/40%

Table 21 : Concentration of Ca-HA/(calcium sulfate) considered blends

Ca-HA/G Blends	Ca-HA Water (ml.cm^{-3})	Gypsum (g.cm^{-3})	Ca-HA$_{Gel}$ (g.cm^{-3})	Density (g.cm^{-3})	Γ_{B2} (Ca-HA/G)
80%/20%	101	16	56	72	0.23
70%/30%	108	29	60	89	0.27
60%/40%	90	38	50	88	0.30

Ca-HA/P Blends	Ca-HA Water (ml.cm^{-3})	Plaster (g.cm^{-3})	Ca-HA$_{Gel}$ (g.cm^{-3})	Density (g.cm^{-3})	Γ_{B2} (Ca-HA/P)
80%/20%	142	18	79	97	0.21
70%/30%	102	22	56	79	0.24
60%/40%	89	30	49	79	0.28

The solid concentration of binary blends (Γ_{B2}) containing either gypsum or plaster (calcium sulfate powder) with Ca-HA$_{Gel}$ was calculated as follows:

$$\Gamma_{B2} = \frac{V_{S_T}}{V_{S_T} + V_{W_T}}$$ [Eq. 6]

With $V_{S_T} = V_{Ca-HA_{Powder}} + V_{CS_{Powder}}$ and $V_{W_T} = V_{Ca-HA_{Water}}$

Where V_{S_T} is the total volume of solid material equal to the sum of Ca-HA$_{Powder}$ volume ($V_{Ca-HA_{Powder}}$) and calcium sulfate powder volume ($V_{CS_{Powder}}$), and V_{W_T} is the total water equal to Ca-HA water volume ($V_{Ca-HA_{Water}}$). The solid concentration increases by increasing the amount of calcium sulfate in the blends. Concentration of

ternary blends is directly correlated to the substituted amount of Ca-HA$_{Gel}$ by gypsum (or plaster). Adding gypsum or plaster to Ca-HA$_{Gel}$ leads to the concentration increase.

III.   Ternary blends

1.   Ca-HA$_{Gel}$/(Water/Plaster) – Ca-HA$_{Gel}$/(Water/Gypsum)

The ternary formulations characterized in this thesis are made from an initial mixture of hemihydrated calcium sulfate, water and dihydrated calcium sulfate with proportions varying from 0.2 to 1.4. The initial mixtures were prepared following the same procedures described in the section 1. Mixtures containing Ca-HA$_{Gel}$ were formed by adding Ca-HA$_{Gel}$ to previously prepared water/plaster or water/gypsum blends. The ternary phase diagram showed in **Figure 39** summarizes the different blends composition. The rheological tests were done on these formulations to evaluate their rheological behavior and to study the influence of water on the structure changes.
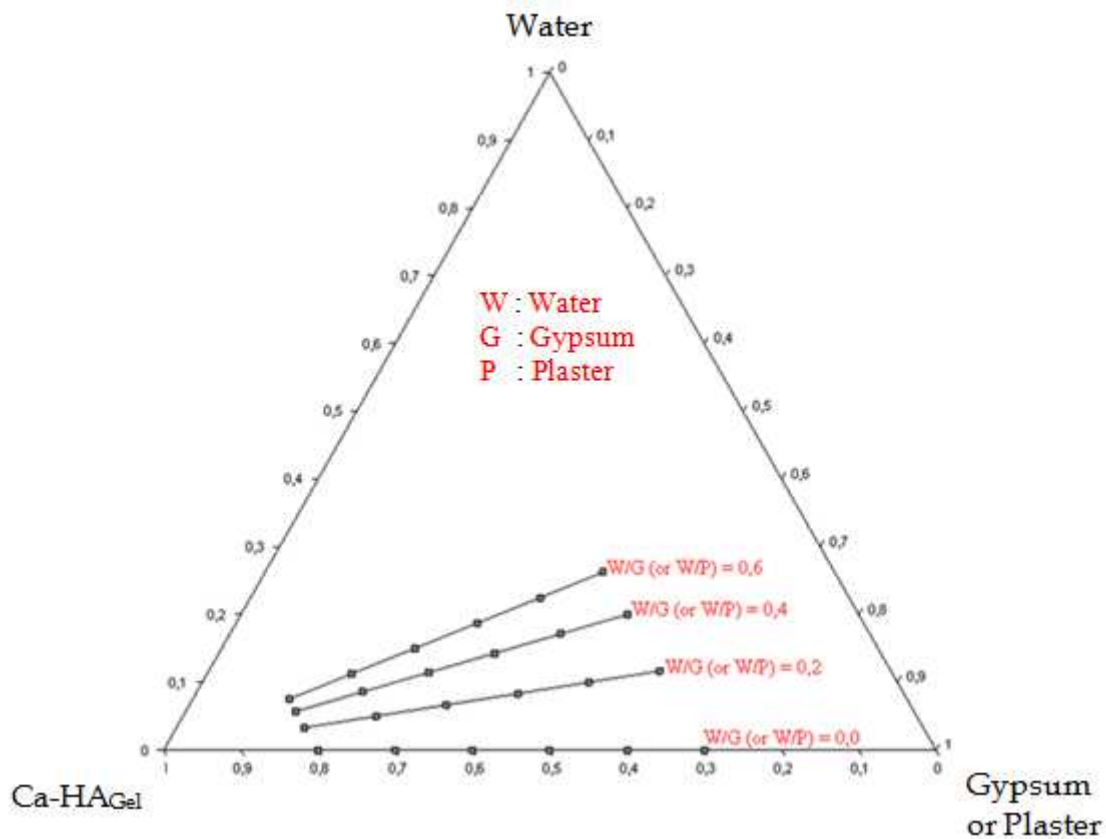
Figure 39: Ternary phase diagram showing different mixtures of Ca-HA$_{Gel}$, Gypsum (<1mm) and plaster

The solid concentration of ternary blends (Γ_{B3}) containing either water/gypsum or water/plaster with mass ratios ranging from 0.2 to 0.6 (calcium sulfate powder) with Ca-HA$_{Gel}$ was calculated as follows:

$$\Gamma_{B2} = \frac{V_{S_T}}{V_{S_T} + V_{W_T}} \qquad\qquad \text{[Eq. 7]}$$

With $V_{S_T} = V_{Ca-HA_{Powder}} + V_{CS_{Powder}}$ and $V_{W_T} = V_{Ca-HA_{Water}} + V_{water}$

Where V_{S_T} is the total volume of solid material equal to the sum of Ca-HA$_{Powder}$ volume ($V_{Ca-HA_{Powder}}$) and calcium sulfate powder volume ($V_{CS_{Powder}}$), and V_{W_T} is the total water equal to Ca-HA water volume ($V_{Ca-HA_{Water}}$) and amount of added water (V_{water}).

2.   Factors influencing the flow

The water dosage and plaster dosage are the main factors influencing the flow of formulations and characterize the optimal water amount leading to plaster hydration and consistency adjustment.

3.   Water dosage

The water dosage is the amount of free water occurring in Ca-HA$_{Gel}$ and added to hydrate plaster. As known, the water dosage adjusts the consistency of formulations and can affect the stability and homogeneity. The water dosage (W_d) in ternary blends is maximum at 0.2 W/P mass ratio and calculated according to the relationship:

$$W_d = \frac{W_T}{(P^* + Ca-HA_{Gel})} \qquad\qquad \text{[Eq. 8]}$$

Where W_T is the total water amount (water of Ca-HA$_{Gel}$ and added water) (g), P* is the hydrated plaster amount (g) and Ca-HA$_{Gel}$ is the introduced hydroxyapatite gel amount (g). The amount of water occurring in Ca-HA$_{Gel}$ hydrates plaster particles and the added water amount regulates the maniability and consistency of blend

pastes. **Figure 40** shows the correlation between water dosage and W/P ratio in Ca-HA/(W/P) formulations.
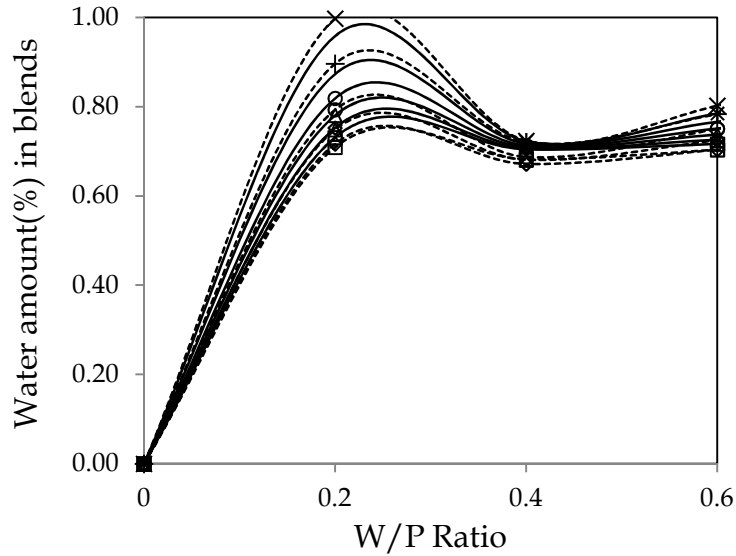
Figure 40: Water dosage of different W/P ratio ranged from 0.2 to 1.0
—□— 80%Ca-HA/20%(W/P) Theoretical, - -□- - 80%Ca-HA/20%(W/P) Experimental
—◇— 70%Ca-HA/30%(W/P) Theoretical, - -◇- - 70%Ca-HA/30%(W/P) Experimental
—△— 60%Ca-HA/40%(W/P) Theoretical, - -△- - 60%Ca-HA/40%(W/P) Experimental
—○— 50%Ca-HA/50%(W/P) Theoretical, - -○- - 50%Ca-HA/50%(W/P) Experimental
—+— 40%Ca-HA/60%(W/P) Theoretical, - -+- - 40%Ca-HA/60%(W/P) Experimental
—×— 30%Ca-HA/70%(W/P) Theoretical, - -×- - 30%Ca-HA/70%(W/P) Experimental

For all formulations, the optimum water dosage was located at 0.2 W/P mass ratio. At 0.4 W/P mass ratio, water amount leading to plaster hydration is constant. It indicates that from this W/P ratio, the water dosage controls the plaster hydration and adjusts the consistency.

4.   Plaster dosage

Plaster dosage (P_d) was calculated for all considered blends using the following equation:

$$P_d = \frac{P^*}{(P^* + Ca-HA_{Gel})} \qquad\qquad \text{[Eq. 9]}$$

Where P* is the hydrated plaster amount (g). **Figure 41** illustrates the plaster dosage in the blends in function of W/P mass ratio.
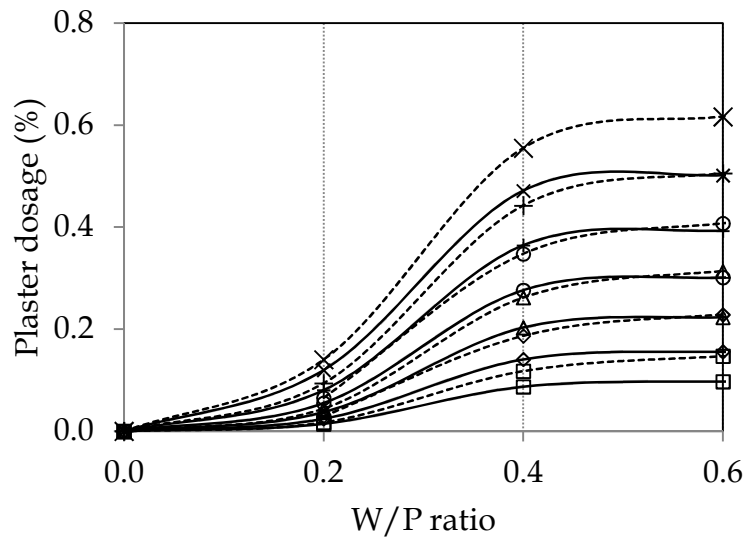
Figure 41: Hydrated plaster dosage in function of W/P ratio
—□— 80%Ca-HA/20%(W/P) Theoretical, - -□- - 80%Ca-HA/20%(W/P) Experimental
—◊— 70%Ca-HA/30%(W/P) Theoretical, - -◊- - 70%Ca-HA/30%(W/P) Experimental
—Δ— 60%Ca-HA/40%(W/P) Theoretical, - -Δ- - 60%Ca-HA/40%(W/P) Experimental
—○— 50%Ca-HA/50%(W/P) Theoretical, - -○- - 50%Ca-HA/50%(W/P) Experimental
—+— 40%Ca-HA/60%(W/P) Theoretical, - -+- - 40%Ca-HA/60%(W/P) Experimental
—×— 30%Ca-HA/70%(W/P) Theoretical, - -×- - 30%Ca-HA/70%(W/P) Experimental

The plaster dosage increases by increase W/P ratio and, remains constant at 0.4 W/P mass ratio. Plaster dosage increases as a function of W/P ratio in the blends. The blends with 0.4 W/P mass ratio presents a good consistency. These results are in agreement with the rheological tests described in the Chapter V.

IV.   Characteristics of formulations

1.   The pH of formulations

The pH of the formulations were measured after rheological tests according to European standard. **Figure 42** shows the recorded pH of considered ternary formulations. As known, the pH of plaster is acidic and the pH of Ca-HA is basic. The addition of Ca-HA$_{Gel}$ changes the pH of the blend. A reaction between plaster and Ca-HA was observed and explains undoubtedly the final pH values.
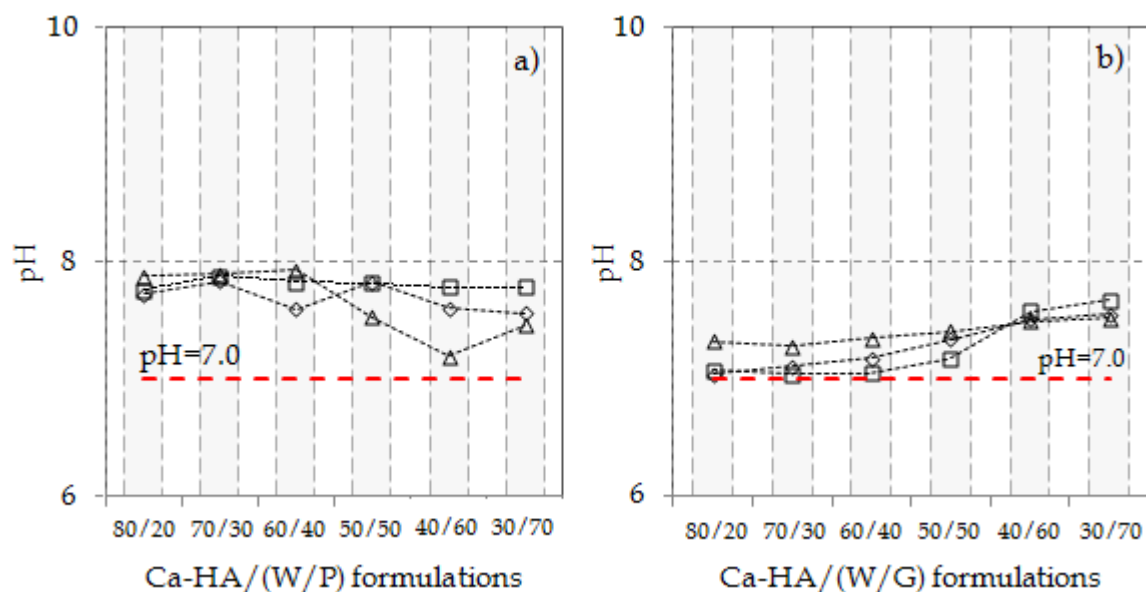
Figure 42 : The pH of blends a) Ca-HA/(W/P) and b) Ca-HA/(W/G)
---◇--- W/P=0.2 (or W/G=0.2), ---□--- W/P=0.4 (or W/G=0.4), ---△--- W/P=0.6 (or W/G=0.6)

The pH of Ca-HA/(W/P) blends becomes basic indicating the reaction between dissolved calcium and sulfate with free phosphate leading to the precipitation of new compounds. The addition of water/plaster mass blend to Ca-HA led to the pH decrease. The decrease in pH is due to the dissolution effect. The pH of formulation based on Ca-HA/(W/G) was basic and increases slightly by increasing the proportion of water/gypsum.

2.   Effect of hemihydrates substitution on Ca-HA non-evaporable water

In order to highlight the influence of the calcium sulfates added amount, the non-evaporable water (NEW) in Ca-HA$_{Gel}$/(W/P) and Ca-HA$_{Gel}$/(W/G) was evaluated by considering that the loss mass in samples at temperature ranging from 105 to 450°C is due to evaporation of chemically bound water which is combined with calcium sulfate. The samples were initially dried at 105°C for 24 h.
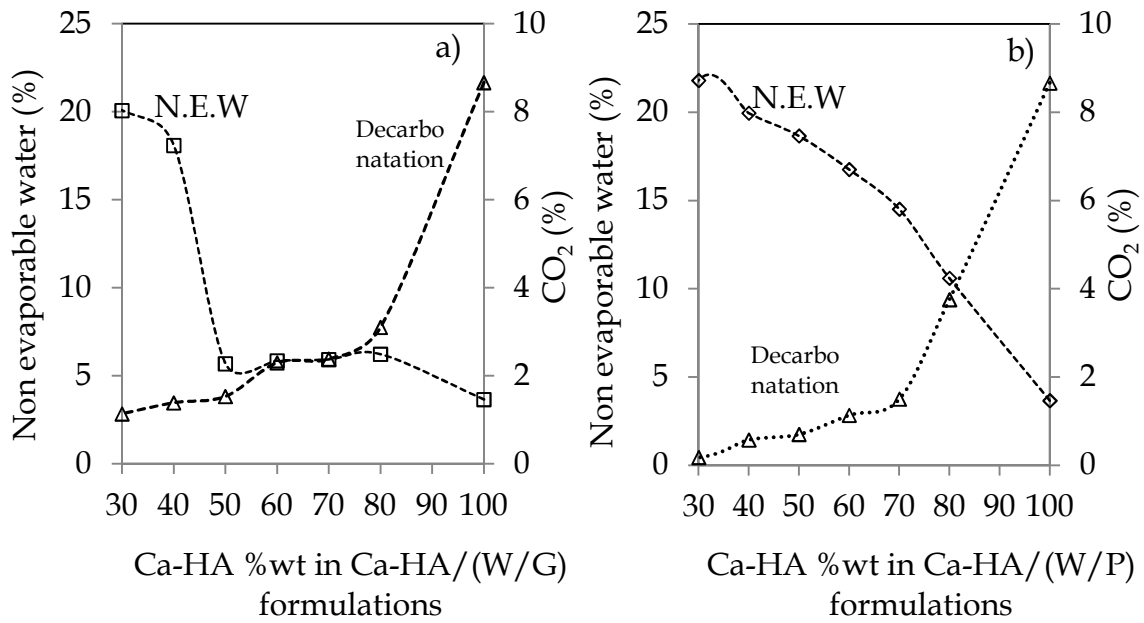
Figure 43: Non evaporable water and rate of decarbonatation as a function of Ca-HA proportions. (a) Ca-HA/(W/G=0.4), b) Ca-HA/(W/P=0.4))

The present relationship allows the determination of the amount of non-evaporable water (NEW) amount present in blends:

$$N.E.W = \frac{W_{105°C} - W_{450°C}}{W_{450°C}}$$ [Eq. 10]

Where $W_{105°C}$ and $W_{450°C}$ are evaporated water at 105°C and 450°C respectively. **Figure 43** illustrates the NEW and sample decarbonatation in the Ca-HA/(W/P=0.4) and Ca-HA/(W/G=0.4) formulations. The NEW decreases by increasing the amount of Ca-HA_{Gel} in the formulations. The NEW present in Ca-HA powder, gypsum and plaster are about 4, 23 and 7% respectively. For formulations containing Ca-HA and water/gypsum mass ratio equal to 0.4, the NEW remains constant at 6% for the substitution rate ranging from 50% to 80%. It has been observed that, for the formulations containing Ca-HA and water/plaster mass ratio equal to 0.4, the NEW decreases dramatically as a function of the amount of Ca-HA. This difference can be explained by the effect of plaster hydration and reaction between plaster and Ca-HA leading to the cohesion between particles. As known, the unreacted calcite in the synthesized Ca-HA is about 14% and gypsum and plaster do not contain calcite as observed in the ATG analysis described in the Chapter III. Decarbonatation increases

134

by increasing the proportions of Ca-HA in the formulations. The decarbonatation decreases of about 43 and 35% when 20% of either W/P or W/G was added to 80% Ca-HA respectively. The decrease of carbon amount is related to the reaction of calcium sulfates with Ca-HA$_{Gel}$. The amount of released calcium from gypsum (or plaster) reacts with the free phosphate in Ca-HA promoting the continuation of calcium phosphate-sulfate hydrate precipitation (see XRD analysis in the Chapter VII).

3.   Microstructure of the formulation

The structure of considered formulation was observed using SEM and environmental SEM (ESEM) to identify the microstructure and surface analysis.
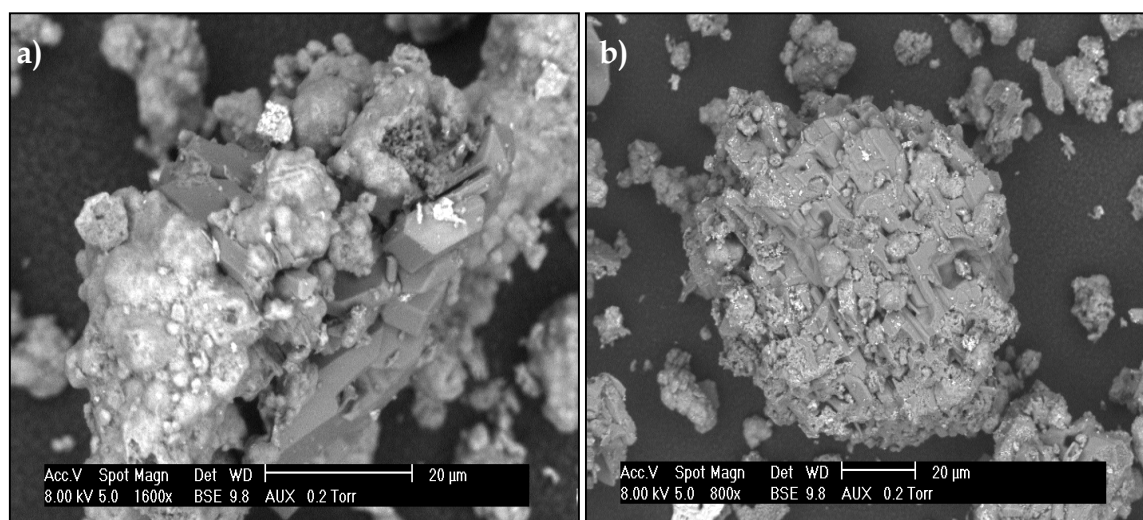
Figure 44 : SEM micrographs of formulation containing a) 80%Ca-HA/20%(W/P) and b) 50%Ca-HA/50%(W/P) with W/P=0.4

The crystalline structure of plaster is characterized by needles readily cleavable. On the other hand, the gypsum is known to be composed of elongated needle-shape particles (Chapter III). Blending the gypsum with Ca-HA leads to the modification of its crystalline structure. **Figures 44** and **45** show the crystalline structure of formulation blended with Ca-HA, water and plaster with W/P mass ratio of 0.4 recorded using SEM and environmental SEM. The picture shown in **Figure 44 a)** illustrates the cohesion between plaster and Ca-HA particles. The interlocking between the deposited irregular-shaped Ca-HA particles and the gypsum. The incorporation of Ca-HA particle in the gypsum crystalline needles causes the

modification of its structure. The Ca-HA particle tangles on the needles of gypsum forming a heterogeneous structure (**Figure 44 b)**). Studies carried out by Greish (2011) have shown that the Ca-HA influences on the growth kinetics of gypsum and causes its deformation [3].

	Wt(%)	At(%)
C	12.24	22.32
O	32.31	44.23
P	15.71	11.11
Ca	35.14	19.20
S	4.61	3.15
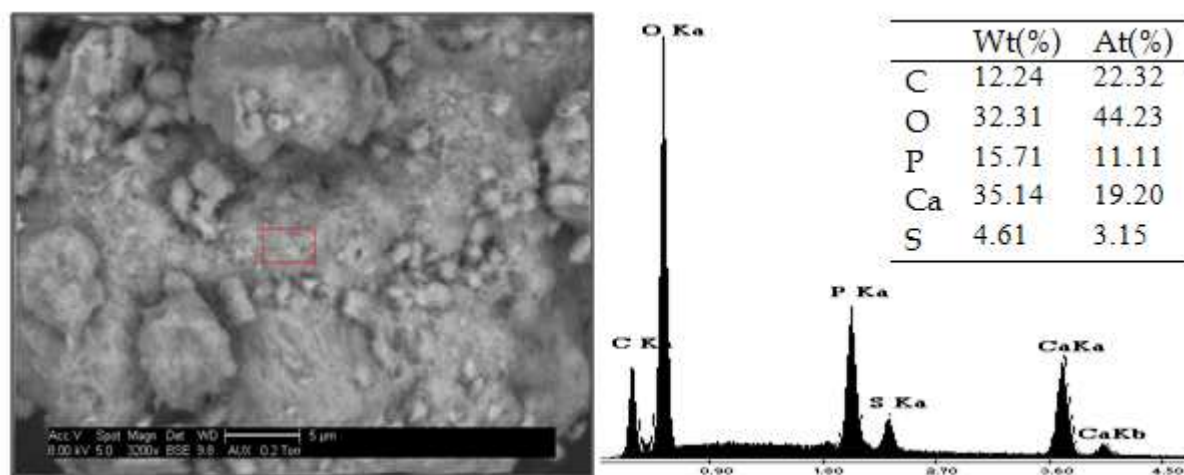
Figure 45 : Environmental SEM of 80%Ca-HA/20%(W/P=0.4) formulation

EDA analysis carried out on localized surface of Ca-HA particle reveals that the Ca/P molar ratio is about 1.72. The presence of sulfur on the surface of Ca-HA indicates the adsorption of sulfate as discussed in Chapter V. The interaction between Ca-HA and plaster may produce new compounds such as calcium sulfate phosphate hydrate. For further information on crystalline structure see chapter VII (XRD analysis).

V. Ca-HA/(Water/Plaster) reaction

The reaction between Ca-HA$_{Gel}$ and plaster was confirmed after rheological tests where bubbling gas was observed. **Figure 46** shows the considered formulations after rheological tests. For formulations (in red color), the bubbling gas has been observed leading to an heterogeneous structure and generation of pores. No reaction was observed in formulations without added water.
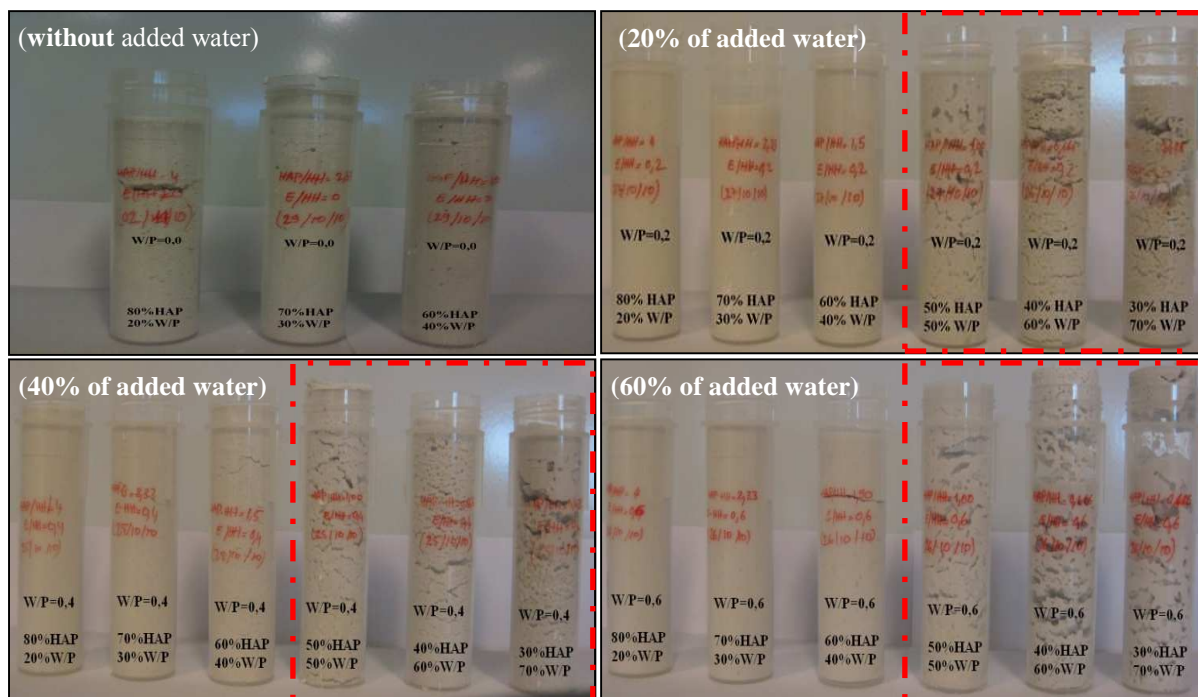
Figure 46: Pictures showing the reaction between Ca-HA$_{Gel}$ and plaster after rheological tests

This results show a strong interaction between particles when water is added. Specially for formulations with 0.6 W/P ratio containing 50%Ca-HA$_{Gel}$/50%(W/P), 40%Ca-HA$_{Gel}$/60%(W/P) and 30%Ca-HA$_{Gel}$/70%(W/P). For these, a bubbling release was observed. The apparance of important voids is probably due to release of gas produced by reaction between unreacted calcite and phosphorus released from hemihydrates and free phosphate in the Ca-HA$_{Gel}$ suspension in contact with acidic water. To quantify the amount of CO_2 released, the experimental set-up illustrated in **Figure 47** was proposed. The procedure is based on the fixation of the released CO_2 in NaOH (0.1M). The chosen formulation was 50%Ca-HA/50%(W/P) with W/P=0.6. The blend was made by introducing 50g of sample (31.3g and 18.8g of Ca-HA$_{Gel}$, plaster and water respectively) in a three-necked round flask. The round flask was connected to N_2 to avoid any reaction with air and to facilitate the passage of CO_2 to the NaOH solution. The stirring speed was set up at 450 rpm and the pressure of N_2 was of 0.2 bar. The reaction was maintained for 90 minutes to ensure homogenization under laboratory conditions (temperature and pressure). The sampling was carried out by extracting 10ml every 5 minutes. The extracted samples were analyzed using SHIMADZU TOC.
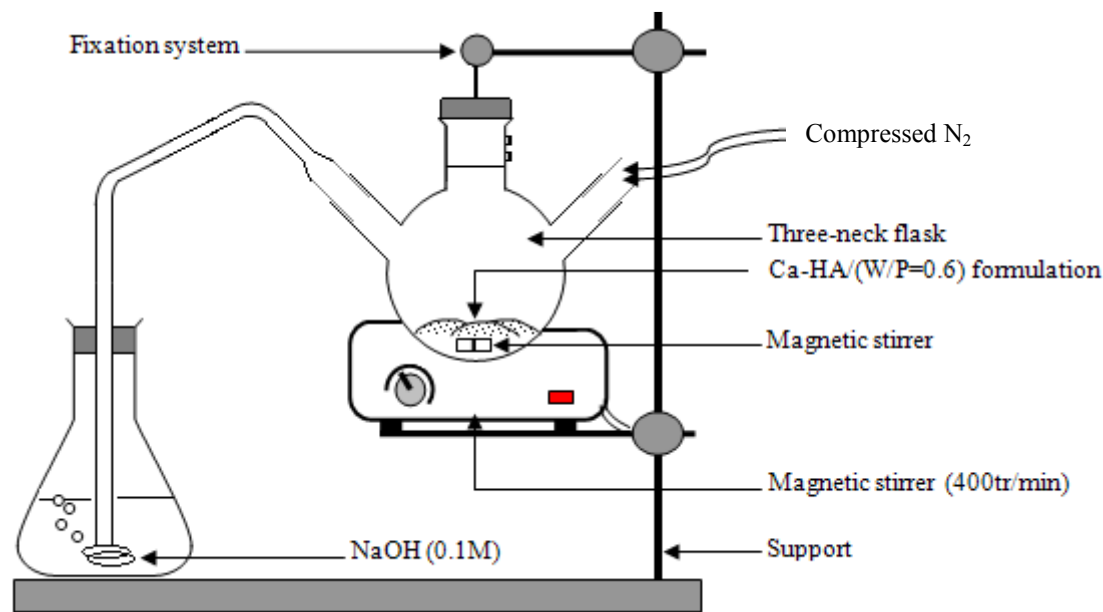
Figure 47: Mounting used to quantify the released dioxide Carbone during the Ca-HA/calcium sulfate reaction

Figure 48 shows the concentration of released CO_2 versus time. In the beginning of the reaction, the released CO_2 increases rapidly to achieve a constant value of 0.1mg.l^{-1} after 45 minutes of reaction.
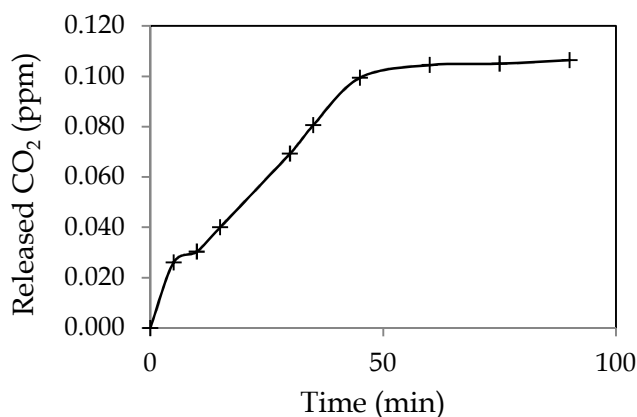
Figure 48 : Amount of released CO_2 as a function of time

The qualitative analysis have shown that the released gas is evidently CO_2. This result is in accordance with those obtained from ATG analysis, where the decrease in the decarbonatation is due to the reaction between Ca-HA and plaster.

VI.   Conclusion

Plaster hydrates following the stoichiometric W/P ratio of 0.2. Above 0.4 W/P mass ratio, plaster particles hydrate perfectly. Water consumption decreases by increasing the W/P mass ratio. The porosity of plaster increases as a function of amount of mixing water. The amount of adsorbed water in plaster solid blended with W/P mass ratio ranging from 0.4 to 1.4, increases with increasing W/P ratio. It was difficult to evaluate the total porosity and the capillary rise of samples based on Ca-HA-Plaster, this could be due to the frequent dissolution and destruction of solid body in water. Concerning the formulations containing Ca-HA, plaster and water, the amount of water dosage and plaster dosage was identified at W/P mass ratio of 0.4. The hydration of plaster according to W/P of 0.4 in Ca-HA$_{Gel}$ controls the consistency of the blends. The reaction between plaster and Ca-HA were observed for each formulations. The reaction led to an heterogeneous structure. The heterogeneity is due to the release of CO_2. However, the release of CO_2 indicates that the unreacted calcite reacts with phosphate (free phosphate of Ca-HA$_{Gel}$ and dissolved phosphate provided by the plaster) to produce calcium-phosphate-sulfate hydrates.

Reference

[1] JAFFEL H., KORB J-P., NDOBO-EPOY J-P., GUICQUERO J-P., and MORIN V., 2006, *Multi-scale approach continuously relating the microstructure and the macroscopic mechanical properties of Plaster pastes during their setting*. J. Phys. Chem. B 2006, 110, Pp18401-18407

[2] JAFFEL HAMOUDA., 2006, *Caractérisation multi-échelle de matériaux poreux en évolution : cas du plâtre*. Thèse soutenue le 08 Décembre 2006, Ecole polytechnique, Palaiseau, Pp56,

[3] GREISH Y., E., 2011, *Phase evolution during the low temperature formation of stoichiometric hydroxyapatite-gypsum composites*, Ceramics International 37, Pp715-723

Chapter V

Rheological behavior of gypsum, plaster and hydroxyapatite gel blends

Introduction

Calcium phosphate is a well-known biomaterial frequently used in the medical domain and as an agricultural fertilizer. It can come from natural sources such as fish or cow bones or as a result of a synthesis process using calcium and phosphate compounds. Calcium phosphate has been investigated as a reactive material, especially in its thermodynamically stable structure with the stoichiometric ratio Ca/P = 1.67 (hydroxyapatite, Ca-HA), to determine its usefulness in treating contaminated water or as a stabilizing agent for hazardous waste [1-3]. Many studies have also shown the capacity of Ca-HA to remediate soil and groundwater [4,5]. Gypsum can have two origins: natural gypsum and synthetic gypsum. Natural gypsum, characterized by a high purity, is an anionic mineral with a C_{2h}^{6} space group. This gypsum is a rock resulting from the evaporation of water from saturated calcium sulfate and geological sedimentation. Synthetic gypsum is a byproduct of industrial activities. It is obtained from a reaction between sulfuric acid and phosphate rock to produce phosphoric acid (H_3PO_4). The precipitate, usually named phosphogypsum (PG), is dihydrated calcium sulfate. This gypsum contains a significant amount of impurities and is considered to be a waste product. The environmental impact associated with PG storage and disposal, as reviewed by *Tayibi et al.*, is negative on the surrounding land, water, and air [6]. Valorization seems to be by far the best way to reuse this hazardous material. Industrial PG can be valorized as a material for soil stabilization. It can be added to Portland cement or to reactive materials such as fly ash to enhance the mechanical properties of the soil and to reduce the plasticity index, moisture, and water content [7]. It can also be used as a hydraulic binder in the design of calcium sulfoaluminate cement [8]. The calcium

sulfates used in this work are industrial gypsum ($CaSO_4 \cdot 2H_2O$) and plaster ($CaSO_4 \cdot 0.5H_2O$). They are by-products of phosphoric acid production and are washed to eliminate the residual fraction (phosphate, fluor, sodium, radionuclides, etc.).

There are three anhydrous or anhydrite forms produced by sintering of hemihydrates or gypsum: the compact form α-$CaSO_4$ or $CaSO_4$-I, obtained at 1200 °C and characterized by a crystalline structure; the stable form β-$CaSO_4$ or $CaSO_4$-II, obtained at 400 °C, which is a natural insoluble anhydrite; the metastable form γ-$CaSO_4$ or $CaSO_4$-III, obtained at low temperature between 130 and 200 °C, which is a soluble anhydrite [9]. The stability of gypsum is also influenced by the relative humidity (RH). At 10−35% RH, the migration of water molecules takes place toward the crystals, while at 100% RH, the migration takes place in the opposite direction [10,11]. The crystalline structure of the gypsum, characterized by a perfect cleavage orientation (010), results in the circulation of water, leading to dissolution on the surface (010) [11,12]. The blending of hemihydrates with water gives a rigid and compact solid body, due to the hydration process.

The main purpose of the work presented in this chapter is to investigate the rheological behavior of water/gypsum, water/plaster, Ca-HA/ gypsum, and Ca-HA/plaster blends. This is a preliminary step in a project devoted to the formulation and characterization of a Ca-HA-based permeable reactive barrier. The evaluation of the rheological behavior of a mixture of *gypsum* and *plaster* on Ca-HA$_{Gel}$ aims to better understand the development of the matrix microstructure and, consequently, to assess its workability.

I.   Materials and methods

1.   Calcium sulfates

The gypsum (G, $CaSO_4 \cdot 2H_2O$) and the plaster calcium sulfate (P$_\alpha$, $CaSO_4 \cdot 0.5H_2O$, prepared by the wet method) used in this work are industrial byproducts of a phosphoric acid (H3PO4) preparation from phosphate rock (PRAYON, Belgium).

The plaster was used as received, and gypsum was sieved to under 1 mm and the larger fraction discarded.

2. Hydroxyapatite-Gel (Ca-HA$_{Gel}$)

Ca-HA$_{Gel}$ was obtained by the reaction between calcite ($CaCO_3$; 98% pure, Fisher Scientific) and ammonium phosphate ($NH_4H_2PO_4$; 99.4% pure, Fisher Scientific) at 25 °C with a molar ratio of Ca/P = 1.67, and the amount of demineralized water is 3 times higher than that of calcite. The equation below describes the overall reaction pathway for the synthesis of Ca-HA. During the formation of Ca-HA$_{Gel}$, bubbling corresponding to the release of CO_2 gas was observed.

$$10CaCO_3 + 6NH_4H_2PO_4 + 2H_2O \rightarrow Ca_{10}(PO_4)_6(OH)_2 + 6NH_4OH + 2H_2O + 10CO_2 \qquad [R. 1]$$
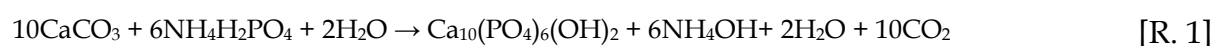
At the beginning of the reaction, the pH value increased gradually from 6 to 8 and then stabilized after 12 h of synthesis. The stabilization of the pH revealed the formation of an ammonium hydroxide buffer and the consumption of calcium carbonate. Ca-HA$_{Powder}$ was prepared by drying Ca-HA$_{Gel}$ at 105 °C for 24 h to obtain a powder with monomodal particle size distribution. The water content calculated after drying at 105 °C was 70%. Ca-HA$_{Gel}$, destined to be used for chemical characterization, was filtered and rinsed with deionized water to dissolve any unreacted phosphate.

3. Physical and chemical characterization

Powder densities were measured using a helium pycnometer (AccuPyc 1330 V2.04N). The specific surface areas of the materials (G, P, and Ca-HA) were determined on a Micromeritics Gemini 2360, by surface analysis using the Brunauer−Emmett−Teller method, and the measurements were performed by nitrogen absorption at liquid-nitrogen temperature followed by desorption (adsorption gas N2; heating temperature 150 °C). The particle-size distribution was determined by LASER granulometry using a Malvern Laser Master Sizer Hydro 2000 instrument (with ethanol as a dispersant shaken by ultrasound). The pH

measurements were made after dispersion of 10 g of powder materials in 25 mL of deionized water and stirring for 1 h at room temperature, with the measurement being carried out after 2 h. The particle charge was evaluated relative to the net charge on the particles' surfaces by evaluation of the pH point zero charge (pH_{PZC}). This determination is based on the electrochemistry and involves the introduction of 50 cm3 of a NaCl (0.01 M) solution in closed vials and adjustment of the initial pH to values between 2 and 12 by the addition of NaOH or HCl (0.1M). A mass of 0.15 g was added to the vials, and the final pH was measured and recorded after stirring for 48 h at room temperature. The pH_{PZC} value corresponds to the intersection point of the titration curves obtained at one ionic strength for the suspension ($pH_{initial}$) and blank solution (pH_{final}).

Zeta potential measurements were performed on a ZETASIZER 3000 HSA (Malvern instruments Ltd).

The rheological measurements were performed using a Rheostress (HAAKE RS 150 Rheometer). The rheological behavior and viscosity η(Pa.s) were evaluated for shear rates ranging from 0 to 500s^{-1} at constant temperature (20±5°C). The sample was placed in a cylindrical vessel and the strain was applied by a double helical ribbon impeller. Samples were homogenized before measuring the shear stress τ(Pa) and the viscosity versus the applied shear rate $\dot{\gamma}$(s^{-1}). The dynamic trails applied on Ca-HA$_{Gel}$ were performed with the same apparatus using oscillation mode with a preselected constant shear stress of 50Pa and a frequency ranging from 1 to 50Hz. The loss and storage module measurements were recorded for 300s at room temperature.

4.   Formulations

Rheological tests were carried out on pure Ca-HA$_{Gel}$, on binary water/gypsum (W/G) and on water/plaster (W/P) blends. Binary blends were prepared by mixing the selected material with de-ionized water according to different mass ratios ranging from 0.4 to 1.4. Solid concentrations of binary blends (Γ_{B1}) and *water/gypsum* and *water/plaster* mass ratios were calculated as follows:

$$\Gamma_{B1} = \frac{V_s}{V_{s+}V_w} \quad ; \quad \frac{W}{G} = \frac{1-\Gamma_B}{\rho_G\Gamma_B} \quad ; \quad \frac{W}{P} = \frac{1-\Gamma_B}{\rho_P\Gamma_B} \qquad \text{[Eq. 1]}$$

Where V_s is the volume of solid phase, V_w is the volume of water and ρ_G and ρ_P are the densities of gypsum and plaster respectively. The Ca-HA$_{Gel}$ content considered was from 0 to 50wt% Ca-HA$_{Gel}$. The rheological behaviors of water-free formulations (Ca-HA$_{Gel}$/G and Ca-HA$_{Gel}$/P) with mass ratios of 50/50, 40/60 and 30/70 were not considered, as the pastes obtained are very thick, and almost solids). The solid concentration of binary blends (Γ_{B2}) containing either gypsum or plaster (calcium sulfate powder) with Ca-HA$_{Gel}$ was calculated as follows:

$$\Gamma_{B2} = \frac{V_{S_T}}{V_{S_T}+V_{W_T}} \qquad \text{[Eq. 2]}$$

$$V_{S_T} = V_{Ca-HA_{Powder}} + V_{CS_{Powder}} \qquad \text{[Eq. 3]}$$

$$V_{W_T} = V_{Ca-HA_{Water}} \qquad \text{[Eq. 4]}$$

Where V_{S_T} is the total volume of solid material equal to the sum of Ca-HA$_{Powder}$ volume ($V_{Ca-HA_{Powder}}$) and calcium sulfate powder volume ($V_{CS_{Powder}}$), and V_{W_T} is the total water equal to Ca-HA water volume ($V_{Ca-HA_{Water}}$).

II.   Results and discussion

1.   Characteristics of the materials

The results of bulk density, specific surface area and pH of materials are given in **Table 22**. It can be seen that the bulk densities were used to calculate the solid concentration in the blends. The specific surface area of plaster is three times higher than that of gypsum. The specific surface area of Ca-HA$_{Powder}$ indicates the surface reactivity of the particles. The net charge of the materials can be evaluated by referring to the pH of the aqueous solutions with the metal surface in a neutral electric state and pH$_{PZC}$. The hemihydrated calcium sulfate and Ca-HA particles are positively charged (pH<pH$_{PZC}$) and dihydrated calcium sulfate particles are negatively charged (pH>pH$_{PZC}$).

Table 22: Physicochemical characteristics of materials

	G_{powder}	P_{powder}	Ca-HA$_{Powder}$	Ca-HA$_{Gel}$
Bulk density ρ (gcm^{-3})	2.3	2.8	2.58	1.23
Surface specific area S_{SA} (m^{2}g^{-1})	26.3	72.8	138	-
pH	8.5	2.9	7.9	8.4
pH$_{PZC}$	7.5	3.3	8.1	-
Residual Moisture 105°C (%)	20	5	-	67
Loss on ignition (at 1000°C) (%)	22	8	59	-
Granulometric fraction (%)				
Sand	79.6	48.9	43.4	9.0
Silt	18.7	49.0	51.7	88.0
Clay	1.7	1.7	4.9	3.0

The classification and identification of materials following the geotechnical designation reveals that plaster and Ca-HA$_{Powder}$ seem to have a silty-sand texture, while gypsum, having a diameter less than 1mm, is sandy-silt and Ca-HA$_{Gel}$ is identified as silty (see **Table 22**).

2.   Rheological behavior

2.1.   Steady rheological properties of Ca-HA$_{Gel}$

Apatite gel is characterized by a specific texture caused by absorption of water and interaction between fine particles. The identification of the behavior and the structure Ca-HA$_{Gel}$ requires an understanding of the influence of parameters such as material deformation, strength and stability. Studies published by KNOWLES et al (2000), have shown that the rheological behavior of a Ca-HA suspension (from Tetrahydrated Calcium Nitrate and Ammonium Phosphate) at 60°C and commercial products have a shear-thinning behavior while Ca-HA synthesized at 80°C has a Newtonian behavior. This behavior evolves towards shear thickening (dilatants) when dispersant agents are added in excess [13].
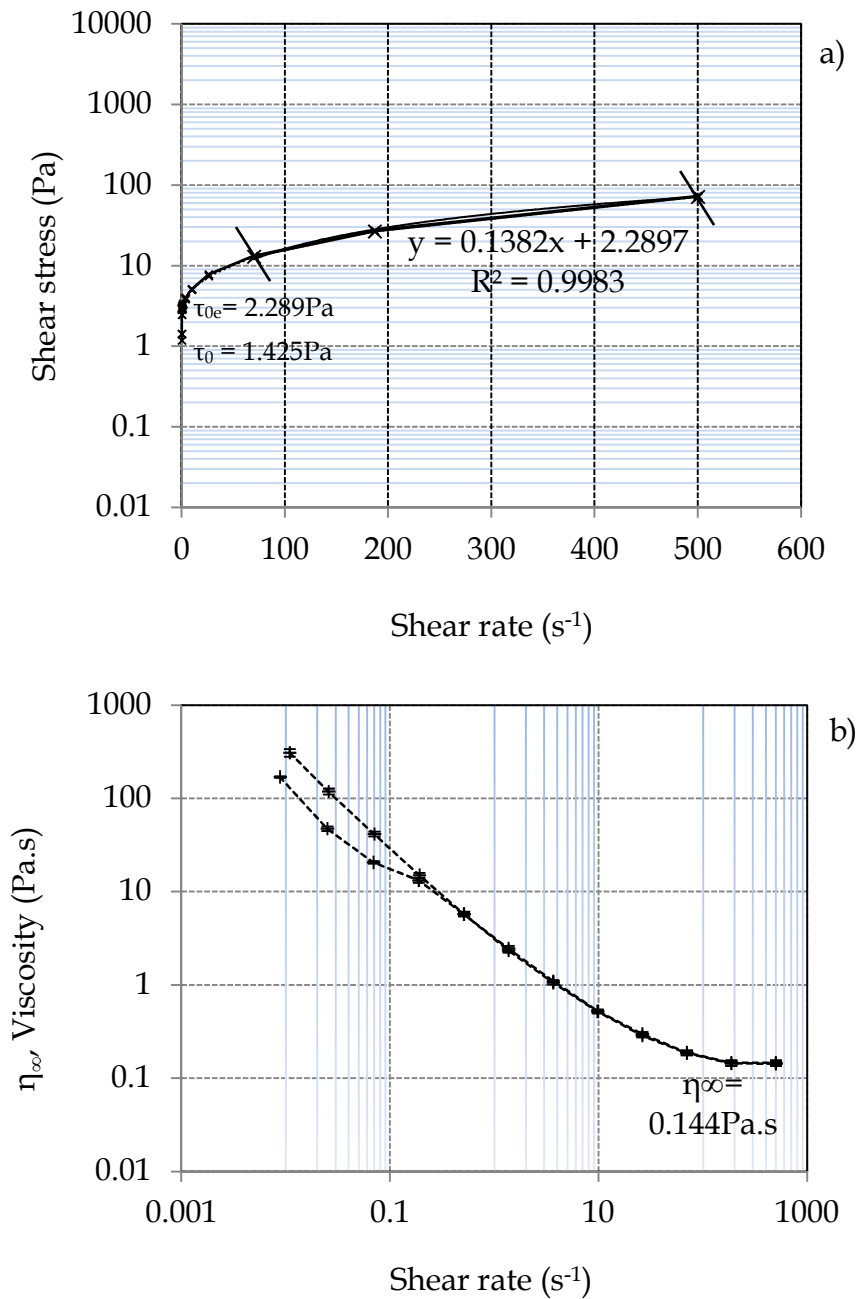
Figure 49: Rheological behavior and viscosity of Ca-HA$_{Gel}$ after 48h of synthesis, a) $\tau = f(\dot{\gamma})$; b) $\log(\tau) = f(\dot{\gamma})$ ($-\times-$Shear stress (Pa), $-+-$Viscosity (Pa.s))

As shown in **Figure 49**, the shear stress increases with the shear rate when the stress exceeds a threshold value τ_0 (1.425Pa), indicating that Ca-HA$_{Gel}$ exhibits a shear thinning, or, specifically, a viscoplastic behavior. Viscosity reaches an apparent value of (η_∞=0.144Pa.s) above $\dot{\gamma}$=200s^{-1}. The critical shear rate corresponding to the Ca-HA dispersion is characterized by an extrapolated maximum yield stress τ_{0e} (2.289Pa) and minimum yield stress τ_0 (1.425Pa), related to the response of the gel to the

deformation. The viscosity of Ca-HA$_{Gel}$ is of 0.144Pa.s at a higher shear stress, and above this value the suspension flows. The increase in the shear stress leads to the disruption of the gel structure, and when the shear stress stops, the suspension tends to recover its original structure (i.e. the flow is reversible). Viscosity does not only depends on the shear rate but it is also correlated to the duration of the applied stress. The internal structure of Ca-HA$_{Gel}$ undergoes an initial homogenization at low shear rate values corresponding to low levels of plasticity. The constraint force is too small to disorganize the structure; it requires an increase in the magnitude of applied force for the flow to occur. Beyond the shear stress threshold, with an increasing shear rate, the flow is enhanced by the gradual dispersion of particles, promoting the separation effect which causes the decrease in viscosity. The viscosity (apparent viscosity) value stabilizes at high shear rates. Once the apparent viscosity is reached there is no further modification observed for the structure of Ca-HA$_{Gel}$.

2.2. Dynamic rheological properties of Ca-HA

To explain the viscoelastic behavior observed for the Ca-HA$_{Gel}$, dynamic oscillatory tests were carried out to investigate the internal structure and response of the gel during the Ca-HA synthesis.

The dynamic rheological (oscillatory) test aims to determine the storage (G′) and loss (G′′) modulus. **Figure 50** represents the results of the frequency-sweep response of a Ca-HA suspension after 12, 24, 48 and 72 hours of synthesis. During the synthesis, the storage and loss modulus (G′, G′′) rose with the increase in the frequency and their values decreased with the aging of the gel.

At low frequencies, the 12h age dispersion (**Figure 50** a)) seems to have a heterogeneous structure at the beginning of the periodic oscillation application. It is observed that G′ is greater than G′′, which corresponds to an elastic behavior. Therefore, when the frequency is increased, the module values increase strongly due to the dispersed state of the particles.
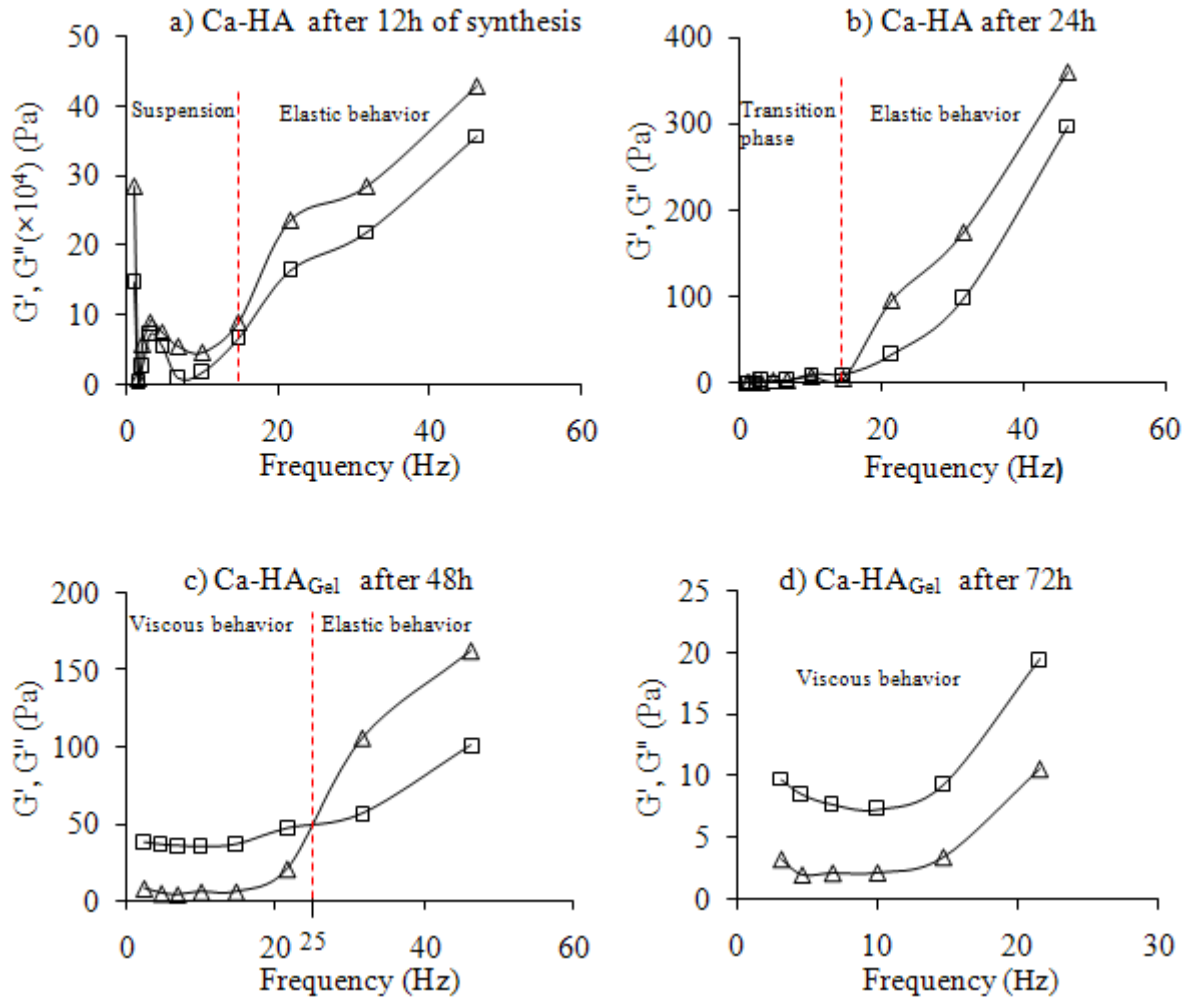
Figure 50: Frequency-sweep curves of Ca-HA as a function of synthesis time
(—△— , storage modulus G′, —□— loss modulus G″). The description of the
behavior of Ca-HA$_{Gel}$ is based on two conditions if G′> G″, elastic behavior, and if
G′< G″, the behavior is viscous.

For 24h age dispersion (**Figure 50** b)), the value of the storage and loss modulus is
almost zero below 15Hz. The strain response at constant stress after 24h of synthesis
is delayed compared to the 12h age dispersion measurement. This change in
behavior, identified at low frequencies, is due to the evolution of the reaction. This
response is related to the precipitation of the Ca-HA suspension occurring when the
pH value buffers around 8, leading to the formation of a colloidal suspension. The
behavior remains elastic at high frequency values.

After 48h of synthesis (case c)), we observe a complete change in behavior at low
frequencies; for frequencies below 25Hz, G′ and G″ increase exponentially at low
stress. Below 25Hz, G″ is greater than G′, indicating viscous behavior. This simply

means that the suspension follows a constant structural deformation where the stress is proportional to the strain rate. When the frequency reaches values higher than 25Hz, G″ becomes smaller than G′, indicating an elastic behavior: the stress is proportional to the deformations (**Figure 50 c**)). However, the viscosity increases progressively, indicating the agglomeration of colloids and the formation of gel-paste calcium phosphate. This result is important since it shows the transition between a suspension and pasty behavior. As demonstrated by KNOWLES et al [14] and BAO et al [14], the mutual approach of particles in solution is correlated to the positive charge of the Ca-HA surface. The behavioral changes show the formation of gel particles or gel-paste structures after 2 days of reaction, exhibiting a viscoelastic behavior. The dynamic rheological properties study carried out by LIU et al (2006) [15] on calcium-phosphate cement slurry (a composite of equimolar tetracalcium (TECP) and dicalcium phosphate anhydrous (DCPA)) under the condition of a 2.0 Powder/Liquid ratio and a 1% strain showed that at the range of low strain and low frequency, the slurry behaved to yield behavior when frequency increases. The slurry began to flow and presented a shear-thinning behavior.

For the 72h age dispersion (case d)), the loss modulus values are higher than the storage modulus values, thus revealing a viscous behavior. Nevertheless, when the frequency increases and the strain exceeds the yield strain, the viscosity decreases. The decrease in G′ and G″ values is due to gel aging and stirring, which cause a large deformation of the gel structure. The disruption of extractible water molecules caused by bonds between particles leads to flow and demonstrates that the Ca-HA$_{Gel}$ exhibits a shear-thinning behavior.

2.3. Rheological behavior of binary blends

The viscosity of the binary matrix was measured and plotted versus the concentration of added powder, as illustrated in **Figure 51** and **Figure 52**. W/G and W/P blends exhibit shear-thinning behavior.
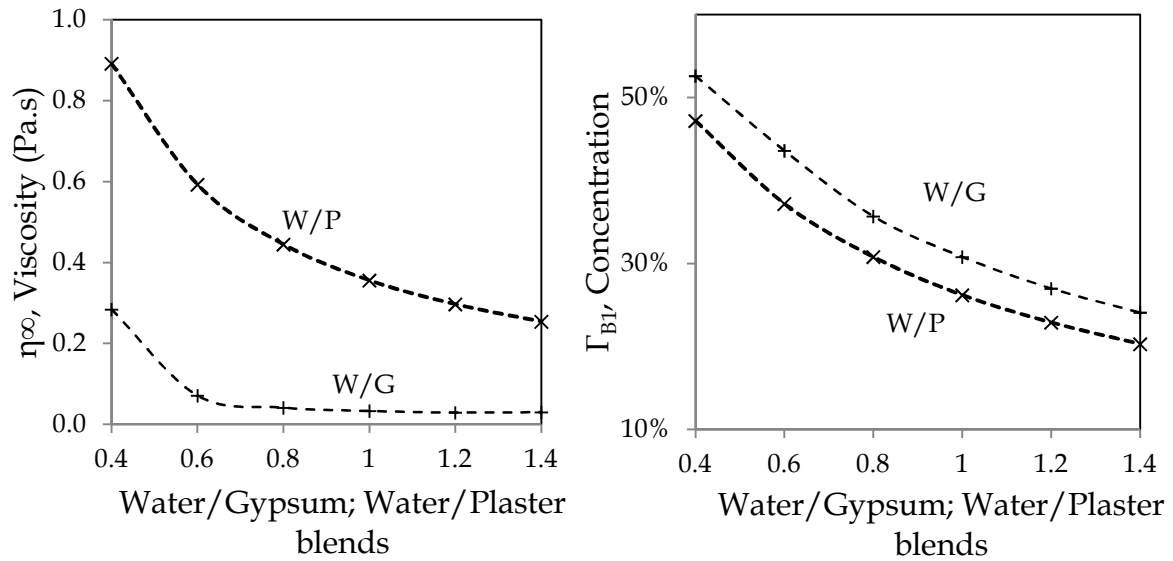
Figure 51: a) Viscosity of W/G and W/P blends at different mass ratios, b) Concentration of gypsum and plaster at different mass ratios

Figure 51 shows that the viscosity of W/G blends decreases with a decreasing gypsum concentration until achieving an almost constant apparent viscosity for W/G ratios above 0.6. The viscosity plateau reveals no influence of water on the particle surface of gypsum and shows that the grains undergo the action of gravity and buoyancy (characterized by an apparent density of 1.25g.cm^{-3} in the cylindrical vessel).

Hydrated gypsum particles present similar double-electric layers of a common charge (negatively charged) which generates *electrostatic repulsion* between particle surfaces (due to the overlap of the electrical double-layers theory). Gypsum grains are mainly negatively charged and surrounded by a diffuse layer of positive average charge. This positive charge layer stabilizes the dispersion through particle repulsion, avoiding particle aggregation. At rest, particles tend to precipitate. If a stress is applied, the suspension is dispersed leading to a decrease in viscosity. The gypsum concentration controls the dispersed state; the repulsive forces tend to stabilize the suspension, because the particles are negatively charged. The apparent viscosity is obtained at a high shear rate where gravity forces are negligible. It can be seen that above a 0.6 W/G ratio, inter-particle distance is large enough to make apparent viscosity independent of gypsum content.

150

With regards the plaster blends (W/P), the viscosity decreases with decreasing plaster concentration. The hydration of hemihydrate particles, requiring 1.5 water molecules, leads to crystallization. In general, the contact of plaster particles with water triggers dissolution, which induces the saturation or supersaturation of the solution in Ca^{2+} and SO_4^{2-}, leading to the formation of gypsum nuclei [16]. Consequently, the hydration controls scenario is correlated to the nucleation and crystal growth mechanism [17,18].

The high specific-surface area of *plaster* particles plays a major role in the multiplication of inter-granular links. Interaction between plaster particles occurs by *electrostatic forces* (i.e. the spread of ions in an extended diffuse layer) and attractive forces (*Van der Waals*) responsible for *adhesion*. Furthermore, adhesion is described as the formation of two Ca^{2+}/SO_4^{2-} layers bound together by ionic interaction constructing a growth slice [16]. The predominance of reactive sites on the grains attracts cations which form a rigid network that surrounds the layer of adsorbed water molecules. It is also known that the attraction of plaster particles requires cohesion between atoms to form the contiguous flakes. The development of this structure (agglomerated structure or plaster paste) depends on the amount hydration water. According to the stochiometry, the α-hemihydrates require a W/P ratio higher than 0.186 to be transformed into gypsum. To improve the consistency of the blends, the hydration rate was chosen from a range of 0.4 to 1.4. In the dynamical study in the linear viscoelastic domain published by FINOT et al (2001), the time-sweep test at 0.015% (ω=10rad.s^{-1}), carried out on W/P=0.7, indicates that the rise in the storage modulus reflects the hydration and setting process. This reveals an increase in the level of crystallized gypsum [19]. Obviously, the viscosity decreases steadily with an increasing amount of water, and the application of shear stress destroys the links between particles, facilitating the decoagulation of the structure and leading to flow. Plaster hydrates during viscosity measurement under stress. The plaster viscosity value depends on the volume fraction of the solids (solid concentration Γ_{B1}), particle size and water excess (free of water after full plaster hydration). At a high shear rate, it is possible to measure the apparent viscosity of the dispersion of agglomerated

hydrated particles. The apparent viscosities of W/G blends are lower than those of W/P blends. Because plaster hydration held the measurement long, the difference observed in apparent viscosity between W/G and W/P cannot be solely attributed to hydration. The difference observed in a specific-surface area may provide an explanation.

Figure 52 show that the viscosity increases when the solids concentration (Γ_{B2}) increases, the latter being calculated relative to the water (by wt %) present in the Ca-HA$_{Gel}$. It should be noticed that the formulations having Ca-HA$_{Gel}$ /G or Ca-HA$_{Gel}$ /P ratios higher than 1.5 are solids, and their rheological properties were not characterized.
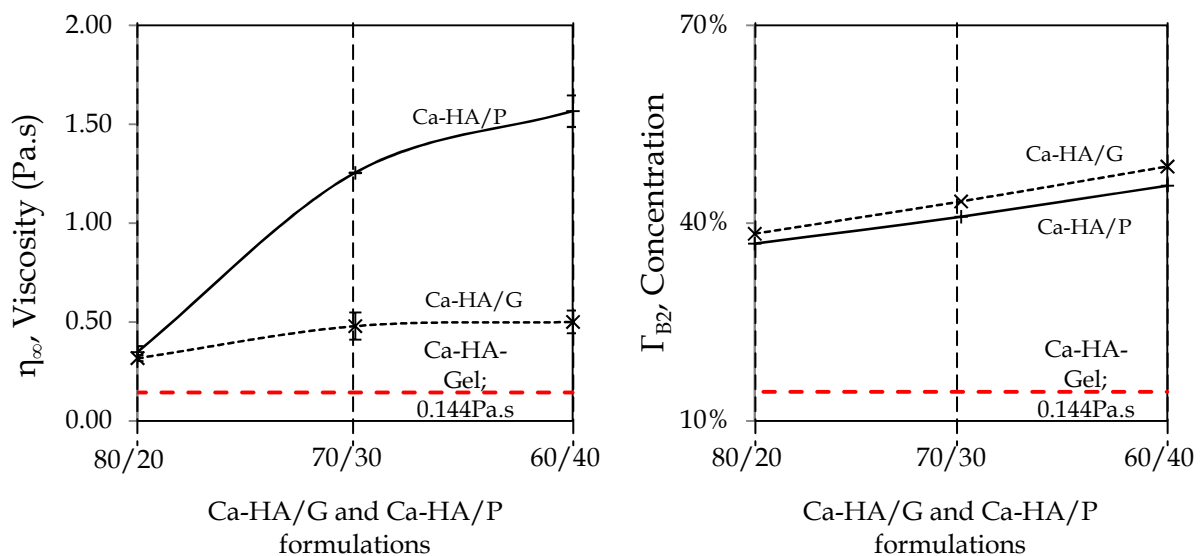
Figure 52: Viscosity of Ca-HA/G and Ca-HA/P formulations

The water content in Ca-HA is more than sufficient to hydrate calcium sulfate hemihydrate particles. In this case, an almost solid paste is formed. Replacing 20% of Ca-HA$_{Gel}$ by gypsum or plaster produced little influence on viscosity, indicating that for this blend there is little influence of calcium sulfate on the rheological properties of Ca-HA$_{Gel}$. As regards the already-hydrated gypsum particles, increasing the gypsum concentration in the blend up to 40% produced a slight increase in viscosity. Blends containing more than 40% of gypsum are almost solids. The addition of plaster to Ca-HA requires a high stress to cause the flow. Plaster particles in contact with Ca-HA water cause plaster hydration, creating strong bonds that encompass the

Ca-HA particles and make difficult the flow of the blend. Hydrated plaster strongly increases the viscosity of Ca-HA$_{Gel}$ by its own weight.

Figure 53 shows the thixotropic behavior of binary blends containing a mass ratio blend of 80% of Ca-HA and 20% of plaster and a mass ratio of 80% of Ca-HA and 20% of gypsum, indicating that the blends recover their initial structure. In this case, viscosity values increase slightly compared to the viscosity of Ca-HA$_{Gel}$ while keeping their flow characteristics.
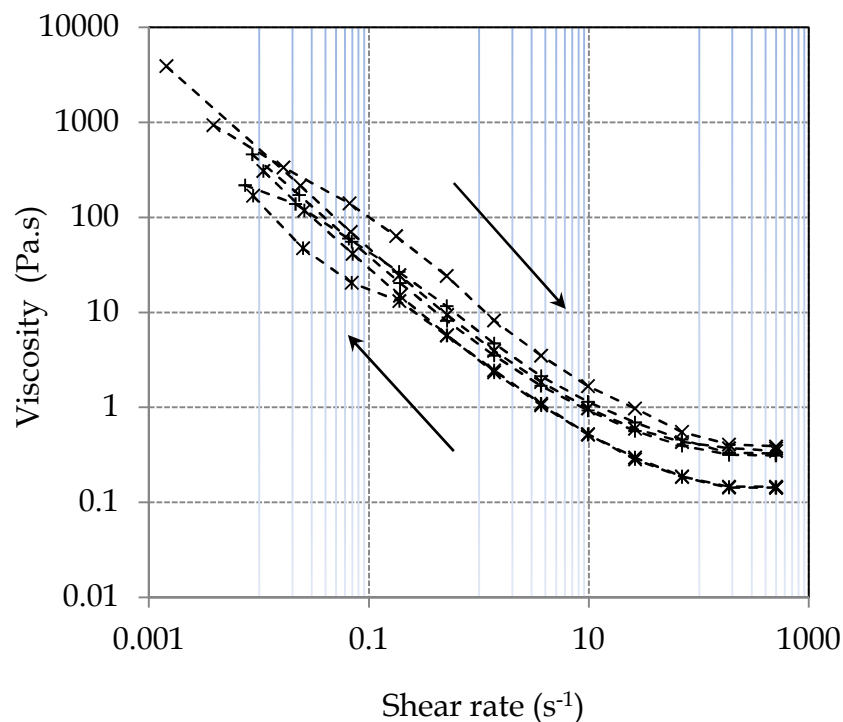
Figure 53: Example of thixotropic hysteresis loop of composites 80%Ca-HA/20%(G) and 80%Ca-HA/20%(P) (--*--Ca-HA$_{Gel}$ ($\eta\infty$= 0.144Pa.s),--×-- 80%Ca-HA$_{Gel}$/20%(P) (Γ=0.369; $\eta\infty$= 0.348Pa.s), --+--80%Ca-HA$_{Gel}$/20%(G) (Γ=0.384; $\eta\infty$= 0.318Pa.s)

2.4.   Interaction between particles

The interpretation of interactions between these compounds is complex. The zeta potential (ζ-potential) has been considered as a mean to understand the interactions, based on the net charge of particles, and hence to describe the suspension structure. The ζ-potential indicates the repulsion forces between particles promoting dispersion stability. **Figure 54** shows that the Ca-HA particles are characterized by a negative ζ-

potential, indicating that particles are positively charged (≈-20mV) [13] and the gypsum particles are negatively charged (≈20mV) [20]. The Ca-HA ζ-potential value indicates the instability of the gelled particles. Adding gypsum to Ca-HA leads to charge modification. High ζ-potential values prevent the presence of repulsive forces and indicate colloidal dispersion. These results support the assumption of sulfate attraction on the Ca-HA surface, indicating the dispersion of particles. However, sulfate adsorption changed the charge distribution, generating the change from positive to negative charge.
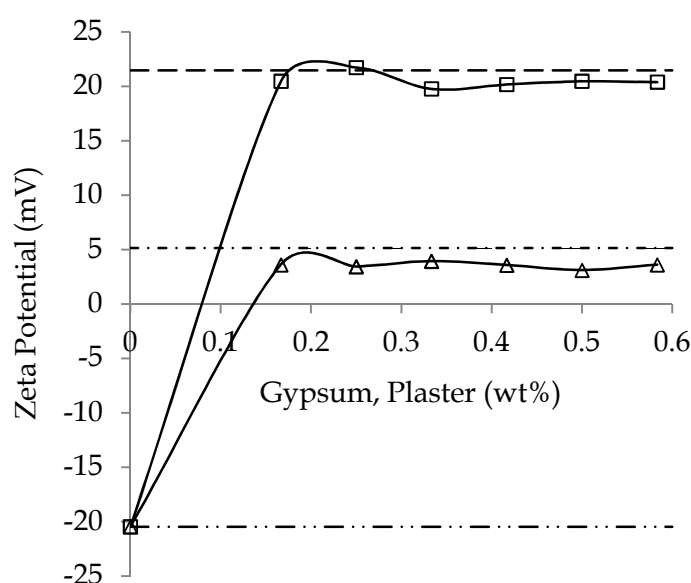
Figure 54: Zeta potential of Ca-HA/(G) and Ca-HA/(P) formulations without added water (–– ζ-potential of gypsum (≈20mv), –··–··– ζ-potential of plaster (≈5mv), –···–···– ζ-potential of Ca-HA (≈-20mv), —□— ζ-potential of Ca-HA /G formulations, —Δ— ζ-potential of Ca-HA /P formulations)

The adsorbed amount of anionic sulfate on Ca-HA particles is equal to the Ca-HA electrical charge sites and the coating of gypsum sulfate Ca-HA particles is the main reason for the modification of ζ-potential. The surfaces of plaster particle are characterized by a positive charge, and hydration changes the surface charge to negative. The formation of a plaster solid body is explained by the cohesion between particles and is illustrated by a low ζ-potential value.

Figure 54 represents the ζ-potential of formulations containing Ca-HA and different proportions of the W/P ratio. With the increase of the amount of plaster, the ζ-

potential remains constant (with similar values to the plaster at the beginning of the hydration process), and the surface charge of Ca-HA changes. The nucleation process of hemihydrated particles starts by the formation of Ca^{2+}/SO_4^{2-} bound double layers, and the concentration of sulfate decreases, indicating that it is consumed during the hydration. However, the fixation of remaining sulfate in solution on the Ca-HA surface leads to the change in the charge.

Conclusion

The rheological test carried out reveals shear-thinning and the thixotropic behavior of Ca-HA$_{Gel}$ for formulations considered. The internal structure of Ca-HA$_{Gel}$ exhibits to viscoelastic behavior after 48h of synthesis.

The negatively-charged gypsum particles cause the repulsion of particles (repulsive forces) and the viscosity of W/G (0.2–1.4) blends remains constant. Plaster is characterized by attractive forces and the particles are positively charged. The hydration of plaster leads to cohesion between particles, which explains the increase in viscosity of W/P blends compared to W/G blends. The ζ-potential of Ca-HA is negative and the dissolution of calcium-sulfate particles saturates the solution in sulfates ions (SO_4^{2-}); the charge of particles becomes positive, due to the fixation of SO_4^{2-} on the Ca-HA surface. The adsorption of sulfate on the Ca-HA particle surfaces influences the structure of formulations and explain why the viscosity is independent of Ca-HA$_{Gel}$ content. Plaster hydration plays a major role in the Ca-HA$_{Gel}$ stabilization structure. The modification in ζ-potential can affect retention capacity, reactivity and mechanical resistance. These aspects will be the subject of later study.

This study has led to the understanding of the rheological and physicochemical behavior on water/calcium sulfates and hydroxyapatite/calcium sulfate blends. These results will be useful in the formulation of permeable reactive barrier.

References

[1] CHEN X., WRIGHT J.V., CONCA J.L., PEURRUNG L.M., 1997, *Evaluation of heavy metal remediation using mineral apatite.* Water, Air, and Soil Pollution 98, Kluwer Academic Publishers. Printed in the Netherlands; Pp57–78

[2] NZIHOU A., SHARROCK P., 2002, *Calcium phosphate stabilization of fly ash with chloride extraction*, Waste Management, Volume 22, Issue 2, Pp235-239

[3] BAILLEZ S., NZIHOU A., BERNACHE-ASSOLANT D., CHAMPION E., SHARROCK P., 2007, *Removal of aqueous lead ions by hydroxyapatites: Equilibria and kinetic processes*, Journal of Hazardous Materials A139, Pp443–446

[4] MOORE R.C., 2005, *Stabilization and Solidification of hazardours,* Radioactive and mixed Wastes, ROGER, D.Spence, SHI, Caijun, Pp98-112

[5] CONCA J., & WRIGHT J., 2006, *An Apatite II permeable reactive barrier to remediate groundwater containing Zn, Pb and Cd.* Applied Geochemistry, *21*(12), Pp2188-2200

[6] TAYIBI H., CHOURA M., A.LOPEZ F., ALGUACIL F.J., LOPEZ-DELGADO A., 2009, *Environmental impact and management of phosphogypsum*, Journal of Environment Management 90, Pp2377-2386

[7] DEGIRMENCI N., OKUCU A., TURABI A., 2007, Application *of phosphogypsum in soil stabilization*, Building and Environment 42, Pp3393-3398

[8] KURYATNYK T., ANGULSKI DA LUZ C., AMBROISE PERA, J., 2008, *Valorization of phosphogypsum as hydraulic binder*, Journal of Hazardous Materials 160, Pp681-687

[9] IRIBARNE A. P., IRIBARNE J. V., & ANTHONY E. J., 1997, *Reactivity of calcium sulfate from FBC systems.* Fuel, *76*(4), Pp321-327.

[10] AUVRAY C., HOMAND F., & HOXHA D., 2008, *The influence of relative humidity on the rate of convergence in an underground gypsum mine.* International Journal of Rock Mechanics and Mining Sciences, *45*(8), Pp1454-1468

[11] FINOT E., LESNIEWSKA E. MUTIN, J.-C, GOUDONNET, J.-P, 1997, *Reactivity of gypsum faces according to the relative humidity by scanning force microscopy*, Surface Science 384, Pp212-217

[12] FAN, C., & TENG, H., 2007, *Surface behavior of gypsum during dissolution.* Chemical Geology, *245*(3-4), Pp242-253.

[13] KNOWLES, J. C., CALLCUT, S., & GEORGIOU, G. 2000, *Characterisation of the rheological properties and zeta potential of a range of hydroxyapatite powders.* Biomaterials,

21(13), Pp1387-1392.Retrieved from http://www.ncbi.nlm.nih.gov/pubmed/10850933.

[14] BAO Y., SENOS A M. R., ALMEIDA M., & GAUCKLER L. J., 2002. *Rheological behavior of aqueous suspensions of hydroxyapatite (HAP)*. Journal of materials science.Materials in medicine, *13*(7), Pp639-43. Retrieved from http://www.ncbi.nlm.nih.gov/pubmed/15348572

[15] LIU C., SHAO H., CHEN F., ZHEN H., 2006, *Rheological properties of concentrated aqueous injectable calcium phosphate cement slurry*, Biomaterials 27, Pp5003-5013

[16] SINGH N.B., MIDDENDORF B., 2007, *Calcium sulphate hemihydrate hydration leading to gypsum crystallization*, Progress in Crystal Growth and Characterization of Materials 53, Pp57-77

[17] BOSBACH D., JUNTA-Rosso J.L., BECKER U., and HOCHELLA JR M.F., 1996, *Gypsum growth in the presence of background electrolytes studied by Scanning Force Microscopy*, GeochimicaetCosmochimicaActa, Vol. 60, No. 17, Pp3295-3304

[18] SIEVERT T., WOLTER A., SINGH N.B., 2005, *Hydration of anhydrite of gypsum (CaSO4.II) in a ball mill*, Cement and Concrete Research 35, Pp623-630

[19] FINOT, E., LESNIEWSKA, E. MUTIN, J.-C, GOUDONNET, J.-P, MUTIN, J-C., DOMENECH, M., AIT KADI, A., 2001, *Correlation surface forces with surface reactivity of gypsum crystals by atomic force microscopy. Comparison with rheological properties of plaster*, Solid State Ionics 141-142, Pp39-46

[20] PENG J., QU J., ZHANG J., CHEN M., WAN T., 2005, *Adsorption characteristics of water-reducton agents on gypsum surface and its effects on the rheology of gypsum plaster*, Cement and Concrete Research 35, Pp527-531

Chapter VI
Rheological behavior of Water — Calcium sulfate — Hydroxyapatite-Gel ternary blends

Introduction

The formulation of a stable matrix from various initial materials requires a better understanding of the mixture and interaction between the components. The assessment of the rheological behavior may help to understand the flow mechanisms such as forces between inter-particles affecting the stability and the workability. Ca-HA was used in the formulation as metal ion stabilizing agent and both plaster and gypsum were used as support materials to enhance the stability of the structure and hydraulic performances of the formulations. The main purpose of this work is to investigate the rheological behavior of blends containing Ca-HA$_{Gel}$, water/gypsum and/or water/plaster with different proportions. The rheological tests aim to evaluate the influence of added water on the rheological properties of Ca-HA$_{Gel}$. This is a preliminary step in a project devoted to the formulation and characterization of a Ca-HA based permeable reactive barrier. The evaluation of the rheological behavior of a mixture of *water/gypsum* and *water/plaster* on the Ca-HA$_{Gel}$ aims to better understand the development of the matrix microstructure, and consequently to assess its stability and workability.

I.   Ternary formulations

Ternary blends were obtained according to material dosages listed in **Table 23**. Rheological tests were carried out on pure Ca-HA$_{Gel}$, on ternary Ca-HA$_{Gel}$/(water/gypsum) and on Ca-HA$_{Gel}$/water/plaster blends.

Table 23: Proportions of ternary blends (Ca-HA/(W/P) – Ca-HA/(W/G))

Blends	W/P=0.2	W/P=0.4	W/P=0.6	Blends	W/G=0.2	W/G=0.4	W/G=0.6
Ca-HA/(W/P)	80%/20%	80%/20%	80%/20%	Ca-HA/(W/G)	80%/20%	80%/20%	80%/20%
	70%/30%	70%/30%	70%/30%		70%/30%	70%/30%	70%/30%
	60%/40%	60%/40%	60%/40%		60%/40%	60%/40%	60%/40%
	50%/50%	50%/50%	50%/50%		50%/50%	50%/50%	50%/50%
	40%/60%	40%/60%	40%/60%		40%/60%	40%/60%	40%/60%
	30%/70%	30%/70%	30%/70%		30%/70%	30%/70%	30%/70%

Ternary blends were prepared by mixing binary blends (W/G or W/P according to different mass ratios ranging from 0.2 to 0.6) with Ca-HA. Solid concentration of ternary blends (Γ_T) was calculated as follows:

$$\Gamma_T = \frac{V_{S_T}}{V_{S_T} + V_{W_T}}$$ [Eq. 1]

$$V_{S_T} = V_{Ca-HA_{Powder}} + V_{CS_{Powder}}$$ [Eq. 2]

$$V_{W_T} = V_w + V_{Ca-HA_{Water}}$$ [Eq. 3]

Where V_{S_T} is the total volume of solid material equal to the sum of Ca-HA$_{Gel}$ volume ($V_{Ca-HA_{Powder}}$) and calcium sulfate powder volume ($V_{CS_{Powder}}$), and V_{W_T} is the total water content which includes water amount of added water (V_w) and the Ca-HA water volume ($V_{Ca-HA_{Water}}$).

II.   Results and discussion

1.   Rheological behavior of ternary blends

This section reported the results obtained with ternary blends. **Figures 55** and **56** illustrates rheological steady test results Ca-HA$_{Gel}$/(W/G) and Ca-HA$_{Gel}$/(W/G) (wt%/wt%) blends.

Ternary blends formulations containing Ca-HA$_{Gel}$ and water/gypsum blends, having W/G ratio ranging from 0.2 to 0.6 (wt %), display a non-Newtonian behavior. The results show that the sample structure depends mainly on binary blend (W/G) composition rather than on Ca-HA$_{Gel}$/(W/G) mass ratio. Solid concentration of Ca-HA$_{Gel}$/(W/G) samples varies depending on W/G mass ratio. For samples having W/G mass ratio below 0.4, solid concentration (Γ) increases when decreasing Ca-HA$_{Gel}$ amount. Above 0.4 W/G mass ratio, solid concentration decreases.
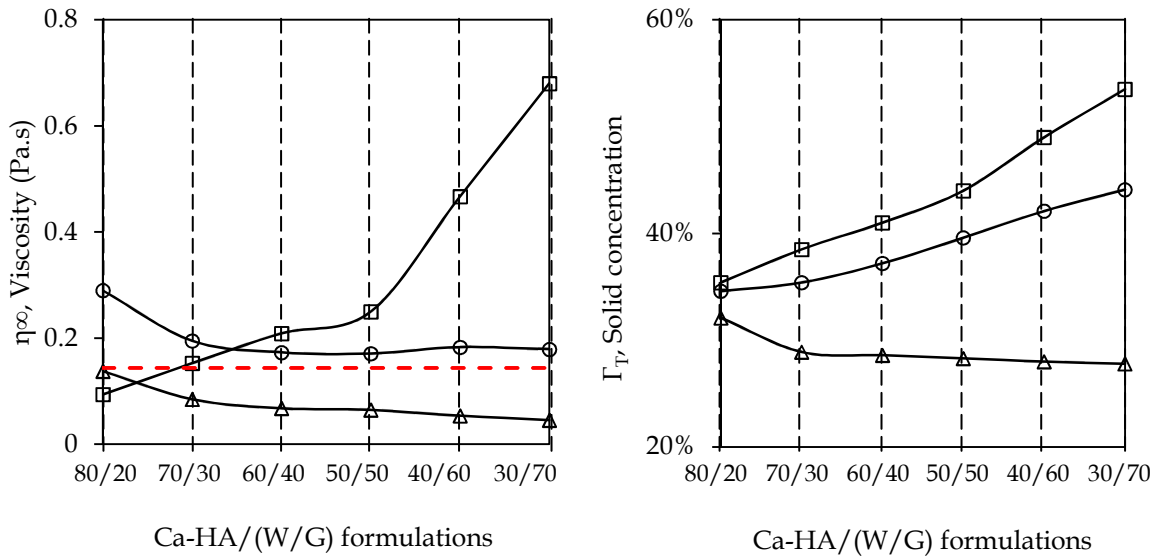
Figure 55: Variation of viscosity of Ca-HA/(W/G) mixtures at different mass ratios
($--$ Ca-HA$_{Gel}$ (0.144Pa.s), $-\square-$ Ca-HA/(W/G=0.2), $-\circ-$Ca-HA /(W/G=0.4), $-\triangle-$Ca-HA/(W/G=0.6))

Decreasing W/G ratio to 0.4-0.2 induces an important changes in blends aspects and viscosity. The formulations with 0.4 W/G mass ratio have viscosity values almost similar to Ca-HA$_{Gel}$. For 0.2 W/G mass ratio blends, viscosity increases by increasing the concentration of total solids. Blends with W/G ratios of 0.6 behaved as low viscosity suspension. It can be seen from **Figure 55** that formulations based on a W/G ratio of 0.6 provides indications of the transformation to liquid phase; viscosity values are similar, exhibiting no influence of added water on rheological behavior and hence on blends workability.

It seems that gypsum interacts with Ca-HA; this can be due to the difference in net charge. Gypsum net charge is negative while Ca-HA has an overall positive charge. Interaction between particles is due to the existence of attractive forces that depends strongly on the creation of low-energy bonds (i.e. *Van Der Walls forces*). The partial dissolution of gypsum in water produces sulfate anions and calcium cations. The sulfate anions (SO_4^{2-}) are attracted to the surface of Ca-HA particles where they get adsorbed. Chemical adsorption seems to be the important process leading the observed phenomena. The attraction of sulfate group can be then explained by its substitution in apatite lattice replacing phosphate group and chemisorption process that occur by inner sphere complexation on surface sites of apatite minerals through

covalent bounding. Consequently, the substitution of phosphate decreases the stability and chemical structure of apatite [1].

As sulfate molecules surround Ca-HA particles, the attractive process leads to the neutralization of Ca-HA particles which are stabilized by interaction effects. However, the charge of Ca-HA becomes negative indicating that the potential of surface reached a maximum of anions adsorption leading to surface saturation that inhibits the attractions effect and provides the decoagulation of particles by electrosteric effects [12]. This electrostatic repulsion effect of gypsum on Ca-HA turns *gypsum* into a dispersing agent.
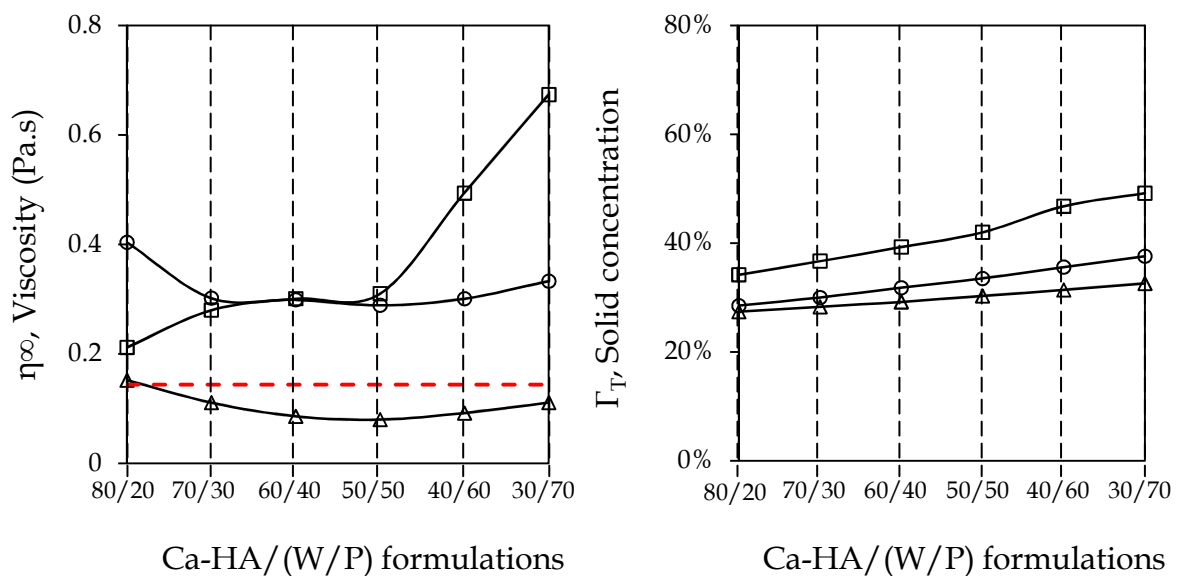
Figure 56: Variation of viscosity of Ca-HA/(W/P) mixtures at different mass ratios ($--$ Ca-HA$_{Gel}$ (0.144Pa.s), $-\square-$Ca-HA/(W/P=0.2), $-\circ-$ Ca-HA/(W/P=0.4), $-\triangle-$ Ca-HA/(W/P=0.6))

As shown in **Figure 56**, the viscosities of Ca-HA$_{Gel}$/(W/P) blends are similar or greater than that for Ca-HA$_{Gel}$ what is not always the case of Ca-HA$_{Gel}$ /(W/G) formulations. For blends with W/P mass ratio varying from 0.2 to 0.6, viscosity mainly depends on W/P mass ratio and little on Ca-HA$_{Gel}$/(W/P) mass ratio. For 0.4-0.6 W/P mass ratios, the system is quite stable and viscosity is almost independent of Ca-HA /(W/P) ratio. Plaster hydration takes place during the binary blend preparation, and its mixture with Ca-HA$_{Gel}$ has little influence on gel structure. For 0.2 W/P mass ratio with different substitutions of Ca-HA$_{Gel}$, the increase in the

solids concentration generates the increase in viscosity (**Figure 56**). Adding of Ca-HA$_{Gel}$ to 0.6 W/P mass ratio blend gives an apparent viscosity of formulations surrounding the viscosity of Ca-HA, despite the increase of the solids concentration.

2.   Interaction between particles

The interpretation of interactions between these compounds is complex. The zeta potential (ζ-potential) can help to better understand the phenomena observed, based on the net charge of particles. The ζ-potential indicates the repulsion forces between particles promoting stability. **Figure 57** represents the ζ-potential of formulations containing Ca-HA and different ratio W/P. **Figure 57** shows that the Ca-HA particles are characterized by a negative ζ-potential, indicating that particles are positively charged (≈-20mV) [3] and the gypsum particles are negatively charged (≈20mV) [4].

The Ca-HA ζ-potential value indicates the instability of the gelled particles. Adding gypsum to Ca-HA leads to charge modification. High ζ-potential values prevent the presence of repulsive forces and indicate colloidal dispersion. These results support the assumption of sulfate attraction on the Ca-HA surface, indicating the dispersion of particles. However, sulfate adsorption changed the charge distribution, generating the change from positive to negative charge. The adsorbed amount of anionic sulfate on Ca-HA particles is equal to the Ca-HA electrical charge sites and the coating of gypsum sulfate Ca-HA particles is the main reason for the modification of ζ-potential. The surfaces of plaster particle are characterized by a positive charge, and hydration changes the surface charge to negative. The formation of a plaster solid body is explained by the cohesion between particles and is illustrated by a low ζ-potential value.
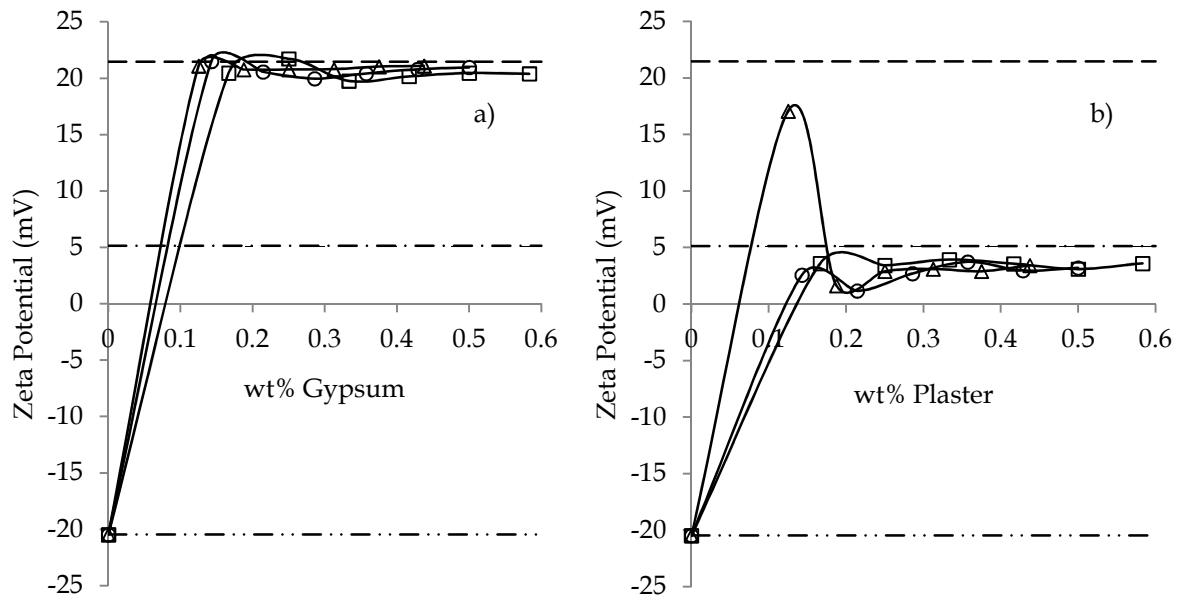
Figure 57: Zeta potential of (a) Ca-HA/(W/G) and (b) Ca-HA/(W/P) formulations (--- gypsum (≈20mv), –·–·– plaster (≈5mv), –···–···– Ca-HA (≈-20mv), —□— Ca-HA /(W/G=0.2) or Ca-HA/(W/P=0.2), —○— Ca-HA /(W/G=0.4) or Ca-HA/(W/P=0.4), —△— Ca-HA /(W/G=0.6) or Ca-HA/(W/P=0.6))

It can be seen from **Figure 57**, the ζ-potential remains constant with increase of plaster content, (with similar values to the plaster at the beginning of the hydration process), and the surface charge of Ca-HA changes. The nucleation process of hemihydrated particles starts by the formation of Ca^{2+}/SO_4^{2-} bound double layers, and the concentration of sulfate decreases, indicating that it is consumed during the hydration. However, the fixation of remaining sulfate in solution on the Ca-HA surface leads to the change in the charge.

Conclusion

The rheological test carried out reveals shear-thinning and the thixotropic behavior of Ca-HA$_{Gel}$ for the formulations considered. The negatively-charged gypsum particles cause the repulsion of particles (repulsive forces). Plaster is characterized by attractive forces and the particles are positively charged. The ζ-potential of Ca-HA is negative and the dissolution of calcium-sulfate particles saturates the solution in sulfates ions (SO_4^{2-}); the charge of particles becomes positive, due to the fixation of SO_4^{2-} on the Ca-HA surface. The adsorption of sulfate on the Ca-HA particle surfaces

163

influences the structure of formulations and explain why the viscosity becomes independent from Ca-HA$_{Gel}$ content. Plaster hydration plays a major role in the Ca-HA$_{Gel}$ stabilization structure. The modification in ζ-potential can affect retention capacity, reactivity and mechanical resistance. These aspects will be the subject of later study.

References

[1] VEIDERMA, M., TONSUAADU, K., KNUBOVETS, R., PELD, M., 2005, *Impact of anionic substitutions on apatite structure and properties*, Journal of Organometallic Chemistry 690, Pp2638-2643

[2] BAO, Y., SENOS, A M. R., ALMEIDA, M., & GAUCKLER, L. J., 2002. *Rheological behavior of aqueous suspensions of hydroxyapatite (HAP)*.Journal of materials science.Materials in medicine, *13*(7), Pp639-43. Retrieved from http://www.ncbi.nlm.nih.gov/pubmed/15348572

[3] KNOWLES, J. C., CALLCUT, S., & GEORGIOU, G. 2000, *Characterisation of the rheological properties and zeta potential of a range of hydroxyapatite powders*. Biomaterials, *21*(13), Pp1387-1392.Retrieved from http://www.ncbi.nlm.nih.gov/pubmed/10850933.

 [4] PENG J., QU J., ZHANG J., CHEN M., WAN T., 2005, *Adsorption characteristics of water-reducton agents on gypsum surface and its effects on the rheology of gypsum plaster*, Cement and Concrete Research 35, Pp527-531

Leaching behavior of calcium sulfate by-product and stabilization using synthesized hydroxyapatite-gel (Ca-HA$_{Gel}$)

I. Introduction

Soil and groundwater contamination are the major environmental problems linked to abusive uses of chemical products. Consequently, the presence of heavy metals and toxic contaminants contributes to the contamination of groundwater by infiltration of pollutants trough the soil. The stabilization of waste materials using a reactive material is now of interest to predict their storage conditions and reutilization. Currently, the elimination of heavy metals present in water and soil using reactive materials (i.e. pollutants immobilization and/or transformation) such as, active carbon, zero valent iron, zeolite, calcite, and apatite, has became of interest in environmental monitoring. It depends on two important factors, the solution-solid equilibrium phase and solubility product of solid phase. Furthermore, precipitation, adsorption, ion exchange, substitution and surface complexation are important mechanisms leading the removal of contaminants depending on chemical properties and affinities.

The assessment of stability is based on leaching test, which categorizes the disposal in landfills and the classification conditions. The management of environmental risks is based on standard protocols to facilitate not only the tests for the characterization of pollutants, but also their application in surveillance, monitoring and protection the natural environment. The EU Landfill Directive prescribes waste acceptance criteria (WAC) based on leaching of metals and inorganic species from a granular waste sample (i.e. solid particles size less than 4mm) leach tested using a leaching procedure based on liquid/solids (L/S) ratio of 10 [1] (NF EN12-457-2). The guidance document classifies the waste material in three categories, inert waste, non-hazardous waste and hazardous waste as a function of the amount of leachable heavy metals. The criteria for the selection of reactive material used for the PRB technology requires that the reactive media does not represent any source of contamination of soil and groundwater, it must be stable, available at low and

reasonable costs and have a large capacity, efficiency and longevity in intercepting pollutants. The main purpose of the preliminary environmental assessment study was to verify the absence of risk of calcium sulfate by-product as support material in reactive media destined to PRB process and to compare or prioritize the actions based on indicative threshold concentrations to reveal significant environmental behavior.

The aim of this work was therefore to determine whether calcium sulfate industrial by-products (plaster and gypsum) could be safely used for PRB. The effect of several leaching parameters on the leachability from calcium sulfate by-product was investigated. The aptitude of hydroxypatite to stabilize the calcium sulfate waste was studied. The interest in the use of waste calcium sulfate was its valorization as support material in PRB.

II.   Experimental procedure

1.   Samples

The hydroxyapatite-Gel ($Ca-HA_{Gel}$) synthesis method is described in the Chapter II. The Ca-HA used in this work is stochiometric with the molar ratio Ca/P=1.67, the more stable phase ($Ca_{10}(PO_4)_6OH_2$). The main advantage of the synthesis method is Ca-HA high quality [2]. The raw materials used in this work are a commercial by-product of phosphoric acid fabrication (PRAYON®, Belgium) (Gypsum (dihydrated calcium sulfate) and Plaster (α) (hemihydrated calcium sulfate)). The raw gypsum was sieved to obtain different fraction sizes ranging from 1 to 4mm (i.e. d_P<1mm, 1<d_P<2mm and 2<d_P<4mm).

2.   Formulations

The considered formulations studied in this work are summarized in **Table 24**. They are based on plaster containing water to ensure plaster hydration up to W/P 0.4 mass ratio.

Table 24 : Gypsum, plaster and Ca-HA$_{Gel}$ considered formulations

Products	Formulation 1 AWP	Formulation 2 AG	Formulation 3 AWPG1	Formulation 4 AWPG2
Ca-HA$_{Gel}$ (%)	80	80	64	56
Plaster (%)	14.28	0	11.43	10
Water (%)	5.72	0	4.57	4
Gypsum (d$_P$<1mm) (%)	0	20	20	0
Gypsum (1-2mm) (%)	0	0	0	10
Gypsum (2-4mm) (%)	0	0	0	20

The formulations were proposed to evaluated the reactivity of Ca-HA$_{Gel}$ to stabilize the calcium sulfates wastes and to select the adequate formulation leading to PRB assessment.

3. Characterization Methods

The chemical composition of used materials was obtained using the mineralization method in accordance with French standard procedure NF X31-151 [3] described in Chapter II. The pH$_{PZC}$ was determined according to the method described in Chapter II. The Ca-HA powder was destined to physicochemical characterization and obtained by drying at 105°C for 24h after filtration and washing with de-ionized water to eliminate the unreacted phosphate and ammonia. The chemical analysis of both calcium sulfates and hydroxyapatite were carried out using inductively coupled plasma spectrometry (ICP-AES) to determine the impurities contents and to verify the Ca/P stoichiometric ratio of Ca-HA$_{Gel}$, respectively. ICP-AES analyses were performed on a ULTIMA-2 (JOBIN YVON HORIBA). Soluble fraction was determined by filtering of 40ml of eluate at 0.45µm and the dry residue was assured by eluate dehydration in a heated sandbox at 103±2°C. Samples intended for infrared spectroscopy and DRX analysis were prepared by heating them at 105°C to eliminate residual moisture and to facilitate characterization conditions. The presence of functional groups in the different materials is confirmed by infrared spectroscopy

using SHIMADZU FTIR (Fourier Transformed Infrared)-8400S spectrometer (**Figure 63**).

4.   Leaching tests

The leaching tests are currently considered as a necessary tool leading to the environmental prediction and assessment of the long-term leachability behavior of wastes and by-products. Consequently, the identification of soluble species promoting the release of pollutants is achieved. In this work, the leaching behavior was carried out on materials and evaluated with two leaching procedure normalized tests (NF EN12-457-2 [4] and acid-base neutralization capacity test (ANC) [5]. These leaching tests have been chosen to study the physicochemical stability of calcium sulfate raw materials and formulations containing Ca-HA$_{Gel}$ as stabilizer reactive material to investigate the relationship between leachability and L/S ratio, particle size, and leachate pH by comparing the two leaching test methods. Two samples were leached and concentration values correspond to average value. All samples were kept after filtration trough 0.45µm in a plastic flask (10ml of eluate diluted 3 times with de-ionized water) and were acidified with 1% nitric acid to avoid any metal precipitation. The trace metal element concentrations investigated in this work are As, Pb, Cu and Zn. The soluble fraction was expressed as the dry weight of the leached sample accumulated values obtained by weighing the dry residue of each of three leachates.

4.1.   NF EN12457-2 description

French environmental characterization standard (EN12457-2) consists in contacting waste material with de-ionized water on a vertical rotary shaker (7rpm). The calcium sulfate (Gypsum and Plaster) and formulations with Ca-HA$_{Gel}$ samples were subjected to an agitation period of 48 h (24 hours was added to ensure the metal concentration stabilization) at room temperature according to a Liquid/Solid (L/S) ratio of 10 l.kg^{-1} dry matter and liquid extraction was carried out by filtration through a 0.45µm pore size membrane filter. The leaching duration was investigated for raw

calcium sulfate samples. This method of leaching was used for the first set of experiments where plaster and gypsum with three particle size fractions (d_P<1mm, 1-2mm and 2-4mm) were used for different leaching durations (72 hours). The second set was dedicated to investigate the effect of L/S (20/1, 40/1, 60/1, 80/1 and 100/1 l.kg^{-1} dry matter) ratio on the leachability of heavy metals from calcium sulfates materials.

4.2. Acid-base neutralization capacity test (ANC)

The behavior and availability of pollutants present in gypsum and plaster have been studied using the ANC test. The test based on the evaluation of the buffering capacity of materials uses an acid or base attack [5]. Samples of material were introduced in solutions of nitric acid and sodium hydroxide for different concentrations with a weight ratio L/S of 10. Concentrations were adjusted so as to obtain the desired pH value. The equilibrium of suspensions has ensured by agitation during 48 hours and the final pH value was measured. The suspensions were filtered throughout 0.45µm and the filtrates were analyzed.

III. Results and discussion

1. Physicochemical characterization

The samples were prepared by drying at 105°C from 24 hours and grounded after leaching tests. The samples were destined to FTIR and XRD analysis. The results are summarized in **Table 25**.

Table 25: Chemical analysis of calcium sulfate waste material

Elements	Plaster (mg.kg^{-1} DM)	G (<1mm) (mg.kg^{-1} DM)	G (1-2mm) (mg.kg^{-1} DM)	G (2-4mm) (mg.kg^{-1} DM)
Al	5055	4984	3196	3375
As	15	65	65	65
Ca	134773	214544	211307	211700
Cd	3810	3956	3660	3671
Fe	5119	5627	4338	4359
K	6773	7016	7234	9460
Mg	15979	10707	9757	10038

Na	4841	5243	3760	5100
P	3783	4573	4969	5581
Pb	2442	2691	2236	2228
SO_4	766237	846295	602523	710884
Sr	26572	24270	13981	27695
Zn	3849	3994	3400	3410
pH	2.88	8.44	9.57	9.64
pH_{PZC}	3.30	7.50	7.50	7.50
Particle charge	Positive	Negative	Negative	Negative
ρ (g.cm^{-1})	2.81	2.25	2.18	2.18
Textural class	Silty-sand	Sandy-silt	Sandy	Sandy

DM: dried materials

It could be seen from these results that the samples considered contain a significant amount of heavy metals such Al, Cd, Fe, Pb, Sr and Zn. Bulk density of gypsum (1-2mm) and gypsum (2-4mm) are similar.

1.1. FTIR analysis

FTIR carried out on pure products (Ca-HA, plaster and gypsum) were shown in Chapter III. **Figure 58** illustrates the FTIR analysis of formulations containing Ca-HA. Infrared spectroscopy analyses were carried out on all considered formulations. The infrared analysis observations show similar spectra. The IR analysis of the AWP and AG formulations both showed the main peak of phosphate at 1022 cm^{-1}. As expected, sulfate peak intensity increases when the plaster concentration in the formulations increases [6].The decrease of the intensity of phosphate bands indicates that the concentration of phosphate decreased by the effect of sulfate substitution. The increase in wave number and decrease of intensity of phosphate band ranging from 1020 to 1035 cm^{-1} by increasing gypsum quantity provide some indications on the apatite arrangement structure modification by the formation of modified hydroxyapatite type calcium phosphate sulfate hydrate. The present interpretation agrees with XRD analysis described hereafter. For blends containing Ca-HA, gypsum and plaster (AWPG1 and AWPG2), the band displacement by increasing gypsum concentration spanning from 1089 to 1085 cm^{-1} and at 1109-1111 cm^{-1} region

absorption band, indicate the presence of phosphate and sulfate groups characterized by overlapping broad bands.

On the other hand, the intensity of sulfate bands increases as plaster amount increases at frequencies varying from 1020 to 1035 cm^{-1} procures the phosphate sites substitution and reduction of its symmetry. Increasing the concentration of gypsum in composites leads the appearance of two bands corresponding to water. The same group is detected at region wave numbers of 1620-1618 cm^{-1} and reveals the presence of strongly held water. Broad absorption band with intensity decrasing as concentration of gypsum increases is attributed to unreacted calcite also present in synthesized Ca-HA$_{Gel}$.
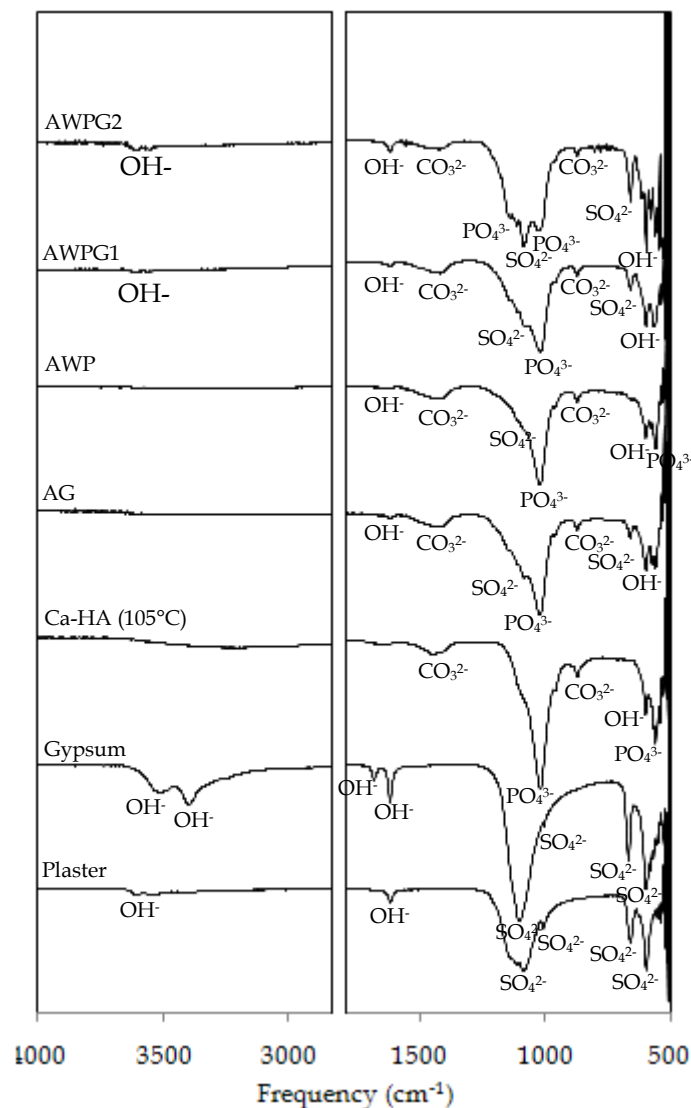
Figure 58 : Infrared spectra of materials and considered formulations

1.2. DRX analysis

Figure 59 represents the XRD analysis of Ca-HA, plaster, gypsum and considered blends. Synthesized Ca-HA is characterized by ten main diffraction peaks (interrecticular distance) similar to the spacing peaks of a synthesized Ca-HA product [7].
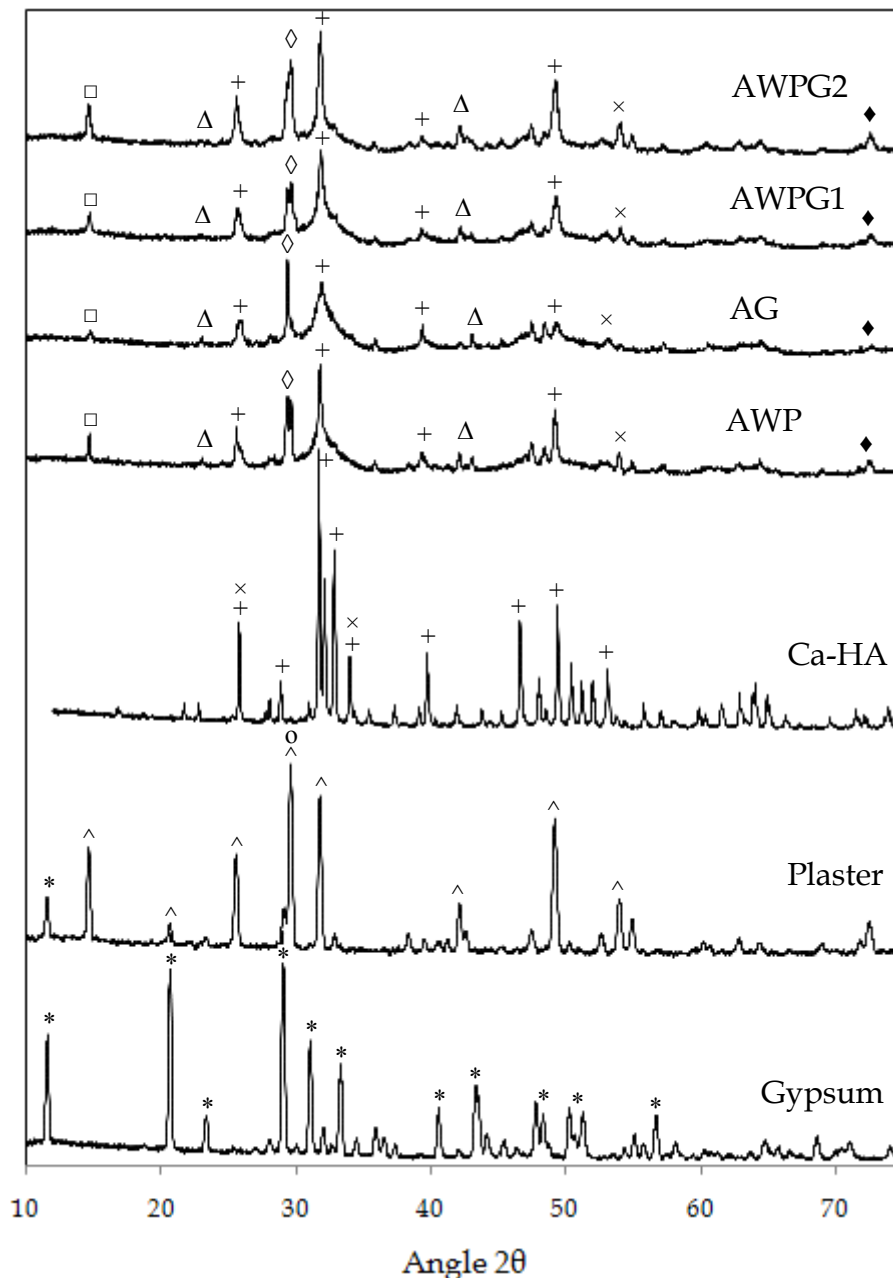
Figure 59 : X-ray diffraction of gypsum (*), plaster (^), Anhydrite (°), Ca-HA (Ca-HA, Hydroxylapatite (+) and Hydroxyapatite (×)) and considered formulations (□ Calcium Sulfate carbonate hydrate ($Ca_2SO_4CO_3.H_2O$), Δ Ardealite ($Ca_2SO_4HPO_4OH.4H_2O$), ◊ Calcium phosphate sulfate hydrate ($Ca(HPO_4)_x(SO_4)_{1-x}.2H_2O$), ♦ Strontium apatite ($Sr_5(PO_4)_3OH$)

The X-ray diffraction patterns of gypsum and plaster have been discussed in Chapter III. The XRD analysis of formulations based on Ca-HA, plaster and gypsum mixtures with different size fraction reveals the apparition of new compounds. The XRD patterns illustrated in **Figure 59** reveal the presence of modified Ca-HA. The main peak in the formulations XRD patterns was also hydroxyapatite as its high proportion in the blends. It should be noted that no sign of gypsum in the XRD patterns of formulation has been detected. The apparition of a new peak in the XRD patterns of formulations proves the formation of a new compound. Calcium sulfate carbonate hydrate was located at 14.7°2θ in the four formulations indicating that unreacted carbonate reacts with sulfates dissolved from gypsum and plaster. Calcium phosphate sulfate hydroxide hydrate ($Ca_2SO_4HPO_4OH.4H_2O$; Ardealite) have been found at 41.2°2θ and at 23.8°2θ in all blends. Calcium phosphate sulfate hydrate ($Ca(HPO_4)_x(SO_4)_{1-x}.2H_2O$) has been located and at 29.5°2θ revealing the formation of double salt phase [6]. The presence of dissolved ions such as Ca^{2+}, PO_4^{3-} (non reacted phosphate from Ca-HA synthesis) and SO_4^{2-} contribute to the formation of calcium phosphate sulfate hydrate. Strontium apatite has been identified at 72.7°2θ indicating that the strontium released from gypsum and plaster has been retained by Ca-HA during the leaching test.

2. Influence of pH

2.1. Acid-base neutralization capacity

The chemical behavior of heavy metals is also controlled by the pH. The influence of pH on the leachability of salts and cations was evaluated by ANC test. **Figure 60** presents the curve of ANC of gypsum and plaster, illustrated by the pH variation as a function of added amount of H^+ (0.1 M) and added amount of OH^- (0.1 M). The pH decreases with increasing volume of acid.
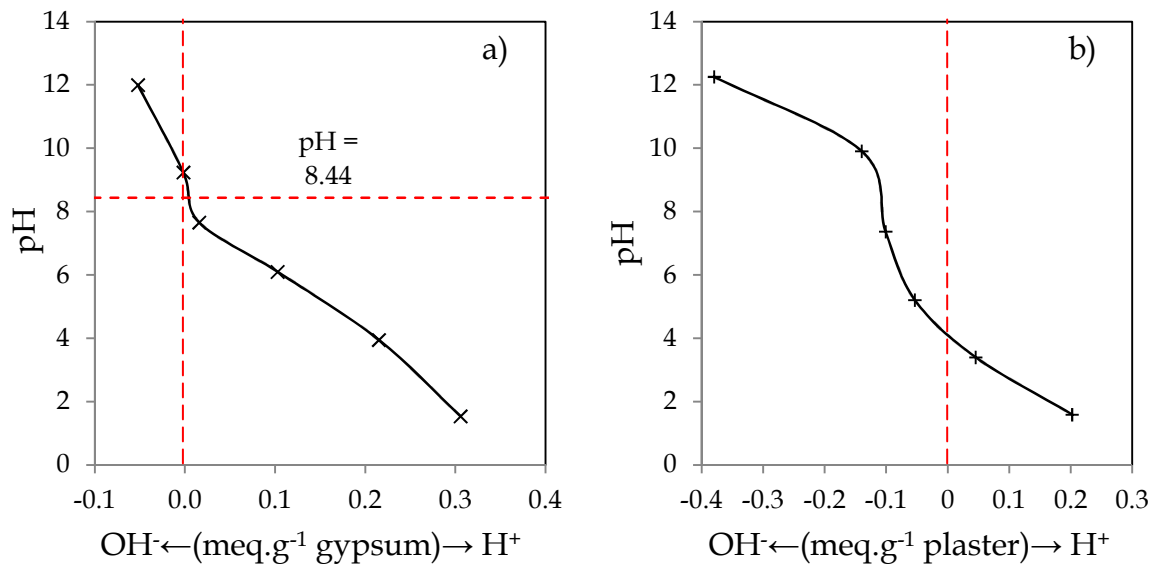
Figure 60: Acid-base neutralization capacity of a) gypsum ($-\times-$) and b) plaster ($-+-$)

The natural pH of gypsum determined in demineralized water is about 8.44. As shown in **Figure 60** a), without added amount of acid or base, the value of pH is the same. By adding the amounts of acid, the pH shifted to pH below 8. The gypsum was characterized by an inflexion point localized at natural gypsum pH (pH=8.44). The plaster (see **Figure 60** b)) is characterized by a plateau in the region of basic pH (10-12) indicating the presence of lime. The inflexion point was observed at pH of 7.4. The inflexion point is shifted to 0.1 meq (OH^-).g^{-1} of plaster. This result can be explained by the presence of small amount of phosphoric acid that modify the pH. For two materials, the acid neutralization was not achieved. **Figure 61** shows the ANC curve of Ca-HA. The pH decreases with increasing added acid volume. The pH of Ca-HA was 8.25 corresponding to inflexion point.
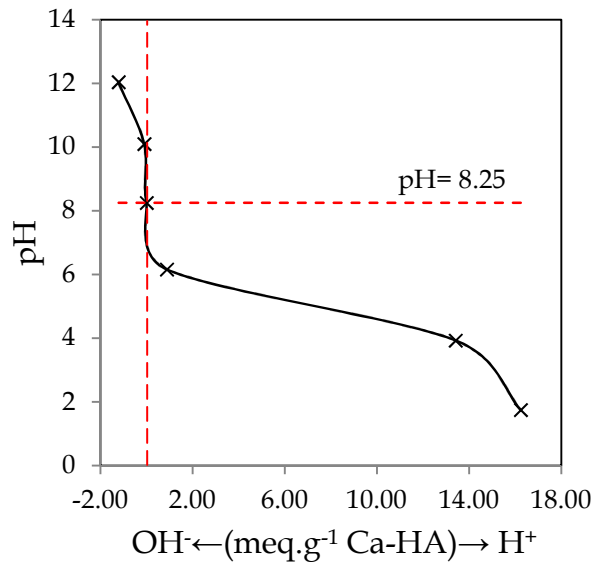
Figure 61 : Acid-base neutralization capacity of Ca-HA

A plateau was observed towards pH ranging from 4 to 6, corresponding to the dissolution of carbonates ions that neutralizes the added acid. It should be noticed that Ca-HA is characterized by a high neutralization capacity or buffer effect.

2.2. Chemical elements availability

The availability of alkaline and metal elements depends on the pH and their solubility. The ANC allows the determination of the leaching behavior and the rate of release of waste material at different pH values. The present leaching test (ANC) depends also on the material pH, the buffering capacity of the material and the pH of solution in contact with the material. The following elements, Al, Ca, Mg, Fe, P, SO_4, Cd, Sr and Zn were selected and their concentrations were plotted against pH. The **Figures 62** and **63** illustrates the release curves of selected elements.
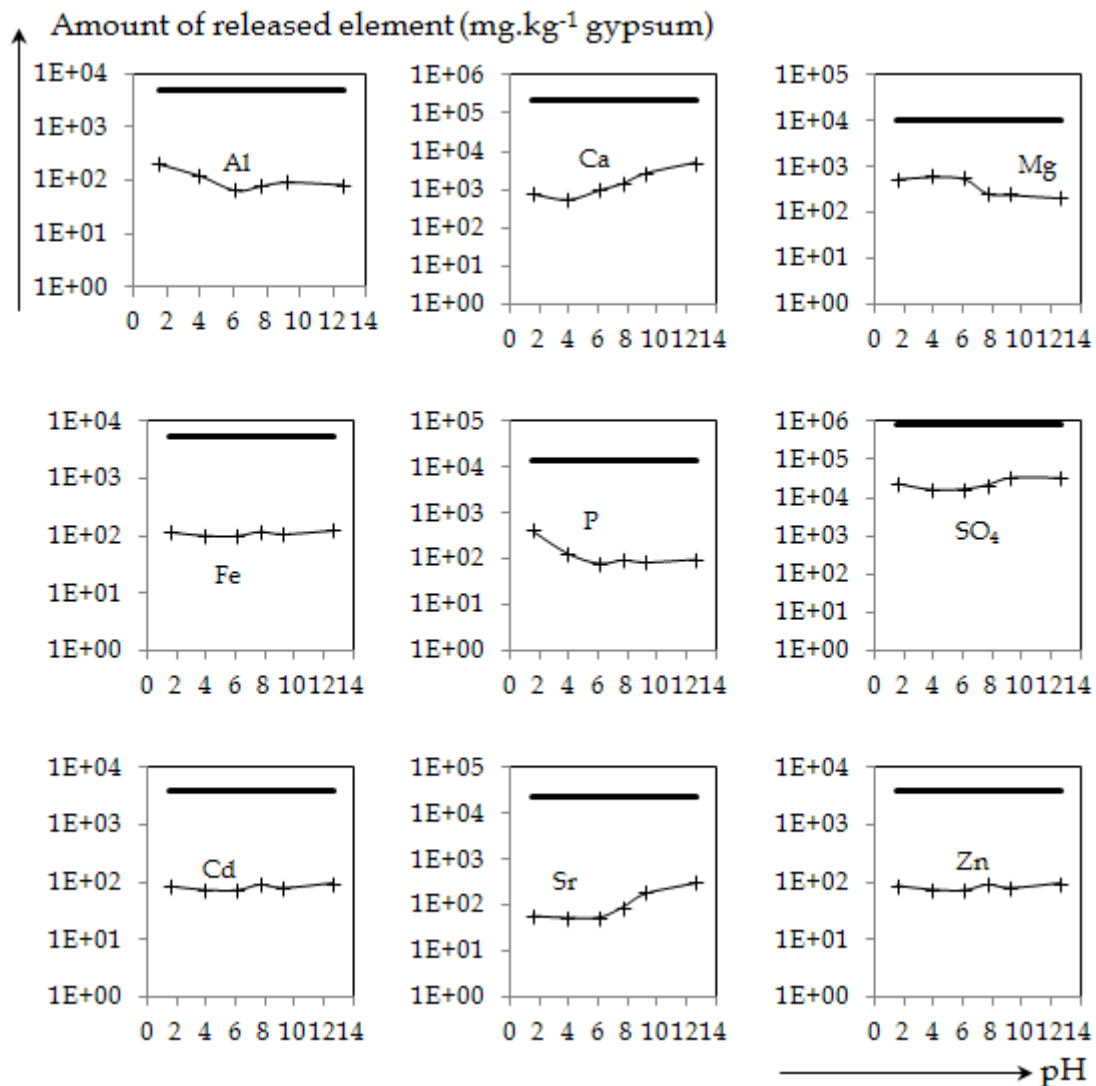
Figure 62 : Amount of released elements from gypsum as a function of pH
(The bold line represents the total amount occurring in the gypsum)

The results of ANC test were expressed in mg.kg^{-1} of dried matter to evaluate the availability of chemical elements. The calcium increases by increasing the pH of leaching solution. The increase of calcium concentration in leached solution was also correlated to the released concentration of sulfate anions. The release rates of calcium from gypsum and plaster were about 1 and 3% respectively. The plaster hydration takes place at basic pH, hence the concentrations of calcium and sulfate were remained constant revealing that the pH change has no influence on the solubility of plaster. The magnesium concentration decreases with increasing the pH of leaching solution. In the case of gypsum, the magnesium was characterized by a rate of release passes from 5% to 2%. The rate of release of magnesium in the case of plaster

decreases from 5 to 1%. In basic region, the magnesium precipitates as hydroxide ($Mg(OH)_2$). The amount of released phosphorus decreases with increasing the pH of the leaching solution and remains constant for pH higher than 6. The rate of release of phosphorus from gypsum was 2% and from plaster was 1%. The phosphorus can be combined to calcium to form calcium phosphate. Concerning the leaching behavior of major elements such as Al and Fe, the rate of release was different in acid and basic regions for Al and no influence of pH was observed for Fe. In acidic environment, the Al was more released with a rate of release ranging from 7 to 9% for plaster and 4 to 2% for gypsum, and its amount was decreased in neutral region where the rate release was 1%. The precipitation of $Al(OH)_3$ in neutral milieu explains the decrease of Al amount. The release rate of Fe was remained constant in both regions of pH for gypsum and plaster with 1 and 2% respectively. The Zn is present in the both gypsum and plaster as Goslarite ($ZnSO_4.7H_2O$). In aqueous medium, the Zn only exists in divalent oxidation state ($Zn(II)$). Its released amount was localized under 100 $mg.kg^{-1}$ of gypsum. No influence of leaching solution (i.e. pH of the solution) on Zn availability has been observed; it can be considered that Zn is also stabilized by its interaction with sulfate. The formation of zinc sulfate in aqueous phase or solid phase controls the Zn availability. The release rate of Zn from gypsum and plaster was 2 and 1% respectively. Cadmium is also associated to zinc, because they have a similar ionic structure and close electronegativity. Cadmium is classified as a chalcophile element. It can be present as sulfide compounds such as Greenockite ($CdS_{(s)}$) and cadmium sulfate. The behavior of cadmium in the gypsum and plaster is slightly controlled by the pH. Whether in acidic or basic conditions, the released amount was the same. As known, the hydrolysis of cadmium begins at high pH and its concentration is limited by different solid phases as a function of pH, redox potential and leaching solution. The more stable predominant solid phase in oxidizing conditions is the combined phase sulfate/hydroxide in alkaline pH.

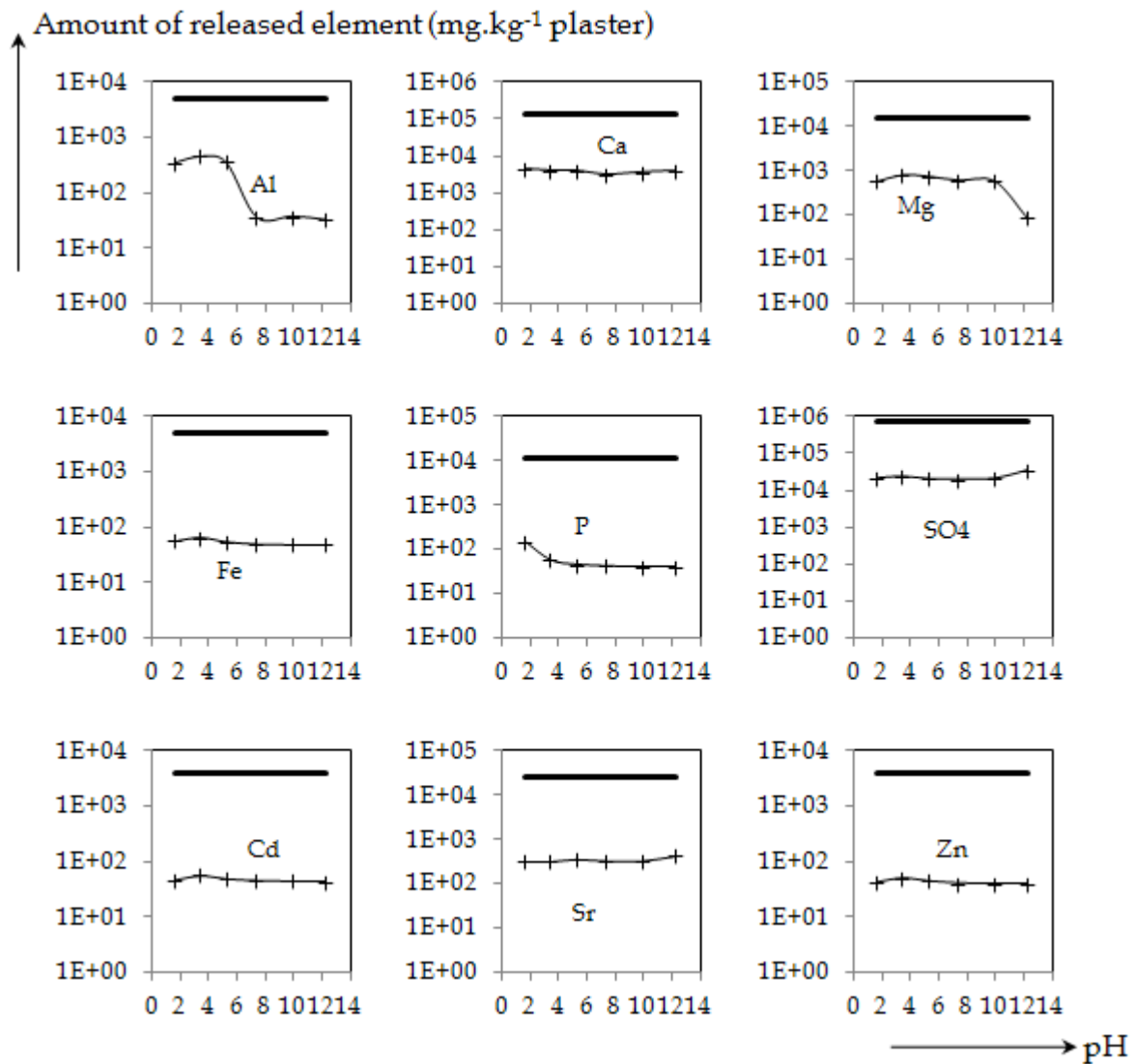**Figure 63 :** Amount of released elements from plaster in function of pH
(The bold line represents the total amount occurring in the plaster)

The rate of release of cadmium from gypsum and plaster was 2 and 1% respectively regarding the total amount in the materials. The strontium occurs in gypsum as Celestine ($SrSO_4$). It's an alkaline metal and its solubility is pH independent and it is controlled by its availability. Strontium was released from gypsum and plaster up to 1 and 2% levels respectively.

The ANC was carried out on washed, filtered and dried Ca-HA. As known, the Ca/P molar ratio of Ca-HA after 48 hours of synthesis is about 2.36. **Figure 64** shows the ANC results of Ca-HA. The leached amount of both calcium and phosphorus are relatively stable at pH ranging from 2 to 4. As observed from ANC carried out on Ca-

HA, Ca-HA particles dissolves totally in acidic solution (pH less than 4). However, the dissolution of Ca-HA particles in acidic solutions leads to the total availability of calcium as Ca^{2+} hyxahydrate $[Ca(H_2O)_6]^{2+}$ and phosphate as H_3PO_4 and $H_2PO_4^{-}$.
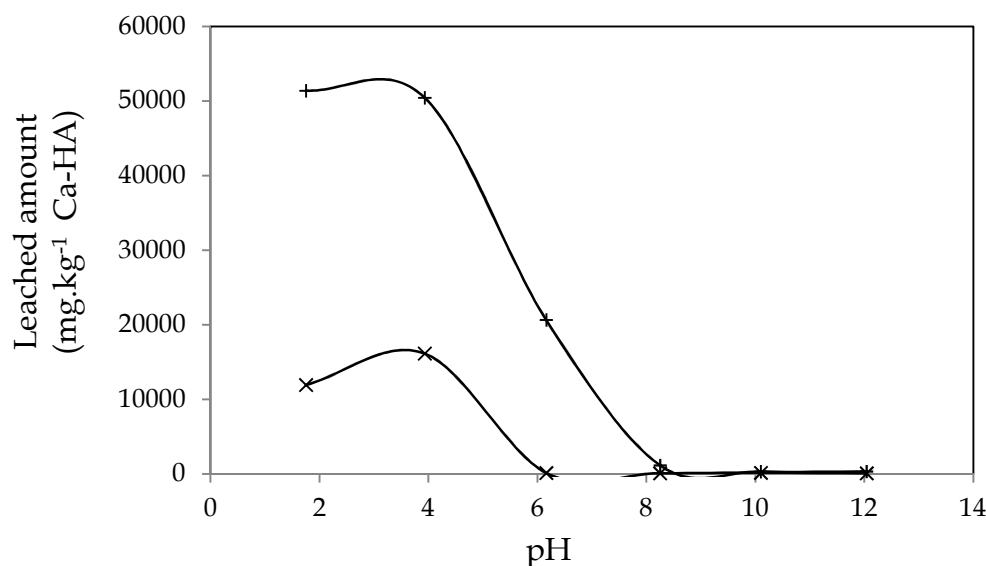
Figure 64 : Amount of calcium ($-+-$) and phosphorus ($-\times-$) released from Ca-HA powder (dried at 105°C during 24 h)

The rates of release of calcium and phosphorus were about 60 and 40% respectively in acidic region (pH less than 4). From pH higher than 4, the amount of calcium and phosphorus decrease slightly. At 6-8 pH region, phosphorus was not released revealing its insolubility near neutral pH.

3.   Effect of leaching duration

The effect of leaching duration on the release of calcium, sulfate, phosphorus and strontium from gypsum and plaster was studied during leaching test. The **Figure 70** illustrates the metal concentrations in the leachate as a function of leaching duration. The leached amount of metals from gypsum was constant during the leaching test (**Figure 65** a)). The pH of leachate increases slightly and achieves a constant value of 8.8 at the end of leaching test.
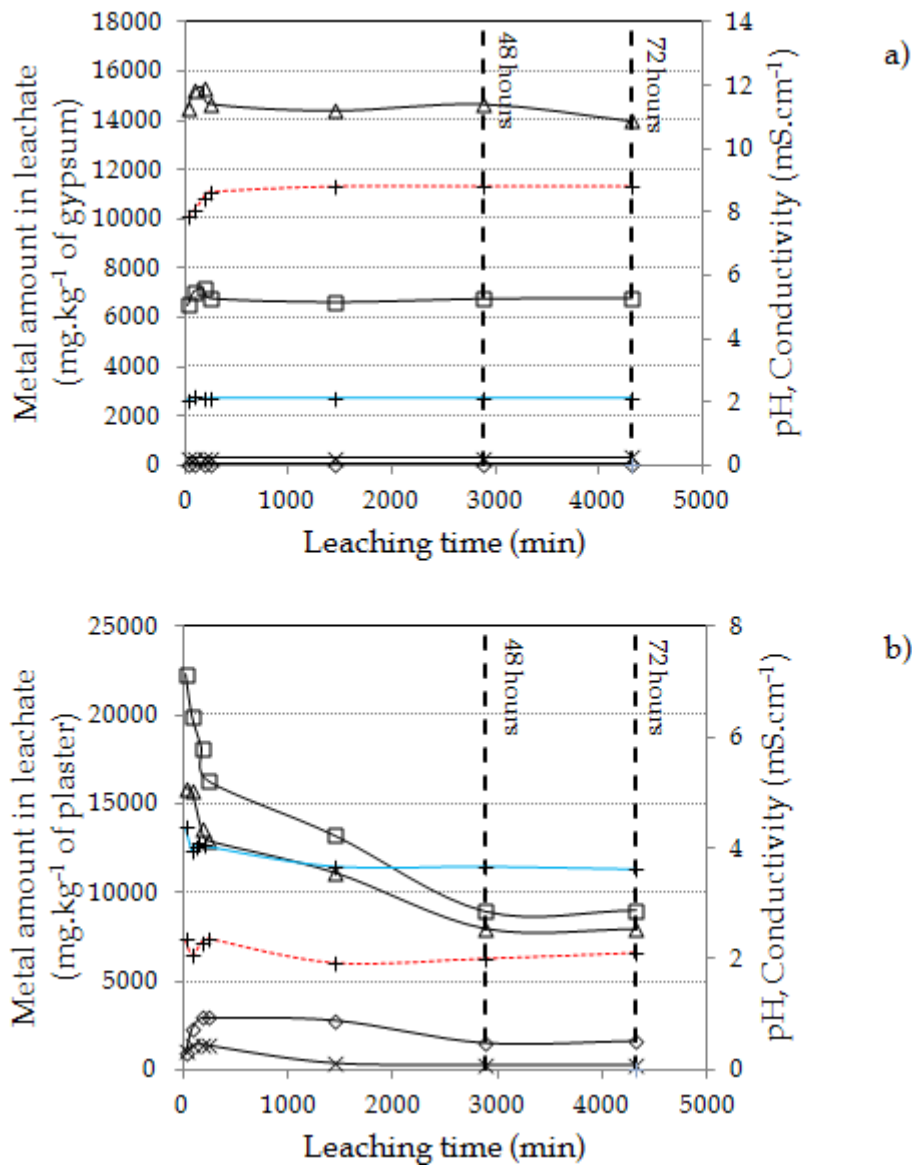
Figure 65 : The effect of leaching duration on the leachability of calcium ($-\square-$), sulfur ($-\Delta-$), phosphorus ($-\lozenge-$) and strontium ($-\times-$) from a) gypsum and b) plaster ($\cdots+\cdots$ pH, $-+-$ Conductivity ($mS.cm^{-1}$))

The phosphorus occurs in the leachate contains HPO_4^{2-}. The rate of release of calcium, sulfate, phosphorus and strontium from gypsum were 3, 5, 1 and 1% respectively. In the case of plaster, the concentrations of calcium and sulfate decrease with increasing leaching duration and remain constant after 48 hours of tumbling. The hydration of plaster is the main process governing the leachability of calcium and sulfate. The release rates of calcium and sulfate from plaster were 7 and 3% at the equilibrium. Otherwise, the concentration of leached phosphorus and strontium increases in the beginning of the leaching test and reach a constant value at the

equilibrium (after 48 hours of leaching). The hydration of plaster may play a major role on the stabilization of metals. The leachate pH of plaster was acidic indicating that the leached solution contains phosphorous in form of H_3PO_4. The release rates of phosphorus and strontium from plaster was about 40 and 1% respectively.

4.   Effect of particle size

In order to study the effect of particle size on leaching, three fraction of gypsum waste, less than 1mm, between 1 and 2mm and between 2 and 4mm have been prepared.
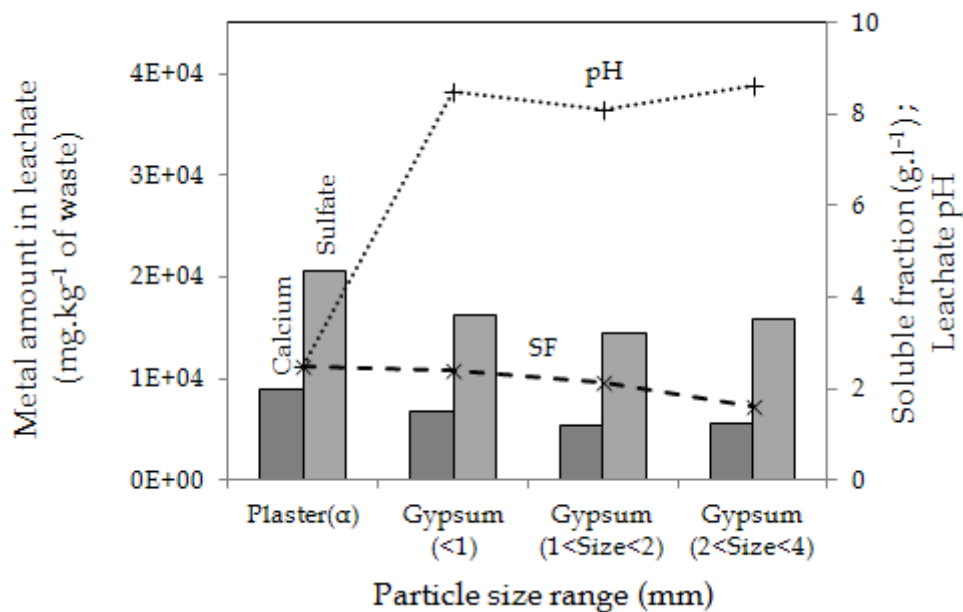
Figure 66 : Leachability of calcium and sulfate from plaster, gypsum (<1mm), gypsum (1-2mm) and gypsum (2-4mm) as a function of the leachate pH (after 48 h of tumbling at 7 rpm) and soluble fraction (SF)

Figure 66 shows the concentration of calcium and sulfate in the leachate as a function of particle size range of plaster and gypsum. It was found that the amount of sulfate leached from plaster is higher than the leached amount from considered fractions of gypsum. The release rate of sulfate from gypsum with particles size less than 1mm, between 1 and 2 mm and between 2 and 4 mm was 2%. The concentration of leached calcium from gypsum was remained constant despite the increase of the gypsum size. The release rate of calcium from all fractions of gypsum was between 3 and 4%. In the case of plaster, the concentrations of calcium and sulfate were slightly higher

than those observed for gypsum fractions with rate of release ranged from 2 to 3% for both elements. The leaching results of plaster and gypsum at different particle size ranges are presented in **Figure 67**.
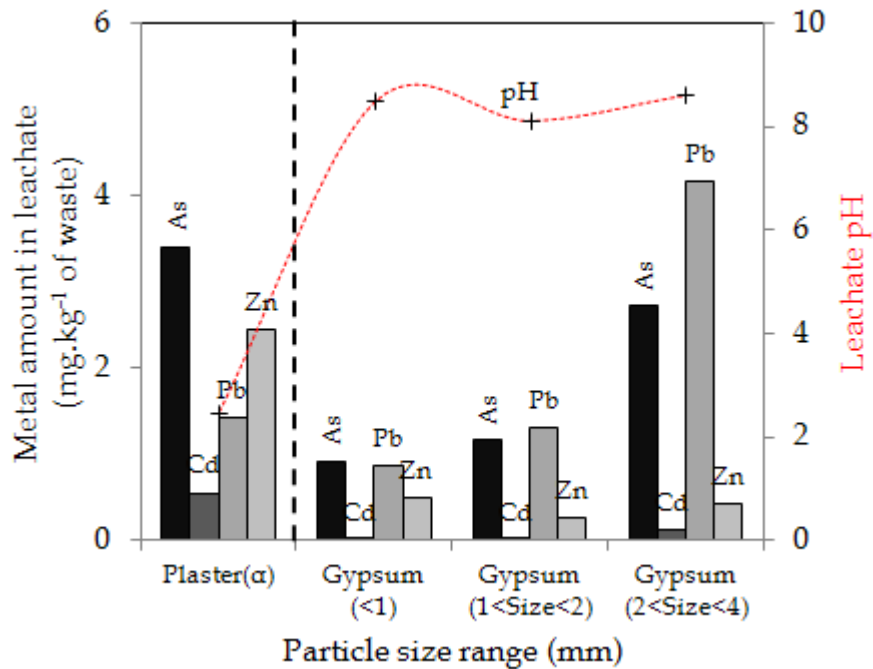
Figure 67 : The amount of As, Cd, Pb and Zn in the leachate as a function of calcium sulfates particle size range tumbled at a speed of 7 rpm for 48h

Calcium sulfate hemihydrated in contact with de-ionized water lead to particles hydration. Plaster powder contains higher amount of heavy metals. Acidic pH of plaster in de-ionized water triggers leaching of As, Cd, Pb, and Zn. In fact, the leached amount is controlled by a higher solubility of metals, the plaster solubility is 9g.l^{-1}. The hydration process plays a major role in heavy metals solidification/stabilization process. Particle size has little influence on Zn concentration in the eluate. However, for Cd, Pb and As, concentration decreases with decreasing particle size. The progressive dissolution of gypsum particles reduces the contact surface leading to heavy metals release, beforehand stabilized and solidified by hydration process. Indeed, during the hydration of calcium sulfate, the metals could be retained and sequestered in the gypsum lattice by nucleation and growth of gypsum particles.

5.   Effect of Liquid/Solid ratio

5.1.   Gypsum leaching test

The effect of liquid to solid ratio (L/S) on the leachability of calcium and sulfate using demineralized water is shown in **Figure 68**. The amount of leached calcium and sulfate from gypsum increases proportionally with increasing the L/S ratio. The pH was basic and increased slightly and decreased after achieved 9.2 at 40 L/S mass ratio. The decrease in the pH value for L/S more than 40 l.kg-1 was explained by the dilution effect (the increase in the volume of demineralized water).
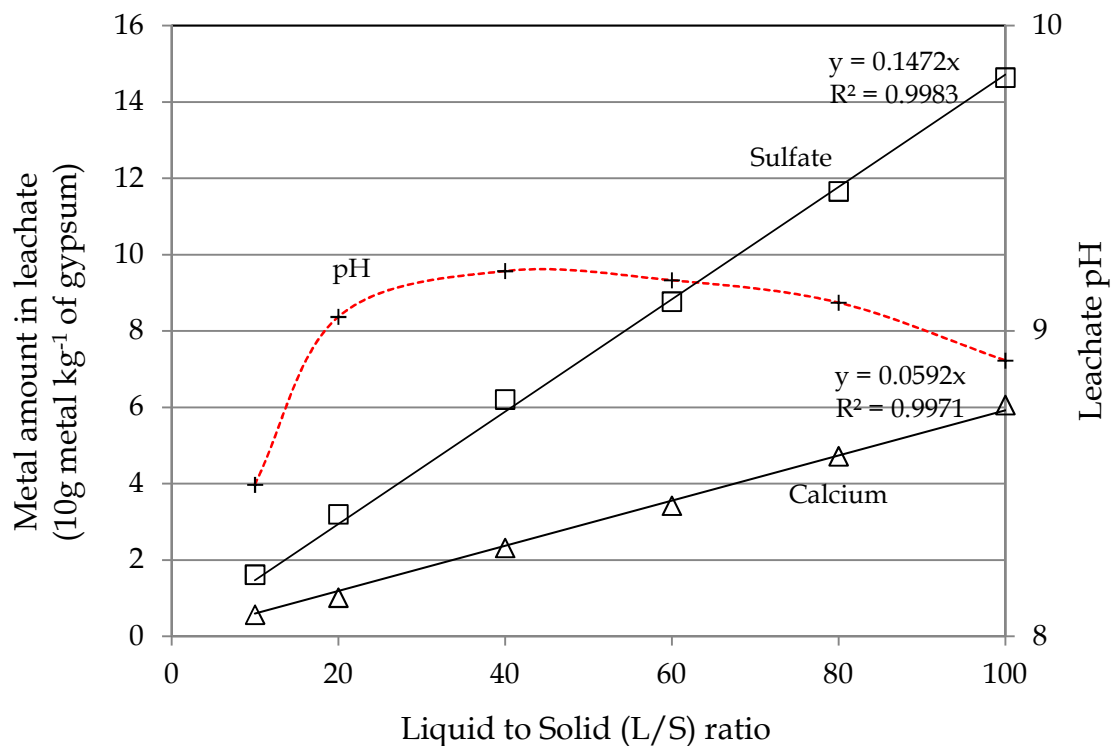
Figure 68 : Leached amount of calcium and sulfate in gypsum (<1mm) at different L/S ratios

The influence of the water dilution is the main mechanism leading to the increase of the concentration of calcium and sulfate in leachate. **Figure 69** illustrates the Ca/SO$_4$ ratio versus L/S ratios ranging from 10 to 100 l.kg-1. The Ca/SO$_4$ ratio increases with increasing L/S ratio and achieves a constant value at 60l.kg-1 L/S ratio.
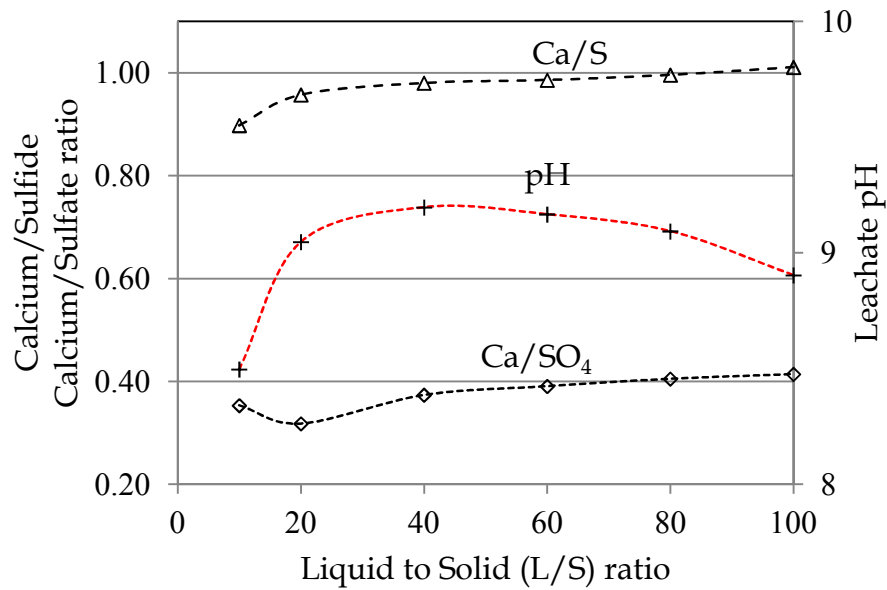
Figure 69 : The Ca/S and Ca/SO$_4$ ratios in function of L/S ratio

Figure 70 : Leachablity of As, Pb and Zn from gypsum (<1mm) (mg.kg^{-1}) at different L/S ratios

The increase of Ca/SO$_4$ was mainly due to the dissolution of water on gypsum particles leading to the modification of gypsum structure. The stabilization of Ca/SO$_4$ at 60 L/S mass ratio indicates that the buffering mechanism was reached as demonstrates by the pH values. The influence of liquid to gypsum solid (L/S) ratio on heavy metals leaching behavior is shown as leachable contents in **Figure 70**. Leachability of gypsum depends also on the solubility. The pH value increases

constantly and remained constant at ≈9.2 as the L/S ratio increases from 40/1 to 60/1 l.kg^{-1}. For L/S ratio more than 60/1 l.kg^{-1}, the leachate pH decreases. The leachable content in gypsum dihydrated increases with increasing L/S ratio; this is due to the de-ionized water dilution. Otherwise, these increased concentrations was correlated and influenced by the stability of pH value.

5.2. Plaster leaching test

The results obtained on the influence of L/S ratio in the leaching capacity of calcium and sulfate from plaster are similar to those obtained for gypsum. **Figure 71** shows the leached amount of calcium, phosphorus and sulfate from plaster against L/S ratio.
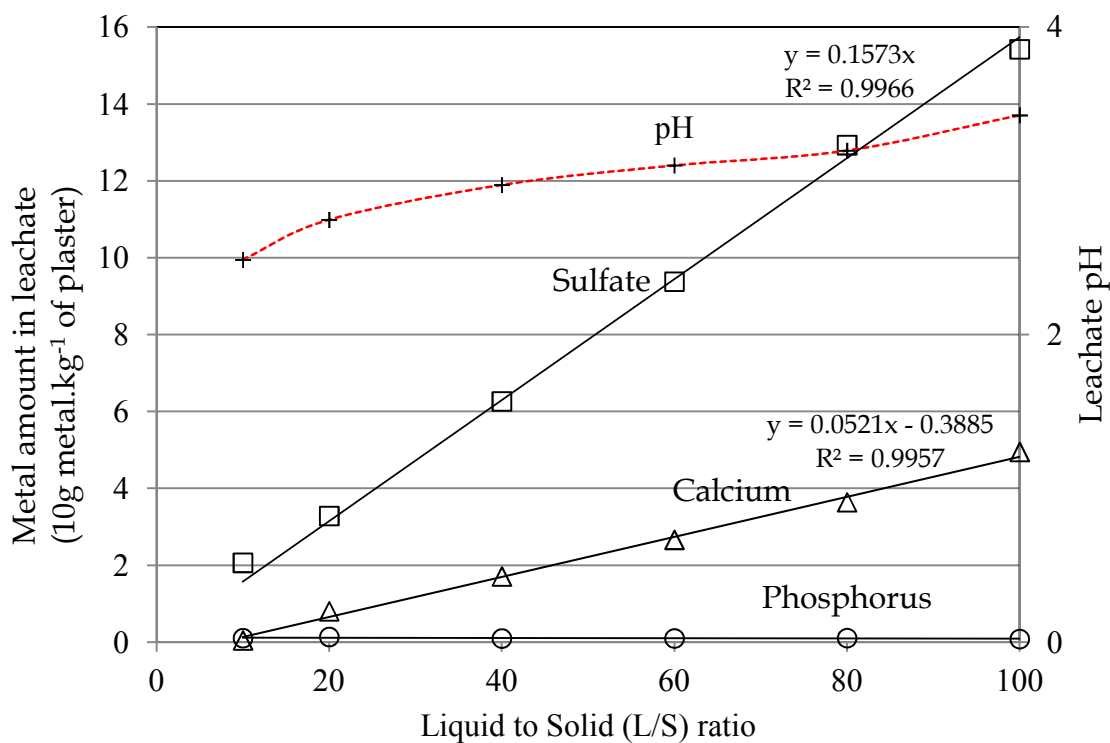
Figure 71 : Leached amount of calcium and sulfate in plaster at different L/S ratios
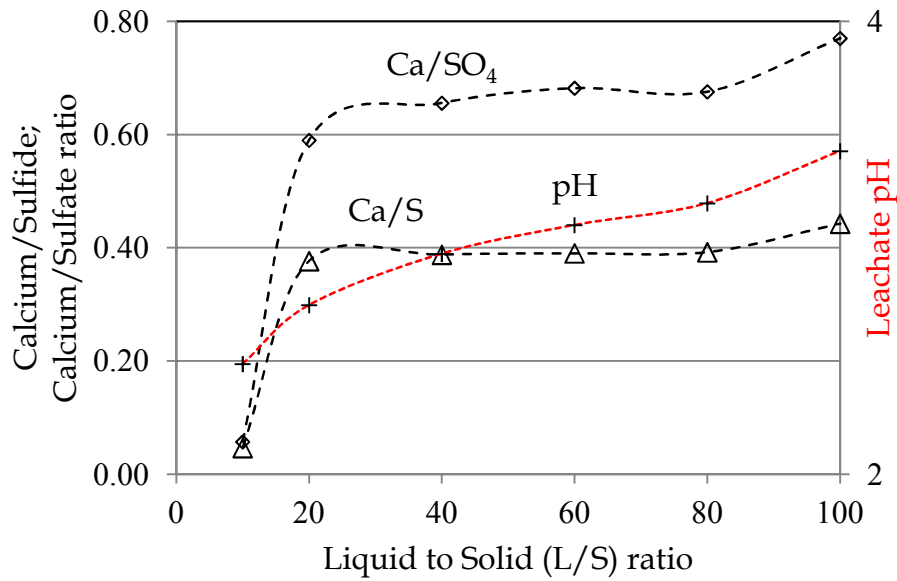
Figure 72 : The Ca/S and Ca/SO₄ ratios in function of L/P ratio

The released amount of calcium and sulfate increases with increasing L/S ratio. The released amount of phosphorus was negligible. The pH value of leachate was acidic at different L/S ratios. As shown in **Figure 72**, the ratio Ca/SO_4 was constant for L/S above 20 l.kg^{-1} indicating that the dissolution of plaster is controlled by the hydration and the 20 L/S ratio may procure indications for the availability and the behavior of heavy metals leachability.
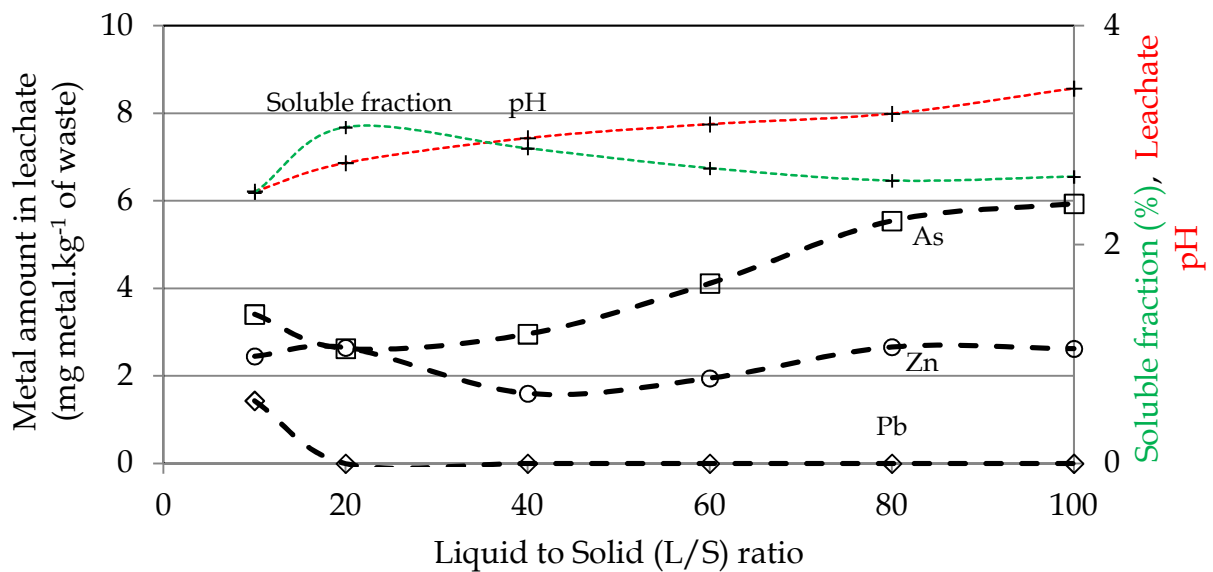
Figure 73 : Leachability of As, Pb and Zn from plaster (mg.kg^{-1}) at different L/S ratios

186

The influence of L/S ratio on the leachability of heavy metals from plaster may be illustrated by plotting the leached amount of selected heavy metals in function of L/S ratio. The **Figure 73** exhibits the leached concentration of As, Pb and Zn from plaster industrial product. From results given in **Figure 73**, acidic leachate pH increases slightly with increasing L/S ratio. Therefore, it can be explained as a buffer effect of de-ionized water. The Pb concentration in plaster leachate is below the detection limit (matter was undetected, this results indicates that Pb remains fixed as Pb-hydroxide when L/S is more than 20/1 l.kg^{-1}. Leached concentration of Zn from plaster hemihydrated particles increased by increasing liquid to solid ratio (L/S) and remains constant at L/S ratio more than 80/1 l.kg^{-1}. Acidic leachate pH plays a major role in alkalinity changes and then influences the leachability of As.

6.   Comparative study (Ca-HA – Plaster – Gypsum formulations)

To study the influence of Ca-HA$_{Gel}$ on the stabilization of sulfate and strontium from calcium sulfate wastes, obtained results of leaching tests on the formulations cited in **Table 24** were discussed. **Figure 74** presents the leaching test carried out on AWP blend. At the beginning of the test, the leached amount of phosphorus decreases in function of leaching time. The amount of leached sulfate increases slightly and achieves a relative stable concentration after 3 hours of leaching.

The pH was neutral during leaching test indicating that the leachate may contain phosphorous in form of $H_2PO_4^-$ or HPO_4^{2-}. The leachable phosphorus is unreacted phosphorus remaining in the Ca-HA suspension and the leachable amount occurring in plaster. The decrease of phosphate indicates the formation of calcium phosphate sulfate hydrate as confirmed by XRD analysis. Ca-HA stabilizes about 70% of released sulfate from plaster. In one hand , phosphate was substituted by sulfate anions in the Ca-HA structure. In the other hand, sulfate may react with free phosphate and calcium leading to calcium sulfate-phosphate hydrate formation. After 50 hours of leaching, phosphorus was relatively constant up to 5%.
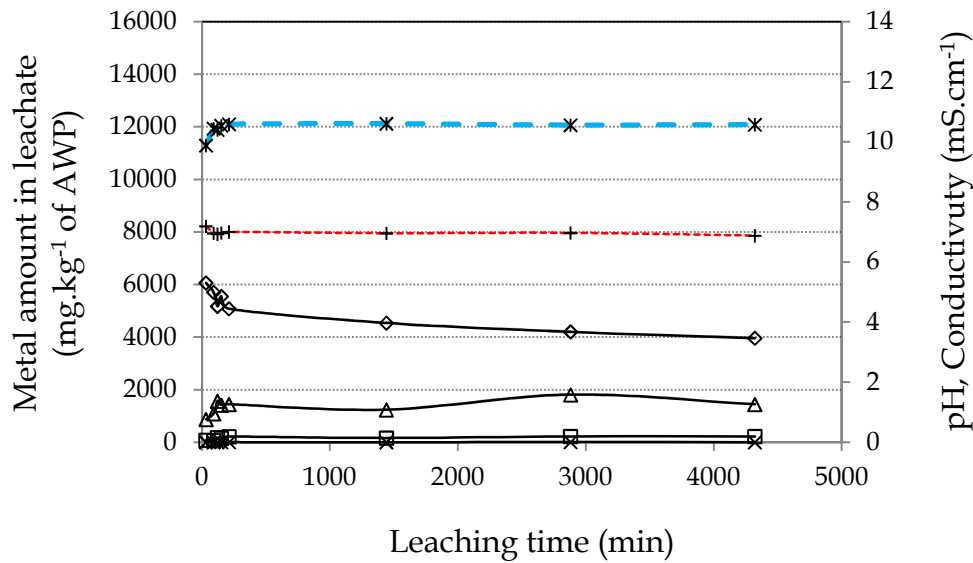
Figure 74 : Leachability of calcium, phosphorus, sulfur and strontium from AWP formulation (—◊— Phosphorus, —□— Calcium, —∆— Sulfur, —×— Strontium, --+-- pH and --*-- conductivity (mS.cm^{-1}))

The release rates of total calcium (plaster and Ca-HA calcium) and sulfate from AWP blend were 0.3 and 5% respectively. The hydration of plaster when blended with Ca-HA suspension leads to the formation of hydrated gypsum and explains the decrease of calcium and sulfate quantities in the leachate. This reveals that the hydration of plaster controls the leachability of sulfate from AWP matrix. The strontium release rate was 0.01% indicating that the released amount was totally adsorbed on Ca-HA particles. The strontium release rate decreases in comparison this release rate to the release rate obtained in the case of plaster leaching test (1%).

Figure 75 shows the concentration obtained for calcium, phosphorus, sulfur and strontium released from formulation based on Ca-HA and gypsum (<1mm) as a function of the leaching time. The released amount of calcium and sulfur increase dramatically in the beginning of the leaching test and remain relatively constant after 150 minutes indicating the equilibrium. The pH of leachate was basic revealing the presence of $H_2PO_4^-$ or HPO_4^{2-} as phosphates. The release rate of calcium and sulfur from AG blend were 2 and 32% respectively.
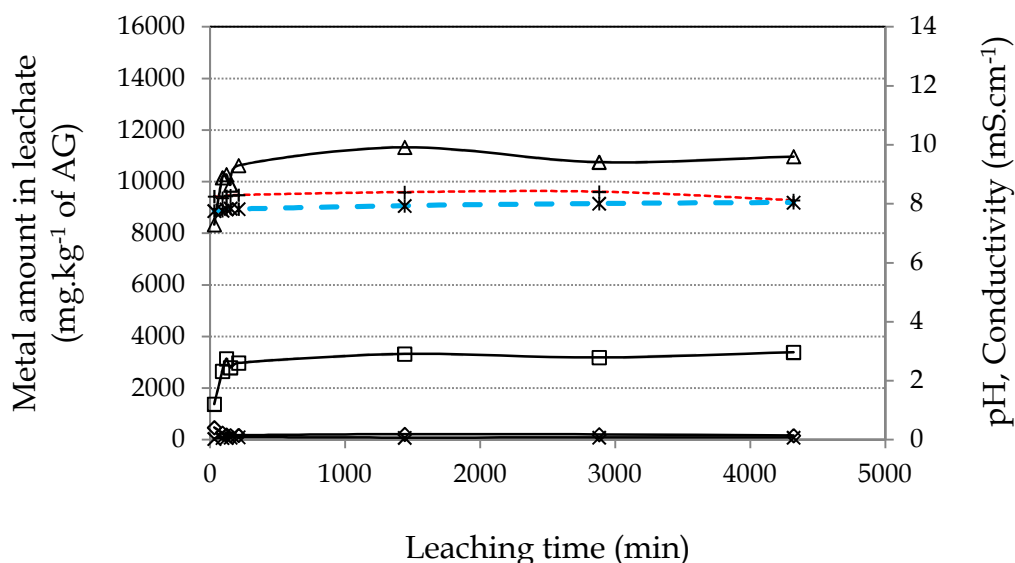
Figure 75 : Leachability of calcium, phosphorus, sulfur and strontium from AG formulation (—◊— Phosphorus, —□— Calcium, —△— Sulfur, —×— Strontium, --+-- pH and --*-- conductivity (mS.cm^{-1}))

Ca-HA$_{Gel}$ plays a major role in the stabilization of released sulfate. In the case of AG blend, about 30% of sulfate was stabilized by adding Ca-HA$_{Gel}$. The released amount of phosphorus and strontium was neglected as far as the high leached amount of calcium and sulfur is concerned. Their release rate from AG blend were 0.3 and 0.4% respectively. Strontium amount released from gypsum was stabilized and retained by Ca-HA. However, more 70% of released strontium was stabilized by Ca-HA$_{Gel}$. The stabilization of strontium may be due to the reaction with phosphate and calcium in the leachate to produce a new compound or to the dissolution/precipitation mechanism. Strontium-hydroxapatite may be presented as Ca$_9$Sr(PO$_4$)$_6$(OH)$_2$ and Ca$_3$Sr$_7$(PO$_4$)$_6$(OH)$_2$ depending on the availability of strontium [8]. **Figure 76** presents the results of leaching test carried out on blend containing Ca-HA, plaster and gypsum (<1mm). The amounts of calcium and sulfate were maintained constant during the leaching test at neutral pH and the release rates of calcium and sulfate from AWPG1 matrix were 2 and 17%.
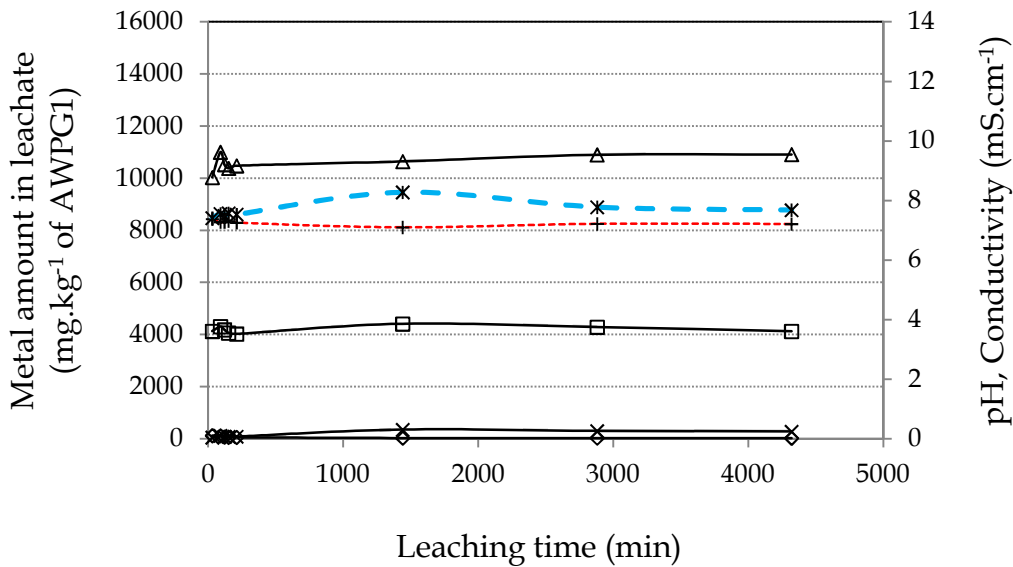
Figure 76 : Leachability of calcium, phosphorus, sulfur and strontium from AWPG1 formulation (—◊— Phosphorus, —□— Calcium, —Δ— Sulfur, —×— Strontium, --+-- pH and --*-- conductivity (mS.cm⁻¹))

The rate of release of phosphorus and strontium from AWPG1 blend were 0.3 and 0.1%. The small released amount of phosphorus indicates its combination with calcium and sulfate in the leachate to generate precipitated compounds. The amount of released strontium decreases when the Ca-HA was added to AWPG1 blend revealing its good stabilization.

Figure 77 : Leachability of calcium, phosphorus, sulfur and strontium from AWPG2 formulation (—◊— Phosphorus, —□— Calcium, —Δ— Sulfur, —×— Strontium, --+-- pH and --*-- conductivity (mS.cm⁻¹))
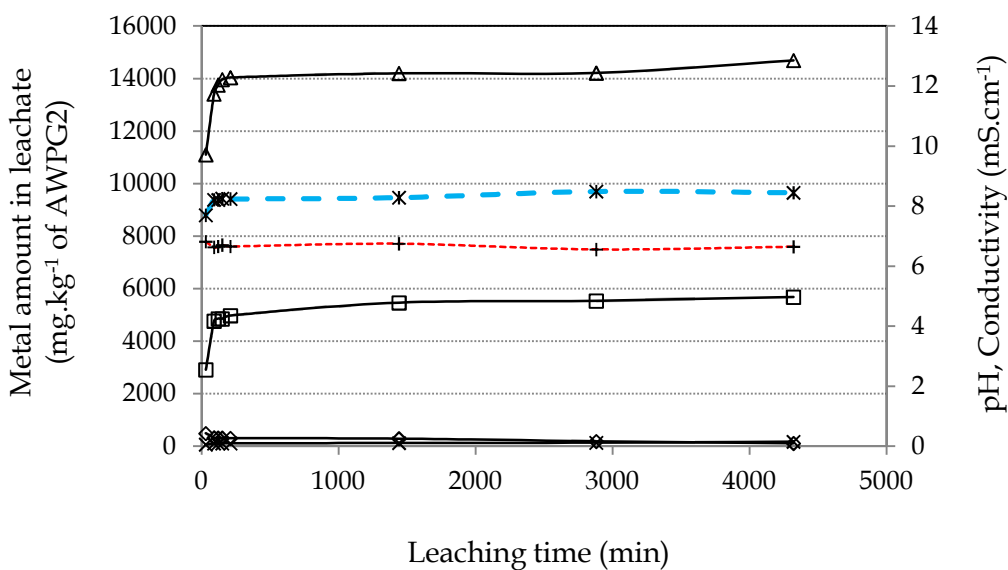
As shown in **Figure 77**, the leached amount of sulfate was higher than at for calcium with Ca/SO$_4$ molar ratio of 0.3. The quantities of calcium (released from Ca-HA, plaster and all gypsum fractions) and sulfate increase with increasing the leaching time. However, the release rates of calcium and sulfate were 2 and 16% respectively. The amount of phosphorus decreases with increasing leaching time and has a concentration ranging from 100 to 500 mg.kg^{-1} of AWPG2. The release rate of phosphorus at the end of leaching test was 0.3% indicating that the phosphate occurring in solid-suspension was reacted with dissolved gypsum and Ca-HA calcium. According to the constant leachate pH, the precipitation of calcium phosphate and calcium sulfate-phosphate hydrates plays a major role to stabilize the AWPG structure and governs the leachability of major elements. The strontium was characterized by a release rate of about 0.03%.

The comparison between formulations in term of released elements was based assuming equilibrium during the leaching test. **Table 26** recapitulates the concentrations of released element. The low value of the conductivity at the equilibrium shows that the leachate from materials and formulations contains less soluble elements. In the case of AWP blend, using Ca-HA$_{Gel}$ led to stabilize above 80% of sulfur. The decrease in the amount of calcium released was explained by the hydration process and the formation of calcium phosphate – sulfate hydrate. The amount of released phosphate was increased in comparison to the amount released from plaster. This could be explained by the presence of free phosphate in Ca-HA$_{Gel}$. The concentration of released strontium (3 mg.kg^{-1} AWP) from AWP blend indicates its retention by Ca-HA particles and/or its reaction with free phosphate leading to strontium apatite precipitation. Strontium amount released from plaster was higher than those released from AWP blend; this result proves that Ca-HA particles and free phosphate play a primordial role in the stabilization of released strontium.

Table 26 : Summary of release of elements at equilibrium from materials and considered blends

	pH	Conductivity (mS.cm^{-1})	Ca (mg.kg^{-1})	S (mg.kg^{-1})	P (mg.kg^{-1})	Sr (mg.kg^{-1})
Plaster	2.4	3.6	10000	10000	2000	200
G 1mm	8.8	2.1	7000	14000	40	300
G 1-2mm	8.1	2.1	5000	6000	4	100
G 2-4mm	8.6	2.1	5000	6000	8	100
AWP	7.0	10.6	200	1600	4000	3
AG	8.4	8.0	3000	11000	200	85
AWPG1	7.2	7.7	4000	11000	30	300
AWPG2	6.7	8.5	6000	14000	200	100

The calcium and sulfur released from the formulation AG were less than those released from gypsum (<1mm). Substituting 80% of gypsum by Ca-HA leads to decrease of calcium and sulfur amount released (i.e. about 60 and 20% of calcium and sulfur were stabilized). The stabilization of calcium and sulfur is essentially due to the re-precipitation of gypsum and the formation of calcium sulfate phosphate hydrate. The phosphorus amount released from AG was five times higher than the released amount from gypsum (<1mm). This can be related directly to free phosphate available from Ca-HA$_{Gel}$. Released strontium was stabilized by Ca-HA particle (above 70% of released strontium was retained). For formulations blended with both plaster and gypsum with different fraction sizes, the total amount of calcium, sulfur, phosphorus and strontium was calculated as a function of plaster and gypsum proportions. Increasing the amount of gypsum in AWPG1 and AWPG2 formulations leads to the increase of leached calcium and sulfur. The amount of released phosphorus decreased, it is correlated to the proportion of Ca-HA$_{Gel}$ introduced and the released amount from plaster. It is difficult to compare the released amount of studied elements from AWPG1 and AWPG2 to those released directly from plaster or gypsum with different fractions. Amount of released strontium from AWPG1 and AWPG2 formulations was approximately similar to amount of strontium released from plaster or gypsum. Nevertheless, this results is commonly related to the amount of gypsum added.

7.   Stabilization of hazardous pollutants

In this present section, the stabilization of cadmium, lead and zinc will be briefly discussed. The leaching results are illustrated by the release rate of heavy metals as presented in **Figure 78**. The release rate of heavy metals from all considered blends was negligible (<0.3%). The release rates were calculated in function of the total amount of selected heavy metals presents in plaster and gypsum with different grain size. The leached amount of cadmium was less than the leached amount of lead and zinc in AWP blend. The rate of release of lead in both AWP and AG blends was higher than that calculated for AWPG1 and AWPG2.
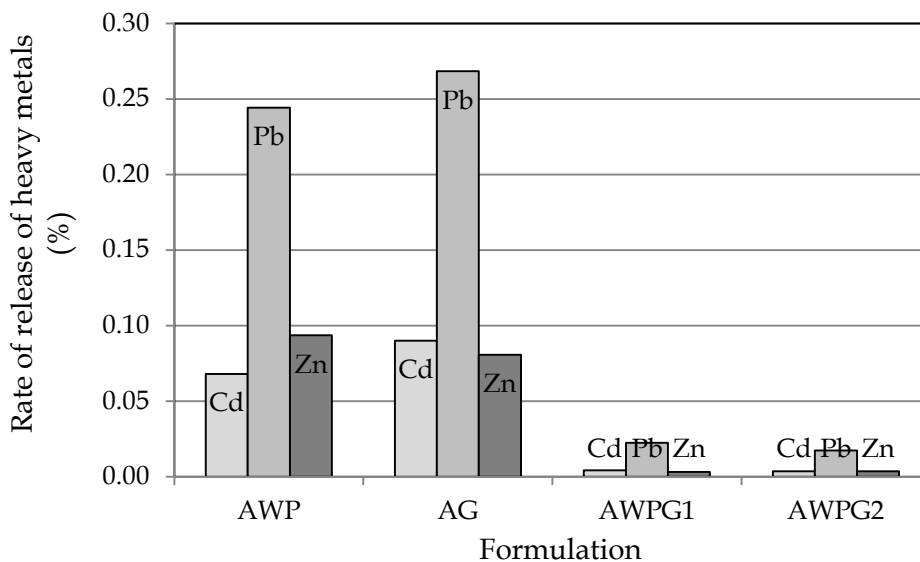
Figure 78 : The release rate of Cd, Pb and Zn in the leachate as a function of considered formulations

The results obtained in the section 3.4 (effect of grain size) have shown that increasing the gypsum fraction, the leached amount of lead increases. Adding Ca-HA$_{Gel}$ to plaster, gypsum (particle size between 1 and 4mm) according to AWPG1 and AWPG2 formulations leads to the stabilization of leached selected heavy metals. Adsorption, cation exchange and precipitation are the main mechanisms of heavy metals stabilization by Ca-HA$_{Gel}$.

8. Conclusion

Different formulations considered in this chapter were characterized by XRD and FTIR. XRD analysis have shown the formation of new compounds like calcium sulfate carbonate hydrate, calcium phosphate sulfate hydroxide hydrate and calcium phosphate sulfate hydrate. FTIR analysis have revealed that the decrease of the intensity of phosphate bands indicates that the symmetry of phosphate decreased because of the effect of sulfate substitution. The increase in wave number and decrease of intensity of phosphate band provide some indications on change of apatite structure. The availability of chemical elements released from Ca-HA, gypsum and plaster was studied using ANC standardized method. Concerning Ca-HA powder particles, calcium and phosphorus were released at pH less than 4. The dissolution of Ca-HA takes place at acidic region. The released amount of calcium and phosphorus from Ca-HA remained constant and negligible indicating that Ca-HA are stable at basic pH zone. The stability of Ca-HA is promoted by the formation of precipitated hydroxide. For gypsum and plaster by-products, the behavior of leached heavy metals depends also on the pH and the solubility. Leaching tests have shown that the leaching duration, particle size and L/S ratio influence the release of calcium, sulfate and selected heavy metals from plaster and gypsum fractions. Leaching tests carried out on considered formulations have revealed that Ca-HA$_{Gel}$ and plaster hydration control sulfate release and the amount of released strontium from plaster and gypsum fraction. Ca-HA$_{Gel}$ stabilized heavy metals released from both plaster and gypsum and AWPG1 and AWPG2 have shown a low heavy metals release rate. The selection of favorable formulation will be based on the determination of hydraulic performance discussed in the Chapter VIII.

References

[1] Environment Agency (EA), 2005. Guidance on Sampling and Testing of Wastes to Meet Landfill Waste Acceptance Procedures.

[2] VERWILGHEN C., CHKIR M., RIO S., NZIHOU A., SHARROCK P., DEPELSENAIRE G., 2009, Convenient conversion of calcium carbonate to hydroxyapatite at ambient pressure, Materials Science and Engineering: C, Volume

29, Issue 3, Development of Nanostructures for Medicine Special Issue, 30 April 2009, Pp771-773

[3] AFNOR, 1993, French standard NF X31-151, Sols, sédiments, boues de station d'épuration - Mise en solution d'éléments métalliques en traces (Cd, Co, Cr, Cu, Mn, Ni, Pb, Zn) par attaques acides.

[4] AFNOR, EN 12457-2, 2002, Characterization of waste – leaching – compliance test for leaching of granular waste materials and sludges. Part 2. One stage batch test at a liquid to solid ratio of 10 l/kg for materials with particle size below 4 mm, European Standard NF, December 2002.

[5] ANC, Test d'influence du pH selon la norme NF CEN/TS14429:

[6] GREISH Y., E., 2011, Phase evolution during the low temperature formation of stoichiometric hydroxyapatite-gypsum composites, Ceramics International 37, Pp715-723

[7] VERWELGHEN C., 2006. Fixation des métaux lourds par des phosphates de calcium dans le traitement des fumes d'usines d'incinération d'ordures ménagères. Thèse soutenue le 13 décembre, 2006, Université Paul Sabatier de Toulouse III. Pp47-60

[8] Verberckmoes S. C., G. J. Behets, L. Oste, A. R. Bervoets, L. V. Lamberts, M. Drakopoulos, A. Somogyi, P. Cool, W. Dorrine´ ,M. E. De Broe, P. C. D'Haese. 2004, Effects of Strontium on the Physicochemical Characteristics of Hydroxyapatite, Calcif Tissue Int (2004) 75: DOI: 10.1007/s00223-004-0260-4 Pp405–415

Chapter VIII

Percolation test and hydraulic performances of hydroxyapatite (Ca-HA$_{Gel}$)/plaster/gypsum permeable reactive barrier (PRB)

I.   Introduction

The Environmental Protection Agency (EPA) defined the Permeable Reactive Barrier (PRB) as a subsurface emplacement of reactive materials perpendicularly to the groundwater flow following a natural hydraulic gradient. PRB performances depend on the pollutant quantity, flux velocity of groundwater and hydraulic properties recognized as durability index. Permeability and porosity are considered the important parameters characterizing the barrier hydraulic capacity and allowing the flux of water and solutes through a geometric reactive media. They are also affected to the PRB performances. Several relationships between permeability and porosity could be used to simulate their evolution based on macro and microscopic morphologies and specific surface areas of materials. The PRB implementation requires that reactive material permeability be sufficient (i.e. permeability coefficient (K) of 10 to 10^{-4} cm.s^{-1}) and more permeable than aquifer permeability to facilitate the drainage and ensure the flux continuity. The permeability is correlated to the porosity and particle size representing the porous structure. Consequently, Kozeny-Carman model (1937) based on the assimilation of porous media as an assembly of capillary connected tubes takes into account the porosity and specific surface area of particles to estimate the intrinsic permeability.

The main purposes of this chapter are to evaluate the hydraulic performances (permeability and porosity) of formulations containing hydroxyapatite gel (Ca-HA$_{Gel}$) and both hemihydrated and dihydrated calcium sulfate. The percolation test will be carried out to evaluate the capacity of Ca-HA to stabilize calcium sulfate wastes. The influence of formulations composition on the physical, chemical and durability performance were investigated.

II. Materials and methods

1. Calcium phosphate / Calcium sulfate Formulations

The considered formulations studied in this work were prepared by mixing Ca-HA_{Gel} and plaster (plaster was blended with water according to W/P mass ratio of 0.4 to ensure its initial hydration) and, Ca-HA_{Gel} and gypsum with proportion of Ca-HA_{Gel} of 80% and 20% of calcium sulfate respectively. Ca-HA used in this work was characterized by Ca/P atomic molar ratio of 2.3. The formulations AWPG1 and AWPG2 were bended with W/P mass ratio of 0.4. **Table 27** summarizes the considered formulations. The formulation AWPG2 was blended with 10% of gypsum (1-2mm) and 20% of gypsum (2-4mm) to investigate the influence of gypsum particle size dissolution in the presence of Ca-HA_{Gel}.

Table 27 : Gypsum, plaster and Ca-HA_{Gel} considered formulations

Products	Formulation 1 AWP	Formulation 2 AG	Formulation 3 AWPG1	Formulation 4 AWPG2
Ca-HA_{Gel} (%)	80	80	64	56
Plaster (%)	14.28	0	11.43	10
Water (%)	5.72	0	4.57	4
Gypsum (d_P<1mm) (%)	0	20	20	0
Gypsum (1-2mm) (%)	0	0	0	10
Gypsum (2-4mm) (%)	0	0	0	20

The formulations were proposed to evaluated the reactivity of Ca-HA_{Gel} to stabilize the calcium sulfates wastes and finally to select the adequate PRB formulation to be assessed.

2. Characterization procedures

The chemical analysis of both calcium sulfates and hydroxyapatite were carried out using inductively coupled plasma spectrometry (ICP-AES) to determine the impurity content. ICP-AES analyses were performed on a ULTIMA-2 (JOBIN YVON HORIBA).

3.   Water absorption capacity

Water Absorption Capacity (WAC) determination was made following the ADEME procedures' (*Agence de l'Environnement et de la Maîtrise de l'Energie*; Environment and Energy Management Agency). Absorption capacity represents stored water amount in the structure of particles. This method describes the behavior of surface exchange between water and surface of particles. It gives indications concerning the amount of water needed to reach a perfect plaster hydration and the influence of gypsum particle size on the retention capacity of water molecules. Water Absorption Capacity (WAC) was determined by a static method consisting in contacting 10g of matter with de-ionized water according to Liquid to Solid (L/S) ratio of 10. The WAC is based on mass loss affected to solubilization and corrosion of particles, volume of stored water and mass of cake after filtration have been determined. Hence, soluble fraction percentage was evaluated by filtering the suspensions and collected water was dehydrated in sandbox heated at $103 \pm 2°C$ and the dry residue was weighed.

Operating mode is described in details as follows:

♦ Weighting the sample (m_0);

♦ Introducing sample in de-mineralized water (L/S=$100ml.10^{-1}g^{-1}$);

♦ Contact during 15min in a closed container to prevent evaporation of water;

♦ Separating sample from water by draining and weighing the wet sample (m_{15min});

♦ Filtration of collected water, weighing the filter cake (G_{15min}),

♦ Determining the soluble fraction in the water (SF) by dehydration at $105 \pm 2°C$ and weighing the dried residue.

WAC (wt%) of samples was calculated according to:

$$WAC = \frac{m_{15min} - [m_0(1-SF) - G_{15min}]}{[m_0(1-SF) - G_{15min}]}$$ [Eq.1]

4. Durability index

4.1. Permeability

Permeability assessment was made using an experimental device illustrated in **Figure 79** to carry out the percolation test. Butterfly valves were installed to control air pressure and water flow. The cell volume of 343.36cm³ was filled by tested sample and applied pressure was a differential pressure attained by compressed air varying from 1.1 to 1.5bars relative pressure. Flow rate was derived by mass of filtered water during 1h of filtration (i.e. to achieve laminar flow). The permeability value (intrinsic permeability, K) was calculated by using Darcy's relationship:

$$K = \frac{Q}{A}\frac{H}{\Delta P}\rho g \qquad\qquad\qquad\qquad \text{[Eq.2]}$$

Where Q is the flow rate of filtered water (cm³.s⁻¹); A is the cross section of sample test (cm²); H is the length of sample test (cm); ΔP is pressure difference (P₂-P₁) (P₁ is the applied pressure of inlet water (Pa) and P₂ is the pressure of outlet water equal to atmospheric pressure (1.013MPa)); ρ is the density of water considered equal to 1.0g.cm⁻³ and g is the gravity constant (9.81m.s⁻²).
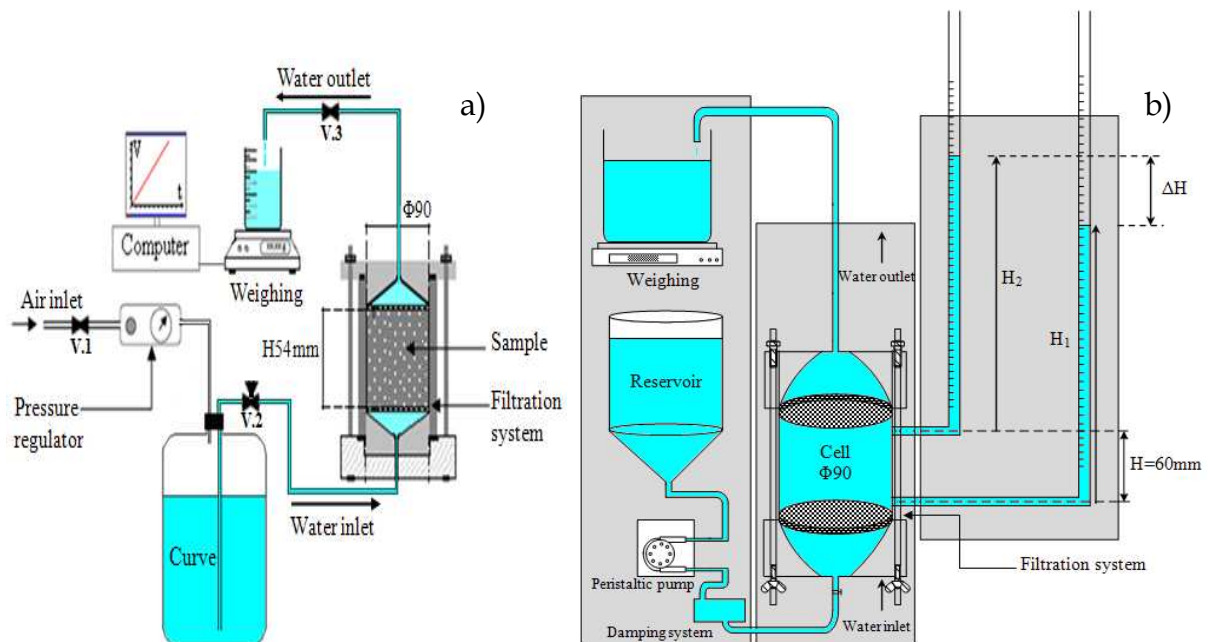
Figure 79: Constant head permeability test, a) permeability device schema for material presenting a high head loss b) permeability device schema destined to evaluate permeability of grain size above 1mm (*V.1 Air pressure valve; V.2 Water flow control and purge valve; V.3 Water flow control valve*)

The method (a)) has been chosen to evaluate the permeability of Ca-HA$_{Gel}$ and Ca-HA$_{Gel}$ with calcium sulfates, i.e. for material presenting a high head loss, and method (b)) was applied to measure the permeability of gypsum grains (1-2mm and 2-4mm).

4.2.   Porosity

The porosity was calculated by evaluating the compactness of formulations. The compactness Φ relationship is as follows:

$$\Phi = \frac{1}{1+\rho_B\frac{W}{S}} \text{ with } \varnothing = 1 - \Phi \qquad \text{[Eq.3]}$$

Where $\varnothing$ is the porosity, ρ_B is the bulk density of the solid (g.cm^{-3}), W is the Ca-HA$_{Gel}$ water (g) and S is the total amount of solid (g). For binary blends, ρ_B is the weighted average of solid densities with Y_{Ca-HA}, Y_P and Y_G are the proportions of Ca-HA$_{Powder}$, plaster and gypsum in the blends respectively ($\rho_B = Y_{Ca-HA} \cdot \rho_{Ca-HA} + Y_P \cdot \rho_P$ or $\rho_B = Y_{Ca-HA} \cdot \rho_{Ca-HA} + Y_P \cdot \rho_G$ with $Y_{Ca-HA} + Y_P = 1$ and $Y_{Ca-HA} + Y_G = 1$).

5.   Percolation test (French standard)

The percolation test was carried out according to NF CEN/TS 14405 French standard [1] to determine the dynamics of release of the materials under standard conditions. The test is applied to compact granular materials in a fixed bed. The column used in this study had a diameter of 90mm (granularity of waste is less than 4mm fraction <80%) and a height of 54mm. A sample fixed bed was prepared in five layers. The demineralized water follows an ascending flow using peristaltic pump following a constant flow rate of 20 ml.min^{-1}. **Figure 80** illustrates the percolation test according to predefined procedure. Filter paper was placed on filtration system to avoid the transport of Ca-HA particles.
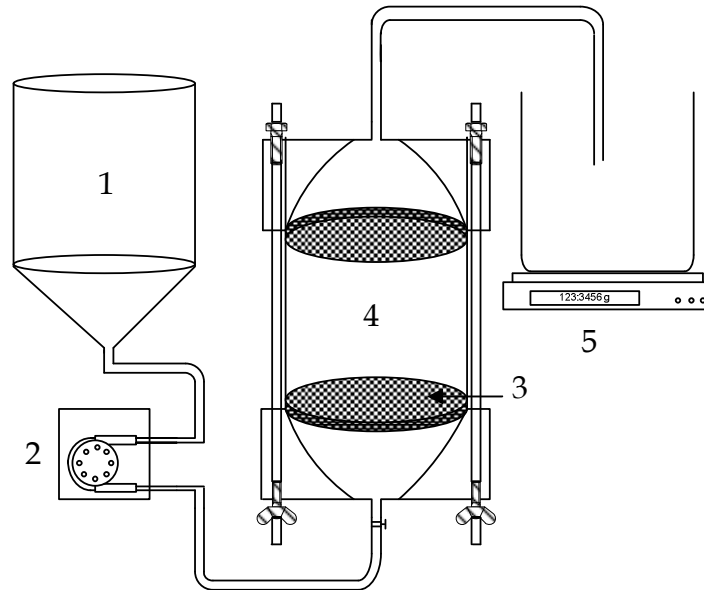
Figure 80: Percolation test system (1: reservoir, 2: peristaltic pump, 3: filter system, 4: permeametric cell, 5: weighing)

The test was stopped when the L/S ratio achieved 10 l.kg^{-1}. The filtrate was recovered by fractions corresponding to 0.1, 0.2, 0.5, 1, 2, 5 and 10 l.kg^{-1} L/S ratio.

III.   Results and discussion

1.   WAC of materials

The results obtained show that the absorption capacity of water by calcium sulfate particles was higher than 50% as shown in **Figure 81**. WAC of plaster was about 60%, indicating that the hydration process of hemihydrated particles is limited at W/P ratio below 10.
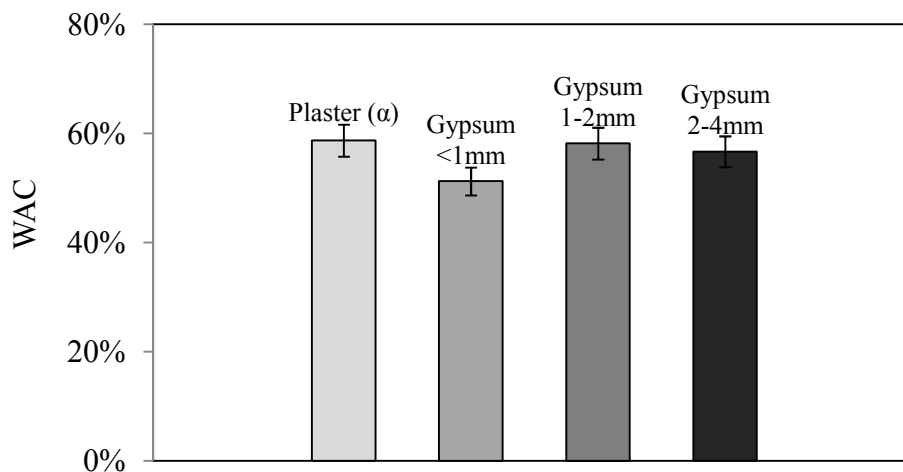
Figure 81 : Water absorption capacity of plaster and gypsum grains

On the other hand, it can be concluded from gypsum stoichiometry that water consumption corresponding to W/P ratio of 10 is about 1.86%. This is explained by the influence of water amount on the hydration by the dissolution and buffering effect of water. Absorption capacity of already hydrated gypsum is influenced by particle size and agglomeration. Absorption capacity increases by increasing size of gypsum grains; this is expected to bring chemical bonds between hydrated particles leading to porosity creation. When all the *open pores* are completely *filled* with water, gypsum grains are saturated, and the stored water is estimated to water absorbed in the case of plaster. As known, present gypsum was obtained by plaster filtration using water to extract remained phosphorus content (phosphoric acid production); plaster filtration implies particle hydration and amount of water added controls porosity rate. Gypsum grains of size ranging from 1-2mm and 2-4mm in contact with water have tendency to absorb water into the void space created by water evaporation during hydration period.

2.   Permeability

2.1.   Material permeability

The permeability of Ca-HA$_{Gel}$ and Ca-HA$_{Powder}$ was determined according to the device illustrated in **Figure 79** a). **Figure 82** shows the flow rate as a function of the section (A) and hydraulic gradient (i). The slopes of the straights represent the permeability values of Ca-HA$_{Gel}$ and Ca-HA$_{Powder}$ that are of 5.10^{-5} and 7.10^{-5} cm.s^{-1} respectively.
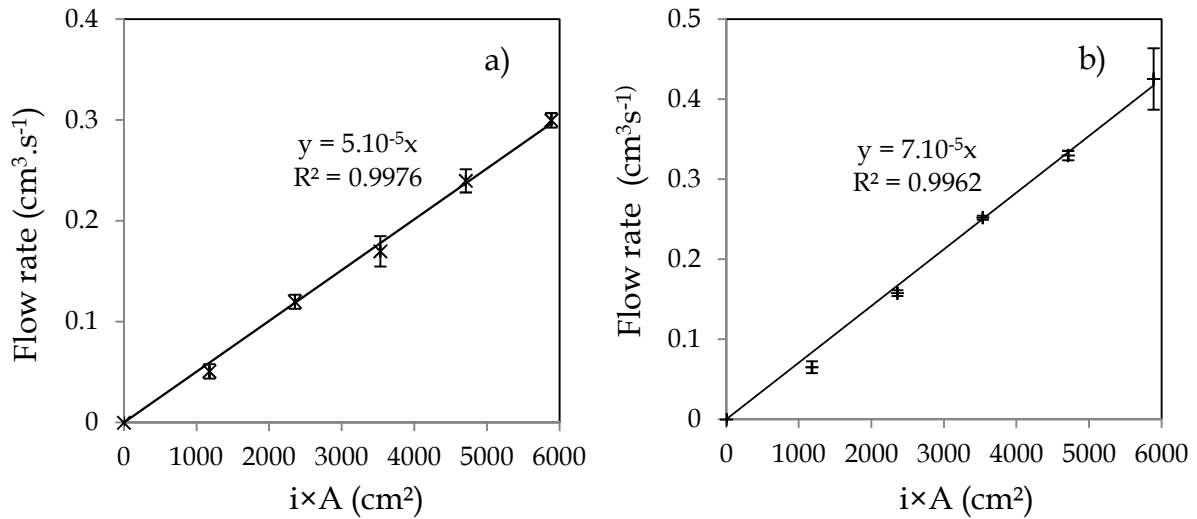
Figure 82 : Permeability of Ca-HA$_{Gel}$ (a) and Ca-HA$_{Powder}$ (b)

Ca-HA is classified as impermeable. Silty texture of Ca-HA describes its impermeability, which is against a good drainage. Permeability using Hazen equation [2] based on d_{10} of Ca-HA particles agrees with the obtained permeability values (i.e. permeability of Ca-HA calculated using Hazen equation was 2.10^{-5} cm.s^{-1}). **Figure 83** shows the flow rate against the section of gypsum and hydraulic gradient.
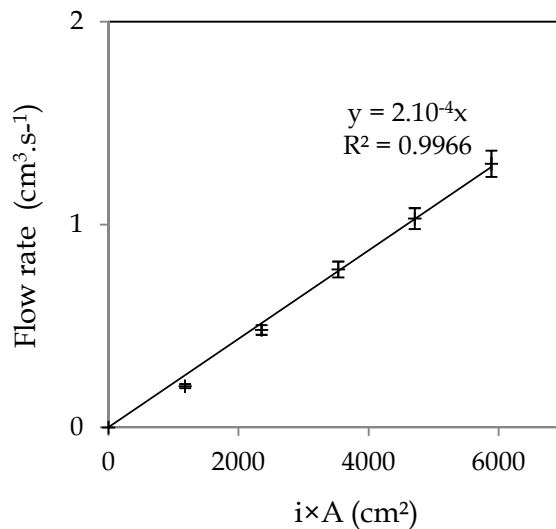
Figure 83 : Permeability of gypsum (<1mm)

Gypsum was classified as sandy-silt and characterized by a permeability of 2.10^{-4} cm.s^{-1}. Consequently, gypsum allows a good drainage of water and could be considered as a permeable material. Permeability test on plaster was not carried out

because the plaster hydration gives a solid with high head loss, making difficult the water flow throughout the solid body. The permeability of plaster was estimated using Hazen equation and its value is about 10^{-4} cm.s^{-1} and it classified as silt. The permeability of gypsum grains vary with particle size between 1 and 2 mm and gypsum grains with particles between 2 and 4 mm was evaluated using the device illustrated in **Figure 79** b). **Figure 84** shows the relationship between flow rate and permeability of gypsum grains as a function of peristaltic pump rotation. Flow rate increases linearly with the rotation velocity. Increasing the rotation velocity leads to the increase in the head pressure and at constant flow rate, permeability is constant.
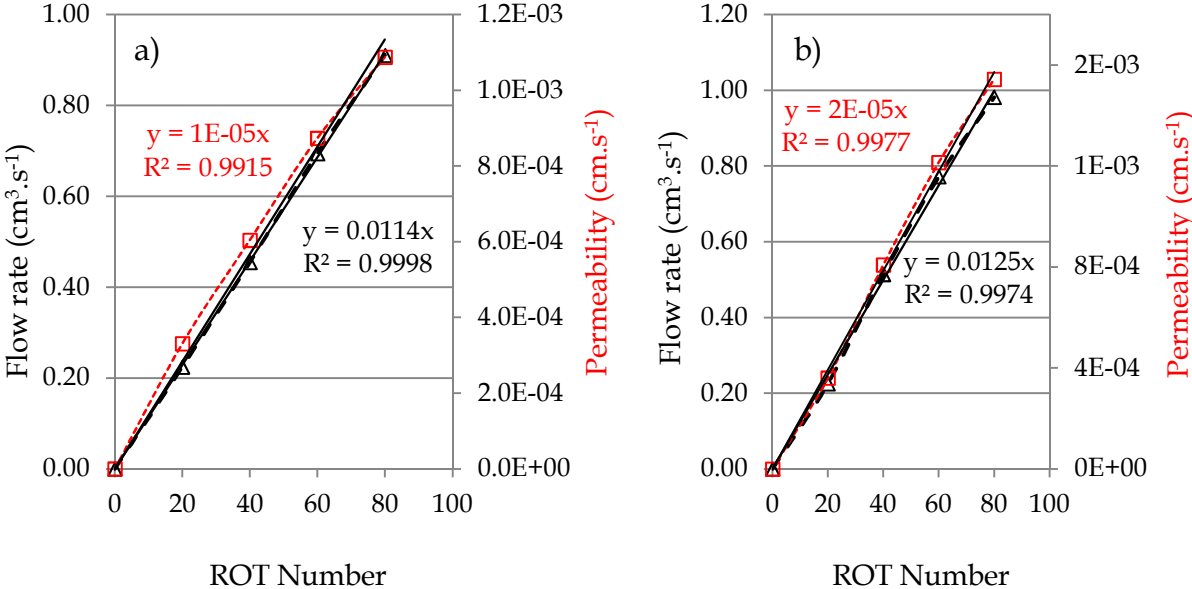
Figure 84 : Permeability of gypsum (1-2mm) (a) and gypsum (2-4mm) (b)

Permeability increases constantly as a function of the pump rotation velocity (flow rate). However, the permeability value of gypsum grains was the average of determined permeabilities at different constant flow rates. The permeability values of gypsum (1-2mm) and gypsum (2-4mm) were 3.10^{-4} and 4.10^{-4} cm.s^{-1} respectively.

2.2.   Considered formulation permeability

The permeability of considered blends was calculated from parameters evaluated from device shown in **Figure 79** a). **Figure 85** illustrates the flow rate in the outlet as a function of sample section and hydraulic gradient. Adding 20% of W/P (0.4) blend to

Ca-HA$_{Gel}$ increases the permeability of Ca-HA$_{Gel}$. The permeability of AWP blend is 9.10^{-5} cm.s^{-1}.
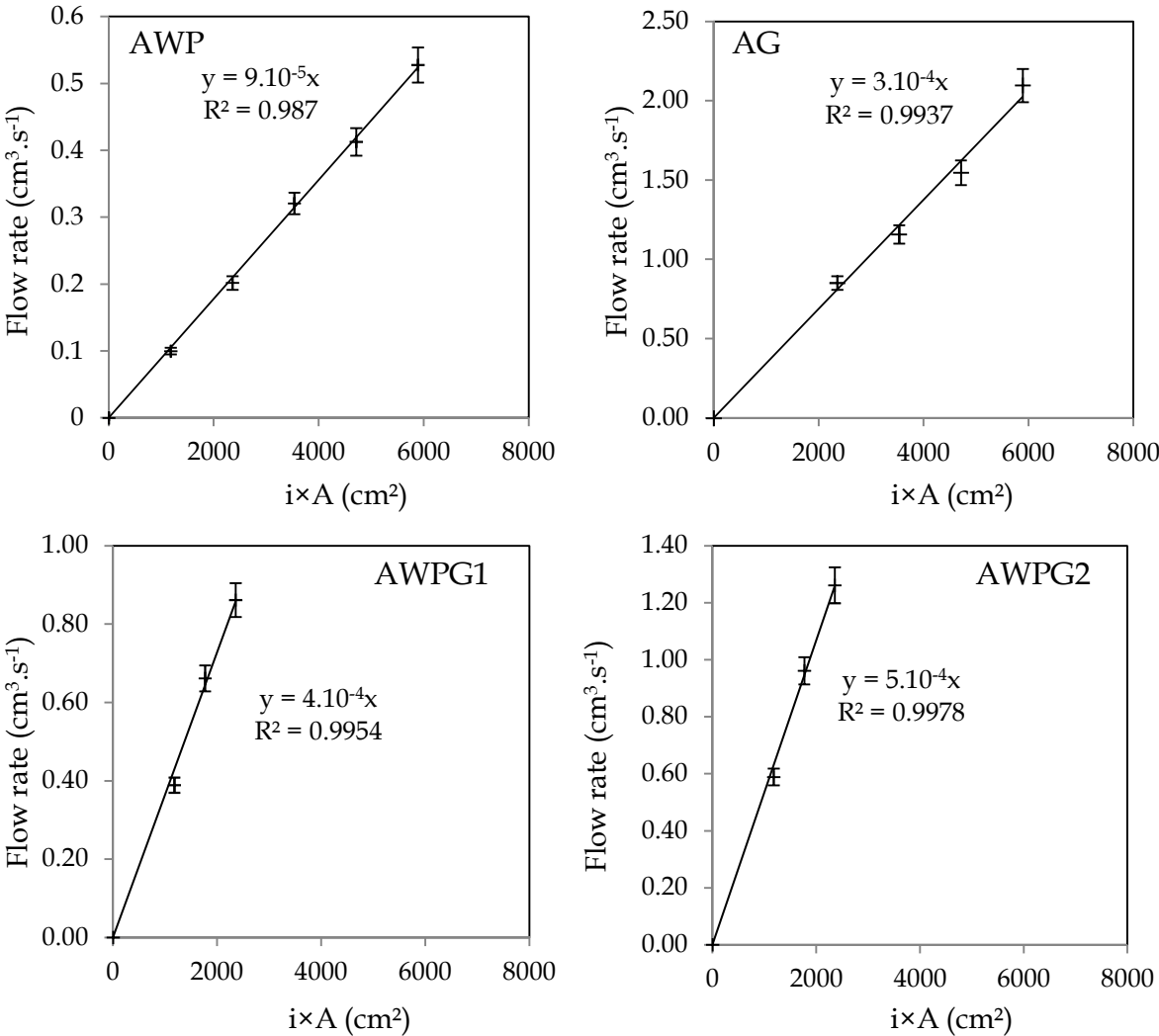
Figure 85 : Permeability of AWP, AG, AWPG1 and AWPG2 considered blends

Increasing the amount and the grain size of gypsum in blends containing Ca-HA$_{Gel}$ leads to the increase in the permeability. Substitution of gypsum with different fractions and plaster hydration govern the permeability and the stability of blends. The permeability of AWPG2 blend was 5.10^{-4} cm.s^{-1} suggesting a good drainage capacity.

3.   Porosity

Porosity of blends was determined from the compactness of solids. **Figure 86** shows the porosity values of AWP, AG, AWPG1 and AWPG2 pastes. Calculated porosity of

formulations decreases by decreasing the amount of Ca-HA$_{Gel}$. The porosity of AWP formulation containing Ca-HA$_{Gel}$ and plaster is higher than the porosity of formulation containing gypsum.
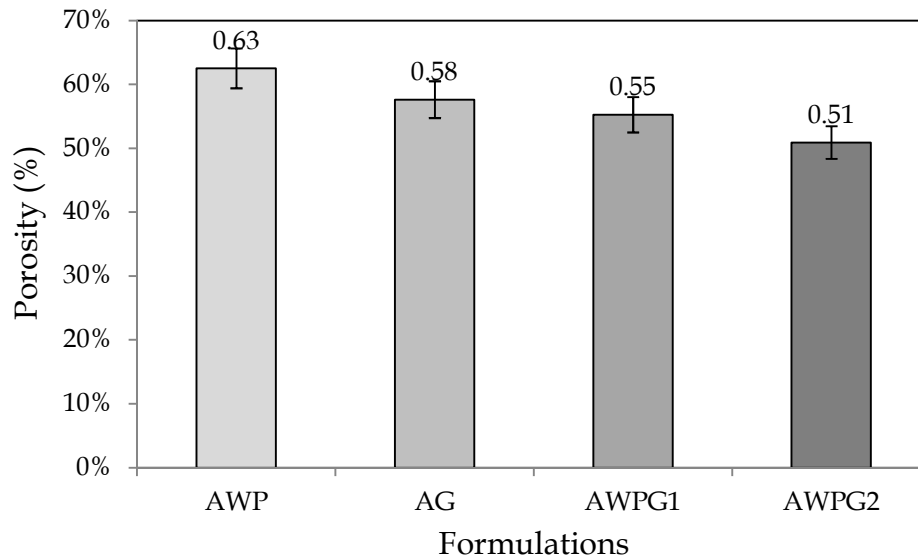
Figure 86 : Calculated porosity of considered formulations

The porosity of AWPG1 blended with gypsum (<1mm) is higher than the porosity of AWPG2 formulated with gypsum having particle size varying from 1 to 4 mm. Consequently, the increase in gypsum particle size leads to the decrease of blends total porosity. It seems that the porosity evaluation from the compactness of blend is not linked with the particle size and the intrinsic porosity but corresponds to the total bulk density of solids. Gypsum grains may absorb up to 50% of free water as determined by WAC method. However, the porosity of considered formulations is equivalent to the saturated water content.

4.   Percolation test results

4.1.   Leachability of Ca-HA$_{Gel}$

Ca-HA$_{Gel}$ contains hydroxyapatite particle and unreacted species such as calcium from calcite and free phosphate from ammonium phosphate. The main purpose of percolation test was to determine the leached quantity of calcium and phosphate from Ca-HA$_{Gel}$. The amount of leached calcium and phosphate corresponds to the

free phosphate and calcium in Ca-HA suspension. **Figure 87** shows the leached amount of calcium and phosphorus against time, conductivity and pH. The pH was basic and its value (pH ≈ 8) indicates the presence of HPO_4^{2-} ions. The conductivity value decreases with increasing percolation time.
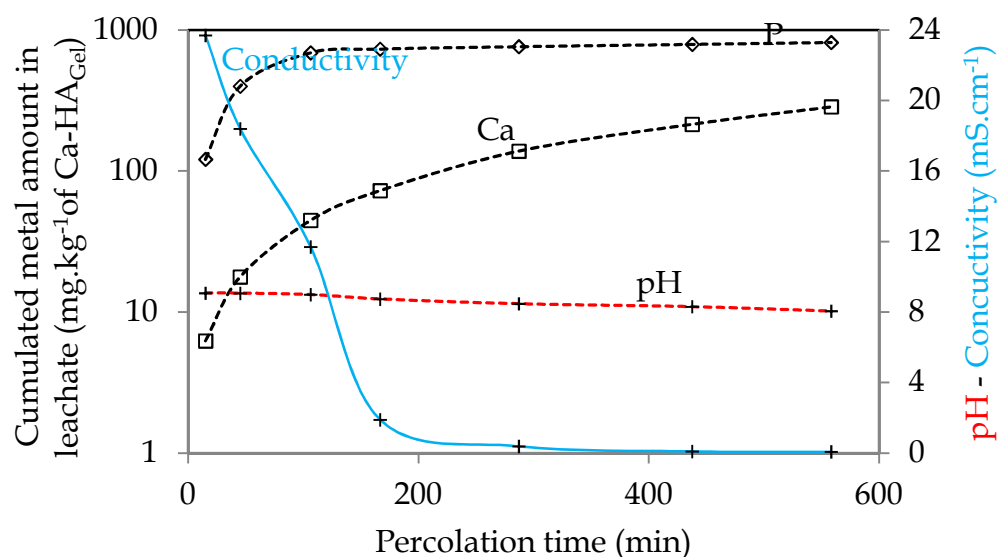
Figure 87: Leached amount of calcium and phosphorus from Ca-HA as a function of leaching time, pH and conductivity (—◊— Phosphorus, —□— Calcium, --+-- pH and --+-- conductivity (mS.cm⁻¹))

It can be noticed that the total amount of calcium and phosphorus percolated from Ca-HA$_{Gel}$ were 400 and 8000 mg.kg⁻¹ Ca-HA$_{Gel}$. The cumulated amount of calcium and phosphorus leached from Ca-HA$_{Gel}$ increases with increasing leaching time. Their concentrations remain stable after 800 minutes (1h30) of leaching time. The release rates of calcium and phosphorus were 13 and 3% respectively. The percolation tests pointed out that there are free calcium and phosphorus, ions that could leached and later precipitate available metal ions in solution.

4.2.   Leachability of plaster and gypsum (<1mm)

Figure 88 compares the concentrations of released calcium, sulfur, phosphorus and strontium from plaster and gypsum respectively. The pH of plaster is acidic and pH of gypsum is basic. The acidic pH of plaster is due to the leaching of phosphoric acid which is present in the percolate (**Figure 88** a)). At the beginning of the percolation

test, H_3PO_4 and $H_2PO_4^-$ are present in the filtrate, and after 600 minutes (10 h) of percolation experiment, only $H_2PO_4^-$ is present following phosphoric acid speciation.
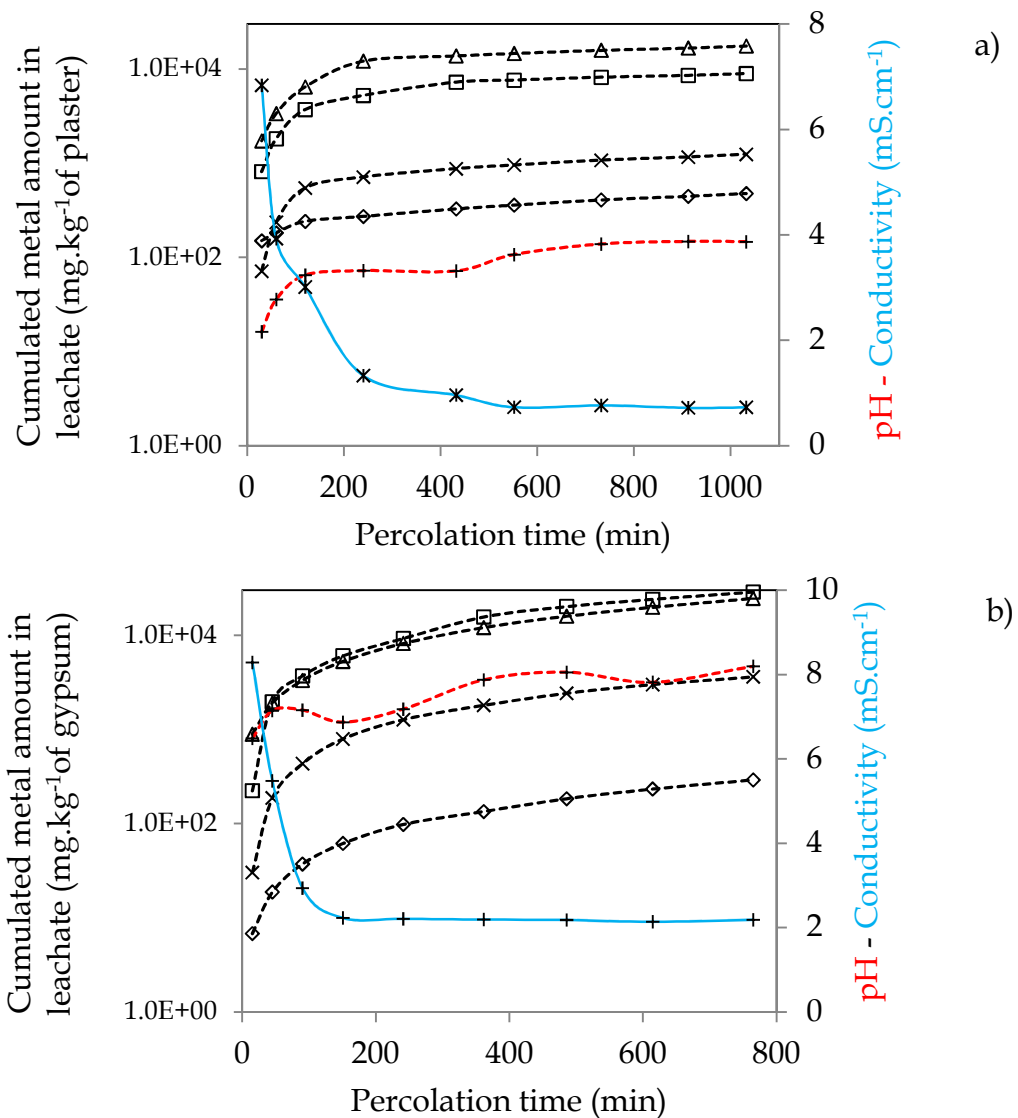
Figure 88: Leached amount of calcium (--□--), phosphorus (--◊--), sulfur (--Δ--) and strontium (--×--) from column percolation test of plaster (a) and gypsum (<1mm) (b) in function of leaching time, pH (--+--) and conductivity (—+—)

The pH of gypsum increases and remains approximately constant after 400 minutes of percolation test. The basic pH of gypsum is correlated to the presence of HPO_4^{2-} ions. The conductivity in both cases decreases with the percolating time indicating the decrease of ionic content in the percolate. Cumulated concentrations increase with increasing percolation time. The release rates of calcium and sulfur were 6 and 7% from plaster, whereas the release rates of calcium and sulfur from gypsum were 12 and 8%. The difference in the release rates was due to the hydration process of

plaster which inhibits and limits the dissolution of calcium and sulfate by the formation of gypsum precipitate. The release of sulfate from plaster and gypsum is <50 000 mg.kg^{-1}. According to waste acceptance criteria, these materials are considered non-hazardous. The release rates of phosphorus from plaster and gypsum were 12 and 5% respectively. For strontium, differences were observed for gypsum and plaster and a rational explanation can be given for these difference that the hydration of plaster stabilizes the strontium. The release rates of strontium from plaster and gypsum were 4 and 13%.

4.3.   Influence of gypsum particle size

In order to explain the leachability of calcium, sulfur, phosphorus and strontium as a function of particle size, percolation test was carried out on gypsum with particle size ranging from 1 to 4 mm (1-2 mm and 2-4 mm). The percolating results are presented in **Figure 89**. The conductivity and pH achieve a constant value after 1 h of percolation test. The pH increases slightly at the beginning and remain constant afterwards. Neutral pH reveals the presence of $H_2PO_4^-$ and HPO_4^{2-} in significant amount. The quantity of percolated calcium, phosphorus, sulfur and strontium increases with percolating time. Amount of calcium and sulfur percolated from gypsum 1-2 mm stabilize after 600 minutes of percolating time. Their release rates were 20 and 10% respectively.
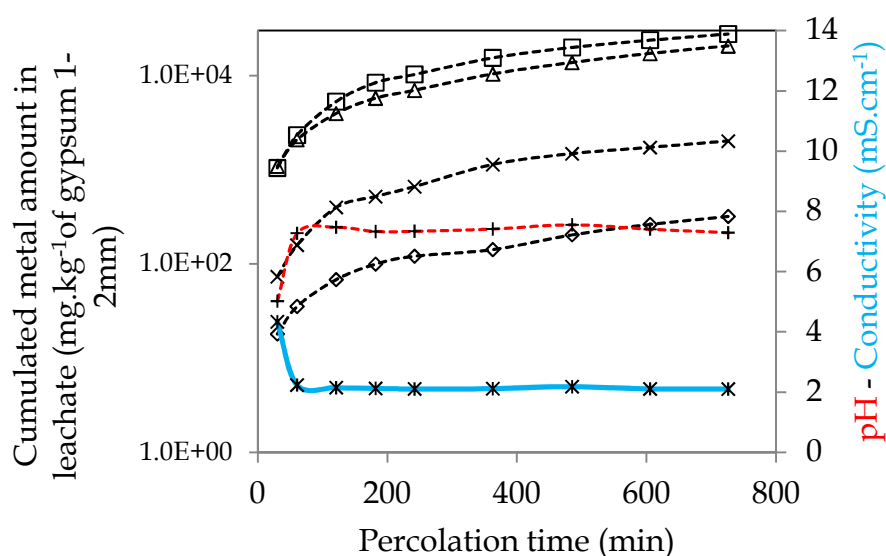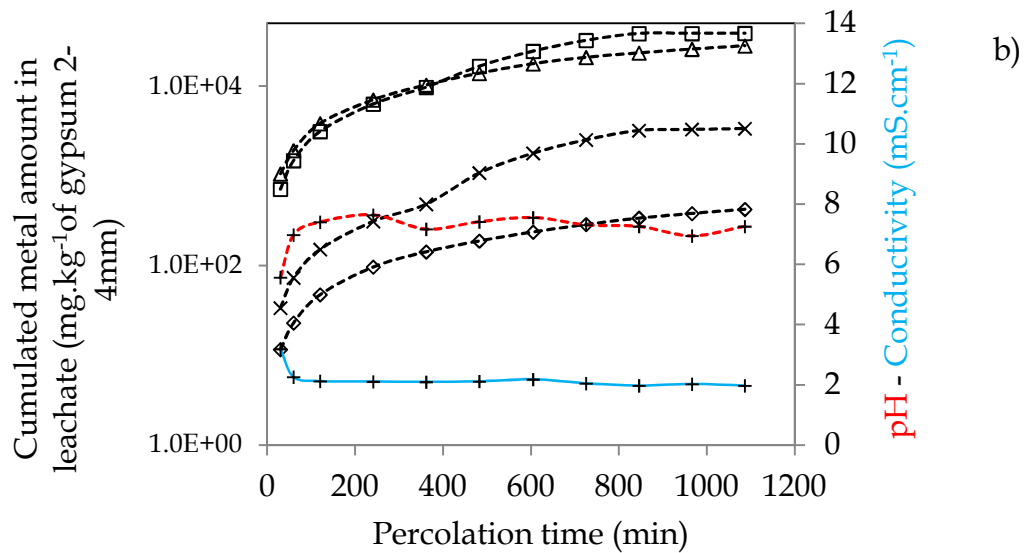
Figure 89: Leached amount of calcium (--□--), phosphorus (--◊--), sulfur (--Δ--) and strontium (--×--) from column percolation test of gypsum (1-2mm) (a) and gypsum (2-4mm) (b) in function of leaching time, pH (--+--) and conductivity (—+—)

Otherwise, the amounts of calcium and sulfur percolated from gypsum (2-4mm) achieve a constant value after 800 minutes of percolation time with rates of release of 18 and 11% respectively. The gypsum particle size has no influence on the percolated amount of calcium and sulfur at the end of percolation test, while the percolation time has. The release rates of phosphorus and strontium were 6 and 12% respectively.

4.4. Leachability of considered formulations

To study the stabilization of sulfate and strontium using Ca-HA$_{Gel}$, the percolation test was carried out on considered formulations. **Figures 90**, **91**, **92** and **93** illustrate the cumulated released concentration of calcium, sulfur, phosphorus and strontium from different considered blends versus L/S mass ratio. The logarithmic plot was used to facilitate the interpretation of the results. The pH and conductivity values were measured to evaluate the ionic amount and element speciation in the percolate.
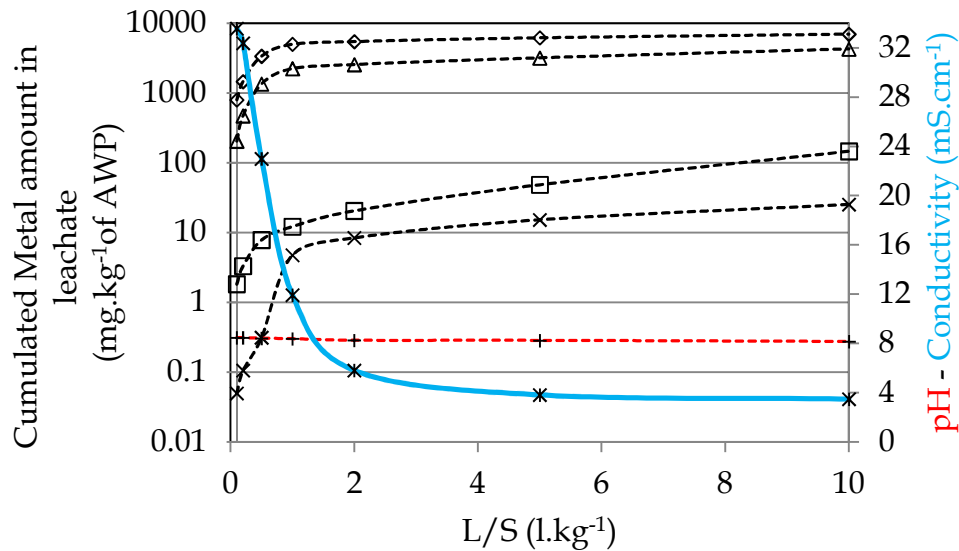
Figure 90 : Percolated amount of calcium (--□--), phosphorus (--◇--), sulfur (--Δ--) and strontium (--×--) from column percolation test of AWP blend in function of leaching time, pH (--+--) and conductivity (—+—)

Conductivity value decreases with L/S mass ratio and achieved a constant value at 5 L/S mass ratio indicating that the free ions were percolated and extracted from AWP formulation. The pH value remained constant at 8.0 for different L/S mass ratio. As it can be seen from **Figure 90**, the concentration of phosphorus and sulfur increases as a function of L/S mass ratio. Their concentrations remained constant from 1 L/S mass ratio. The release rates of phosphorus and sulfate from AWP blend were 0.5 and 0.1% respectively. The cumulated concentration of strontium and calcium increases with increasing L/S mass ratio. From **Figure 91**, the cumulated concentration of calcium, phosphorus and strontium stayed constant at 2 L/S mass ratio.

For comparison, concentration of calcium released from AG blend was approximately 5 times higher than calcium released from AWP blend. This can be explained by plaster hydration and the precipitation of calcium sulfate phosphate hydrates. The release rate of phosphorus was 0.5 and the rate of release of calcium was negligible despite the high released cumulated concentration. The release rate of sulfate and strontium were 0.1 and 0.04%.
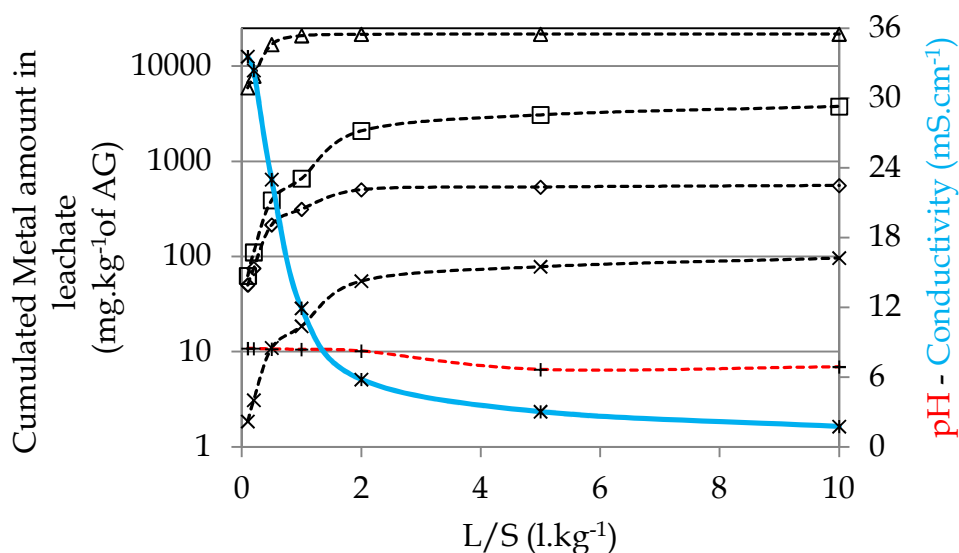
Figure 91 : Percolated amount of calcium (--□--), phosphorus (--◇--), sulfur (--Δ--) and strontium (--×--) from column percolation test of AG blend in function of leaching time, pH (--+--) and conductivity (—+—)

The obtained results demonstrate the capacity of Ca-HA$_{Gel}$ to control the release of sulfate and strontium from gypsum wastes. **Figure 92** shows the accumulated concentrations of calcium, phosphorus, sulfur and strontium from AWPG1 blend. Conductivity value measured on recovered filtrate decreases as a function of L/S mass ratio. At 2 L/S mass ratio, the conductivity value was constant revealing the total leachability of dissolved ions (i.e. phosphate and sulfate). The pH value was acidic and the phosphate may be present as $H_2PO_4^-$ and HPO_4^{2-}.

The cumulated concentrations of calcium, phosphorus, sulfur and strontium increases with increasing L/S mass ratio. The rates of release of calcium and phosphorus were 0.02 and 0.03% respectively. The rates of release of sulfate and strontium were negligible. Ca-HA$_{Gel}$ stabilizes sulfate and strontium released from gypsum.
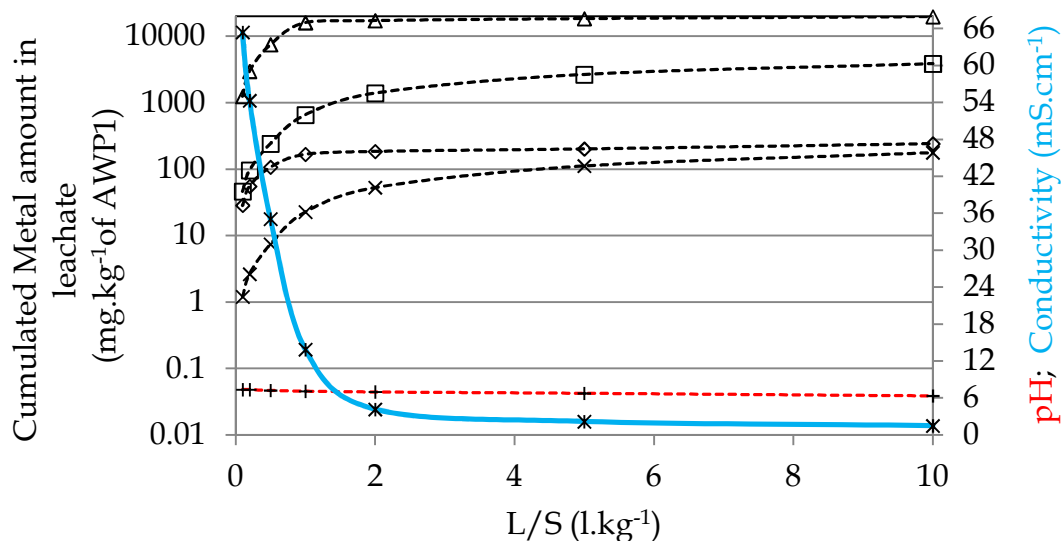
Figure 92 : Percolated amount of calcium (--□--), phosphorus (--◊--), sulfur (--Δ--) and strontium (--×--) from column percolation test of AWPG1 blend in function of leaching time, pH (--+--) and conductivity ($—+—$)

Figure 93 : Percolated amount of calcium (--□--), phosphorus (--◊--), sulfur (--Δ--) and strontium (--×--) from column percolation test of AWPG2 blend in function of leaching time, pH (--+--) and conductivity ($—+—$)
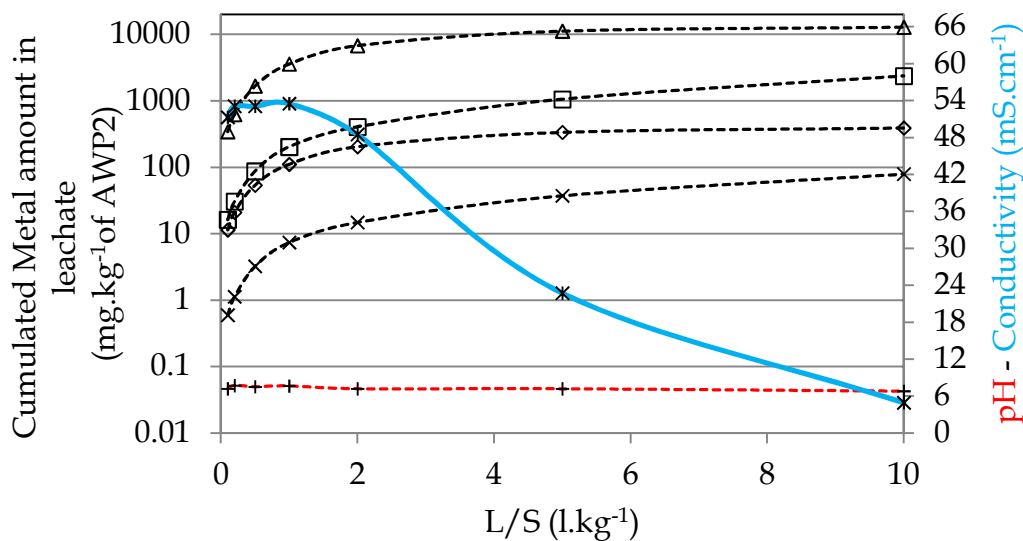
As it can be observed in **Figure 93**, the conductivity value decreases with increasing L/S mass ratio indicating the dissolution of Ca-HA particles and gypsum grains. The rate of release of calcium and phosphorus from AWPG2 blend were 0.01 and 0.04% respectively. Amount of released sulfate and strontium was decreased in the case of gypsum grains. The recovery of gypsum grains by Ca-HA particles stabilizes the blend structure. AWPG2 formulation presents adequate hydraulic performances

(50% porosity and 5.10^{-4} cm.s^{-1}) and chemical properties and can be chosen to evaluate its reactivity and purification performance and soil stabilization.

5.   Pilot trails

5.1.   Reactivity of AWPG2

Selected heavy metals (Cd(II) and Pb(II)) aqueous solutions were prepared by dissolving nitrate salts ($Cd(NO_3)_2,2H_2O$, $Pb(NO_3)_2$) in de-ionized water (10 liter). The Pb(II) and Cd(II) multi-element system had an initial concentrations of 2000ppm and 1000ppm respectively. The pH of initial solutions was determined. A single column lab-scale study was proposed to evaluate the capacities and capabilities of AWPG2 formulation filter-reactive media to remove contaminants (Cd(II) and Pb(II)). The column in composed of a transparent cylindrical cell having 90 mm internal diameter and 30 cm of length, limited by porous plates closed with caps fixed by 4 screws and maintained vertically. The solution flows from the bottom to the top using WATSON-MARLOW 400 peristaltic pump following a constant flow rate of 0.2 cm^3.s^{-1}. Flow rates were recorded as a function of experimental time using weighing coupled to computer. **Figure 94** illustrates the pilot set up.

Figure 94 : Picture of pilot experiment

Figure 95 shows the schema of pilot test. Filter paper was placed on filtration system to avoid the transport of Ca-HA particles. Filtration through AWPG2 porous media describes the flow of elements through total volume of 1907.55 cm^3. The column test experiment was carried out by packing the AWPG2 blend in the cylindrical column.
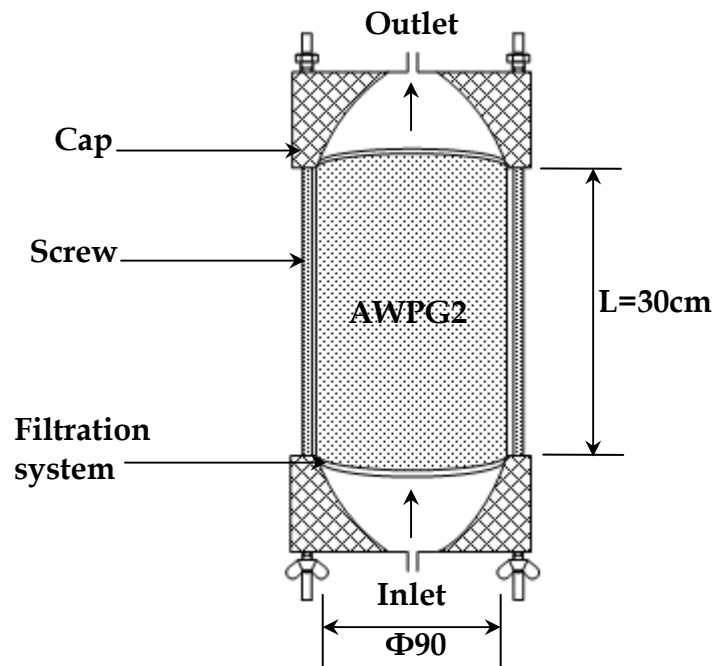
Figure 95: Experimental configuration of AWPG2 column test

Percolation tests were programmed by flushing the AWPG2 reactive media with selected solution. Collected effluents were analyzed using the same techniques as described in the batch test studies. The pilot test was maintained 1 hour and filtered mass was recorded as a function of percolation time. The pH and conductivity values were determined during column test. Conductivity value indicates the ionic composition variation in the filtrate. The porosity and permeability of AWPG2 considered formulation were 50% and 5.10^{-4} cm.s^{-1} respectively.

5.2. Pressure head

Pressure at inlet and outlet of the column was measured using differential pressure sensor (DPS, ASHCROFT 0.2 – 5 bars). Differential pressure sensor was coupled to computer to record the detected pressure value. It should be noticed that the

pulsation of peristaltic pump may influence the pressure value. **Figure 96** shows the head loss profile in the column at L/S mass ratio in function of percolation time.
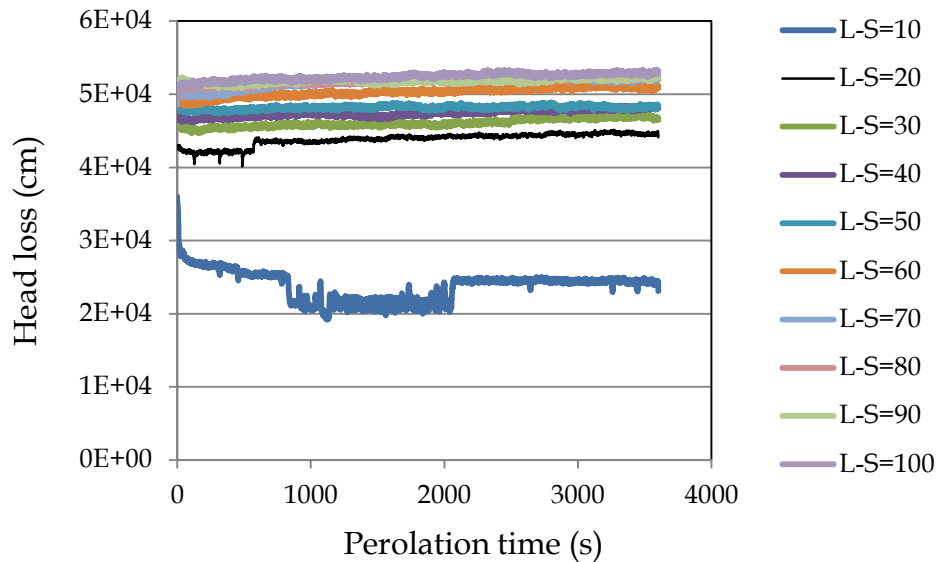
Figure 96 : Head loss as a function of time at different L/S mass ratio ranging from 10 to 100

Increasing cumulated L/S mass ratio, head loss in the column increases. The increase of head loss is directly related to the flow rate by the equation:

$$L/S = t \times Q \hspace{4cm} \text{[Eq.4]}$$

Where L/S is filtered volume on total solid (ml.g^{-1}), t is the percolation time (s) and Q is the flow rate (ml.s^{-1}). As known, the flow rate was maintained constant during the experiment, at the first hour of experiment (L/S=10) corresponds to the flux equilibration. The flux equilibration is correlated to the calibration of column cell and at L/S higher than 10, the head loss was increased explaining the elimination of the water quantity initially present in AWPG2 blend (added water and water constituting gelled particles) and compaction effect. From L/S higher than 60, the head loss is constant ($\approx 5.10^{+4}$ cm) indicating that the structure of AWPG2 paste was stabilized.

5.3. Interaction with lead and cadmium

To highlight the reactivity of selected formulation (AWPG2) to remove lead and cadmium heavy metals, the obtained results of the column test were illustrated in **Figure 97** and discussed elsewhere. The conductivity value decreases with increasing L/S mass ratio and was characterized by two stabilized value regions. The encompassment of gypsum (gypsum particles and gypsum grains) with Ca-HA particles explains the first contact of lead and cadmium with Ca-HA particles was hypothesized. The first one was localized between 40 and 60 L/S mass ratio revealing the formation of hydroxypyromorphite ($Pb_{10}(PO_4)_6(OH)_2$) and cadmium apatite ($Cd_{10}(PO_4)_6(OH)_2$). The main mechanisms of the lead and cadmium retention are ions exchange, surface complexation and precipitation [3-5]. The interaction of both lead and cadmium with Ca-HA is the main mechanism leading to the removal of selected heavy metals.

The second region was observed between 80 and 100 L/S mass ratio corresponding to the precipitation of cadmium sulfate. The pH was constant during the column test at basic value promoting the precipitation and adsorption mechanisms. At the beginning of column test, the amount of released sulfur increases dramatically in function of L/S mass ratio.
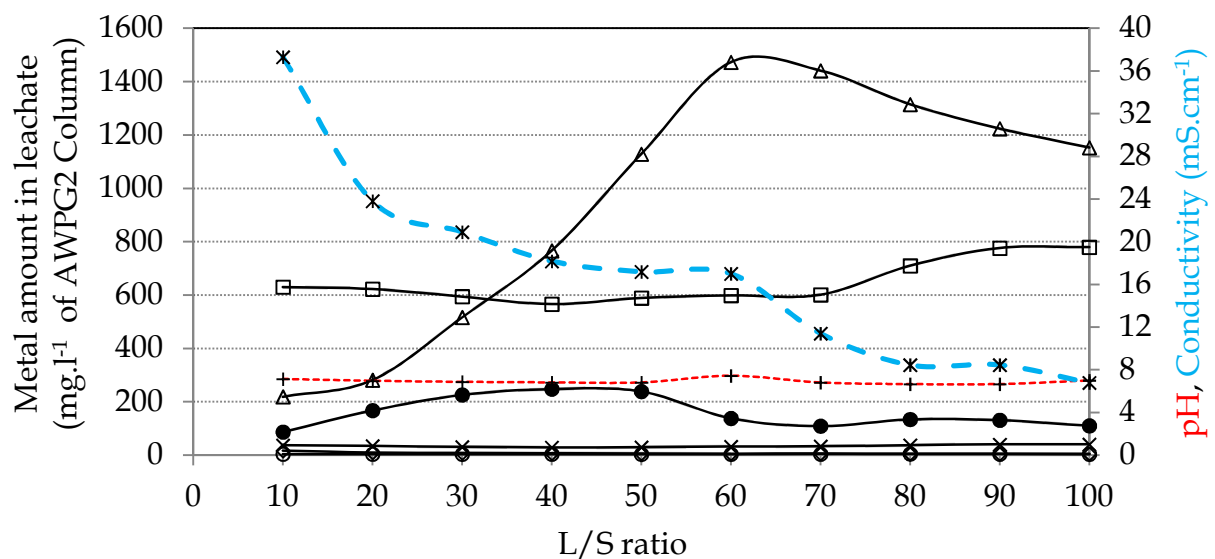
Figure 97 : Concentration of calcium (−□−), phosphorus (−◊−), sulfur (−Δ−), strontium (−×−), lead (−○−) and cadmium (−●−) in the filtrate at different L/S mass ratio (pH (--+--) and conductivity (−+−))

The increase of sulfur concentration in the outlet of column is essentially due to the dissolution of gypsum particles. This amount achieves a maximum at 60 L/S mass ratio and decreases slightly at L/S mass ratio between 60 and 100 l.kg^{-1}. However, the decrease of sulfur concentration is mainly related to the interaction with Ca-HA$_{Gel}$ (Ca-HA particles, free-phosphate and calcium) and both selected heavy metals. The release rate of sulfur from AWPG2 flushed with Pb-Cd multi-metal is 0.03%. The quantity of released calcium was constant at L/S mass ratio between 10 and 70 l.kg^{-1}. The release rate of calcium determined at the end of column experiment is negligible (0.01%). The amount of calcium and sulfur released from AWPG2 blend (percolation test) and from AWPG2 blend (column test) flushed with lead and cadmium are similar (0.01% for calcium and 0.03% for sulfur). It can be hypothesized that gypsum does not intervene in the removal of lead and cadmium. Retention capacity of Pb and Cd was calculated at 100 L/S mass ratio (It has been considered that the equilibrium was achieved at this mass ratio). The concentration of Pb^{2+} in the effluent is negligible and the retention capacity of AWPG2 to stabilize Pb^{2+} is about 99.8%. Retention capacity of Cd^{2+} is evaluated to 88%. The competitivity between lead and cadmium to be removed by Ca-HA particles was also reviewed in literature. The selectivity is also correlated to the exchange affinity and to lead and cadmium hydrated radius (Pb2+ (0.12 nm) and Cd2+ (0.097 nm)). As can be analyzed from lead and cadmium retention capacity results, the concentration of removed lead was higher than concentration of removal cadmium. The selectivity depends also on the reactive material composition, crystallinity, sorption capacities and specific surface area.

IV. Conclusion

This chapter highlighted the hydraulic performances of considered blends. Porosity of initial materials was estimated to water absorption capacity. Amount of added water leading to plaster hydration controls effectively porosity rate (porosity of hydrated plaster is 60%). Gypsum porosity differs as a function of grain size. Agglomerated gypsum (gypsum 1-2mm and gypsum 2-4mm) particles was

characterized by a porosity value about 60% indicating that volume of void space is similar. Porosity of considered blends calculated from solids compactness depends directly to the bulk density and solids proportions. Adding gypsum grains to blend containing plaster and Ca-HA$_{Gel}$ leads to increase in the permeability. Hence, gypsum promotes hydraulic performances of blend. Results of percolation tests carried out on initial materials have shown that the release rates of calcium, sulfur, phosphorus and strontium are higher than those calculated for considered blends. **Table 28** summarizes the release rate of calcium, sulfur, phosphorus and strontium calculated at 10 L/S mass ratio. The decrease of calcium, sulfur and phosphorus release rate is mainly due to the precipitation of calcium sulfate-phosphate hydrate as discussed in the Chapter VII.

Table 28 : Release rate of elements calculated at 10 L/S mass ratio

	pH	Conductivity (mS.cm^{-1})	Ca (%)	S (%)	P (%)	Sr (%)
Ca-HA	7.3	1.97	13	-	3	-
Plaster	3.9	0.73	6	7	12	4
G 1mm	8.2	2.19	12	8	5	13
G 1-2mm	7.3	2.10	20	8	6	13
G 2-4mm	7.3	1.97	18	8	11	12
AWP	8.1	3.48	0.005	0.1	0.5	0.04
AG	6.9	1.77	0.03	0.01	0.01	0.08
AWPG1	6.4	1.48	0.03	0.02	0.01	0.001
AWPG2	6.8	4.90	0.01	0.03	0.02	0.002

The stabilization of strontium was totally ensured by Ca-HA$_{Gel}$. The retention capacities can achieve 99% and 99.4% for plaster and gypsum respectively. The release rate calculated for AWPG1 and AWPG2 was very low indicating its total stabilization. Column test carried out on AWPG2 flushed with solution containing lead and cadmium has shown that the adsorption of lead and cadmium is attributed to Ca-HA particles.

Reference

[1] NF CEN/TS 14405 – Juillet 2005, Caractérisation des déchets - Essai de comportement à la lixiviation - Essai de percolation à écoulement ascendant (dans des conditions spécifiées)

[2] HAZEN, A., 1892, Some physical properties of sands and gravels, with special reference to their use in filtration, 24th Annual Rep., Massachusetts State Board of Health, Pub. Doc. No. 34, Pp539-556

[3] Wu, L., Forsling, W., and Schindler, P. W., 1991. Surface Complexation of Calcium Minerals in Aqueous Solution. Journal of Colloid and Interface Science, 147: Pp178-185

[4] Bailliez, S., Nzihou, A., che, E. B. and Flamant G., 2004, Removal of lead (Pb) by hydroxyapatite sorbent. Trans IChemE Part B, 82: Pp175-180

[5] GOMEZ DEL RIO, J., SANCHEZ P., MORANDO, P.J., CICERNO, D.S., 2006, Retention of Cd, Zn and Co on hydroxyapatite filters, Chemosphere 64, Pp1015-1020

General conclusions & perspectives

The main purpose of this thesis was the formulation of stable matrix based on calcium phosphate (Ca-HA) and the evaluation of its hydraulic performances and reactive capacity. Calcium sulfate was chosen to enhance Ca-HA$_{Gel}$ suspension and different blends were considered.

Bibliographic research highlighted the PRB configurations and its use to remediate groundwater, the main physicochemical properties of calcium phosphate and calcium sulfate and a description of porous media and the relationships leading to the determination of porosity and permeability. Particle size distribution has allowed the identification of material classification in the term of the texture. Ca-HA particles were identified as loamy texture and plaster and gypsum with particle size less than 1mm were classified as silty-sand and sandy-loam texture respectively. Physicochemical characterization (DRX and FTIR) of initial materials has shown the same characteristic bands and peaks of phosphate and sulfate present in apatite and gypsum also discussed in literature. Raman and FTIR analysis carried out on initial materials have shown similar main peaks assignment corresponding to symmetric stretch. Calcium sulfate has shown a high capability to stabilize Ca-HA$_{Gel}$ suspension.

Hydration of plaster industrial product is perfect at W/P mass ratio of 0.4. The consistency of Ca-HA$_{Gel}$ is controlled by the plaster hydration leading to Ca-HA/(W/P=0.4) stabilization structure. Rheological tests carried out on all ternary considered formulations based on Ca-HA$_{Gel}$, gypsum and plaster with or without added water have exhibited a shear-thinning and thixotropic behavior. Shear-thinning behavior and the thixotropy revealed the favorability of blends set up. Gypsum particles are negatively charged causing repulsion and improving stability. The positively-charged plaster particles play a major role in the structure stabilization by the attractive affect generated by hydration process. Interaction between Ca-HA and plaster (or Ca-HA and gypsum) leads to modification of Ca-HA

charge. The fixation of dissolved sulfate from plaster on Ca-HA particles explains the Ca-HA charge modification improving its stability.

From rheological results, 4 formulations were considered to study their leaching behavior under paste form. The formulations containing plaster were blended with 0.4 W/P mass ratio as the amount of plaster paste stabilizes Ca-HA structure at proportions less than 80%. Gypsum with different fraction size (Gypsum 1mm, Gypsum 1-2mm and Gypsum 2-4mm) was used to assess its stability by Ca-HA. Characterization of formulations carried out using XRD analysis has shown the formation of new compounds such as sulfate carbonate hydrate, calcium phosphate sulfate hydroxide hydrate and calcium phosphate sulfate hydrate. Environmental behavior of initial material has shown that the release of heavy metals is in accordance with waste acceptance criteria. The release of calcium, sulfate, phosphorus, strontium and selected heavy metals was also influenced by L/S mass ratio, particle size and leaching duration. Ca-HA stabilizes heavy metals released from gypsum and plaster in AWPG1 and AWPG2 blends. Porosity of considered blends was higher than 50%. Permeability of blends containing gypsum grains was increased 10 times that of Ca-HA$_{Gel}$ permeability. Gypsum grains plays a major role in the enhancement of hydraulic performances of considered blends. The release rate of calcium, sulfur and phosphorus decreases in the cases of AWPG1 and AWPG2 blends in comparison with initial materials. The AWPG2 blend was chosen as matrix presenting adequate hydraulic performances (porosity of 50% and permeability of 5.10^{-4} cm.s^{-1}) to carry out the column test. The results of column tests carried out on AWPG2 blend have shown that lead and cadmium were perfectly removed with retention capacity of 99 and 88% respectively. Surface complexation onto phosphate surface groups, ionic exchange in surface calcium sites and the dissolution/precipitation are the main mechanisms governing the removal of lead and cadmium. AWPG2 formulation may be applied as PRB to treat groundwater following the hydraulic performances and reactivity.

Further work would be interesting to be done on:

- The determination of permeability can be carried out using oedometric trails. This test may provide same indications concerning the intrinsic porous structure and the influence of strain on the permeability value.

- The long term column tests may be performed to describe the behavior of heavy metals through selected porous media and to monitor the principal phenomena governing solute transport and treatment of contaminated water and to model the flow of solute water.

- The modeling could be applied using Phreeqc and Hydrus software. Several results could be obtained from transport modeling to facilitate the interpretation of different phenomena governing the heavy metals removal.

- The clogging and saturation of reactive material is the main drawback of porous filters. It manifests itself by the precipitation of carbonate and hydroxide or the retention of suspended matter leading to the decrease of porous volume. To study the effect of clogging on the porous media performance, floating spheres model based on Kozeny-Carman equation allows the clogging and saturation prediction.

Appendix

Appendix 1 : Granulometric characteristic of materials

Interpretation of granulometric curves is based on the determination of d_X defined as the diameter for which the underflow is X%. HAZEN coefficient (HC) also named coefficient of uniformity and defined by the follow relationship: HC = $\frac{d_{60}}{d_{10}}$ where d_{60} and d_{10} are the diameters corresponding to 60 and 10% of passing accumulated mass.

$$CC = \frac{d_{30}^2}{d_{60}.d_{10}}$$
$$Spacing = \frac{d_{90} - d_{10}}{d_{50}}$$

|	HC	CC	Spacing	d_{10}	d_{30}	d_{50}	d_{60}	d_{90}
Gypsum (<1mm)	01.16	00.58	02.50	17.13	14.10	231.77	19.94	597.30
Plaster (α)	04.10	00.98	02.06	11.86	23.77	61.69	48.61	138.99
Ca-HA$_{Powder}$	13.91	10.77	17.67	04.05	49.55	30.82	56.32	548.62
Ca-HA$_{Gel}$	19.81	15.34	03.29	04.59	80.05	14.69	90.95	52.92

HC : HAZEN Coefficient; CC : Curvature Coefficient; S : Spacing

Appendix 2: Rheological behavior

In general, the rheology is the study of matter flow behavior under constraint applied. As a result, the relative sliding of underlying layers on top of each other is the result of the application of shear stress, which makes the material deformable fluid without mass transfer. The constant friction between the molecules of the layer leads to a delay effect in the transmission of a relative motion to a second underlying layer, so the speed of the first layer decreases. Hence we can define the viscosity of a fluid such as a flow resistance of a material subjected to shear stress; in fact, it depends on the physicochemical composition of the material, temperature, pressure, velocity gradient and evidently the time.

Shear stress results of pressure forces application on a surface; it is expressed by the following relation; $\tau = \frac{\overrightarrow{dF}}{dS}$ (Pa). Perpendicular forces to the surface layers are not involved in the movement of shear. Shear rate or shear rate $\dot{\gamma}$ noted is determined when the shear strain is maximum, it is located at the upper limit of the moving plane, and contact with the fixed plane influence on the decrease of shear rate according to the displacement interval dn (**Figure 98**). Shear deformation is the displacement at a given time interval reported to travel; $\gamma(n,t) = \frac{dx(n,t)}{dn}$. The derivative of the shear strain γ is the shear rate, it is written as follows: $\dot{\gamma} = \frac{d\gamma}{dt}$ (s^{-1}). The devices widely used to evaluate the behavior of liquefied materials, the rotational or coaxial viscometer (Rheometer) (cylinder-cylinder), with cone-plate and plate (plate-plate).
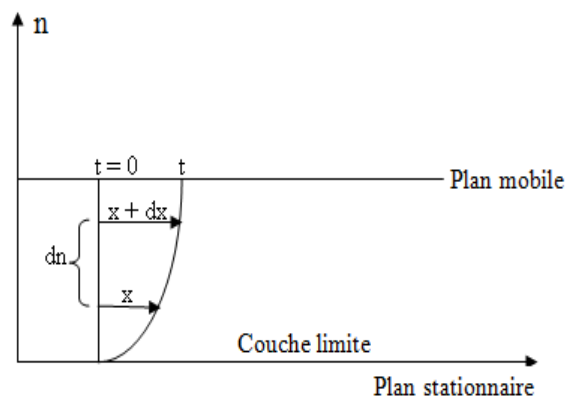
Figure 98: Fluid flow in two parallel planes at a uniform speed

225

Dynamic rheology is based on the application of oscillatory mechanical stress for evaluation of the internal structure of the material. In principle, it is used to denote viscous or elastic behavior of materials and obeys Hooke's law, $\tau = G.\gamma$ where G is the dynamic modulus of viscosity which varies with time for the viscoelastic material and γ is the sinusoidal deformation. The application of a low amplitude sinusoidal deformation allows measure resulting sinusoidal stress measurement. The dynamic modulus of time-dependent viscosity noted G^* is correlated with $G\,'$(storage modulus) characterizes the energy stored in the material as elastic and G''(loss modulus), which refers to the viscous property of the material and characterizes the energy dissipated in the material, the following relations : $G' = G^*\cos(\varphi)$ et $G'' = G^*\sin(\varphi)$, where φ is the phase difference or phase shift, as can be expressed by replacing G^* modulus by the report σ_0/γ_0, with σ_0 is the initial shear stress and γ_0 is the initial shear rate.

Rheological flow

Graphical representation of the rheological behavior is reflected in the establishment of the relationship $\tau = f(\dot{\gamma})$ is the flow curve. Figure 5 identifies the different rheological behavior. Newtonian behavior (exclusively linear viscous behavior) is deduced from the dynamic viscosity (or apparent viscosity) by the equation rheological $\mu = \frac{\tau}{\dot{\gamma}}$ (Pa.s or Poiseuille), and it should be noted that μ is independent of shear rate. The constant value of μ obtained at different shear rates is the absolute viscosity, often denoted η. Moreover, when the viscosity is no longer independent of shear rate, it is useful to describe the mechanical behavior of materials based on the empirical law of viscosity or the power Ostwald law model $\tau = K\dot{\gamma}^n$ with K is the consistency index and n is the flow index, and the value of n, we can characterize the nature of the behavior, which for n=1, the behavior is Newtonian, n<1, the behavior is shear-thinning (or pseudo-plastic) and n>1, the behavior is shear-thickening.

Shear thickening and shear-thinning behaviors are not linear, this can be explained by the fact that lower applied stress causes the flow and the shear force is not always proportional to the shear rate (i.e. variation of viscosity for shear variables).

Another behavior (non-Newtonian) is defined when the flow occurs only through the application of shear stress to a value greater than the yield stress (the yield stress or plasticity threshold τ_0). The representation of a material level, taking into account the plastic viscosity η_{pl} is independent of shear rate, resulting in the following relation, $\tau = \tau_0 + \eta_{pl}\dot{\gamma}$, is the Bingham behavior. The generalization of this power law model is written as follows $\tau = \tau_0 + K\dot{\gamma}^n$, allows the identification of the shear-thinning behavior (or Casson behavior) (n <1) and thickening behavior (n> 1) (**Figure 99**). Non-Newtonian fluids depends on the time, that is to say the duration of the flow is often correlated with the apparent viscosity of the fluid.
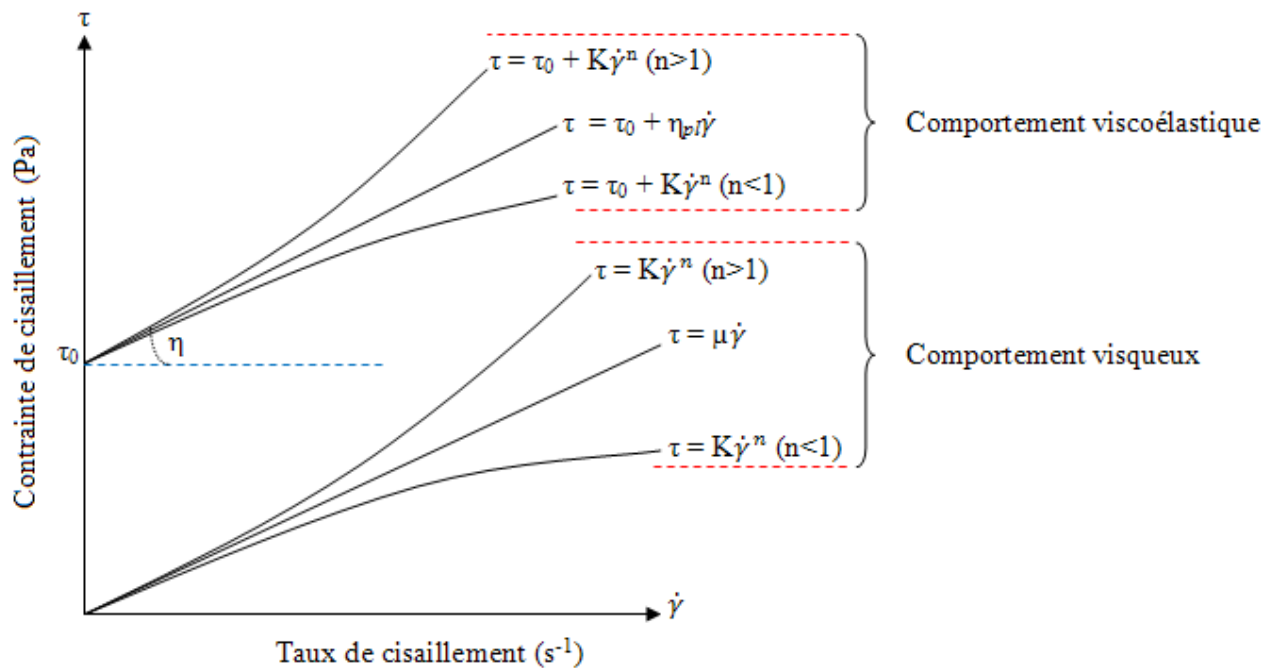
Figure 99: Different flow curves for viscous and viscoelastic behavior

The time index can then characterize the change in the structure into two distinct behaviors, thixotropy and rheopexy (antithixotropie), reversible modification or not of structure (disruption of the structure by shear) corresponding to the thixotropy when the viscosity apparent decreases with constant shear rate duration, and when the viscosity increases, we talk about the rheopexy (organization structure).

Appendix 3 : Thresholds of safe drinking water and waste acceptance criteria

|	Water Potability (mg.l^{-1})		Waste Acceptance Criteria (mg.kg^{-1})		
			Inert	Non-Hazardous	Hazardous
	WHO (2011)	EC (1998)	(i)	(nd)	(d)
Al	0.2	-	-	-	-
As	0.01	0.01	0.5	2	25
B	0.5	1.0	-	-	-
Ba	0.7	-	20	100	300
Cd	0.003	0.005	0.04	1	5
Cr Total	0.05	0.05	0.5	10	70
Cu	2.0	2.0	2	50	100
Fe	-	0.2	-	-	-
Hg	0.006	-	0.01	0.2	2
Mn	0.04	0.05	-	-	-
Mo	0.07	-	0.5	10	30
Na	0.4	-	-	-	-
Ni	0.07	-	0.4	10	40
Pb	0.01	-	0.5	10	50
Sb	0.02	0.005	0.06	0.7	5
Se	0.04	0.01	0.1	0.5	7
Sr*	4	-	18000	18000	
U	0.3	-	-	-	-
Zn	3.0	-	4	50	200
Chloride	-	250	800	15 000	25 000
Fluoride	1.5	1.5	10	150	500
Sulfate	500	250	1 000	20 000	50 000
TOC	-	-	500	800	1 000
SF	1200	-	4 000	60 000	10 000
L.O.I	-	-	-	-	100 000
pH	6.5<pH<9.5	-	-	>6	-

TOC: Total Organique Carbone; SF: Soluble fraction; L.O.I: Loss on igniation

WHO Word Health 2011.Organization. *Guidelines for drinking water quality*. Fourth Edition. ISBN 9789241548151. available on http://whqlibdoc.who.int/publications/2011/9789241548151_eng.pdf. Pp472-475

EC European Commission 1998. *Directive 98/83/CE du conseil du 3 Novembre 1998 relative à la qualité des eaux distinées à la consummation humaine.* disponible sur http://eurlex.europa.eu/LexUriServ/LexUriServ.do?uri=OJ:L:1998:330:0032:0054:FR:PDF. Pp42-45

* ICDF The Idaho Comprehensive Disposal Facility, Complex Waste Acceptance Criteria, Norme A-1B ISO 19005-1, Pp A-10, Available on: http://ar.inel.gov/images/pdf/200910/2009100100577TUA.pdf

Appendix 4: Calibration of peristaltic pump and permeability device
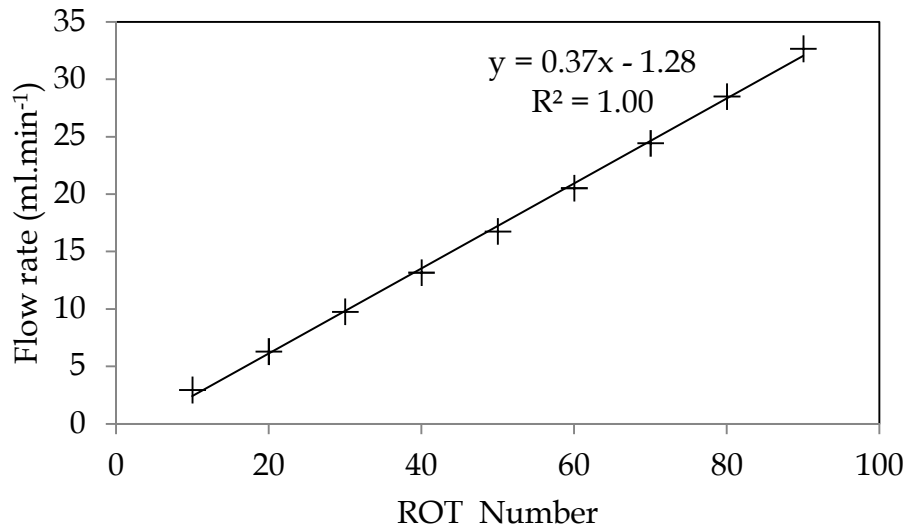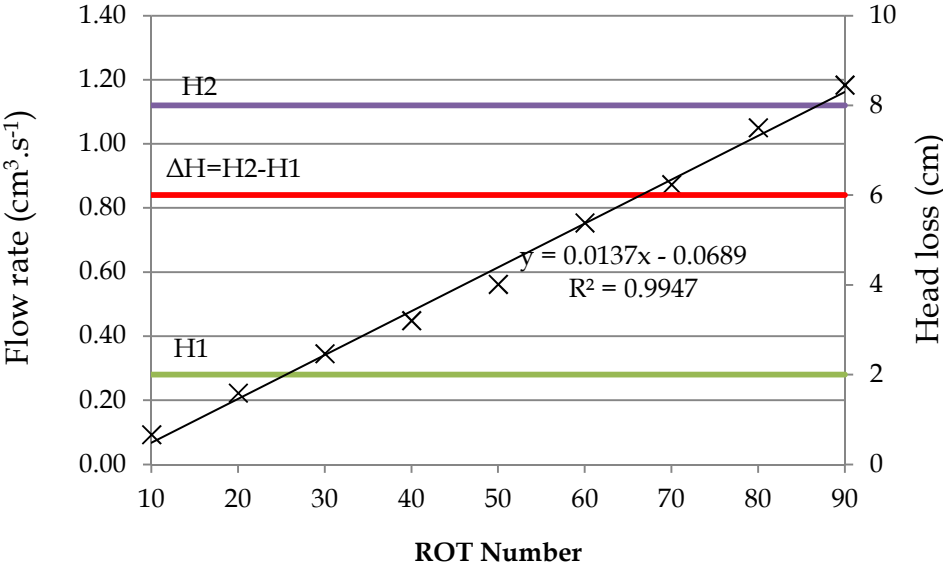

Flow rate as a function of rotation number of peristaltic pump

Calibration for device used to determine the permeability of plaster, Ca-HA$_{Gel}$ and Ca-HA$_{Powder}$:
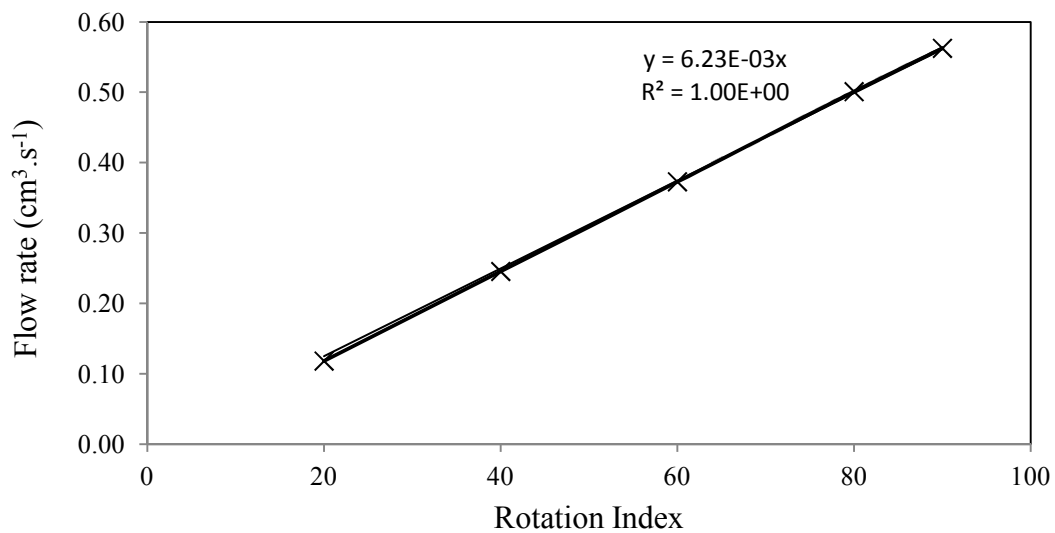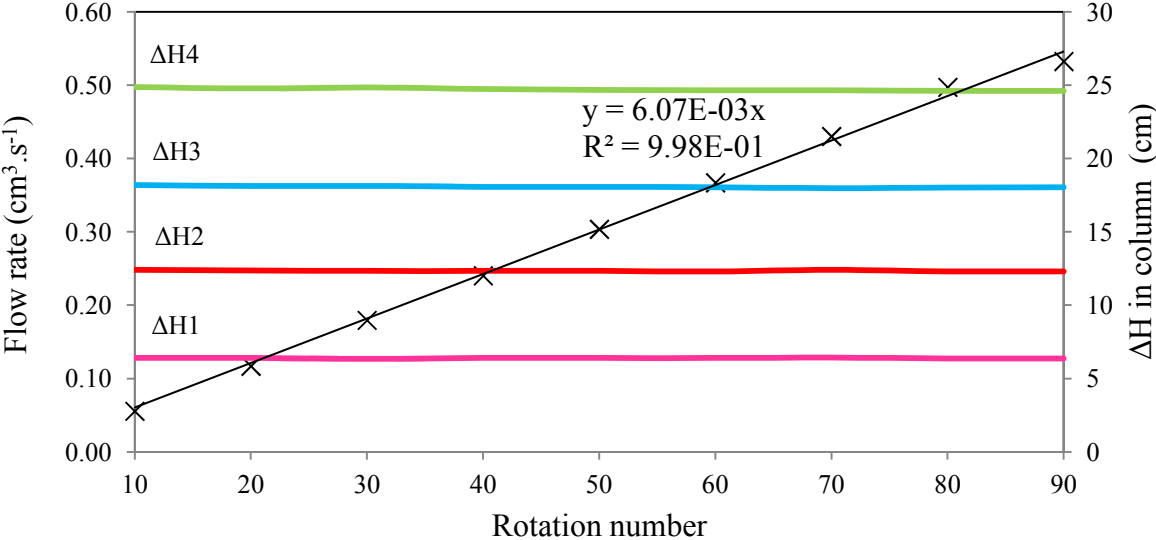

Flow rate as a function of rotation number of peristaltic pump

Calibration for device used to determine the permeability of gypsum with different fraction sizes:

Flow rate and head loss as a function of rotation number of peristaltic pump

Calibration of column used for pilot trail

Flow rate and head loss as a function of rotation number of peristaltic pump